Aus dem Biomedizinisches Centrum
Lehrstuhl: Molekularbiologie
Institut der Ludwig-Maximilians-Universität München
Vorstand: Prof. Dr. Peter B. Becker

Histone methyltransferase SETDB1 regulates fetal hematopoiesis

Dissertation
zum Erwerb des Doktorgrades der Naturwissenschaften
an der Medizinischen Fakultät der
Ludwig-Maximilians-Universität zu München

vorgelegt von

Maryam Kazerani Pasikhani

aus
Rascht / Iran

2020

Mit Genehmigung der Medizinischen Fakultät
der Universität München

Betreuer: Prof. Dr. rer. nat. Gunnar Schotta

Zweitgutachter: Prof. Dr. rer. nat. Heinrich Leonhardt

Dekan: Prof. Dr. med. dent. Reinhard Hickel

Tag der mündlichen Prüfung: 28.10.2020

Eidesstattliche Versicherung

Ich erkläre hiermit an Eides statt, dass ich die vorliegende Dissertation mit dem Thema

“Histone methyltransferase SETDB1 regulates fetal hematopoiesis”

selbständig verfasst, mich außer der angegebenen keiner weiteren Hilfsmittel bedient und alle Erkenntnisse, die aus dem Schrifttum ganz oder annähernd übernommen sind, als solche kenntlich gemacht und nach ihrer Herkunft unter Bezeichnung der Fundstelle einzeln nachgewiesen habe.

Ich erkläre des Weiteren, dass die hier vorgelegte Dissertation nicht in gleicher oder in ähnlicher Form bei einer anderen Stelle zur Erlangung eines akademischen Grades eingereicht wurde.

Munich, 27.05.2020 Maryam Kazerani Pasikhani

Ort, Datum Unterschrift, Doktorandin

My PhD project focused on understanding the role of histone methyltransferase SETDB1 during mouse fetal liver hematopoiesis. The work of my doctoral thesis is assembled into a manuscript for publication in a peer-reviewed journal.

Histone methyltransferase SETDB1 regulates fetal hematopoietic stem and progenitor cell function and lineage fate determination

Kazerani M, Cernilogar F, Pasquarella A, Hinterberger M, Klein L, Schotta G.

In addition to my PhD work, I supported other scientific project leading to the following publication:

Pasquarella, A., Ebert, A., Pereira de Almeida, G., Hinterberger, **M., Kazerani**, M., Nuber, A., Ellwart, J., Klein, L., Busslinger, M., and Schotta, G. (2016). Retrotransposon derepression leads to activation of the unfolded protein response and apoptosis in pro-B cells. Development *143*, 1788–1799.

I. Table of Contents

II. Abstract

Hematopoietic stem cells (HSCs) are characterized by two unique features, the ability to self-renew and to differentiate, that are tightly controlled by transcription factors functioning in concert with epigenetic regulators. The histone methyltransferase SETDB1 is known for its role in epigenetic silencing. Studies of SETDB1 during early development and in different cellular systems pointed to a pivotal role of this histone methyltransferase enzyme in the maintenance of cell identity and genome integrity. SETDB1-mediated silencing of endogenous retroviruses is well-established; however, there is a poor understanding of its role in gene regulation. Besides, the questions of how and by which mechanisms SETDB1 regulates HSC self-renewal, and lineage specification remained mostly unanswered. Here, we show that ablation of *Setdb1* in the fetal liver HSCs (*Setdb1*^{vav}) generates a progressive phenotype from fetal to postnatal. Increased fetal liver long-term hematopoietic stem cells (LT-HSCs) number, enhanced cycling, and normal survival of these cells is followed by enhanced apoptosis and subsequent depletion of LT-HSCs at the postnatal stage, which is indicative of "stem cell exhaustion," leading to hematopoiesis failure and postnatal lethality. *Setdb1*-deficient hematopoietic stem and progenitor cells (HSPCs) display compromised lymphoid lineage differentiation and enhanced myeloerythroid output. Despite the expansion of *Setdb1*^{vav} HSPCs, they generate fewer and smaller colonies *in vitro* and fail to repopulate the bone marrow in competitive transplantation experiments, in part, due to the compromised homing potential. Coherently, HSC gene signature and gene sets implicated in cellular communication and homing downregulated in *Setdb1*^{vav} HSPCs. Strikingly, we observe substantial downregulation of critical regulators of lymphoid development in *Setdb1*^{vav} HSPCs, whereas myeloerythroid lineage affiliated genes show upregulation. Direct silencing function of SETDB1 in fetal liver HSPCs is attributed to the deposition of the H3K9me3 mark on the promoters of non-hematopoietic genes and retrotransposons. Interestingly, we further showed that SETDB1 loss changes the chromatin state toward a more accessible state, as demonstrated by the higher number of ATAC peaks in *Setdb1*^{vav} LSKs, which is the direct consequence of H3K9me3 hypomethylation. Specifically, the accessible chromatin regions containing PU.1 and CTCF motifs embedded in ERVs (class III) and B3 subfamily of B2 SINEs retrotransposons, respectively, lost the H3K9me3 mark. Surprisingly, significantly deregulated genes neighboring these putative motifs are associated with the hematopoietic phenotype.

In conclusion, we demonstrated that *Setdb1* deletion in FL HSPCs generates a unique phenotype compared with the adult counterparts, which is the loss of HSPCs identity and skewed differentiation toward myeloerythroid lineage. Beyond gene promoters and retrotransposon silencing, SETDB1 fine-tunes gene expression by organizing the chromatin

accessibility through deposition of H3K9me3 at inappropriate PU.1 and CTCF motifs. Putative binding of TFs, especially CTCF, to their corresponding unprotected motifs in the absence of *Setdb1*, lead to transcriptional changes, which at least in part, underlies the compromised HSPCs function and skewed lineage specification.

III. Zusamenfassung

Hämatopoetische Stammzellen (HSZ) zeichnen sich durch zwei einzigartige Fähigkeit aus, die zur Selbsterneuerung und die zur Differenzierung. Beide werden durch Transkriptionsfaktoren, die zusammen mit epigenetischen Regulatoren wirken, streng kontrolliert. Die Histonmethyltransferase SETDB1 ist für ihren Beitrag zur epigenetischen Stilllegung bekannt. Studien an SETDB1 während der frühen Entwicklung und in verschiedenen zellulären Systemen zeigten eine zentrale Rolle dieser Histon-Methyltransferase bei der Aufrechterhaltung von Zellidentität und Genomintegrität. Die SETDB1-vermittelte Stilllegung endogener Retroviren ist bestens bekannt. Bezüglich ihrer Rolle in der Genregulation mangelt es jedoch an Verständnis. Außerdem blieben die Fragen, wie und durch welche Mechanismen SETDB1 die HSZ-Selbsterneuerung und die Spezifikation der Abstammungslinien reguliert, größtenteils unbeantwortet. Hier zeigen wir, dass die Entfernung von Setdb1 in den HSZ der fötalen Leber (*Setdb1*^{vav}) einen progressiven Phänotyp von fötal bis postnatal erzeugt. Erhöhte LT-HSZ Zahlen in der fötalen Leber, ein erhöhter Zyklusdurchlauf und ein normales Überleben dieser Zellen werden von erhöhter Apoptose und einer anschließenden Abnahme von LT-HSZ im postnatalen Stadium gefolgt. Dies weist auf eine „Stammzellenerschöpfung“ hin, die zum Versagen der Hämatopoese und einer postnatalen Letalität führt. Setdb1-defiziente Stamm- und Progenitorzellen (HSPZ) zeigen eine beeinträchtigte Differenzierung der lymphoiden Linien und eine verbesserte Myeloerythroid-Produktion. Trotz der Expansion von *Setdb1*^{vav}-HSPZ erzeugen sie in vitro immer weniger Kolonien und können das Knochenmark in kompetitiven Transplantationsexperimenten nicht neu bevölkern, was teilweise auf das beeinträchtigte Homing-Potenzial zurückzuführen ist. Damit zusammenhängend sind die HSZ-Gensignatur und die Gensätze, die an der zellulären Kommunikation und dem Homing beteiligt sind, in *Setdb1*^{vav}-HSPZ herunter reguliert. Bemerkenswerterweise beobachten wir bei *Setdb1*^{vav}-HSPZ eine erhebliche Expressionsminderung kritischer Regulatoren der Lymphoidentwicklung, während Gene, die mit der Myeloerythroid-Linie verbunden sind, eine Hochregulierung aufweisen. Die direkte Stummschaltungsfunktion von SETDB1 in fötalen Leber-HSPZ wird auf die Anreicherung der H3K9me3-Markierung auf den Promotoren nicht hämatopoetischer Gene und Retrotransposons zurückgeführt. Interessanterweise haben wir weiter gezeigt, dass der Verlust von SETDB1 den Chromatin-Zustand in einen zugänglicheren Zustand ändert, wie die höhere Anzahl von ATAC-Peaks in *Setdb1*^{vav}-LSK, als direkte Folge der H3K9me3-Hypomethylierung, zeigt. Insbesondere die H3K9me3-Markierung an zugänglichen Chromatinregionen, die PU.1- und CTCF-Motive enthielten, wie die in ERVs (Klasse III) bzw. B3-Unterfamilie von B2 SINEs-Retrotransposons eingebetteten, gingen

verloren. Überraschenderweise sind signifikant deregulierte Gene, die diesen mutmaßlichen Motiven benachbart sind, mit dem hämatopoetischen Phänotyp assoziiert.

Zusammenfassend haben wir gezeigt, dass die Deletion von *Setdb1* in FL-HSPZ im Vergleich zu den adulten Gegenstücken einen einzigartigen Phänotyp erzeugt, der den Verlust der Identität von HSPZ und die verzerrte Differenzierung zur myeloerythroiden Linie darstellt. Über Genpromotoren- und Retrotransposon- Stilllegung hinaus optimiert SETDB1 die Genexpression, indem es die Zugänglichkeit des Chromatins durch Ablagerung von H3K9me3 an ungeeigneten PU.1- und CTCF-Motiven organisiert. Die mutmaßliche Bindung von TFs, insbesondere CTCF, an ihren entsprechenden Motiven in Abwesenheit von SETDB1 führt zu Transkriptionsänderungen, die zumindest teilweise der beeinträchtigten HSPZ-Funktion und der verzerrten Abstammungsspezifikation zugrunde liegen.

1. Introduction

1.1. Hematopoiesis: development and regulation

1.1.1. From embryo to adult: development of hematopoiesis in mice

The hematopoietic system is the complex system involved in the continuous creation of blood cells in different organs and tissues during development. The detailed studies of the process of hematopoietic development have been started in the early 1900s (Clark, 1909; Stockard, 1915; Sabin, 1920). Ever since, our understanding of this complex developmental system has expanded through several milestones.

In mice, the development of the hematopoietic system occurs in two waves: (1) primitive hematopoiesis; and, (2) definitive hematopoiesis (Figure 1.1). The first wave of hematopoiesis, primitive hematopoiesis, also known as embryonic hematopoiesis initiates at embryonic day (E) 7.0-E9.5 in the yolk sac blood islands which mainly produces primitive embryonic erythrocytes and some myeloid cells with no lymphoid potential (Moore and Metcalf, 1970; Palis et al., 1999; Lux et al., 2008). The major function of erythrocytes which are nucleated and express fetal hemoglobin, is to facilitate oxygen transport to the fast-growing embryonic tissues (Barker, 1968; Steiner and Vogel, 1973) The primitive hematopoiesis has short-term reconstituting potential (Cumano et al., 1996); therefore, it is soon followed by definitive hematopoiesis. At E9.5-E10.5, the first definitive hematopoietic stem cells (dHSCs) emerges in the aorta-gonad-mesonephros (AGM) region. dHSCs isolated from the AGM region have the long-term and autonomous capacity to generate adult-type hematopoietic cells upon transplantation to wild type irradiated recipients (Medvinsky and Dzierzak, 1996). Subsequently, definitive hematopoiesis continues with the colonization of other hematopoietic organs. In parallel with the AGM region, at E10.5-E11.0, placenta harbors dHSCs. The placental dHSC pool increase dramatically by E12.5 and decrease afterward upon peak migration of dHSCs to the next hematopoietic site, the fetal liver (FL) (Müller et al., 1994;Godin and Cumano, 2002; Gekas et al., 2005; Ottersbach and Dzierzak, 2005). The onset of hematopoiesis in the FL occurs as early as E10 (Houssaint, 1981). The immature hematopoietic cells and macrophages are detected by light and electron microscopy, as showed by Sasaki and his colleague (Sasaki and Sonoda, 2000). At E11, the first dHSCs arrive in the FL from the placenta and AGM region (Müller et al., 1994; Gekas et al., 2005). However, Kieusseian et al. present a new developmental stage in HSC development during FL hematopoiesis. They show that FL is colonized primarily at E9.0 by erythro-myeloid progenitors directly from the yolk sac followed by migration of immature HSCs from para-aortic

splanchnopleura (P-Sp), an intraembryonic region that evolves into AGM region later, and AGM region at E10. Moreover, they characterized these immature HSCs by phenotype and reconstitution potential. Importantly, they give rise to HSCs in situ (Kieusseian et al., 2012). From E11-E12, hematopoietic compartment expands in the FL, which is mainly comprised of the formation of erythroblasts islands, leading to erythroid development after E12 (Sasaki and Sonoda, 2000). Concomitantly, lymphoid progenitors migrate from FL and seed fetal thymus around E11 (Kawamoto et al., 1998; Kawamoto et al., 1999; Douagi et al., 2002).

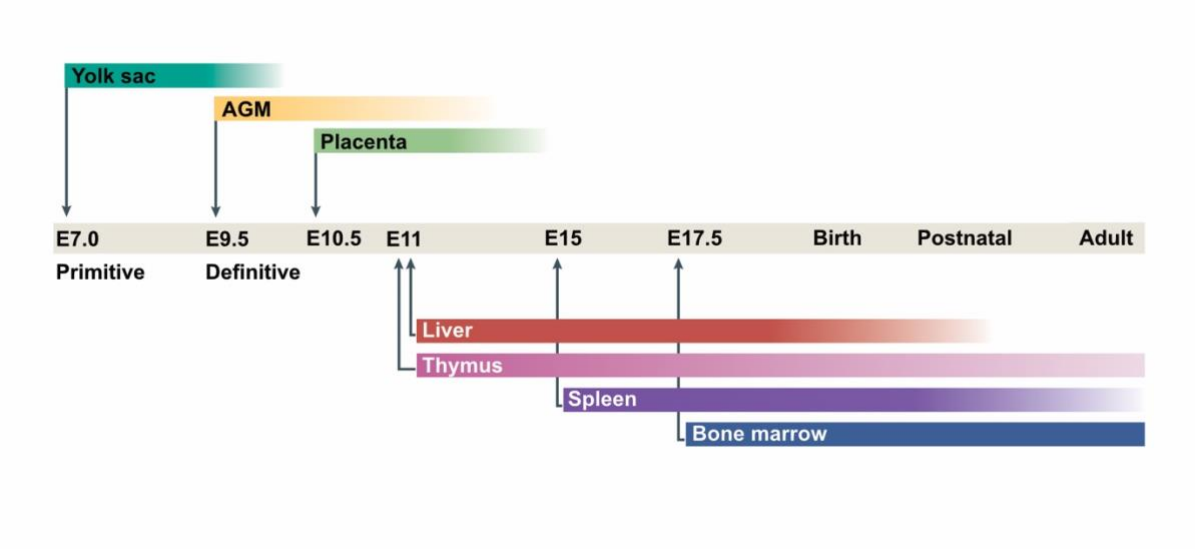

Figure 1.1 | Timeline of hematopoiesis in mice

The development of the hematopoietic system in mice initiates at different time points and locations. Hematopoiesis occurs in two waves, the primitive and definitive hematopoietic waves. The primitive wave mainly generates erythroid progenitors, while the definitive wave gives rise to the hematopoietic stem cells (HSCs) to ensure lifelong maintenance of hematopoiesis. AGM, aorta-gonad-mesonephros; E, embryonic day. Figure is modified from (Wang and Wagers, 2011).

The peak of FL hematopoiesis initiates from E12.5-E15.5 when the FL is the primary active site of hematopoietic development. HSC pool expands massively and reaches a maximum of ~1000 HSCs around E15.5. HSCs undergo commitment and differentiation to generate the first single-potent progenitors and differentiated cells, respectively, fueling the hematopoietic system in the growing embryo. By E15.5-E16.5, HSC production in the FL hits the plateau and decreases (Morrison et al., 1995; Ema and Nakauchi, 2000; Gekas et al., 2005). Around E15, FL HSCs seed fetal spleen (Sasaki and Matsumura, 1988). After that, HSCs activity increases until E17.5 (Christensen et al., 2004). However, the HSC pool resides in the fetal spleen until two weeks after birth (postnatal), contributing to hematopoiesis during the hematopoietic site transition from FL to bone marrow (BM) (Wolber et al., 2002;

Christensen et al., 2004). Moreover, spleen provides an additional site for erythropoiesis and myelopoiesis during fetal and postnatal life (Djaldetti et al., 1975; Bertrand et al., 2006).

Upon development of the skeletal system, functional circulating HSCs of FL origin home to the fetal BM at E17.5. Engraftment and proliferation of HSCs in the newly generated fetal BM niche ensures hematopoietic system establishment at this stage (Christensen et al., 2004; Gekas et al., 2005). The shift of hematopoietic development from FL to fetal BM marks the final transition of the hematopoietic site where BM maintains hematopoiesis until after birth, postnatal, and later during adult life.

1.1.2. Hematopoietic hierarchy

Pioneering studies that proposed the concept of hematopoietic stem cell initiated around 60 years ago by Till and McCulloch. They provided the first evidence that a single progenitor exists in the adult BM and is potent for self-renewal and multi-lineage differentiation. They observed the formation of colonies in the spleen of irradiated recipient mice ten days after transplantation with BM cells (Till and McCulloch, 1961; Wu et al., 1968)

Upon development of new technologies, in 1988, purification of mouse adult BM HSCs becomes possible using fluorescence-activated cell sorting (FACS) and monoclonal antibodies (Muller-Sieburg et al., 1986; Spangrude et al., 1988). The Weissman lab was first to enrich the HSC population characterized by Thy-1^{low} Lin^{-} Sca-1^{+} surface markers. They further demonstrated that these cells are capable of long-term reconstitution of the hematopoietic system after transplantation into the lethally irradiated mice (Spangrude et al., 1988). Ever since, different surface markers identified to optimize HSCs purification including CD34, c-kit, and SLAM (signaling lymphocyte activation molecule) markers (Ikuta and Weissman, 1992; Kiel et al., 2005; Oguro et al., 2013). In 1994, Weissman lab showed that the Thy-1^{low} Lin^{-} Sca-1^{+} population could be fractionated based on the expression of the lineage markers Mac1 and CD4 to three populations: long-term hematopoietic stem cells (LT-HSC), short-term hematopoietic stem cells (ST-HSC) and multipotent progenitors (MPP). They demonstrated that ST-HSC sustained transient reconstitution potential, while the MPP population lost the self-renewal potential of HSCs (Morrison and Weissman, 1994). Later studies demonstrated that the enrichment of HSC cells in $CD34^{-/low}$ c-Kit^{+} Sca-1^{+} Lin^{-} population is enough for long-term myelolymphoid reconstitution in lethally irradiated mice upon single-cell transplantation (Osawa et al., 1996). Further studies identified the presence of hematopoietic intermediate progenitors comprised of common lymphoid progenitors (CLP), common myeloid progenitors (CMP), Granulocyte-monocyte progenitors (GMP), and Megakaryocyte-erythrocyte progenitors (MEP). However, later studies questioned the presence of CMP by identification

of FLT3^{hi} CD34^{+} c-Kit^{+} Sca-1^{+} Lin^{-} lymphoid-primed multipotent progenitors (LMPPs). Gene expression profiling of these population revealed a gradual decrease in the Megakaryocyte-erythrocyte (MkE) transcriptional initiation, an increase in lymphoid specific gene expression, and maintained Granulocyte-monocyte (GM) transcriptional initiation from LT-HSCs to LMPPs. Interestingly, the LMPPs were defined during FL hematopoiesis (Mansson et al., 2007). In parallel, heterogeneity in the MPP population demonstrated using different surface marker combinations (Akashi et al., 2000; Adolfsson et al., 2005; Pietras et al., 2015).

The tree-like hierarchical model of hematopoietic system in mouse has been shaped by Weissman lab to demonstrate the relationship between HSCs, their immediate progenitors, and the sequential differentiation process (Morrison et al., 1997; Akashi et al., 2000; Manz et al., 2002). In this classical model, HSCs, at the apex of the hierarchy, go through a series of stages comprised of multipotent, bipotent, and unipotent progenitor cells. In this process, the self-renewal and lineage potential is restricted in a stepwise manner. Each stage encompasses cells with defined immunophenotype and binary lineage branchpoint, which shapes a tree-like hierarchical model (Figure 1.2).

This model considers HSCs to be functionally homogeneous cell population which carry a balanced differentiation potential. However, this model has been challenged thanks to the recent advances in the functional and transcriptomic analysis at the single-cell level, suggesting that lineage commitment already occurs in HSC or MPP compartments (Mercier and Scadden, 2015; Paul et al., 2015; Notta et al., 2016; Karamitros et al., 2018).

The establishment of either of the models is mainly based on the phenotypic, functional, and transcriptomic analysis of hematopoietic compartments in the adult BM. Since the very first HSCs differentiation takes place in the FL, several studies sought to characterize the hematopoietic cell populations in the FL. The presence of HSCs in the FL was first demonstrated by the identification of labeled clones derived from retrovirally-marked HSCs after transplantation in unirradiated adult mice (Capel et al., 1990; Jordan et al., 1990). Using comprehensive flow cytometry-based cell separation and transplantation experiments, Akashi and his colleagues characterized the intermediate progenitor cells in the FL analogous to the phenotypically defined progenitor cells in the adult BM (Mebius et al., 2001; Traver et al., 2001). Moreover, SLAM markers allowed for the high purification of FL HSCs as of the BM counterparts (Kim et al., 2006). Taken together, the classical model of the hematopoietic hierarchy is conserved in the FL. However, several developmental differences exist between FL and BM HSCs.

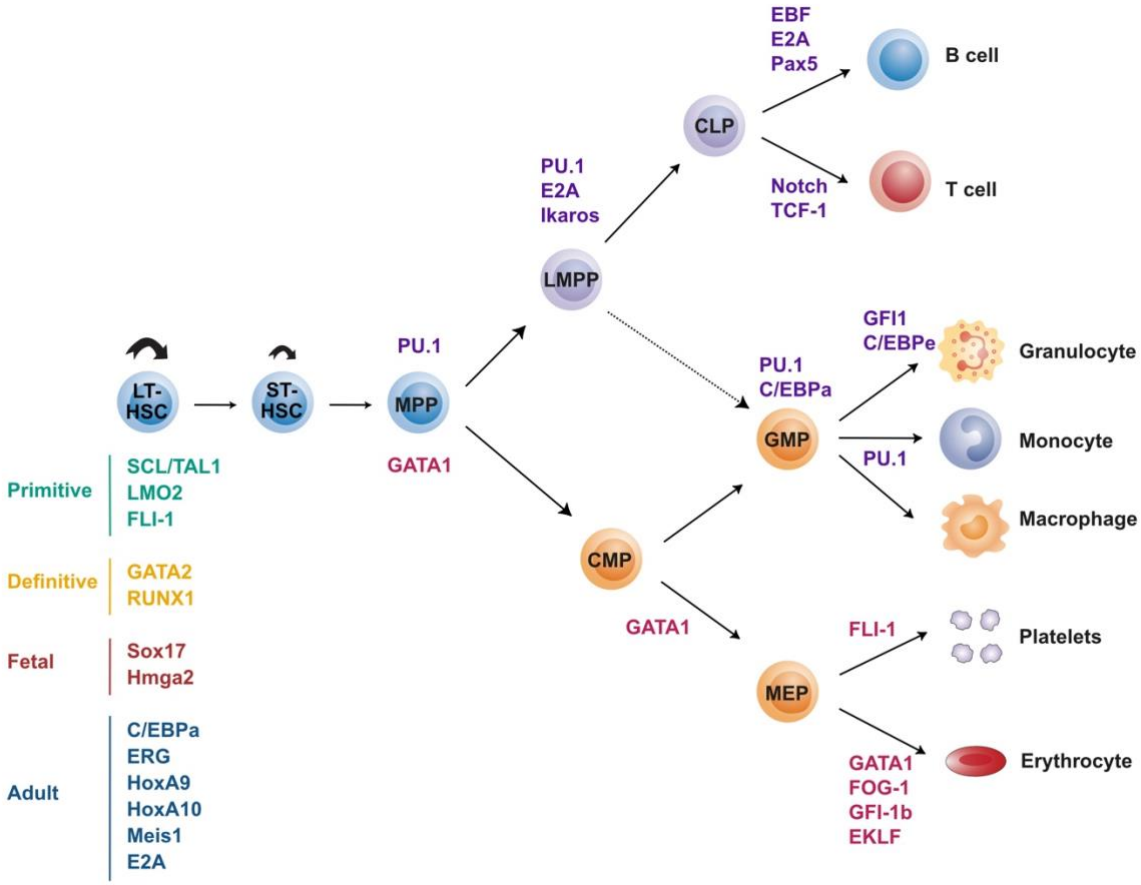

Figure 1.2 | Hierarchical model of hematopoietic system

Maintenance of the hematopoietic system is dependent on the self-renewing HSCs at the apex of the hematopoietic hierarchy. HSCs are divided based on the temporal reconstitution potential to LT-HSCs and ST-HSCs. HSCs give rise to MPPs, providing the bifurcation point toward either lymphoid lineage or myeloerythroid lineage. The formation and survival of HSCs depend on the combinatorial function of TFs at the onset of both primitive and definitive hematopoiesis. Moreover, several other TFs demonstrated to have a prominent role in the maintenance of HSCs during fetal and adult hematopoiesis. Upon lineage commitment, the generation of each population depends on the expression of one or a combination of several TFs. LT-HSC, long-term hematopoietic stem cell; ST-HSC, short-term hematopoietic stem cell; MPP, multipotent progenitors; LMPP, lymphoid-primed multipotent progenitor; CLP, common lymphoid progenitor; CMP, common myeloid progenitor; GMP, granulocyte–monocyte progenitor; MEP, megakaryocyte–erythrocyte progenitor. Figure is modified from (Manz and Boettcher, 2014).

1.1.3. Developmental changes in hematopoietic stem cell characteristics from fetal to adult

The difference in biological characteristics between fetal and adult hematopoietic cells was revealed by detecting the clones of differentiating hematopoietic cells (CFU-S) in the spleen of irradiated mice, two weeks after transplantation (Till and McCulloch, 1961). CFU-S assay quantitively demonstrated that fetal cells bear higher cycling activity, which is in contrast with the very low cycling life of adult CFU-S (Becker et al., 1965). Moreover, the repopulating

potential of fetal CFU-S was much higher than adult CFU-S after transplantation in the irradiated recipient mice (Schofield, 1970).

During the development of HSCs from FL to adult BM, several phenotypic and functional changes occur (Table 1.1). As long as phenotypic differences are concerned, FL HSCs express AA4.1 (CD93), Mac-1 (CD11b), and CD34 surface markers, while adult BM HSCs do not (Jordan et al., 1990). In addition, FL HSCs transiently express VE-cadherin (CD144) at E13.5 to E16.5 (Kim et al., 2005). Apart from the phenotypic differences, fetal and adult HSCs bear functional differences. First, FL HSCs demonstrate high cycling activity, while the adult BM HSCs are mainly in a quiescent state. The fraction of cycling HSCs drops from almost 100% in the FL to around 10% in the adult BM (Fleming et al., 1993; Morrison et al., 1995; Bowie et al., 2006). Importantly, the cycling status of HSCs showed to be independent of the location of the HSCs as the fetal HSCs remain in the cycle from FL to the BM until three weeks after birth when they precipitously become quiescent in the period of one week, highlighting the presence of an intrinsic mechanism which regulates this timely developmental switch (Bowie et al., 2006; Bowie et al., 2007). One of the mechanisms suggested to play a role in modulating this switch is the decrease of *C/EBPa* expression in a developmentally regulated manner. *C/EBPa*-deficient adult HSCs acquired the FL HSCs characteristics in terms of cell cycle status and transcriptional profile, suggesting an inhibitory impact for C/EBPα on the HSCs cell cycle (Ye et al., 2013). Second, another differentiating feature is the self-renewal potential. The rate at which the E14.5 FL HSCs regenerate hematopoiesis is higher compare to BM HSCs (Bowie et al., 2007; Rebel et al., 1996a; Rebel et al., 1996b). In addition, FL HSCs demonstrate superior regenerative activity in competitive repopulating unit (CRU) assay to that of BM (Pawliuk et al., 1996). Interestingly, this property changes simultaneously with the decrease in the cell cycle activity between 3 and 4 weeks after birth (Bowie et al., 2007). Third, not only the self-renewal potential is timely regulated, but also the lineage output potential undergoes the developmental changes. FL HSCs generate ~twofold higher granulocytes and monocytes ($Mac1^+$ and/or $Ly6g^+$) upon transplantation, while the contribution of the adult BM HSCs to lineage reconstitution is balanced (Bowie et al., 2007). Forth, it was shown that FL HSCs divisions are symmetrical, while adult BM HSCs divide asymmetrically, explaining the substantial number of FL HSCs as compared with BM HSCs (Morrison et al., 1995; Takano et al., 2004). Lastly, it was shown that the strikingly cycling FL HSCs require substantially different metabolic pathways for energy production. Adult BM HSCs are mainly fueled by glycolysis. During differentiation, the decrease in glycolysis is accompanied by an increase in oxidative phosphorylation (OxPhos) (Suda et al., 2011; Klimmeck et al., 2012). Intriguingly, a recent study revealed that, in addition to glycolysis, FL HSCs use OxPhos to generate ATP efficiently and to fuel their tremendous expansion. In this study, FL HSCs showed a remarkably higher

level of OxPhos, and citric acid cycle (TCA) gene expression compared with BM HSCs (Manesia et al., 2015).

Table 1.1 | Phenotypic and functional differences between fetal liver and adult bone marrow HSCs

Property	Fetal liver HSC	Adult bone marrow HSC	References
Surface marker	AA4.1 (CD93) $^{+}$ Mac-1 (CD11b) $^{+}$ $CD34^{+}$ VE-cadherin (CD144) $^{+}$	AA4.1 (CD93) $^{-}$ Mac-1 (CD11b) $^{-}$ $CD34^{-}$ VE-cadherin (CD144) $^{-}$	(Jordan et al., 1990) (Kim et al., 2005)
Proliferation activity	Cycling	Quiescent	(Fleming et al., 1993) (Morrison et al., 1995) (Bowie et al., 2006)
Regenerative activity	Superior	Normal	(Pawliuk et al., 1996)
Lineage output potential	Myeloid biased	Balanced	(Bowie et al., 2007)
Cell division mode	Symmetrical	Asymmetrical	(Morrison et al., 1995) (Takano et al., 2004)
Metabolic pathway	Glycolysis Oxidative phosphorylation (OxPhos)	Glycolysis	(Suda et al., 2011) (Manesia et al., 2015)

1.1.4. Mechanisms to regulate hematopoietic stem cell function

The two unique and opposing functions of HSCs – self-renewal capacity and multilineage differentiation – are regulated by coordinated mechanisms encompassing extrinsic and intrinsic factors. Extrinsic factors refer to the specialized cells and factors that create the microenvironment or ‘niche’ while intrinsic factors concern transcription factors and epigenetic mechanisms.

In 1978, Schofield proposed the concept of the niche. He described that the input from microenvironment or ‘niche’ is required for both primitive and definitive hematopoiesis and that the behavior of HSCs is determined by its association with other cells (Schofield, 1978). Today, the niche includes signals harmonized in a spatially and temporally dependent manner. Such signals are provided by specific cells and soluble molecules. During definitive hematopoiesis, colonization of FL depends on the expression of CXCL12 chemokine (SDF1) by FL stromal cells and its ligand CXCR4 (CD184) by HSCs (Nagasawa et al., 1996; Ma et al., 1998; McGrath et al., 1999). Besides, production of SCF cytokine by stromal cells and expression of its receptor c-Kit (CD117) on the surface of HSPCs showed to be an essential mechanism for HSCs function and homing (McCulloch et al., 1965; Broxmeyer et al., 1991; Christensen et al., 2004). Moreover, FL stromal cells produce Insulin-like growth factor 2 (IGF2) and angiopoietin-like factors, which are essential for HSCs function (Zhang and Lodish, 2004; Zhang et al., 2006). Additionally, fetal HSCs migration and engraftment rely on the adhesion such as α4 integrin, neural cadherin (N-cadherin), and osteopontin (Qian et al., 2007; Toyama et al., 2012;

Cao et al., 2019). Likewise, responsible mechanisms for homing and engraftment of HSCs to the BM include CXCR4/CXCL12, cKit/SCF, Ang-1/Tie2, and signaling pathways (Frenette, 2008). Extrinsic pathways meet to activate the expression of hematopoietic TFs.

TFs serve as the significant intrinsic determinants involved in HSCs development, function, and lineage-restricted differentiation (Orkin, 2000). The implication of TFs in hematopoiesis regulation has been determined through gene knock out strategies (Rossi et al., 2012). The important TFs governing the early stage of the HSCs formation and primitive hematopoiesis include SCL/TAL1, LMO2, and FLI-1 (Robb et al., 1995; Yamada et al., 1998; Manaia et al., 2000; Robertson et al., 2000; Göttgens et al., 2002). Complete deletion of the *Scl/Tal1*, the helix-loop-helix transcription factor, leads to the embryonic lethality and defective fetal HSC production (Robb et al., 1995; Shivdasani et al., 1995). The development of HSCs depends on SCL already in the yolk sac (Robb and Begley, 1997). However, SCL remains essential for megakaryocyte and erythroid development in the adult mouse (Hall et al., 2003). LIM-only TF LMO2 was found to be fundamental in primitive erythropoiesis and also in definitive hematopoiesis (Yamada et al., 1998). In developing hematopoietic and endothelial cells, *Fli-1* is expressed (Truong and Ben-David, 2000; Vlaeminck-Guillem et al., 2000). The *Fli-1* mutation is embryonically lethal and show an impaired mature megakaryocytes production which leads to hemorrhage in the central nervous system, implying the role of FLI-1 in the hematopoiesis regulation (Hart et al., 2000; Spyropoulos et al., 2000). Moreover, FLI-1 jointly with GATA2 and ELF-1 was found to be part of an enhanceosome crucial for the transcription of the *Scl* gene and establishment of the HSC formation transcriptional program *in vivo* (Göttgens et al., 2002). The two critical TFs involved in the definitive hematopoiesis include GATA2 and RUNX1 (Tsai et al., 1994; Wang et al., 1996). GATA2 modulates the generation, development, and survival of HSCs during definitive hematopoiesis. *Gata2* deletion in mice leads to embryonic lethality, and ES cells generated from *Gata2* knockout (ko) mice showed impaired production of hematopoietic cells in transplanted mice (Tsai et al., 1994; de Pater et al., 2013). Moreover, GATA2 regulates the proliferation and cell cycle progression of hematopoietic stem and progenitor cells (Tsai and Orkin, 1997). Deletion of *Gata2* and *Runx1* using *VE-cadherin/cdh5 (Cre)* revealed that both TFs were required for the HSC formation during the endothelial-to-hematopoietic transition (EHT) (Chen et al., 2009). Additionally, *Vav-Cre* mediated deletion of *Runx1* did not produce any defect on the HSCs in the FL (Chen et al., 2009; Tober et al., 2013).

Several TFs are pivotal for FL but not adult HSCs. FL and postnatal HSCs are endowed with the expression of *Sox17*. Kim and his colleagues demonstrated that *Sox17*, the endodermal marker, is 1) restrictively expressed in mouse FL and postnatal HSCs, and 2) involved in FL but not adult BM HSCs maintenance. The expression of *Sox17* gradually

decreases at the postnatal stage, reaching to undetectable level eight weeks after birth. *Sox17* depletion was independent of the quiescent state of the adult BM HSCs. Furthermore, the deletion of *Sox17* using *Tie2-Cre* revealed that *Sox17* is required for the production and maintenance of definitive HSCs since hematopoietic cells from yolk sac and embryo at E11.5 illustrated a marked reduction in the reconstitution potential (Kim et al., 2007). Another study revealed that the forced expression of *Sox17* enhanced myeloid lineage output in adult BM HSCs, indicative of FL HSC property (He et al., 2011). Similarly, Hmga2, Lin28b (RNA-binding protein), and let-7 miRNA implicated the differential expression pattern in E14.5 FL HSCs compared with those in adult BM. In mouse, the Lin28b-let-7-Hmga2 pathway serves as an intrinsic clock to modulate the FL HSCs self-renewal and developmental transition from fetal to the adult at 3-4 weeks after birth. FL HSCs show a higher expression of Lin28b, which is repressive for let-7 miRNA expression; therefore, it permits the enhanced level of Hmga2. Consequently, the elevated level of Hmga2 induces the FL HSCs self-renewal (Copley et al., 2013).

Apart from the FL HSCs-specific TFs, several TFs express exclusively in adult BM HSCs. It was shown that the C/EBPα endowed the adult HSCs with the quiescent state by a gradual decrease in the expression pattern from FL HSCs to adult BM HSCs (Ye et al., 2013). Bmi1, a member of the polycomb-repressive complex, was the first TF demonstrated to be involved in adult HSC maintenance (Park et al., 2003). Correspondingly, Gfi1, and Tel/Etv6 showed to be pivotal in modulating the survival of adult HSCs (Hock et al., 2004a; Hock et al., 2004b). Besides, members of ETS family TFs have also been shown to be indispensable for the maintenance of adult HSCs. A member of this family is the E-twenty-six (ETS)-related gene (ERG), which is shown to be critical for definitive hematopoiesis and the function of adult HSCs (Loughran et al., 2008; Ng et al., 2011). At the functional level, *Erg* coordinates the balance between self-renewal and differentiation by restricting the adult HSC premature differentiation (Knudsen et al., 2015). A few more examples of essential TFs in adult HSCs development and maintenance are HoxA9 and HoxA10 (homeobox factors), Meis1 (TALE family), and E2A (Helix-loop-Helix proteins)(Lawrence et al., 2005; Magnusson et al., 2007; Yang et al., 2008; Semerad et al., 2009; Ariki et al., 2014).

The first lineage segregation occurs in HSCs/MPPs – mediated by PU.1 and GATA1 – which is the branchpoint for either myeloid/lymphoid or erythroid/megakaryocytic the cell lineage (Shivdasani et al., 1997; Laslo et al., 2006). PU.1 is a member of the ETS family of TF, encoded by the *Spi1* gene. It has been shown that the efficient production of LMPPs from HSCs is dependent on PU.1 and that it promotes the formation of CLPs, subsequently (Pang et al., 2018). During LMPPs generation, PU.1, E2A, and Ikaros function to promote the

myeloid/lymphoid branch at the expense of the erythroid/megakaryocytic lineage (Dias et al., 2008; Semerad et al., 2009; Ng et al., 2009). As mentioned earlier, LMPPs are potent to generate GMPs, CLPs, and (early T-cell progenitors) ETPs. While several studies demonstrated the essential role of PU.1, E2A, and Ikaros for induction of the lymphoid transcriptional network, it has been shown that myeloid cell fate in the GMP compartment is much dependent on the collaboration of PU.1 and C/EBPα (Laslo et al., 2008). GATA1, a zinc finger TF encoded by the *Gata1* gene, is the master regulator of erythroid/megakaryocytic lineage specification (Ferreira et al., 2005). Intriguingly, GATA1$^+$ MPPs demonstrated myeloerythroid potential and lacked lymphoid potential. At the same time, the PU.1$^+$ MPPs (the closest equivalent to LMPPs) harbored the granulocyte/monocyte/lymphoid-restricted progenitor activity lacking megakaryocyte/erythroid differentiation, suggesting the reciprocal activation of GATA1 and PU.1 coordinates the lineage fate determination at the first HSCs/MPPs bifurcation (Arinobu et al., 2007). Furthermore, the lineage-committed cells such as eosinophils, mast cells or basophils also expressed GATA1 (Martin et al., 1990; Zon et al., 1993). Supporting evidence raised from the study, which carried single-cell RNA-seq analysis on myeloid progenitors and demonstrated the heterogeneity of GMPs and distinct myeloid differentiation pathways based on GATA1 expression. The GATA1$^+$ pathway generated megakaryocytes, erythroid cells, eosinophils, mast cells, and, while the GATA1$^-$ pathway gave rise to lymphocytes, neutrophils, and monocytes introducing two discrete subsets within GMPs (Drissen et al., 2016).

Of note, TFs are not the sole determinants of cell fate decisions and lineage priming. A myriad of evidence has described the function of TFs in concert with epigenetic regulators.

1.2. Epigenetic control of chromatin state

1.2.1. Epigenetic mechanisms

The genetic information flows from DNA to RNA and subsequently to the protein according to the central dogma of gene expression (Cobb, 2017). Intriguingly, the zygote and differentiated cells share the same genetic information (Bird, 2002). The field of epigenetics has been established based on this fundamental question of how one genome gives rise to many different cellular phenotypes. Conrad Waddington, who was first to coin the term “epigenetics,” described it as a branch of biology to understand the connection between genotype and phenotype (Waddington, 1942). Broadly speaking, epigenetics entails the mechanisms which, without modifying the DNA sequence, alter the outcome of a locus or

chromosome, heritably and stably (Goldberg et al., 2007). Therefore, the generation of diverse cell types upon development and differentiation in a multicellular organism proposed to be driven by the change in the "epigenetic landscape," as conceptualized by Waddington. (Waddington, 1957). The epigenetic landscape of a cell has taken shape based on the modifications of the chromatin – a complex of DNA and its associated proteins – through epigenetic mechanisms. The core epigenetic mechanisms encompass DNA methylation, histone modifications, and chromatin remodeling.

DNA methylation. In mammals, methylation of the cytosine residues of CpG dinucleotides is mediated by DNA methyltransferases (DNMTs). While DNMT3a and DNMT3b are responsible for *de novo* methylation after DNA replication, DNMT1 mediates maintenance methylation during DNA replication by adding the methyl groups to hemi-methylated DNA (Jaenisch and Bird, 2003). Moreover, a high frequency of CpGs in parts of the genome shape CpG islands (CGIs), and methylation of CGIs associates with transcriptional repression (Goll and Bestor, 2005). Besides, DNA methylation is involved in the control of the centromeric region, silencing of repetitive elements, X chromosome inactivation, and genomic imprinting (Scelfo and Fachinetti, 2019; Greenberg and Bourc'his, 2019)

Histone modifications. In eukaryotic cells, the highly conserved core histone proteins and DNA form nucleosomes, which are the building blocks of the chromatin. Each nucleosome consists of a histone octamer containing two molecules of each histone proteins (H2A, H2B, H3, and H4) and 147 bp of DNA, which wraps around them. The linker histone H1 binds to and protects the free DNA between the nucleosomes (Luger and Richmond, 1998; Kornberg and Lorch, 1999) The protruded histone tails undergo several post-translational modifications (PTMs). Several covalent histone modifications have been characterized, including methylation, acetylation, phosphorylation, ubiquitination, sumoylation, poly (ADP)-ribosylation, and deamination. Post-translational histone modifications are carried out by different enzymes that regulate the addition or removal of a modification dynamically on different amino acid residues (Berger, 2007; Kouzarides, 2007).

Chromatin remodeling. Along with covalent modification, chromatin structure is also regulated by noncovalent mechanisms such as chromatin remodeling. Chromatin remodeling complexes utilize ATP hydrolysis to change histone-DNA contacts by altering the nucleosome arrangement (sliding) or nucleosome ejection (Saha et al., 2006).

1.2.2. Histone modifications define chromatin state

Chromatin provides the template for storage and organization of the genetic information in the nuclei of the eukaryotic cells (Jenuwein and Allis, 2001). Nucleosomes, which are the building block of the chromatin, contribute to the first level of chromatin compaction. Post-translational modifications of histones control the degree of chromatin compaction, thereby governing the DNA accessibility to the transcriptional machinery and distinct pattern of gene expression. Therefore, proper organization of the chromatin, which is mediated by post-translational modifications of histones, is central to many developmental processes and cellular differentiation (Greer and Shi, 2012). Some of the histone modifications, such as trimethylation of lysine 4 (H3K4me3) or acetylation of lysine 14 of histone H3 (H3K14ac), are associated with the genomic regions which are actively transcribed, indicative of open or accessible regions. In contrast, other histone marks, such as H3K27me3 or H3K9me3, are correlated with transcriptionally repressed genes, which are the typical feature of close or inaccessible regions (Sparmann and Van Lohuizen, 2006). It has been postulated that the combination of different histone modifications constitutes “histone code,” which defines the chromatin state. In this context, the distinct histone code governs the dynamic mutual passage from transcriptionally active to transcriptionally silent chromatin states by allowing for the binding of specific chromatin remodeling factors, while blocking the others (Jenuwein and Allis, 2001) (Figure 1.3). Accordingly, disruption of proper chromatin state leads to inappropriate gene expression and genomic instability (Sparmann and Van Lohuizen, 2006).

Thanks to the genome-wide studies, the profiling of the genomic distribution of histone modifications in combination with transcriptome analysis highlighted the central interaction between regulation of the chromatin state and function of the genome. Among the histone modifications, Lysine (Lys) methylations seem like a dynamic modification since they are indicative of both transcriptionally active and silent chromatin. The modification is carried out by Lys methyltransferases (KMTs) at several degrees as mono- (me1), di- (me2), or trimethylation (me3) in particular Lys residue at different positions within histone. Histone Lys methylations associated with transcriptional activation include methylations of histone H3 Lys 4 (H3K4) and H3K36, whereas methylation of histone H3 Lys 9 (H3K9), H3K27 and H4K20 are implicated in gene silencing (Eissenberg and Shilatifard, 2010; Wagner and Carpenter, 2012; Mozzetta et al., 2015). H3K9 methylation marks are mediated by SUV39 family of methyltransferases. SETDB1, a member of this family, is involved in the chromatin compaction (heterochromatinization) of the euchromatin regions (Huisinga et al., 2006).

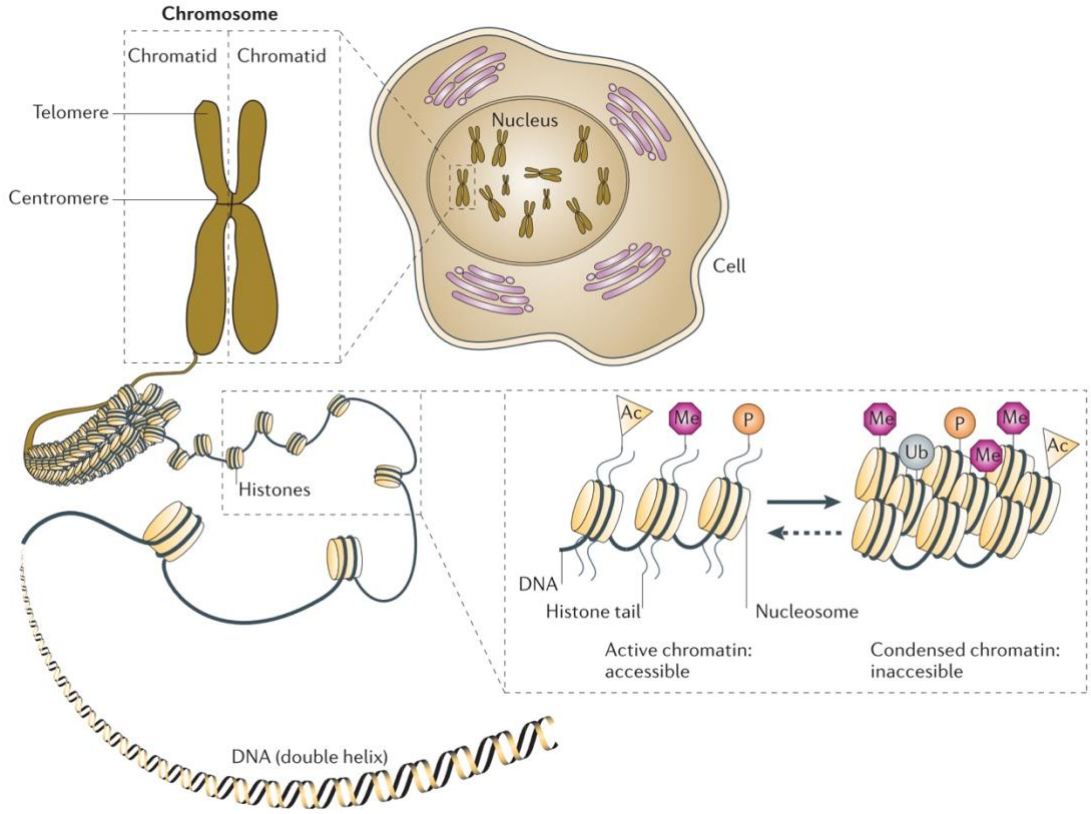

Figure 1.3 | Histone modifications define chromatin state

In eukaryotic cells, chromosomes contain genetic information. They are composed of the DNA double helix, which is wrapped around histones, creating nucleosomes that further fold to form the higher-order chromatin. For many cellular processes, including transcription, the precise organization of chromatin is fundamental. Post-transcriptional histone modifications define the dynamic changes between transcriptionally active and silent states. Figure is modified from (Sparmann and Van Lohuizen, 2006).

1.3. The histone lysine methyltransferase SETDB1

1.3.1. SETDB1 structural features

SET domain bifurcated 1 (SETDB1) belongs to the SUV39 family of methyltransferases Yang et al., 2002). The enzyme is responsible for the deposition of the H3K9me3 mark outside of pericentric heterochromatin (Bilodeau et al., 2009; Dambacher et al., 2010; Karimi et al., 2011). The catalytic activity of this family depends on the SET-domain (similar to other KMTs) and the two unique cysteine-rich domains called pre-SET and post-SET domains (Rea et al., 2000; Schultz et al., 2002). In SETDB1, the SET domain is bifurcated by the insertion of hundreds of amino acids (Schultz et al., 2002; Falandry et al., 2010). In addition, SETDB1 contains a putative methyl-CpG-binding domain (MBD), which might bind to methylated DNA (Kang, 2015). SETDB1 also possesses two Todur domains which are positioned consecutively and are involved in binding to methylated Lys and protein-protein interaction (Yang et al., 2002;

Ponting, 1997)(Figure 1.4). Studies of SETDB1 deletion during mouse development and in different cellular contexts highlighted the importance of SETDB1 function in the maintenance of the cell identity and genome integrity.

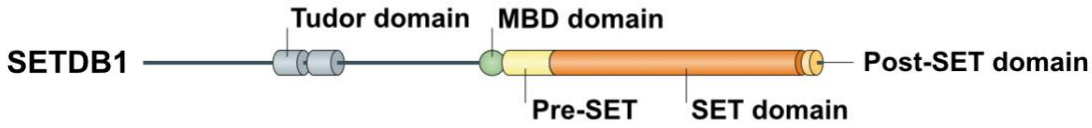

Figure 1.4 | The domain composition of SETDB1

SETDB1 encompasses two Tudor domains implicated in protein interaction, a putative methyl-DNA binding domain (MBD). Besides, the methyltransferase activity of SETDB1 is attributed to the Pre-SET, SET, and Post-SET domains. Figure is modified from (Mozzetta et al., 2015).

1.3.2. SETDB1 and its H3K9me3-marked targets during development and differentiation

During early development, SETDB1 demonstrated a severe phenotype. *Setdb1* ko mice die at the pre-implantation stage between E3.5 and E5.5 (Dodge et al., 2004; Keniry et al., 2016). Besides, no mESC lines were established by *Setdb1* ko blastocyst outgrowth, which was consistent with the impaired proliferation and survival of mESC upon *Setdb1* depletion (Yuan et al., 2009; Lohmann et al., 2010). SETDB1 is crucial to maintain the mESC pluripotent state. mESC devoid of *Setdb1* differentiated into the trophectoderm lineage cells. SETDB1 was recruited to the promoter of the trophectoderm genes (*Tcfap2a* and *Cdx2*) by the stem cell-specific transcription factor Oct4, thereby repressing the transcription by deposition of H3K9me2/3 (Bilodeau et al., 2009; Yuan et al., 2009; Lohmann et al., 2010). Interestingly, a subset of these genes carried the features of bivalent genes marked by H3K4me3 and H3K27me3 modifications catalyzed by Trithorax and Polycomb group proteins, respectively. *Setdb1* ablation led to a concomitant increase of H3K4me3 activation mark and depletion of H3K27me3 repression mark, thus losing the mESC pluripotent state (Bilodeau et al., 2009; Lohmann et al., 2010). However, these genes lack DNA methylation (Karimi et al., 2011). In parallel, a set of germline genes showed to be the direct SETDB1 targets which lost H3K9me3 and became upregulated in *Setdb1* ko mESC (Karimi et al., 2011).

Importantly, SETDB1 played a fundamental role in silencing the retrotransposons during development. Retrotransposons are composed of non-LTR (long-terminal direct repeats) and LTR retrotransposons. The non-LTR is constituted by long interspersed elements (LINEs) and

short interspersed elements (SINEs). The LTR retrotransposons comprised around 10% of mouse genome and derived from endogenous retroviruses (ERV) superfamily, which were classified into three groups (class I, II, and III) (Stocking and Kozak, 2008). In mESC, SETDB1 is responsible for the deposition of H3K9me3 and subsequent transcriptional repression of ERVs MLV and GLN (class I) and IAP, MusD, ERVK10C (class II) (Matsui et al., 2010; Karimi et al., 2011; Maksakova et al., 2011; Maksakova et al., 2013). Besides, upregulation ERVs neighboring genes via the generation of chimeric transcripts observed upon *Setdb1* loss in mESC (Karimi et al., 2011).

In germline cells, depletion of *Setdb1* in spermatogonial stem cell (SSC) led to reduced viability due to enhanced apoptosis and decreased level of H3K9me3. Among the apoptosis-associated genes, the promoter of the cytochrome oxidase *Cox4i2* gene showed enrichment for SETDB1-mediated H3K9me3 and DNA methylation. In the rescue experiment, ko of *Cox4i2* restored cell viability (An et al., 2014). Conditional deletion of *Setdb1* in male primordial germ cells (PGCs) at E13.5, led to the decreased number of germ cells and impaired gametogenesis in postnatal and adult mice. Partial loss of H3K9me3 and H3K27me3 was accompanied by an increase of global DNA methylation at the H3K9me3-targeted regions. Additionally, ERVs including IAPEz and ERVK10C, upregulated upon *Setdb1* loss, which led to the upregulation of the neighboring genes and generation of chimeric transcripts (Liu et al., 2014).

Setdb1 was highly expressed in neural progenitor cells (NPC) at E9.5 but downregulated over time. Proper expression of neuronal and non-neuronal genes such as the astrocyte marker *Gfap* and gliogenesis regulator *Sox9* was dependent on SETDB1. *Setdb1*-deficient NPC demonstrated impaired neurogenesis, increased apoptosis (only in deep layer neurons), compromised proliferation, enhanced astrocyte differentiation, and reduced level of global H3K9me3. Subsequently, mice died 10 days after birth. Finally, *Setdb1* deletion induced derepression of IAPs (class II) and upregulation of genes in their vicinity by generating the chimeric transcripts (Tan et al., 2012).

Deletion of *Setdb1* in postnatal forebrain neurons showed normal gross cytoarchitecture; however, adult mice brains were smaller. Nevertheless, no premature cell death or neuronal loss observed. Hi-C chromosome conformation capture revealed no change in the 3D organization of the genome. However, 110 long-range chromosomal contacts were lost in the mutant neurons. Analysis of the topologically associated domains (TAD) revealed the loss of a super TAD that encompassed 77 genes, including the regulators of neuronal connectivity, *Pcdha*, *Pcdhb*, and *Pcdhg*. Similar to CD19+ B lymphocytes and mESC, H3K9me3 hypomethylated regions in the clustered *Pcdh* locus showed enrichment for CTCF motifs. Accordingly, CTCF binding to the exposed CTCF motif in mutant neurons increased, thereby

enhancing the insulation. However, the insulation was lost at the *Pcdh* cluster due to the structural collapse. Concomitantly, loss of DNA methylation, accumulation of histone hyperacetylation, and upregulation of the genes in this cluster observed. Multiple KRAB zinc finger proteins, like ZFP143 recognition sequences, showed enrichment in the new CTCF binding sites, indicating the role of SETDB1-mediated H3K9me3 in preventing the excessive CTCF binding (Jiang et al., 2017).

In mice bone mesenchymal cells, the deletion of *Setdb1* using *Prx1* showed skeletal malformation in newborn mice. Growth plate chondrocytes were disorganized, and concomitantly, chondrocyte hypertrophy was accelerated. Moreover, the formation of epiphyseal plate (physis) was impaired (Yang et al., 2013). Ablation of *Setdb1* using the same deleter in mesenchymal stem cell (MSC) inhibited their differentiation into osteoblasts (Lawson et al., 2013a). Both studies demonstrated that the interaction of Runx2 with SETDB1 and HDAC4 regulates the expression of Runx2 target genes, like *osteocalcin* (Lawson et al., 2013b; Yang et al., 2013). Articular chondrocytes devoid of *Setdb1* demonstrated enhanced hypertrophy, apoptosis, and underwent terminal differentiation (Lawson et al., 2013b).

Deletion of *Setdb1* in proliferating myoblasts led to impaired proliferation and differentiation accompanied by downregulation of muscle-specific genes such as *MyoD* and *myogenin* (Song et al., 2015). However, when *Setdb1* is deleted shortly before terminal differentiation, decreased self-renewal, and enhanced commitment occurred. Loss of *Setdb1* led to the decreased H3K9me3 on SETDB1 binding sites and consequent upregulation of myeloblast differentiation genes like *Ankrd1*, which were targeted directly by SETDB1 at the enhancer. Moreover, in proliferating myoblasts, the artificial increase of the canonical Wnt3a signaling, which is critical for embryonic myogenesis, induced redistribution of *Setdb1* to the cytoplasm (Beyer et al., 2016).

In the hematopoietic system, SETDB1 was studied in different cell populations. Macrophages devoid of *Setdb1* using *LysM-Cre* increased expression of TLR4-mediated proinflammatory cytokines like interleukin-6 (IL6) following lipid A stimulation. Due to the enhanced response after LPS treatment, mutant mice were prone to endotoxin shock. Mechanistically, SETDB1-mediated H3K9me3 reduced on the proximal promoter region of *IL6* and enhanced the recruitment of NF-κB p65, which was induced by LPS. Subsequently, the promoter activity of *IL6* enhanced. Therefore, *Setdb1* was able to regulate the expression of the proinflammatory cytokine in macrophages (Hachiya et al., 2016).

Ablation of *Setdb1* under the *Cd4-Cre* promoter in SP CD4+ T cells resulted in a partial decrease of the T cell reservoir. Transcriptome analysis did not reveal any bias toward a

specific T helper (Th) lineage. However, when Th cells were challenged in IL-12-mediated Th1 differentiation assay, *Setdb1*-mutant T cells showed Th1 priming demonstrated by enhanced secretion of Th1- specific cytokines. Moreover, in the Th2-instructing condition, the acquisition of the Th2 phenotype by *Setdb1*-deficient T cells was impaired. Furthermore, stable commitment to the Th2 cells in vitro and the Th1-Th2 balance in vivo were compromised in *Setdb1*-mutant T cells. There were no SETDB1-mediated H3K9me3 at the Th1-specific genes in wildtype Th2 cells; however, 74% of ERVs – harboring H3K9me3 as SETDB1 direct targets – overlapped or flanked enhancers of Th1-related genes such as *T-Bet*, *STAT4*, *IRF-1*, and *RUNX3*. Thus, SETDB1 regulated Th2 cell integrity at the chromatin level (Adoue et al., 2019).

Deletion of *Setdb1* using thymocyte-specific *Lck-Cre*, resulted in decreased cellularity in the thymus, lymph nodes, and spleen (Martin et al., 2015; Takikita et al., 2016). During thymocyte development, a partial block in the double-positive (DP) to single-positive (SP) transition was observed. Moreover, DP thymocytes underwent enhanced apoptosis, which was attributed to the shift toward negative selection. In fact, DP thymocytes displayed enhanced responsiveness to the TCR agonism. Although contradictory in the context of TCR inhibition, upregulation of the TCR inhibitory receptor, *FcγRIIb*, in mutant thymocytes showed to be the consequence of the H3K9me3 loss at the promoter. Finally, the authors suggested that inhibition of LAT, the modulator of TCR signaling, by FcγRIIb led to the hyperactive TCR signaling and subsequent apoptosis (Martin et al., 2015). However, another study that used the same *Cre* deleter suggested that FcγRIIb decreased the activation of ERK by phosphorylation, which defected positive selection. Moreover, the expression of IAP and MusD (class II) elements was induced in thymocytes (Takikita et al., 2016).

Specific deletion of *Setdb1* in pro-B cells using *Mb1-Cre* abolished bone marrow and splenic late-stage B-cells due to the enhanced apoptosis. However, the expression of *Bcl2*, the anti-apoptotic gene, partially rescued splenic B cells. Impaired function of pro-B cells to generate B cells and to form colonies was confirmed to be intrinsic in both in vitro and in vivo assays, respectively. Immune-related and non-hematopoietic genes showed upregulation in *Setdb1*-deficient pro-B cells (Collins et al., 2015; Pasquarella et al., 2016). In addition, several genes belonging to the unfolded protein response (UPR) pathway were upregulated. *Setdb1* deletion in pro-B cells resulted in the loss of H3K9me3 and derepression of the several ERVs elements, including MLV, VL30 (class I) and MMTV (class II). Translation of excessive viral protein led to the endoplasmic reticulum (ER) stress, activation of UPR and, subsequent apoptosis. Indeed, envelop protein (Env) of the MLV was detected on the surface of mutant pro-B cells. Similarly, ectopic expression of Env protein led to the enhanced apoptosis and subsequent trigger of the UPR pathway (Pasquarella et al., 2016). Additionally, the

upregulation of MLV elements led to the upregulation of genes in their vicinity (Collins et al., 2015; Pasquarella et al., 2016).

In hematopoietic stem and progenitor cells, tamoxifen-induced deletion of *Setdb1* in mice transplanted with *Cre-ERT*; *Setdb1* $^{fl/fl}$ bone marrow cells was lethal at 3 weeks after induction due to the massive BM failure. The BM cellularity, number of HSCs, MPPs, CMPs, GMPs, except for MEPs, decreased dramatically. Apoptosis enhanced in LSK cells (HSCs and MPPs) but not in LK cells (CMPs, GMPs, and MEPs). Concomitantly, the cell cycle was impaired in LSK cells, as showed by Pyronin Y staining and BrdU incorporation assay. No significant changes observed in the global DNA methylation and H3K9me3 level in mutant GMP. However, a significant decrease of H3K9me3 observed at the promoter of coding genes and ERVs such as ERV1 (class I), IAP (class II), and ERVL (class III). Correspondingly, the ERV1 (class I), IAP, and Etn (class II) demonstrated mild up-regulation in both *Setdb1*-mutant LSK and GMPs. In contrast to mESC, NPC, PGCs and similar to pro-B cell, no chimeric transcripts detected for the highly expressed genes. The majority of upregulated genes in *Setdb1*-mutant LSK and GMPs showed to be non-hematopoietic genes, including gluconeogenesis enzymes *Fbp1/2*. Accordingly, these genes lost H3K9me3 at the promoter and DNA methylation level around TSS and in the gene body in *Setdb1*-mutant GMPs. Up-regulation of these gluconeogenic enzymes led to decreased ATP levels, impaired metabolic hemostasis, and subsequently compromised HSPC function (Koide et al., 2016).

2. Summary and objectives

Studies of SETDB1 during early development and in different cellular systems pointed to a pivotal role of this histone methyltransferase enzyme in the maintenance of cell identity and genome integrity. Indeed, SETDB1 not only demonstrated a cell type-specific phenotype, but it also represented a cell stage-specific phenotype. In particular, SETDB1 was dispensable for the survival of differentiated cells, whereas cell function (macrophage) and cell lineage integrity ($CD4^+$ T cell) were tightly controlled by SETDB1-mediated silencing. In committed progenitors, *Setdb1* ablation led to apoptosis and partial (T cell progenitor) or complete (pro-B cell) developmental arrest. Intriguingly, *Setdb1* deletion in stem cells and early progenitors resulted in either skewed (mESC, and NPC) or blocked differentiation (MSC). However, in profound contrast to other stem cells, *Setdb1*-deficient adult hematopoietic stem and progenitor cells represented a severe phenotype as they underwent extensive apoptosis, which was due to the non-hematopoietic events. The questions of how and by which mechanisms SETDB1 regulates HSC self-renewal and lineage specification remained mostly unanswered. Given that fetal liver and adult HSCs differ in many phenotypic and functional features (reviewed in section 1.1.3), I decided to move the window of the analysis to the earlier time points during hematopoietic development.

Therefore, the main objectives of the current thesis were to understand 1) the significance of SETDB1 in FL hematopoietic stem and progenitor cell function, 2) SETDB1 mode of action with regard to gene regulation.

To this end, I planned the following sub-objectives:

- Characterization of *Setdb1* implications in the HSC self-renewal and differentiation. I wondered which phenotypic changes would occur during FL and postnatal hematopoiesis, and how it differed from adult hematopoiesis. Moreover, the functional features of HSPCs devoid of *Setdb1* were studied by standard functional assays *in vitro* and *in vivo*.

- Investigation of transcriptional changes underlying the defined phenotype. Given the fact that HSPCs encompass a heterogeneous population, to gain a better resolution for SETDB1-mediated gene regulation, I performed transcriptome analysis distinctly in FL LT-HSCs and MPPs.

- Identification of SETDB1 targets in HSPCs. In order to dissect SETDB1 direct/indirect silencing function in transcriptional regulation of its targets, I planned to map the genome-wide H3K9me3 mark as the readout of SETDB1 function in HSPCs.

- Interrogation of SETDB1 implication on chromatin dynamics. I assessed the genome-wide chromatin accessibility, integrated it into the transcriptome, and H3K9me3 data to unravel the SETDB1 mode of action on gene regulation.

3. Results

3.1. Characterization of *Setdb1* ablation during fetal and postnatal hematopoiesis

3.1.1. *Setdb1^{vav}* embryos develop normal but show increased lethality at postnatal stage

To study the function of SETDB1 during fetal and postnatal hematopoiesis, we established a mouse model in which *Setdb1* was deleted in the HSCs that emerged at E10.5 (Ogilvy et al., 1999). To achieve that, we crossed *Setdb1$^{flox/flox}$* mice with *Vav-cre* mice to delete *Setdb1* exon 4 flanked by two loxP sites, hereafter called *Setdb1^{vav}* (Figure 3.1A). Embryos and mice with *Setdb1$^{flox/+}$; Vav-cre* or *Setdb1$^{flox/+}$;* +/+ used as control. E14.5 embryos normally developed as *Setdb1^{vav}* embryos were indistinguishable from the control ones, and the cellularity of the fetal liver remained unchanged (Figure 3.1B, C). *Setdb1^{vav}* mice were born at the Mendelian ratio; however, they did not reach the adult stage and died around 3-4 weeks after birth. At postnatal (2 weeks after birth), *Setdb1^{vav}* mice looked slightly smaller, as compared with the control littermates, which became prominent at 3-4 weeks after birth (Figure 3.1D). Histological analysis revealed the hypocellularity of *Setdb1^{vav}* BM (Figure 3.1E). Indeed, BM cellularity decreased significantly (Figure 3.1H). Additionally, postnatal *Setdb1^{vav}* mice had enlarged spleen and severe thymus atrophy, which resulted in a 200-fold decrease in thymus cellularity (Figure 3.1F-H). Postnatal lethality of *Setdb1^{vav}* mice was probably due to the hematopoiesis failure in the central hematopoietic organs. Therefore, besides E14.5 fetal liver, we analyzed the hematopoietic phenotype shortly before death at 2 weeks after birth.

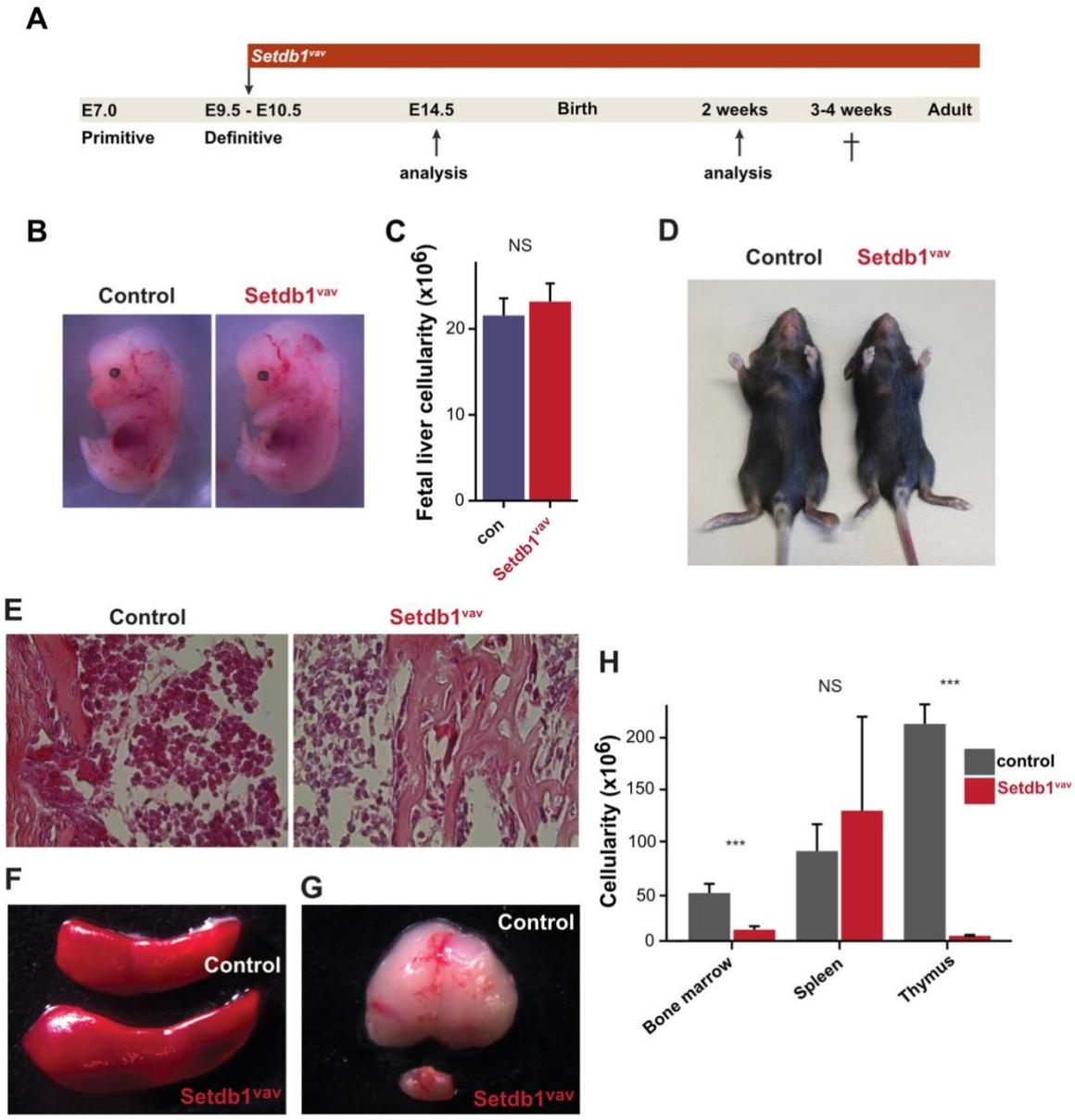

Figure 3.1 | *Setdb1*^{vav} embryos develop normal but show increased lethality at postnatal stage

(A) Timeline of *Setdb1* deletion and analyses time points. (B) Representative photos of E14.5 control (*Setdb1*$^{flox/+}$*; Vav-cre* or *Setdb1*$^{flox/+}$*;* +/+) and *Setdb1*^{vav} (*Setdb1*$^{flox/flox}$*; Vav-cre*) embryos. (C) Comparison of total cell number between control and *Setdb1*^{vav} E14.5 FLs (n=10). Data are shown as mean ± SD. (D) Representative photo of 2-week-old control (*Setdb1*$^{flox/+}$*; Vav-cre* or *Setdb1*$^{flox/+}$*;* +/+) and *Setdb1*^{vav} (*Setdb1*$^{flox/flox}$*; Vav-cre*) mice. (E) H&E staining of decalcified BM sections from 2-week-old control and *Setdb1*^{vav} mice. (F) Spleen of 2-week-old control and *Setdb1*^{vav} mice. (G) Thymus of 2-week-old control and *Setdb1*^{vav} mice. (H) Comparison of total cell number between control and *Setdb1*^{vav} bone marrow, spleen and thymus in of 2-week-old mice (n=20). Data are shown as mean ± SD. ***P<0.001 (unpaired two-tailed Student's t-test); NS, not significant.

3.1.2. Deletion of *Setdb1* abrogates lymphoid lineage

Thymocyte development occurs in the thymus following the migration of early T-cell progenitors from the BM. In the thymus, early T-cell progenitors pass through the double-negative (DN) stages from DN1 to DN4 and then to the CD4/CD8 double-positive stage (DP). The DP cells generate either CD4 or CD8 single-positive cells (SP) before they enter the periphery. In *Setdb1*^{vav} mice, the marked reduction of thymus cellularity was suggestive of the possibility of impaired thymocyte development. Indeed, FACS analysis of early thymocytes at 2 weeks after birth (2wk) showed a significant increase in the frequency of *Setdb1*^{vav} DN1 ($CD44^+$ $CD25^-$), DN2 ($CD44^+$ $CD25^+$), and DN3 ($CD44^-$ $CD25^+$) followed by a decrease in DN4 ($CD44^-$ $CD25^-$) population, indicating a severe developmental transition block from DN3 to DN4 stage (Figure 3.2A, B).

The second developmental block observed at the DP to both CD4 and CD8 SP cells resulted in a ~ 50% decrease in the frequency of $CD4^+$ and $CD8^+$ T cells (Figure 3.2C, D). Concomitantly, both $CD4^+$ and $CD8^+$ T cells showed a 10-fold decrease in the spleen of *Setdb1*^{vav} mice, demonstrating that the few generated T cells were not able to enter the periphery (Figure 3.2E, F, G). We previously showed that the deletion of *Setdb1* impairs B cell development (Pasquarella et al., 2016). Similarly, *Setdb1*^{vav} B cells ($B220^+$ $CD19^+$) were absent in the FL (Figure 3.2H, I) as well as BM and spleen (data not shown), suggesting that the overall lymphoid output is severely impaired in *Setdb1*^{vav} mice. We then analyzed if the common lymphoid progenitors (CLPs) were generated in the absence of *Setdb1*. Surprisingly, there was no significant difference in the frequency of CLPs (Lin^- $IL7ra^+$ $Sca\text{-}1^{low}$ $ckit^{low}$) neither in the FL (Figure 3.2J, K) nor in the BM (data not shown), illustrating that *Setdb1*^{vav} lymphoid progenitors were generated, but they failed to populate the thymus efficiently. Besides, the few CLPs that migrated to the thymus showed impaired T-cell development. Likewise, *Setdb1*^{vav} CLPs were compromised to generate B cells.

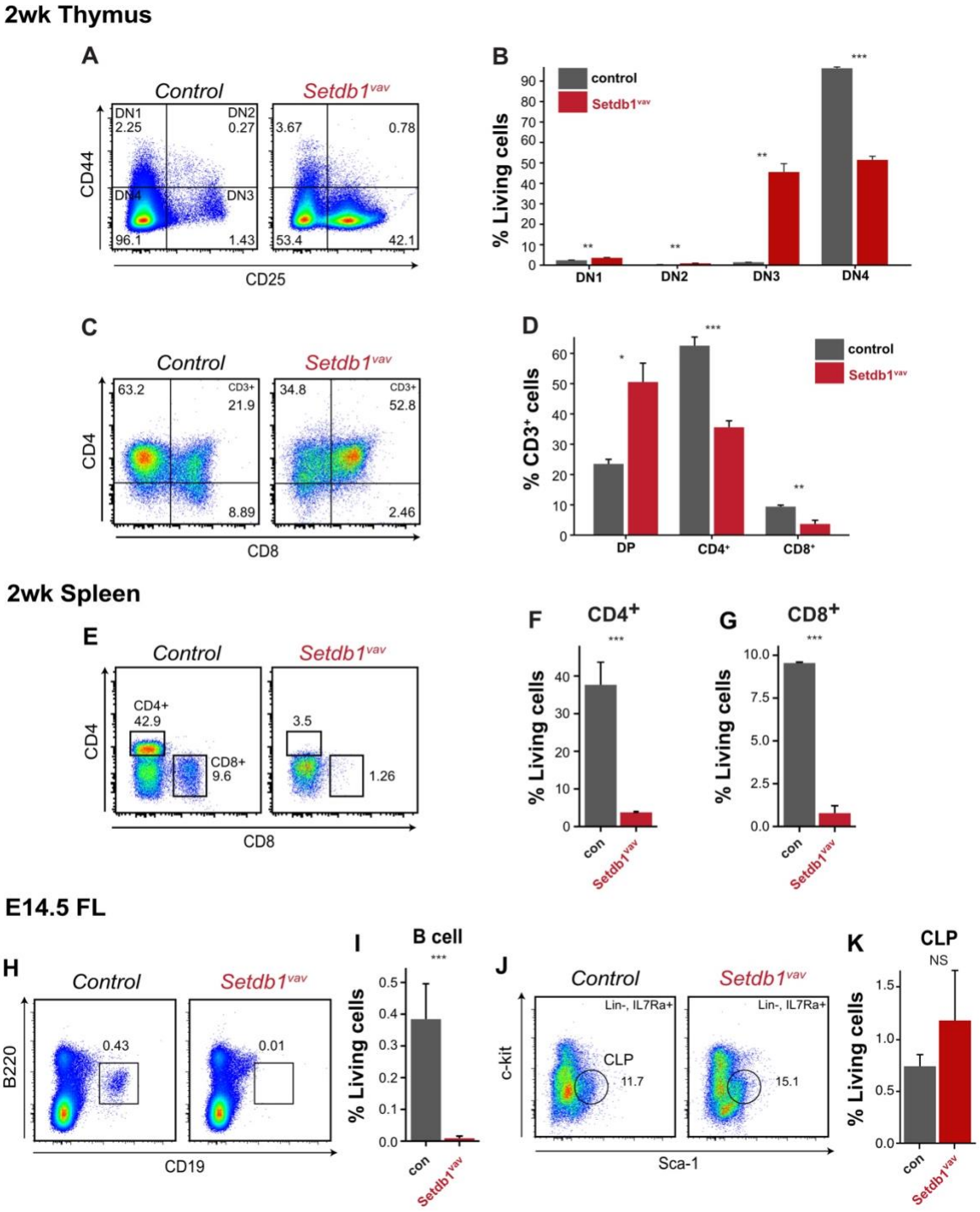

Figure 3.2 | Deletion of *Setdb1* abrogates lymphoid lineage

(A) Representative FACS plots of DN thymocytes in the thymus of control and *Setdb1*^{vav} mice at 2wk (B) Frequencies of DN thymocytes in the thymus of control and *Setdb1*^{vav} mice at 2wk (n=3). Data are shown as mean ± SD. (C) Representative FACS plots of SP, CD4$^+$, and CD8$^+$ thymocytes in the thymus of control and *Setdb1*^{vav} mice at 2wk (D) Frequencies of SP, CD4$^+$, and CD8$^+$ thymocytes in the thymus of control and *Setdb1*^{vav} mice at 2wk (n=3). Data are shown as mean ± SD. (E) Representative FACS plots of CD4$^+$ and CD8$^+$ T cells in the spleen of control and *Setdb1*^{vav} mice at 2wk. (F) Frequencies of CD4$^+$ and (G) CD8$^+$ T cells in the spleen of control and *Setdb1*^{vav} mice at 2wk (n=3). Data are shown as mean ± SD. (H) Representative FACS plots of B cells in control and *Setdb1*^{vav} E14.5 FLs. (I) Frequencies of B cells in control and *Setdb1*^{vav} E14.5 FLs (n=3). Data are shown as mean ± SD. (J) Representative FACS plots of CLPs in control and *Setdb1*^{vav} E14.5 FLs. (K) Frequencies of CLPs in control and *Setdb1*^{vav} E14.5 FLs (n=3). Data are shown as mean ± SD. *P<0.05, **P<0.01, ***P<0.001 (unpaired two-tailed Student's t-test); NS, not significant.

3.1.3. *Setdb1* ablation leads to the expansion of myeloerythroid lineage

At E14.5, FL is the primary site of erythropoiesis and myelopoiesis. In parallel at E15, spleen provides an additional site for erythroid and myeloid cell generation until postnatal life (Bertrand et al., 2006). To evaluate how *Setdb1* loss affected myeloerythroid lineage, we analyzed erythroblast in both FL and 2wk spleen. Interestingly, the frequency of *Setdb1*^{vav} pro-erythroblasts (ProE) (CD71^{+} TER119^{-}) demonstrated ~2-fold and a 15-fold increase in FL and spleen, respectively. Moreover, TER119^{+} erythroblasts significantly augmented by 2-fold in the *Setdb1*^{vav} spleen (Figure 3.3A-F). Likewise, the analysis of myeloid compartment revealed a marked increase in the percentage of Gr-1^{+} Mac-1^{+} for ~ 2-fold in FL and ~ 3-fold in the spleen (Figure 3.3G-J). The higher presence of erythroid and myeloid lineage prompted us to analyze the corresponding progenitors in the *Setdb1*-deficient FL. Therefore, we measured the common myeloid progenitors (CMPs), granulocyte-macrophage progenitors (GMPs), and megakaryocyte-erythroid progenitors (MEPs) in the *Setdb1*^{vav} FL and 2wk BM. Interestingly, *Setdb1* ablation significantly led to a decrease in the frequency of CMPs (c-kit^{high} CD34^{+}CD16/32$^{-/low}$) and an increase in the frequency of GMPs (c-kit^{high} CD34^{+}CD16/32^{+}) in the FL (Figure 3.3K-M) and BM (data not shown). Surprisingly, the percentage of MEPs (c-kit^{high} CD34^{-}CD16/32^{-}) did not show any significant difference in *Setdb1*^{vav} FL compared to control (Figure 3.3K, N) and even showed an insignificant decrease in 2wk BM (data not shown). In summary, both erythroid and myeloid lineages expanded in the absence of *Setdb1* in FL and spleen. However, analysis of the progenitors revealed that the commitment of CMPs was more prone toward GMPs, resulting in the reduction of CMPs and overrepresentation of GMPs. In contrast to the erythroid cells, the MEPs remained unchanged, suggesting that the enhanced differentiation toward erythroid lineage happened at later stages of erythroid development.

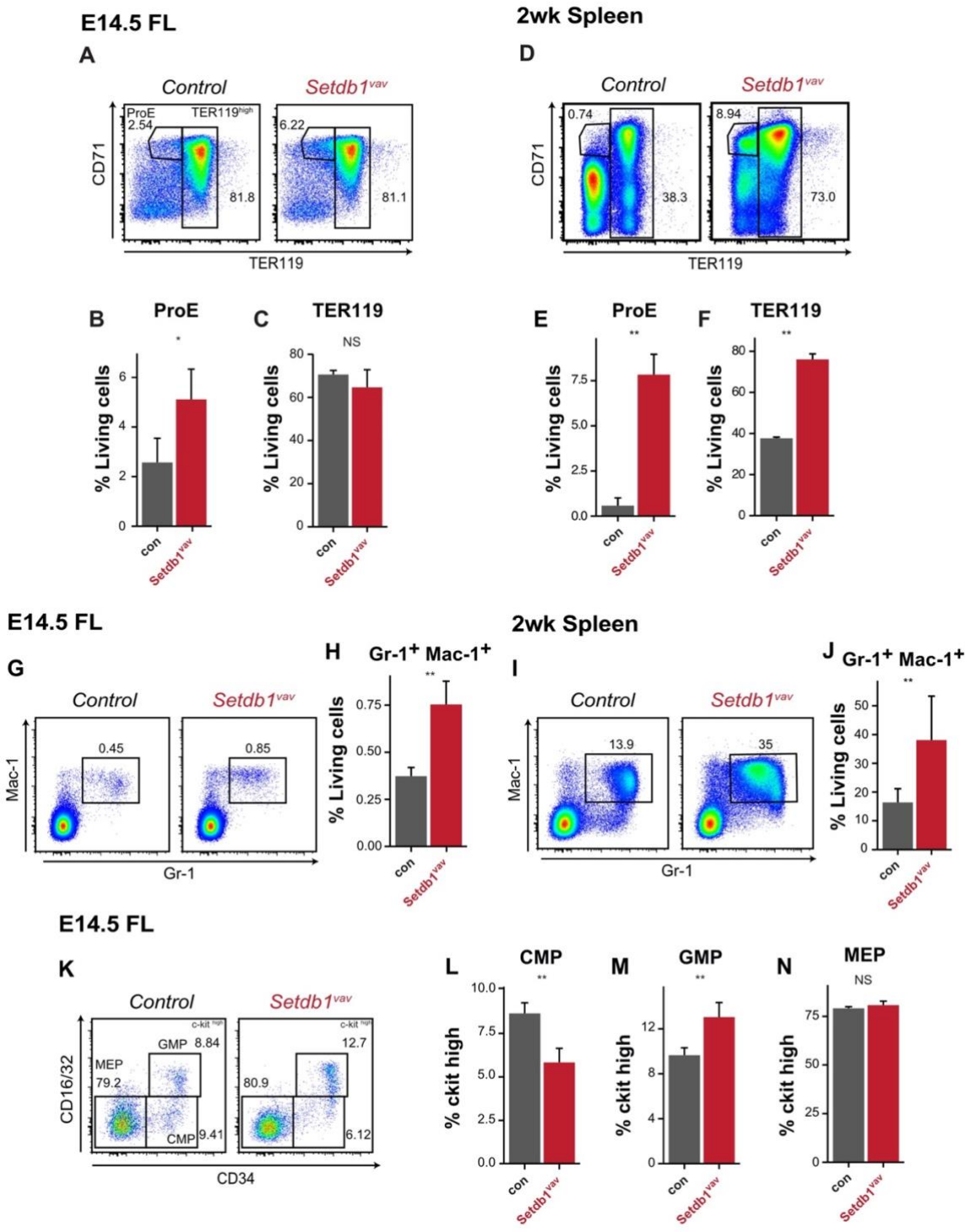

Figure 3.3 | *Setdb1* ablation leads to the expansion of myeloerythroid lineage

(A) Representative FACS plots of ProE and TER119$^+$ erythroblasts in control and *Setdb1*^{vav} E14.5 FLs. (B) Frequencies of ProE and (C) TER119$^+$ erythroblasts in control and *Setdb1*^{vav} E14.5 FLs (n=4). Data are shown as mean ± SD. (D) Representative FACS plots of ProE and TER119$^+$ erythroblasts in the spleen of control and *Setdb1*^{vav} mice at 2wk. (E) Frequencies of ProE and (F) TER119$^+$ erythroblasts in the spleen of control and *Setdb1*^{vav} mice at 2wk (n=3). Data are shown as mean ± SD. (G) Representative FACS plots of Gr-1$^+$ Mac-1$^+$ cells in control and *Setdb1*^{vav} E14.5 FLs. (H) Frequencies of Gr-1$^+$ Mac-1$^+$ cells in control and *Setdb1*^{vav} E14.5 FLs (n=4). Data are shown as mean ± SD. (I) Representative FACS plots of Gr-1$^+$ Mac-1$^+$ cells in the spleen of control and *Setdb1*^{vav} mice at 2wk. (J) Frequencies of of Gr-1$^+$ Mac-1$^+$ cells in the spleen of control and *Setdb1*^{vav} mice at 2wk (n=6). Data are shown as mean ± SD. (K) Representative FACS plots of myeloid progenitors in control and *Setdb1*^{vav} E14.5 FLs. (L) Frequencies per ckit high$^+$ of CMP (M) GMP and (N) MEP in control and *Setdb1*^{vav} E14.5 FLs (n=4). Data are shown as mean ± SD. *P<0.05, **P<0.01 (unpaired two-tailed Student's t-test); NS, not significant.

3.1.4. Absence of *Setdb1* causes fetal liver expansion and postnatal loss of LT-HSCs

To assess how *Setdb1* ablation implicated the hematopoietic stem and progenitor cells (HSPCs, also known as LSK), we measure the percentage of LSK cells and their subpopulations, including long-term hematopoietic stem cells (LT-HSCs), and multipotent progenitors (MPPs) in *Setdb1*^{vav} FL and 2wk BM.

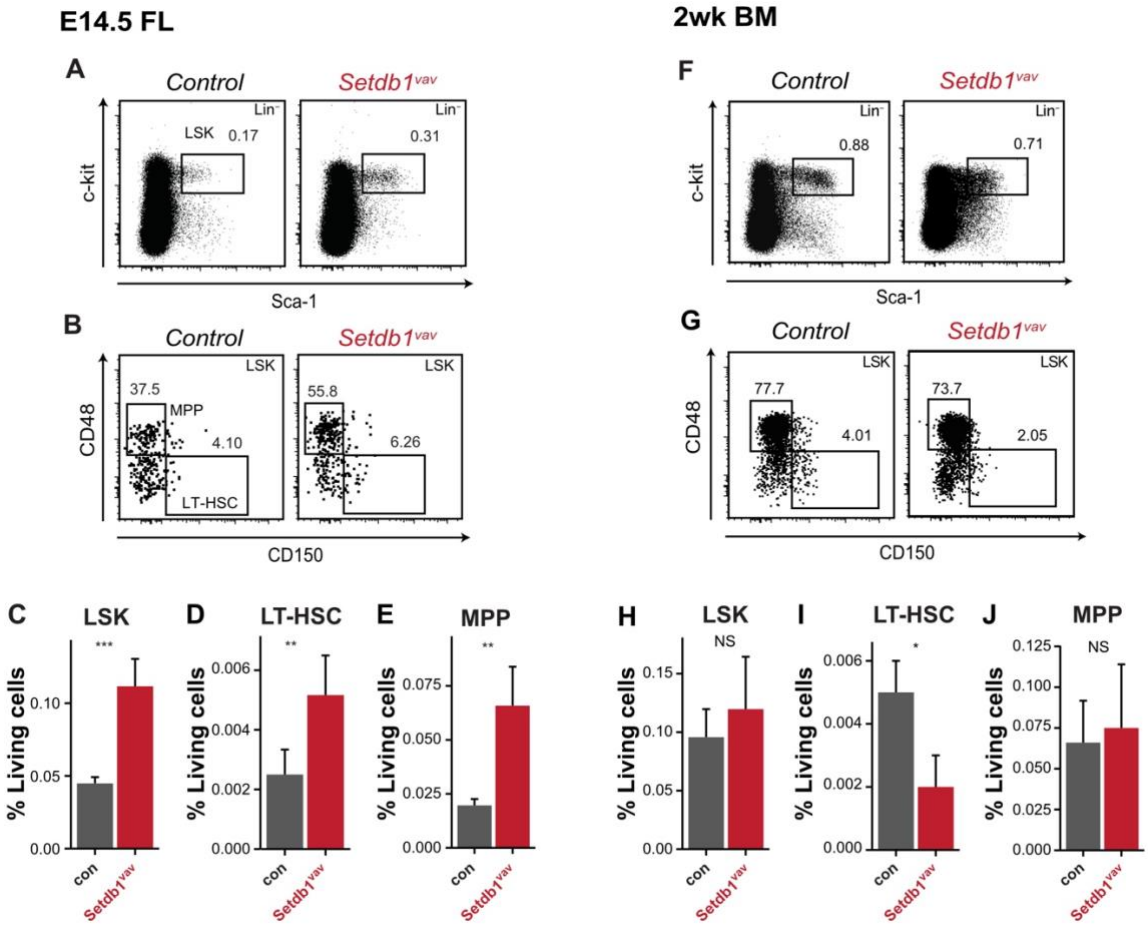

Figure 3.4 | Absence of *Setdb1* causes fetal liver expansion and postnatal loss of LT-HSCs

(A) Representative FACS plots of LSK (B) LT-HSC and MPP populations in control and *Setdb1*^{vav} E14.5 FLs. (C) Frequencies of LSK (D) LT-HSC (E) MPP populations in control and *Setdb1*^{vav} E14.5 FLs (n=4). Data are shown as mean ± SD. (F) Representative FACS plots of LSK (G) LT-HSC and MPP populations in the BM of control and *Setdb1*^{vav} at 2wk. (H) Frequencies of LSK (I) LT-HSC (J) MPP populations in the BM of control and *Setdb1*^{vav} at 2wk (n=4). Data are shown as mean ± SD. *P<0.05, **P<0.01, ***P<0.001 (unpaired two-tailed Student's t-test); NS, not significant.

Setdb1-deficient FL contained 2-fold more LSK (Lin$^-$ Sca-1$^+$ c-kit$^+$) compared to control (Figure 3.4A, C). Consistently, the frequency of LT-HSCs (LSK CD150$^+$ CD48$^-$) and MPPs

(LSK CD150$^-$ CD48$^+$) showed a significant increase of ~ 2 and 3-fold, respectively (Figure 3.4B, D, E). However, analysis of the hematopoietic stem and progenitor counterparts in 2 wk BM revealed a comparable percentage of LSKs in *Setdb1^{vav}* and control BM, indicating that the *Setdb1^{vav}* LSKs were decreasing from fetal to postnatal (Figure 3.4F, H). Intriguingly, the percentage of LT-HSCs showed a marked reduction in 2wk BM, whereas, the MPPs remained unchanged (Figure 3.4G, I, J).

Thus, *Setdb1* ablation led to a progressive loss of LT-HSCs, which resulted in minimizing the difference between *Setdb1^{vav}* and control LSKs and MPPs from fetal to the postnatal stage. The phenotype of *Setdb1^{vav}* LT-HSC is suggestive of stem cell exhaustion in which after the initial expansion, the population of LT-HSC declined progressively.

3.2. Phenotypic and functional profiling of *Setdb1* deficient HSPCs

3.2.1. Postnatal but not fetal liver *Setdb1^{vav}* LT-HSCs show enhanced apoptosis

To gain insight into the survival of hematopoietic stem and progenitor cells, we assessed apoptosis on these cells in E14.5 FL and 2wk BM.

Setdb1-ablated LSK showed a lower percentage of AnnV$^+$ cells compared to control (Figure 3.5 A, B). Moreover, there was no difference in the percentage of apoptotic cells in both LT-HSCs and MPPs (Figure 3.5 A, C, D). In 2wk BM, *Setdb1^{vav}* LSK showed a significant increase in the percentage of apoptosis (Figure 3.5 E, F). Strikingly, there was a 10-fold increase in the apoptosis of LT-HSCs. Moreover, MPPs demonstrated higher, but not significant, apoptosis rate (Figure 3.5E, G, H).

To sum, FL hematopoietic stem and progenitor cells showed normal survival followed by enhanced apoptosis at postnatal, more specifically in LT-HSCs, which is indicative of stem cell exhaustion.

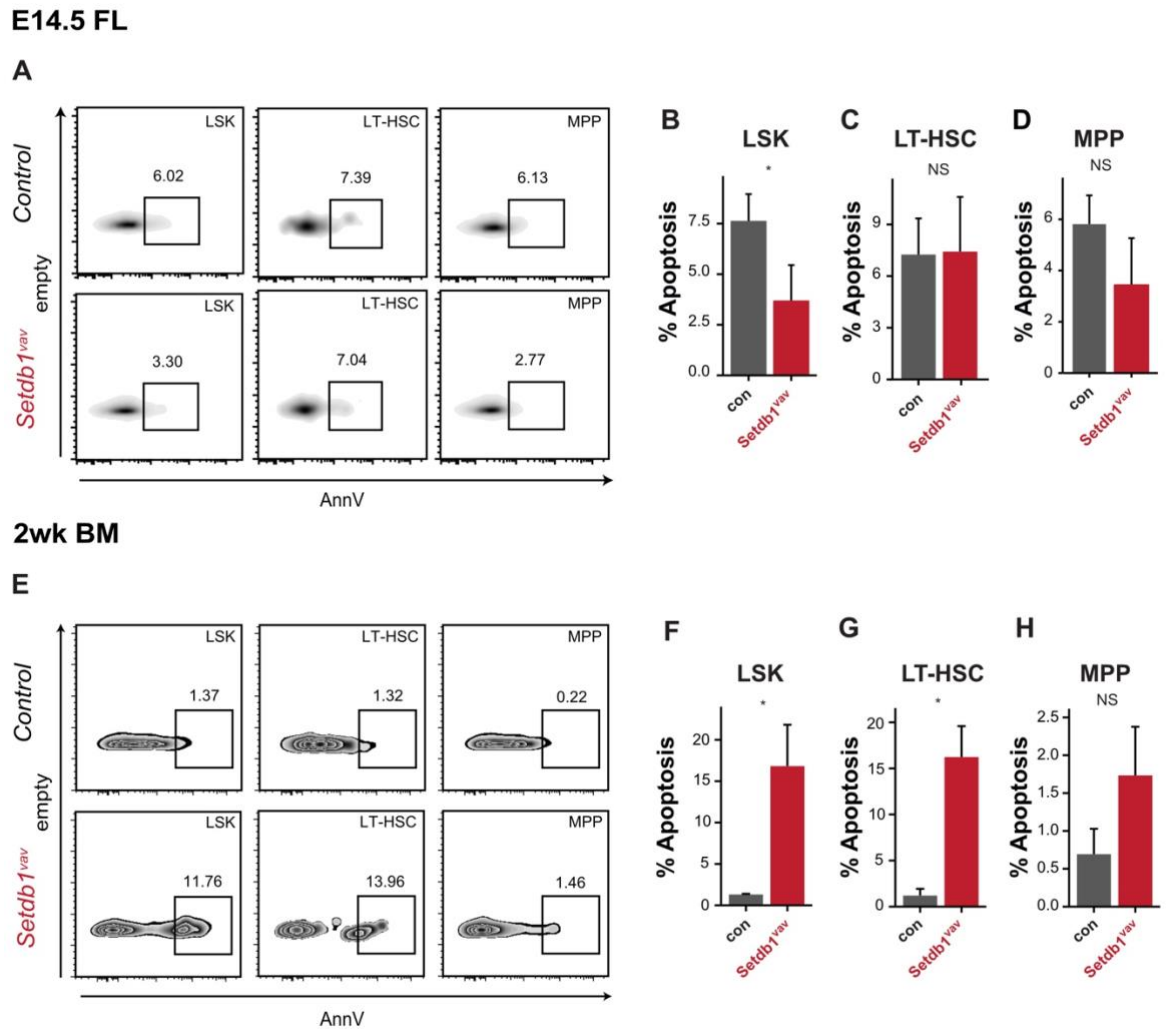

Figure 3.5 | Postnatal but not fetal liver *Setdb1*^{vav} LT-HSCs show enhanced apoptosis

(A) Representative FACS plots apoptotic cells (AnnV^{+}) in LSK, LT-HSC, and MPP in control and *Setdb1*^{vav} E14.5 FLs. (B) Frequencies of apoptotic cells in LSK, (C) LT-HSC, and (D) MPP in control and *Setdb1*^{vav} E14.5 FLs (n=4). (E) Representative FACS plots apoptotic cells in LSK, LT-HSC, and MPP in the BM of control and *Setdb1*^{vav} at 2wk. (F) Frequencies of apoptotic cells in LSK, (G) LT-HSC, and (H) MPP in the BM of control and *Setdb1*^{vav} at 2wk (n=4). Data are shown as mean ± SD. *P<0.05 (unpaired two-tailed Student's t-test); NS, not significant.

3.2.2. *Setdb1* loss augments cell cycle entry of fetal liver LT-HSCs

To determine whether enhanced hematopoietic stem and progenitor cells population were due to the change in cell proliferation, we analyzed the cell cycle profile by measuring the Ki-67 proliferation marker. We observed that in the absence of *Setdb1*, the fraction of LT-HSCs in the G0 phase significantly decreased with a concomitant increase of cells in the G1 phase (Figure 3.6A, C). Likewise, a higher percentage of *Setdb1*-deficient LSK and MPPs showed to be in cycle compare to control (Figure 3.6A, B, D). These data are consistent with normal survival and expansion of the *Setdb1*-ablated hematopoietic stem and progenitor cells.

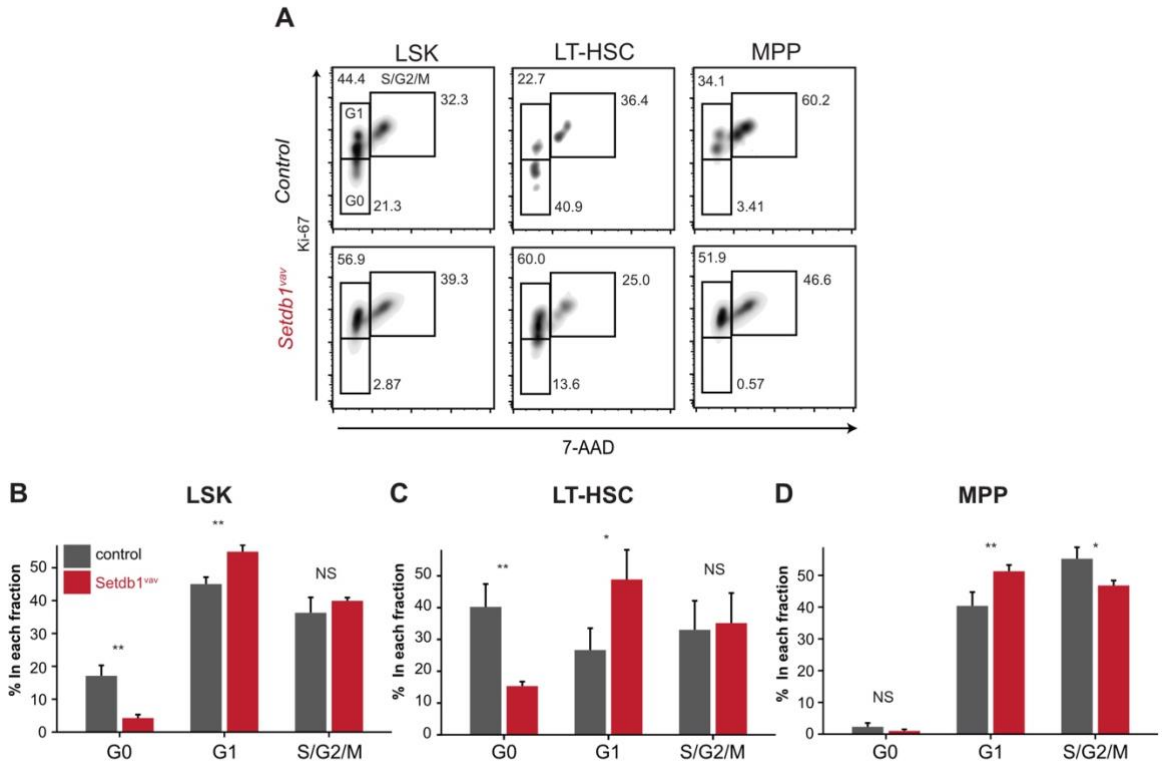

Figure 3.6 | *Setdb1* loss augments cell cycle entry of fetal liver LT-HSC

(A) Representative FACS plots of the cell cycle distribution in LSK, LT-HSC, and MPP in control and *Setdb1*^{vav} E14.5 FLs. (B) Frequencies of LSK, (C) LT-HSC, and (D) MPP in each cell cycle phase in control and *Setdb1*^{vav} E14.5 FLs (n=4). Data are shown as mean ± SD. *P<0.05, **P<0.01 (unpaired two-tailed Student's t-test); NS, not significant.

3.2.3. Function of fetal liver HSPCs is impaired in absence of *Setdb1 in vivo* and *in vitro*

The early lethality of *Setdb1*^{vav} mice and severe decrease in the BM cell number precluded evaluation of *Setdb1* loss in 2wk BM HSPCs. Therefore, to assess the significance of *Setdb1* on the function of HSPCs, we conducted the gold standard competitive transplantation experiment using E14.5 FL cells. For this purpose, we transplanted the *Setdb1*^{vav} or control CD45.2 donor FL cells with CD45.1 competitor FL cells at the ratio of 1:1 to the lethally irradiated recipient CD45.1/2 mice. We then monitored the percentage of CD45.2 donor cells in the peripheral blood of the recipient mice every two weeks for two months after transplantation. *Setdb1*^{vav} FL cells did not show any contribution to the peripheral blood at any assessment time points, whereas control FL cells demonstrated a 50% donor contribution (Figure 3.7A, B). Analysis of BM cells from the moribund mice, 8 weeks after transplantation, revealed that *Setdb1*^{vav} donor FL cells had competitive disadvantage and ultimately failed to reconstitute the hematopoietic compartment in the recipients, as shown by the ratio of CD45.2

to CD45.1 donor cell (Figure 3.7C). Therefore, this experiment showed that *Setdb1* is required for the HSPCs function. Despite the double frequency of LSK cells in *Setdb1*-deficient FL, the absence of *Setdb1* severely impaired HSPCs function.

We next tested the colony formation potential of FL progenitors *in vitro* using the methylcellulose medium supplemented with either SCF, IL-3, IL-6, and EPO (MethoCult M3434) or IL-7 (MethoCult M3630) supporting the myeloerythroid and pre-B cell colonies, respectively. Compare to control, *Setdb1*^{vav} FL cells not only generated a fewer number of myeloerythroid colonies, but the colonies were also smaller in size (Figure 3.7D). As expected, no pre-B cell colony was formed by *Setdb1*-ablated FL cells (Figure 3.7E). In summary, *Setdb1* loss compromised both myeloerythroid and lymphoid colony-forming potential of progenitors. However, the reduced number of myeloerythroid colonies was in contrast with higher myeloerythroid differentiation potential in FL of *Setdb1*^{vav} embryos, probably due to their susceptibility in *in vitro* culture.

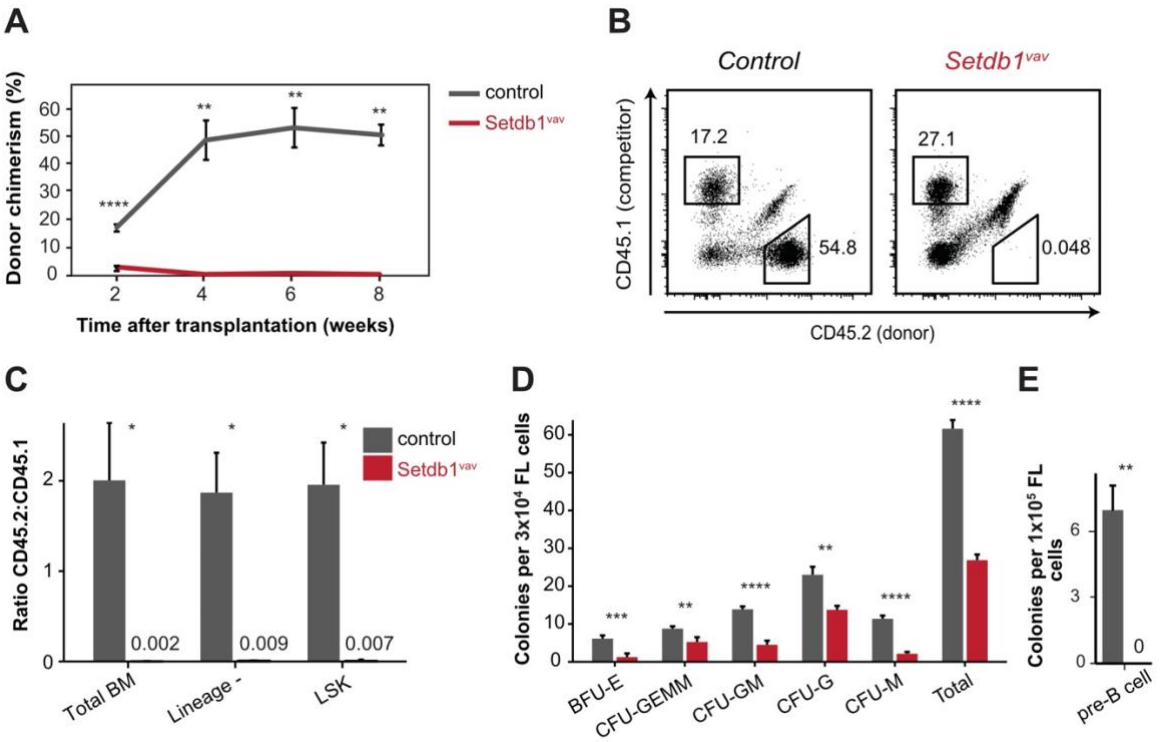

Figure 3.7 | Function of fetal liver HSPCs is impaired in absence of *Setdb1 in vivo* and *in vitro*

(A) Frequency of CD45.2$^+$ donor cells in the PB of recipient mice at different time points after transplanation (n=3). (B) Representative FACS plots distinguishing the contribution of CD45.1$^+$ (competitor) and CD45.2$^+$ (donor) cells in the BM of recipient mice, 8 weeks after transplantaion. (C) The ratio between control or *Setdb1*^{vav} and competitor cell frequency of total BM, lineage$^-$, and LSKs in the the BM of recipient mice, 8 weeks after transplantaion (n=3). (D) Average myeloerythroid and (E) pre-B cell colonies generated from control and *Setdb1*^{vav} FLs in methylcellulose colony forming assays perfomed in MethoCult M3434 and MethoCult M3630, respectively (n=4). Data are shown as mean ± SD. *P<0.05, **P<0.01, ***P<0.001, ****P<0.0001 (unpaired two-tailed Student's t-test).

3.2.4. Lack of *Setdb1* partially compromises homing potential of fetal liver HSPCs

Given that *Setdb1*^{vav} HSPCs demonstrated severely impaired functionality in transplantation, we wondered if HSPCs devoid of *Setdb1* were capable of migrating to the bone marrow efficiently. To address this, we performed a homing experiment by injecting the CFSE-labeled *Setdb1*^{vav} and control FL lineage$^-$ cells to the lethally irradiated recipient mice and analyzed the percentage of CFSE$^+$ cells in the BM after 16h. Although not significant, the frequency of *Setdb1*^{vav} CFSE$^+$ cells exhibited a decreasing trend. To substantiate this, we measured the expression of known homing surface markers on LSKs from *Setdb1*^{vav} and control FL cells. Intriguingly, both CD62L and VLA-4 surface markers significantly decreased on *Setdb1*^{vav} LSKs. Collectively, these data indicate that *Setdb1* deficiency compromised, at least partially, the homing potential of FL HSPCs.

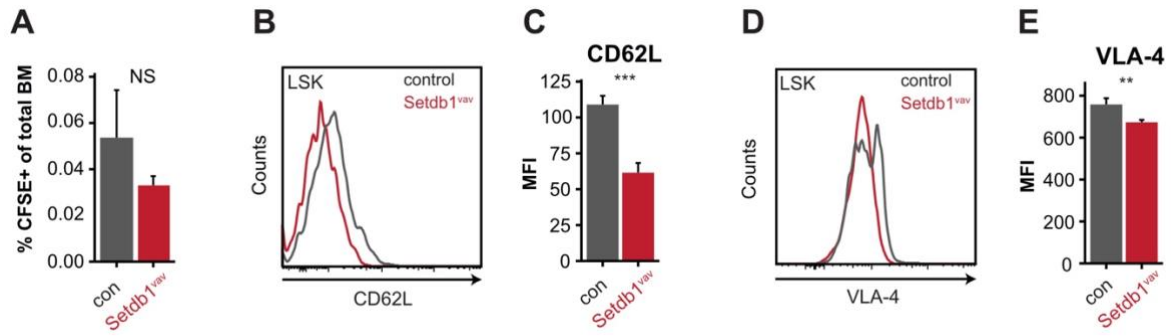

Figure 3.8 | Lack of *Setdb1* partially compromises homing potential of fetal liver HSPCs

(A) Frequencies of control and *Setdb1*^{vav} CFSE$^+$ cells in the BM of lethally irradiated recipient mice 16h after injection (n=3). (B) Representative histogram indicating the expression of CD62L homing marker on control and *Setdb1*^{vav} FL LSKs. (C) Comparison of the mean fluorescence intensity (MFI) of CD62L expression on control and *Setdb1*^{vav} FL LSKs (n=4). (D) Representative histogram indicating the expression of VLA-4 homing marker on control and *Setdb1*^{vav} FL LSKs. (E) Comparison of the mean fluorescence intensity (MFI) of VLA-4 expression on control and *Setdb1*^{vav} FL LSKs (n=4). Data are shown as mean ± SD. **P<0.01, ***P<0.001, (unpaired two-tailed Student's t-test)); NS, not significant.

3.3. Transcriptome analysis of fetal liver LT-HSCs and MPPs

3.3.1. Genes are dysregulated in *Setdb1*-deleted LT-HSCs and MPPs

To decipher the molecular basis underlying *Setdb1*-regulated HSPCs maintenance and differentiation, we performed high-throughput bulk RNA sequencing (RNA-Seq) on LT-HSCs and MPPs sorted from *Setdb1*^{vav} and control FL cells. On Integrative Genomics Viewer (IGV), the deletion of *Setdb1* exon 4 in LT-HSC and MPP was evident (Figure 3.9A). Principal component analysis (PCA) of transcriptome data of all samples projected 52% and 92%

transcriptional variance based on the first component (PC1), which separated well the *Setdb1*^{vav} and control samples in LT-HSCs and MPPs, respectively (Figure 3.9B, C). Differential expression analysis of all coding genes demonstrated that 285 and 2719 were significantly dysregulated in *Setdb1*^{vav} LT-HSCs and MPPs, respectively, relative to control ($P_{adj} < 0.05$). In LT-HSCs, out of 285 dysregulated genes, 144 genes were upregulated, and 141 genes were downregulated (Figure 3.9D). Interestingly, in MPPs, more genes deregulated upon *Setdb1* loss. Out of 2719 dysregulated genes in MPPs, 1213 genes were upregulated, and 1506 genes were downregulated (Figure 3.9E). The majority of the highly upregulated genes in both *Setdb1*^{vav} LT-HSCs and MPPs revealed to be tissue non-specific genes. Among upregulated genes in both *Setdb1*^{vav} LT-HSCs and MPPs, we found testis-specific genes (*Iqcg*, *4930550L24Rik*, *Dnah8*, *M1ap*, and *Tex19.1*), oocyte-specific gene (*Stag3*), germ cell-specific gene (*Gm1564*), neuronal gene (*Akap5*), and gene encoding ion channel membrane protein (*Tmem150c*). The upregulation of the *Tex19.1* gene was also reported in *Setdb1*-knockdown ES cells (Yuan et al., 2009). The liver and muscle-specific gluconeogenic enzymes, *Fbp1 and Fbp2*, respectively, were previously shown to be upregulated in *Setdb1*-deficient adult HSPCs (Koide et al., 2016). Similarly, expression of both genes increased in *Setdb1*^{vav} MPPs, whereas, only *Fbp2* demonstrated upregulation in *Setdb1*^{vav} LT-HSCs. Moreover, the cell cycle-related gene *Gstp2*, G1 to S phase transition protein 2, was among the upregulated genes, implying the enhanced cell cycle progression. Interestingly, a couple of hematopoietic specific genes showed strong upregulation. *Setdb1*-ablated pro-B cells and T cells showed upregulation of the *Fcgr2b* gene (Pasquarella et al., 2016; Takikita et al., 2016). Likewise, both *Setdb1*^{vav} LT-HSCs and MPPs expressed high levels of the *Fcgr2b* gene. Lastly, strong expression of the erythroid-specific enzyme, *Car1*, observed in *Setdb1*^{vav} LT-HSCs and MPPs.

Although SETDB1 was known for its silencing function, we also looked at the downregulated genes that could be indirectly regulated by SETDB1. Surprisingly, we found the established SETDB1 target *H19,* and *H19*-regulated gene *Igf2*, both belonged to the Imprinted Gene Network (IGN), downregulated in *Setdb1*^{vav} LT-HSCs and MPPs. Intriguingly, several immune-related genes such as chemokine receptors (*Ccr2*, *Ccr9*), adhesion molecule (*Vcam1*), pattern-recognition receptor (*Clec7*) demonstrated strong downregulation in *Setdb1*^{vav} MPPs, suggesting the requirement of *Setdb1* for proper expression of immune-related genes.

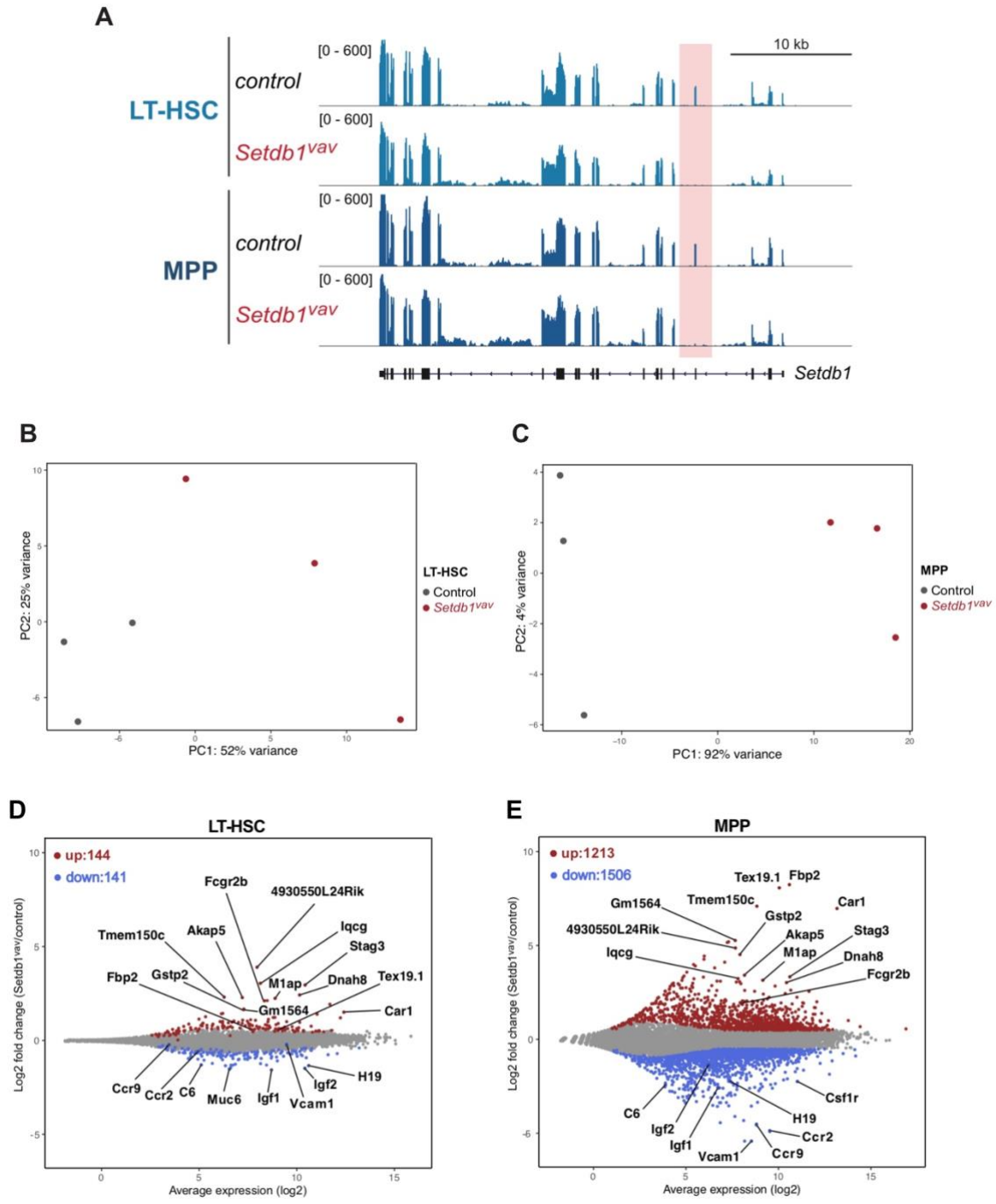

Figure 3.9 | Genes are dysregulated in *Setdb1*-deleted LT-HSCs and MPPs

(A) Genome browser view of *Setdb1* locus. Red-colored box indicates the exon 4 deletion in *Setdb1*^{vav} LT-HSC and MPP. (B) Principal component analysis (PCA) of transcriptional profiles of control and *Setdb1*^{vav} LT-HSC. (C) As in A, but for control and *Setdb1*^{vav} MPP. (D) Average expression of all protein-coding genes versus log2 fold change in control vs *Setdb1*^{vav} LT-HSC. Highlighted in red are significantly upregulated genes in *Setdb1*^{vav} LT-HSC. Highlighted in blue are significantly downregulated genes in *Setdb1*^{vav} LT-HSC ($P_{adj} < 0.05$, n=3 for each group). (E) Same as D, but for MPP ($P_{adj} < 0.05$, log2 fold change > 0.5, n=3 for each group).

3.3.2. Hallmark gene sets related to cell cycle are enriched in *Setdb1^{vav}* LT-HSCs and MPPs

We next, performed Gene Set Enrichment Analysis (GSEA) for hallmark gene sets comparing *Setdb1^{vav}* and control LT-HSCs and MPPs. Consistent with the enhanced cell cycle activation, several gene sets associated to cell cycle enriched significantly in *Setdb1^{vav}* LT-HSCs as well as MPPs (Figure 3.10 A, B). Moreover, we observed enrichment for the oxidative phosphorylation (OxPhos) gene set. OxPhos was reported as the FL additional source for energy production to meet the demand of the highly proliferating FL HSPCs (Manesia et al., 2015). In addition, the unfolded protein response (UPR) gene set demonstrated marked enrichment; however, in contrast to pro-B cells (Pasquarella et al., 2016), we have not observed any apoptosis in *Setdb1^{vav}* HSPCs (Figure 3.5 A-D). In support of the higher erythroid lineage output, the heme metabolism-related genes enriched in *Setdb1^{vav}* MPPs.

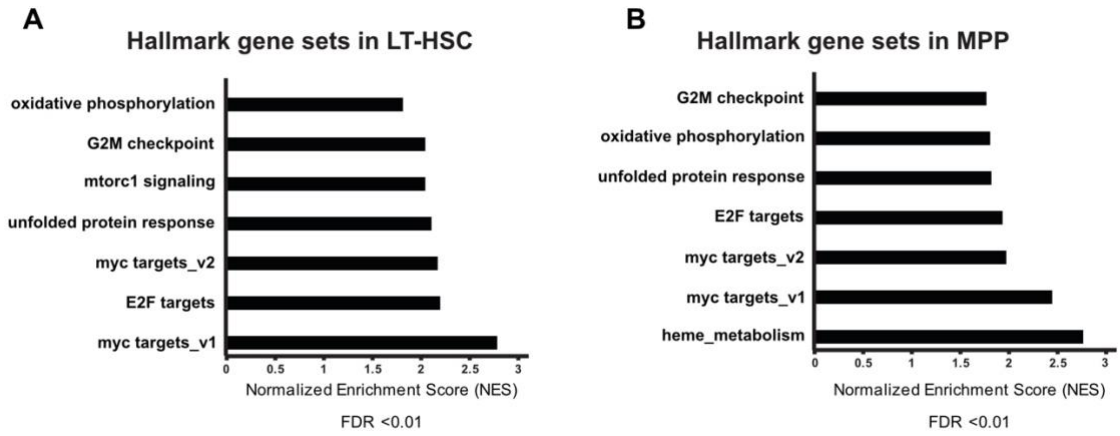

Figure 3.10 | Hallmark gene sets related to cell cycle are enriched in *Setdb1^{vav}* LT-HSCs and MPPs

(A) Gene Set Enrichment Analysis (GSEA) of RNA-seq data for hallmark gene sets enriched in *Setdb1^{vav}* LT-HSC performed by GSEA software (Subramanian et al., 2005). Shown are the highly enriched gene sets. (B) Same as A, but for MPP. FDR, false discovery rate.

3.3.3. *Setdb1^{vav}* LT-HSCs and MPPs show loss of transcriptional identity and biased lineage specific gene expression

Apart from non-hematopoietic genes (described in section 3.3.1), we detected several hematopoietic genes deregulated in *Setdb1*-deficient HSPCs. Strikingly, the absence of *Setdb1* in LT-HSCs led to the downregulation of *Hoxa10*, *Hoxa9*, *Smad7*, *Flt3,* and FL specific *Hmga2* genes involved in survival and self-renewal of LT-HSCs (Figure 3.11A).

By GSEA, we observed that the gene signature specific to LT-HSC is completely depleted in *Setdb1*^{vav} LT-HSCs, suggesting the significance of *Setdb1* in the maintenance of the HSC transcriptional identity (Figure 3.11B). Likewise, not only the expression of HSC-specific genes decreased in *Setdb1*^{vav} MPP, but the transcriptional gene signature related to HSPCs also depleted (Figure 3.11C, D). Consistent with the phenotypic profiling, we observed downregulation of many genes involved in lymphoid development. Transcription factor PU.1 (encoded by *Spi1*) showed to be critical in lymphoid lineage priming from multipotent progenitors by regulating its two target genes encoding key cytokine receptors Flt3, IL-7Ra (DeKoter et al., 2002; Carotta et al., 2010; Pang et al., 2018). In MPPs, *Setdb1* ablation led to a significant downregulation of *Spi1*, *Flt3,* and *Il7r*. (Figure 3.11C). Interestingly, expression of another PU.1 target, *Mef2c*, that showed to regulate lymphoid versus myeloid fate choice in MPPs (Stehling-Sun et al., 2009) markedly decreased (Figure. 3.11C). Accordingly, the gene signatures related to both B and T cell development were lost in *Setdb1*^{vav} MPPs (Figure 3.11E).

Coherence with the myeloerythroid lineage expansion in the absence of *Setdb1*, we observed the upregulation of the erythroid-affiliated genes, *Gata1*, *Zfpm1* (*FOG-1*), *Tal1*, *Klf1*, *Epor*, and *Car1* (Figure. 3.11C). Moreover, the gene signature related to nucleated erythrocyte, which encompassed genes implicated in erythropoiesis were positively enriched in *Setdb1*^{vav} MPPs (Figure 3.11F), which corroborated the enriched heme metabolism gene signature in the hallmark genes (Figure 3.10B). In addition to the highly expressed myeloid related gene *Fcgr2b*, we detected upregulation of the *Cebpe* gene, which was shown previously to be crucial for terminal differentiation and function of granulocytes (Lekstrom-Himes, 2001)(Figure. 3.11C).

To sum, our data demonstrated that *Setdb1* was required for the maintenance of the HSPCs transcriptional identity and the regulation of balanced lineage priming.

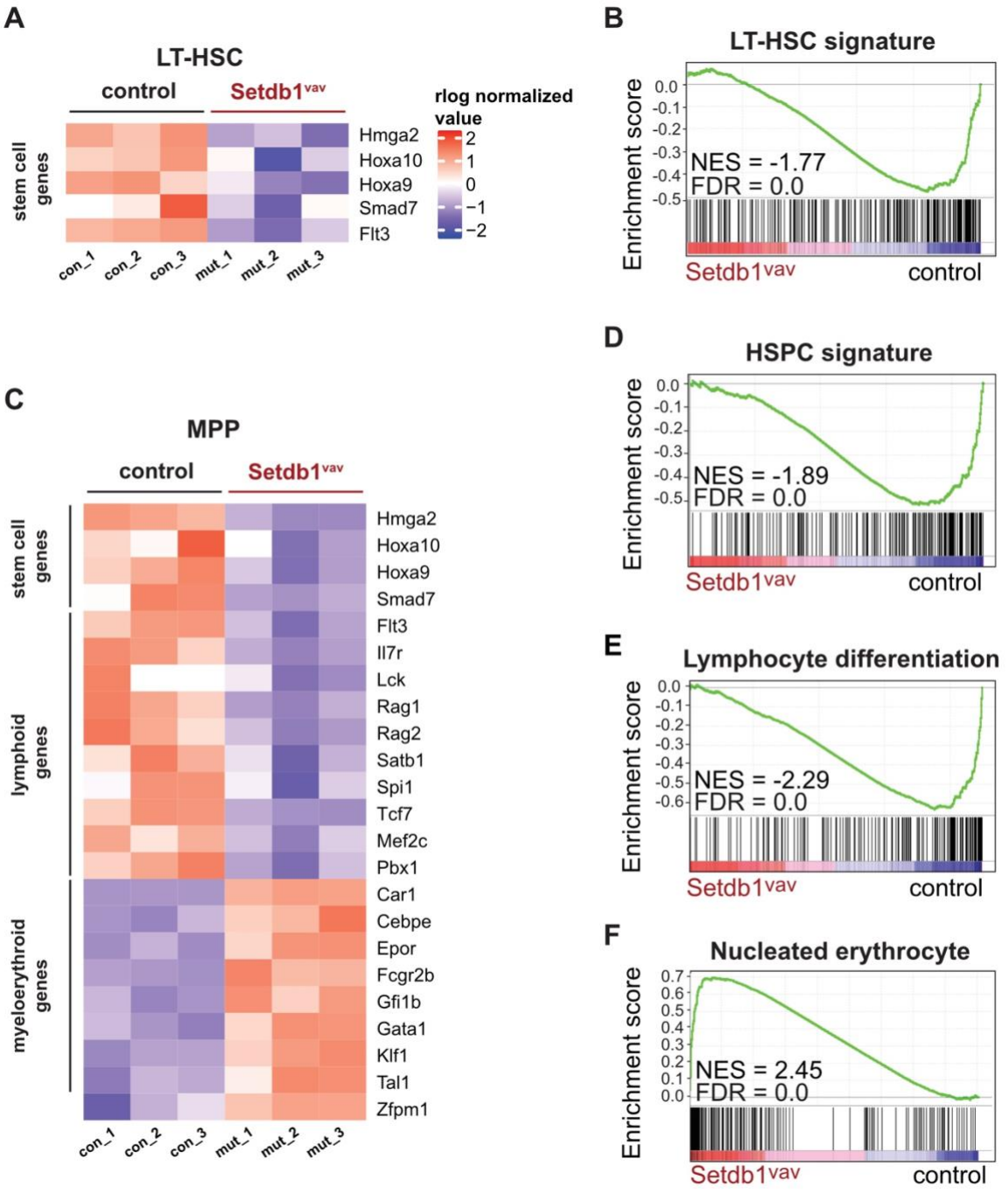

Figure 3.11 | *Setdb1*^{vav} LT-HSCs and MPPs show loss of transcriptional identity and biased lineage specific gene expression

(A) Heatmap showing selected hematopoietic stem cell-related gene expression in control (con) and *Setdb1*^{vav} (mut) FL LT-HSC (P_{adj} < 0.05). (B) Gene Set Enrichment Analysis (GSEA) with LT-HSC gene signature (Ivanova et al., 2002) for RNA-seq data from control and *Setdb1*^{vav} FL LT-HSC. (C) Heatmap indicating selected hematopoietic stem cell-, lymphoid-, and myeloerythroid-associated gene expression in control (con) and *Setdb1*^{vav} (mut) FL MPP (P_{adj} < 0.05, log2 fold change > 0.5). (D) Gene Set Enrichment Analysis (GSEA) with hematopoietic stem and progenitor cell (HSPC) gene signature (Ivanova et al., 2002) for RNA-seq data from control and *Setdb1*^{vav} FL MPP. (E) Gene Set Enrichment Analysis (GSEA) with GO lymphocyte differentiation gene signature for RNA-seq data from control and *Setdb1*^{vav} FL MPP. (F) Gene Set Enrichment Analysis (GSEA) with nucleated erythrocyte gene signature (Chambers et al., 2007) for RNA-seq data from control and *Setdb1*^{vav} FL MPP. NES, normalised enrichment score; FDR, false discovery rate.

3.3.4. *Setdb1*-deleted MPPs downregulate expression of genes associated with cellular communication

By KEGG pathway analysis, we observed depletion of gene sets related to cellular communications, e.g., cell adhesion molecules (CAMs) and Cytokine-cytokine receptor interaction (Figure 3.12A, B). The chemokine receptors CCR9 and CCR7 were required for the seeding of lymphoid progenitors in the thymus (Ramond et al., 2014). In *Setdb1*^{vav} MPPs, expression of both *Ccr9* and *Ccr7* genes showed a marked decrease (Figure 3.12C). In addition, HSPCs homing markers, LFA-1 (*Itgal*), CD62L (*Sell*), CXCR4 (*Cxcr4*), VLA-4 (*ITGA4*), were significantly downregulated in *Setdb1*^{vav} MPPs (Figure 3.12C). These data confirmed a partial decrease in the homing capability of *Setdb1*-ablated HSPCs *in vivo* (Figure 3.8A-E).

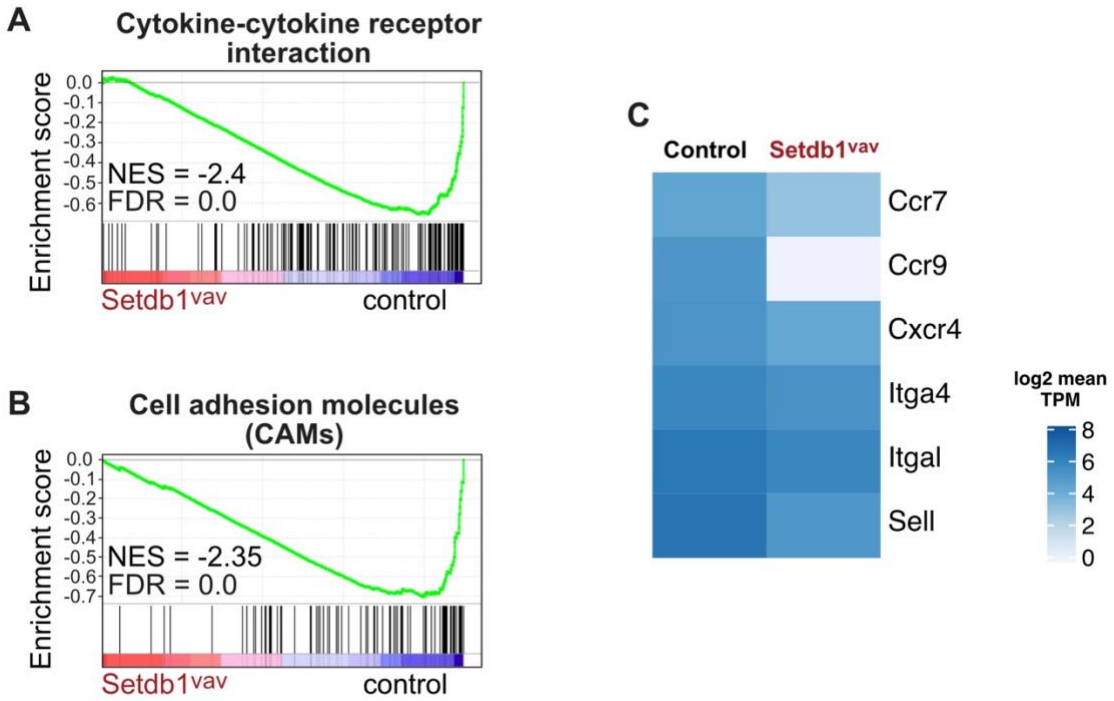

Figure 3.12 | *Setdb1*-deleted MPPs downregulate expression of genes associated with cellular communication

(A) Gene Set Enrichment Analysis (GSEA) for KEGG pathway gene signature related to cytokine-cytokine receptor interaction for RNA-seq data from control and *Setdb1*^{vav} FL MPP. (B) As in A, but for KEGG pathway gene signature related to cell adhesion molecules (CAMs). (C) Heatmap showing expression (given by TPM) of selected genes in control and *Setdb1*^{vav} FL MPP ($P_{adj} < 0.05$). . NES, normalised enrichment score; FDR, false discovery rate; TPM, transcripts per million.

3.3.5. Retrotransposons are derepressed in *Setdb1*^{vav} LT-HSCs and MPPs

Setdb1 depletion in a variety of cellular systems led to derepression of different families of retrotransposons. To verify which families gained transcriptional activity in the absence of *Setdb1*, we analyzed the differential expression of all annotated retrotransposon defined in the University of California Santa Cruz (UCSC) genome browser in our RNA-seq data from *Setdb1*^{vav} LT-HSCs and MPPs compared to control. The significant expression was observed in all classes of ERVs in both LT-HSCs and MPPs such as MuLV and MMVL30 (class I), RLTR50A, MMERVK10C, and IAPLTR3 (class II), and MER74C (class III) (Figure 3.13A, B). Interestingly, we detected significant but mild expression of non-LTR retrotransposons such as LINE-L1 and B2 SINE in *Setdb1*^{vav} MPPs (Figure 3.13C, D). Mild expression of LINE-L1 was observed in visceral endoderm (XEN) cells (PhD thesis, Zeyang Wang); however, B2 SINE exhibited an exclusive expression pattern in *Setdb1*-deleted FL MPPs.

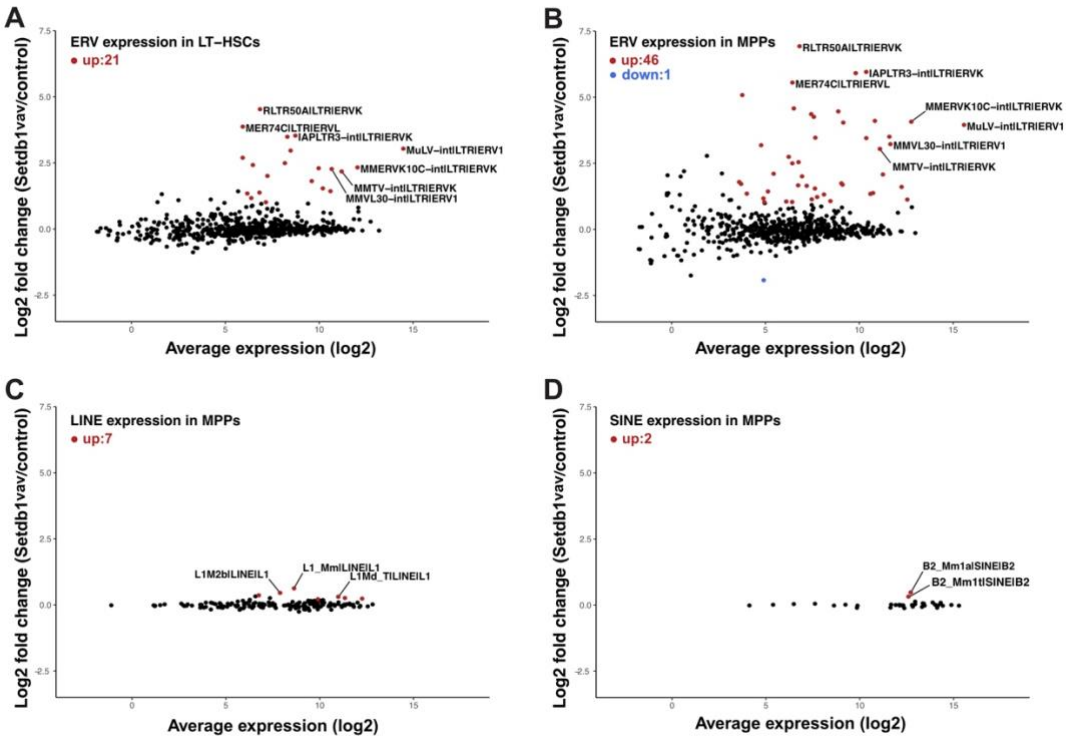

Figure 3.13 | Retrotransposons are derepressed in Setdb1^{vav} LT-HSCs and MPPs

(A) Dot plot indicating average expression versus log2 fold change of ERV families in control vs *Setdb1*^{vav} LT-HSC. Highlighted in red are significantly upregulated ERVs in *Setdb1*^{vav} LT-HSC. (P_{adj} < 0.01, log2 fold change > 1, n=3 for each group). (B) Same as A, but for MPP. Highlighted in red are significantly upregulated ERVs in *Setdb1*^{vav} MPP. Highlighted in blue are significantly downregulated ERVs in *Setdb1*^{vav} MPP. (P_{adj} < 0.01, log2 fold change > 1, n=3 for each group). (C) Dot plot indicating average expression versus log2 fold change of LINEs in control vs *Setdb1*^{vav} MPP. Highlighted in red are significantly upregulated SINEs in *Setdb1*^{vav} MPP. (P_{adj} < 0.01, log2 fold change > 0.2, n=3 for each group). (D) Dot plot indicating average expression versus log2 fold change of SINE families in control vs *Setdb1*^{vav} MPP. Highlighted in red are significantly upregulated SINE in *Setdb1*^{vav} MPP. (P_{adj} < 0.01, log2 fold change > 0.2, n=3 for each group).

3.4. Identification of SETDB1 targets

3.4.1. SETDB1 directly targets non-hematopoietic genes

SETDB1-mediated silencing is heralded by the deposition of the H3K9me3 mark on its target regions. To investigate whether the upregulation of genes was the direct consequence of *Setdb1* ablation, we mapped the H3K9me3 mark as the readout of SETDB1 enzymatic activity in *Setdb1*^{vav} and control LSK cells using chromatin immunoprecipitation followed by high-throughput sequencing (ChIP-Seq). However, the number of FL LSK cells was the limiting factor to employ regular ChIP protocols. Therefore, we utilized the ultra-low-input micrococcal nuclease-based native ChIP (ULI-NChIP) and sequencing method (Brind'Amour et al., 2015). We asked whether the level of H3K9me3 mark changed at transcriptional start sites (TSS) of coding genes (-4.0 kb to +1.0 kb from TSS) upon *Setdb1* deletion in LSK cells and that the loss of H3K9me3 led to the transcriptional changes observed in MPPs, which encompassed the substantial fraction of LSK cells. Interestingly, we observed that the promoter of non-hematopoietic genes in FL LSK cells was enriched for the SETDB1-mediated H3K9me3 mark. The deletion of *Setdb1* resulted in a reduction of the H3K9me3 level at these gene promoters such as *Fbp2*, *Dnah8*, *Gstp2*, and *M1ap*. This observation was coherent with the transcriptome analysis since many of these genes exhibited a significantly higher expression in *Setdb1*^{vav} MPP cells (Figure 3.14). Loss of H3K9me3 at the promoter of *Fbp2* in *Setdb1*^{vav} FL LSKs was consistent with that of adult BM HSPCs (Koide et al., 2016).

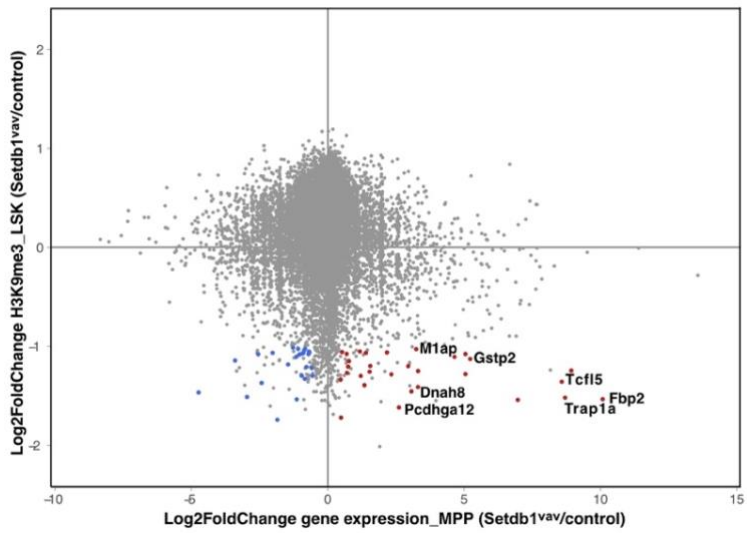

Figure 3.14 | SETDB1 directly targets non-hematopoietic genes

Scatter plot indicating the correlation between the expression of genes in *Setdb1*^{vav} vs control MPP and H3K9me3 levels in *Setdb1*^{vav} vs control LSK. Highlighted in red are significantly upregulated genes ($P_{adj} < 0.05$, log2 fold change > 0.5) demonstrating reduced H3K9me3 levels (log2 fold change > 1).

3.4.2. SETDB1 mediates silencing on ERVs

We next analyzed H3K9me3 enrichment at different families of retrotransposons and asked if there is a correlation between the loss of H3K9me3 mark and the derepression of retrotransposons. Surprisingly, not all families of the derepressed retrotransposons in *Setdb1*^{vav} MPPs demonstrated H3K9me3-hypomethylation. ERVs class I and II, whose expression was detected in *Setdb1*^{vav} MPPs, such as MuLV and MMVL30 (class I), RLTR50A, MMERVK10C showed loss of H3K9me3. In contrast, IAPLTR3 (class II), and MER74C (class III) exhibited maintained H3K9me3 level, suggesting that SETDB1-mediated silencing did not control the expression of these elements (Figure 3.15A). Mild reduction of H3K9me3 level at LINEs was reported in *Setdb1* knockout MEF cells (Kato et al., 2018). Similarly, we observed H3K9me3-hypomethylation at LINE-L1 (Figure 3.15B). Despite significant but slight derepression of B2 SINE, the H3K9me3 level showed a reduction trend; however, it did not pass the set threshold (Figure 3.15C).

In *Setdb1*-ablated mESCs, neural progenitor cells, and PGCs, activation of ERVs, such as IAPs, and generation of chimeric transcripts starting from ERVS, led to the upregulation of neighboring genes (Karimi et al., 2011; Tan et al., 2012; Liu et al., 2014). However, such transcripts have been detected neither in pro-B cells nor in LSK and GMP cells upon *Setdb1* deletion (Koide et al., 2016; Pasquarella et al., 2016). In *Setdb1*^{vav} MPPs, by visual inspection of genomic regions of upregulated genes on IGV browser, we detected several genes such as *Fcgr2b* and *Def8* that laid in the vicinity of derepressed ERVs; however, the orientation of the derepressed ERVs with respect to the neighboring genes dismissed the generation of read-through transcripts (Figure 3.15D). For example, *Fcgr2b*, the only hematopoietic-related gene, bore the head-to-head orientation with respect to its neighboring MuLV-int ERV.

To sum, SETDB1 mediated silencing at the promoters and retrotransposons. However, SETDB1-mediated repression at the promoters was limited to non-hematopoietic genes.

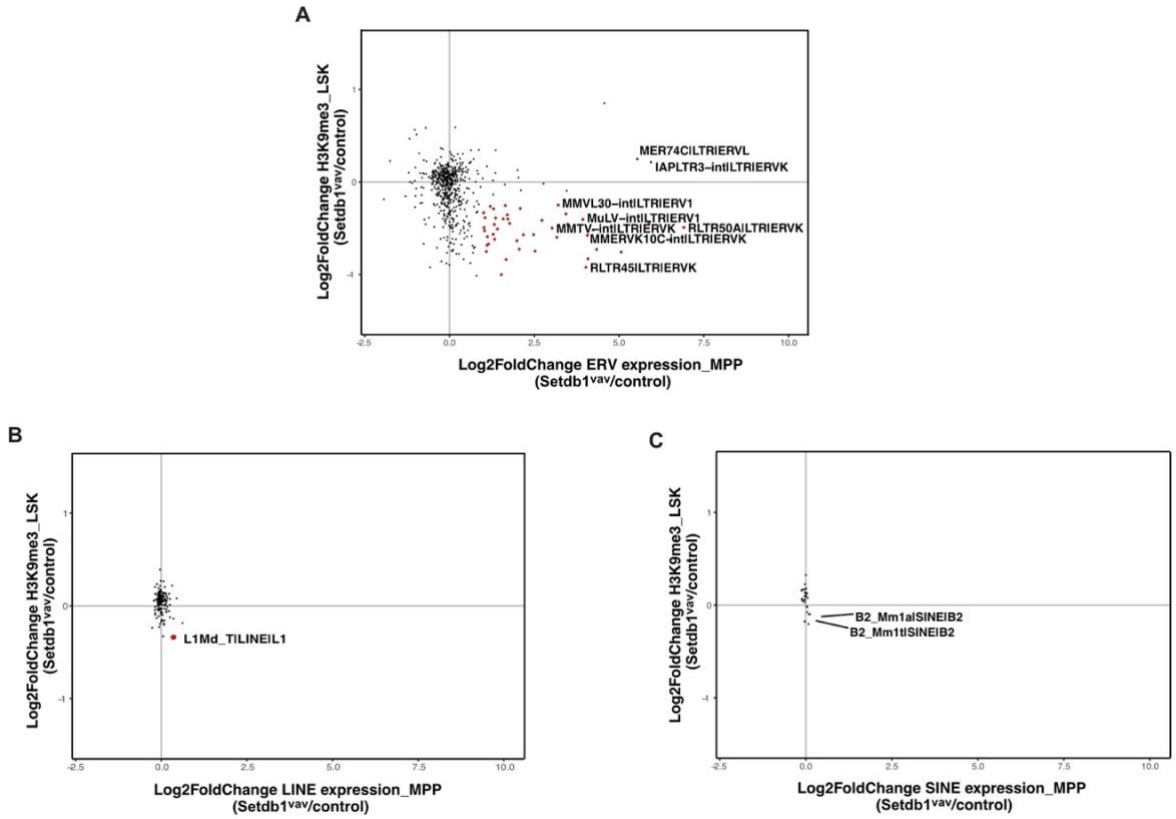

Figure 3.15 | SETDB1 mediates silencing on ERVs

(A) Scatter plot indicating the correlation between the expression of ERV families in *Setdb1*^{vav} vs control MPP and H3K9me3 levels in *Setdb1*^{vav} vs control LSK. Highlighted in red are significantly upregulated ERVs (P_{adj} < 0.01, log2 fold change > 1) demonstrating reduced H3K9me3 levels (log2 fold change > 0.2). (B) Scatter plot indicating the correlation between the expression of LINEs in *Setdb1*^{vav} vs control MPP and H3K9me3 levels in *Setdb1*^{vav} vs control LSK. Highlighted in red are significantly upregulated LINEs (P_{adj} < 0.01, log2 fold change > 0.2) demonstrating reduced H3K9me3 levels (log2 fold change > 0.2). (C) same as B, but for SINEs.

3.5. Assessment of genome-wide chromatin accessibility and motifs in correlation with H3K9me3 and gene expression

3.5.1. Chromatin accessibility is altered in *Setdb1^{vav}* LSK cells

Given that the correlation of *Setdb1*-mediated silencing to the observed *Setdb1^{vav}* hematopoietic phenotype was weak, we wondered whether SETDB1 governed the gene transcription by modulating the chromatin dynamic. Therefore, we used the improved protocol of assay for transposase-accessible chromatin using sequencing (Omni-ATAC-seq) (Corces et al., 2017) to gain insight about SETDB1 regulatory function beyond promoters and retrotransposons by identifying the genome-wide chromatin accessibility landscape in LSK cells. In total, we identified 29774 non-promoter accessible regions. The PCA analysis of non-promoter ATAC peaks projected 82% variance based on the first component (PC1), which distinguished well the *Setdb1^{vav}* and control LSK samples (Figure 3.16A).

Assessment of the differential accessible regions (log2 fold change > 2) revealed 708 regions, which gained accessibility in *Setdb1^{vav}* LSK cells and 135 regions, which lost accessibility (Figure 3.16B). Using Homer motif analysis, we asked if the 708 newly emerged ATAC peaks in *Setdb1^{vav}* LSK cells harbored TF binding sites. Interestingly, three of the five top-scoring motifs matched to PU.1 and other ETS TFs. The other two motifs were enriched for the critical transcriptional regulator and genome organizer CTCF and its paralog BORIS (Figure 3.16C). Notably, the average ATAC-seq coverage on PU.1 and CTCF motifs increased in *Setdb1^{vav}* LSK cells compared to controls, corroborating the presence of the motifs in the accessible regions (Figure 3.16D, E). Intriguingly, except for Boris (TPM<1), CTCF and other ETS TFs such as PU.1 were expressed at different levels in both *Setdb1^{vav}* and control LSK cells, suggesting the binding potentiality of these TFs to their corresponding motifs (Figure 3.16F).

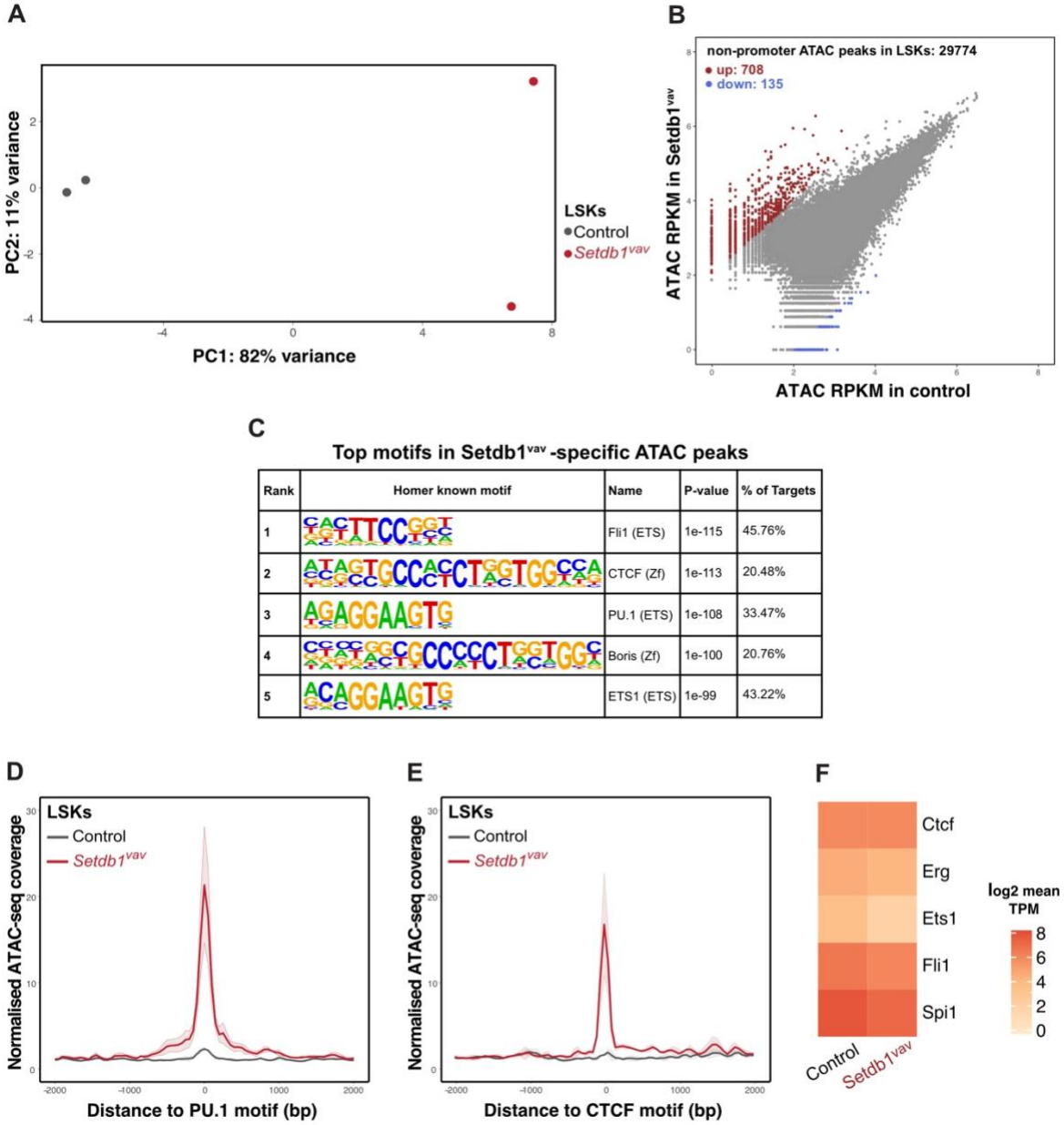

Figure 3.16 | Chromatin accessibility is altered in *Setdb1^{vav}* LSK cells

(A) Principal component analysis (PCA) of non-promoter ATAC peaks in control and *Setdb1^{vav}* LSKs. (B) Dot plot showing ATAC-seq coverage (given by RPKM) in control vs *Setdb1^{vav}* LSK. Highlighted in red are the gained ATAC peaks in *Setdb1^{vav}* LSK (log2 fold change > 2). Highlighted in blue are the lost ATAC peaks in *Setdb1^{vav}* LSK (C) Motif analysis in gained ATAC peaks in *Setdb1^{vav}* LSK. The first five top-scoring motifs are listed. (D) ATAC-seq coverage (given by RPKM) on PU.1 motifs in gained ATAC peaks in *Setdb1^{vav}* LSK (n=2). Mean coverage ± SD (shaded area) is shown. (E) Same as D, but for CTCF motifs. (F) Heatmap showing expression (given by TPM) of motif-associated TFS in control and *Setdb1^{vav}* FL MPP. TPM, transcripts per million.

3.5.2. TF binding sites found in *Setdb1^{vav}*-specific open chromatin lose SETDB1-mediated H3K9me3 protection

We then asked if the altered chromatin accessibility was directly mediated by SETDB1. Among the expressed ETS TFs in LSK cells that could potentially bind to ETS motif, only PU.1 is known as the master regulator of lineage fate determination (Arinobu et al., 2007)(Figure 3.16E). Therefore, we determined the level of H3K9me3 over PU.1 and CTCF motifs detected in the *Setdb1^{vav}*- specific ATAC peaks in control and *Setdb1^{vav}* LSK cells. Of note, we detected a high density of H3K9me3 on both PU.1 and CTCF motifs in control LSK cells. Intriguingly, striking hypomethylation was observed on PU.1 and CTCF motifs in *Setdb1^{vav}* LSK cells, at the same level as the input sample (Figure 3.17 A, B). Importantly, the H3K9me3 reduction was specific for the motifs mentioned above since the H3K9me3 mark remained unaltered at the other part of the genomes, for example, at those repressed ERVs, which maintained the low level H3K9me3 mark in control and *Setdb1^{vav}* LSK cells (Figure 3.17 C). In conclusion, loss of H3K9me3 protection on PU.1 and CTCF binding motifs in *Setdb1^{vav}* LSK cells led to enhanced accessibility, thereby providing additional binding sites for the readily available corresponding TFs.

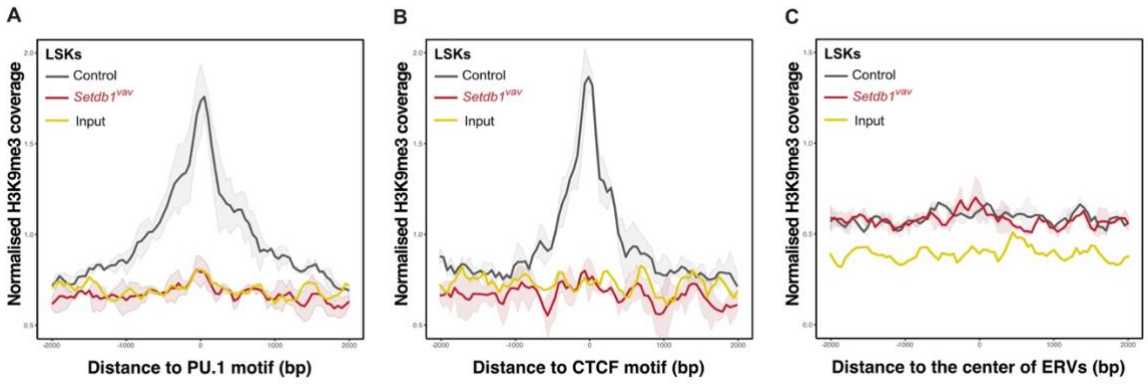

Figure 3.17 | TF binding sites found in *Setdb1^{vav}*-specific open chromatin lose SETDB1-mediated H3K9me3 protection

(A) H3K9me3 coverage (given by RPKM) on PU.1 motifs in gained ATAC peaks in *Setdb1^{vav}* LSK (n=3). Mean coverage ± SD (shaded area) is shown. (B) As in A, but on CTCF motifs. (C) H3K9me3 coverage (given by RPKM) on a subset of represed ERVs with maintained H3K9me3 in *Setdb1^{vav}* LSK (n=3). Mean coverage ± SD (shaded area) is shown.

3.5.3. Potential target genes associated with TF binding sites are deregulated

We next interrogated if the exposed TF binding sites found in the *Setdb1*^{vav}- specific open chromatin regions that could potentially be bound by PU.1 and CTCF, modulated the transcription of the neighboring genes. Therefore, we first filtered the TSS of all coding genes for the ones which were within the ± 100 kb window around the PU.1 and CTCF binding motifs. In total, we found 417 and 389 genes either up or downstream of PU.1 and CTCF motifs, respectively. To gain insight into the transcriptional changes, we overlapped the significantly deregulated genes in *Setdb1*-deficient MPPs with those of PU.1 and CTCF motif-associated. Interestingly, 29 out of 417 PU.1 motif-related genes showed significant upregulation, and the same number of the genes showed downregulation in *Setdb1*^{vav} MPPs (Figure 3.18A, B). Likewise, 25 and 38 out of 389 CTCF motif-associated genes were significantly up and downregulated, respectively, in *Setdb1*^{vav} MPPs (Figure 3.18C, D).

To understand the biological function, we analyzed the genes in the intersection of each Venn diagram with the ShinyGO tool for the GO biological process terms and KEGG pathways (Ge et al., 2020). PU.1 motif-related upregulated genes did not show significant enrichment for defined terms and pathways. Nevertheless, we observed cases where an exposed PU.1 motif correlated with an upregulated gene such as *Fech* gene locus (Figure 3.18E). The gene encodes the ferrochelatase enzyme involved in heme metabolism, which showed enrichment among the hallmark gene sets in *Setdb1*^{vav} MPP (Figure 3.10B). However, this gene is not the PU.1 target. Interestingly, PU.1 motif-related downregulated genes enriched for the KEGG pathway, such as cytokine-cytokine receptor interaction (Figure 3.18F). The illustration was at *IL16* gene locus, where the loss of H3K9me3 observed at PU.1 binding motif in a region with enhanced accessibility upstream of the *IL16* locus (Figure 3.18G). Of note, the emerged PU.1 motif demonstrating H3K9me3 deficit related to *Fech* and *IL16* genes resided in ORR1E and ORR1B1 subfamilies of ERVs class III retrotransposons, respectively. However, no transcriptional changes observed for these elements in *Setdb1*^{vav} MPPs (Figure 3.13B, Figure 3.15A).

We applied the same approach to the CTCF motif-associated genes. Our analysis revealed that upregulated genes related to the CTCF motif enriched for GO biological process terms associated with nuclear division (Figure 3.18H). For instance, the upregulated *Spire2* gene, involved in the nucleation of actin filaments, bore a hypomethylated B3 retrotransposon, the subfamily of B2 SINE, which uncovered a CTCF binding motif (Figure 3.18I). Strikingly, we observed a strong representation of downregulated CTCF motif-related genes in GO biological process terms such as “antigen processing and presentation” and “immune response” (Figure 3.18J). CTCF showed to be central for the regulation of human major histocompatibility

complex (MHC) class II genes (Majumder and Boss, 2010). *Setdb1*^{vav} MPPs demonstrated a significant downregulation of several genes in the large MHC II locus, encompassing two hypomethylated CTCF motifs within the B3 subfamily in an open chromatin environment. Further illustration was observed at the upstream of *Cx3cr1* locus, the chemokine receptor related to the "immune response" GO biological process term (Figure 3.18K). However, despite the fact that we observed significant but slight upregulation of B2 SINE in *Setdb1*^{vav} MPPs (Figure 3.13D), loss of H3K9me3 occurred at CTCF-containing B3 subfamily of B2 SINE elements did not result in transcriptional activation of these loci.

Collectively, these data showed that *Setdb1*-dependent loss of H3K9me3 at retrotransposons, which still remained repressed, altered the chromatin dynamic toward the more accessible state, which exposed the cryptic PU.1 and CTCF binding site. Putative binding of the corresponding TFs could eventually, and partly explain the gene deregulation in *Setdb1*-ablated HSPCs.

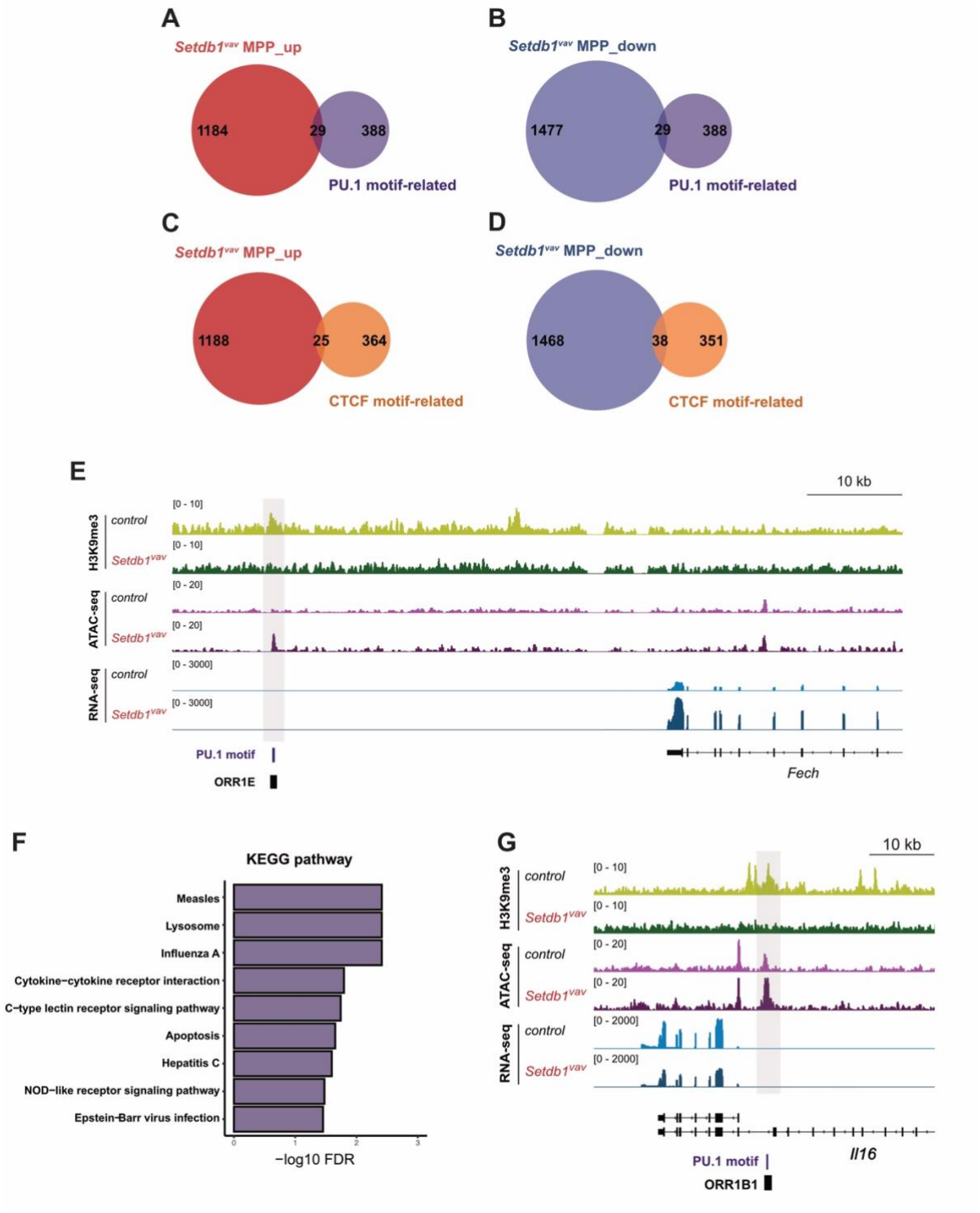
A
Setdb1vav MPP_up
1184
29
388
PU.1 motif-related
B
Setdb1vav MPP_down
1477
29
388
PU.1 motif-related
C
Setdb1vav MPP_up
1188
25
364
CTCF motif-related
D
Setdb1vav MPP_down
1468
38
351
CTCF motif-related
E
10 kb
H3K9me3
control
Setdb1vav
ATAC-seq
RNA-seq
[0 - 10]
[0 - 20]
[0 - 3000]
PU.1 motif
ORR1E
Fech
F
KEGG pathway
Measles
Lysosome
Influenza A
Cytokine−cytokine receptor interaction
C−type lectin receptor signaling pathway
Apoptosis
Hepatitis C
NOD−like receptor signaling pathway
Epstein−Barr virus infection
−log10 FDR
G
10 kb
[0 - 2000]
PU.1 motif
ORR1B1
Il16

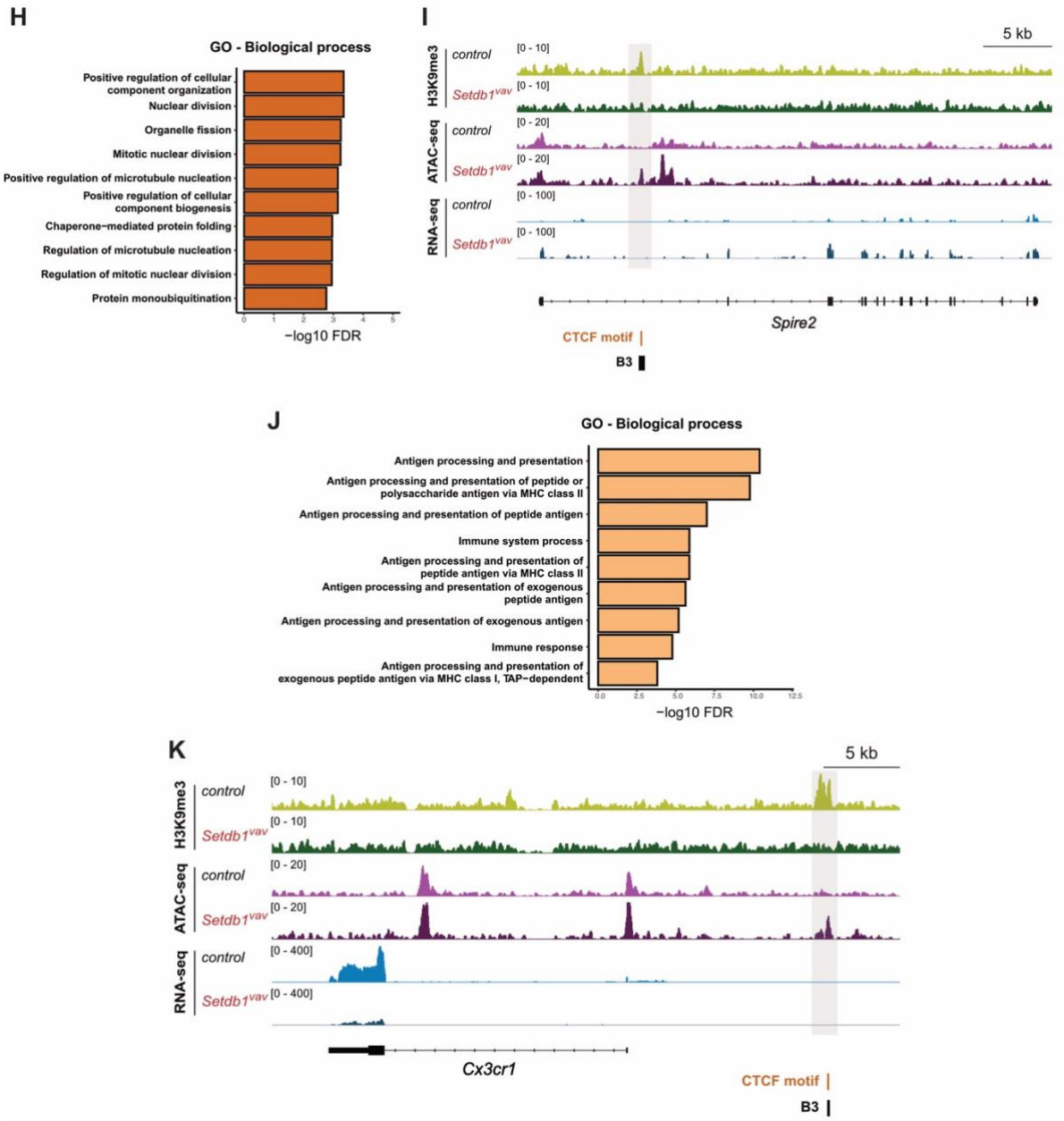

Figure 3.18 | Potential target genes associated with TF binding sites are deregulated

(A) Scaled Venn diagram indicating the overlap of the significantly upregulated genes (P_{adj} < 0.05, log2 fold change > 0.5) and PU.1 motif-related genes (TSS within ± 100 kb window around PU.1 motif). (B) Scaled Venn diagram indicating the overlap of the significantly downregulated genes (P_{adj} < 0.05, log2 fold change > 0.5) and PU.1 motif-related genes (TSS within ± 100 kb window around PU.1 motif). (C) Scaled Venn diagram indicating the overlap of the significantly upregulated genes (P_{adj} < 0.05, log2 fold change > 0.5) and CTCF motif-related genes (TSS within ± 100 kb window around CTCF motif). (D) Scaled Venn diagram indicating the overlap of the significantly downregulated genes (P_{adj} < 0.05, log2 fold change > 0.5) and CTCF motif-related genes (TSS within ± 100 kb window around CTCF motif). (E) IGV snapshot of the *Fech* locus at the intersection in A. Shaded region indicates the hypomethylated motif in the gained ATAC peak in *Setdb1*^{vav} LSK. Black box indicates ERV coordinate. (F) KEGG pathway analysis using ShinyGO tool (Ge et al., 2020) for the genes at the intersection in B. (G) IGV snapshot of the *Il16* locus at the intersection in B. Shaded region indicates the hypomethylated motif in the gained ATAC peak in *Setdb1*^{vav} LSK. Black box indicates ERV coordinate. (H) GO biological pathway analysis using ShinyGO tool for the genes at the intersection in C. (I) IGV snapshot of the *Spire2* locus at the intersection in C. Shaded region indicates the hypomethylated motif in the gained ATAC peak in *Setdb1*^{vav} LSK. Black box indicates B3 subfamily of B2 SINE coordinate. (J) GO biological pathway analysis using ShinyGO tool for the genes at the intersection in D. (K) IGV snapshot of the *Cx3cr1* locus. Shaded region indicates the hypomethylated motif in the gained ATAC peak in *Setdb1*^{vav} LSK. Black box indicates B3 subfamily of B2 SINE coordinate.

4. Discussion

4.1. SETDB1 demonstrates a progressive and developmentally distinct phenotype during hematopoiesis

Definitive hematopoiesis in mice peaks at E14.5 in FL, and then moves to BM until after birth (reviewed in section 1.1.1). During this period, HSCs demonstrate developmentally distinct phenotypic and functional features to ensure proper development and maintenance of the hematopoietic system (reviewed in section 1.1.3). The pivotal role of histone methyltransferase SETDB1 in the maintenance of cell identity during early development and different cellular contexts, as well as adult HSPCs (reviewed in section 1.3.2), prompted us to investigate its significance during FL and postnatal hematopoiesis. In this study, we deleted *Setdb1* at E9.5-E10.5, the earliest developmental time point of definitive hematopoiesis using *Vav-Cre* deleter. Interestingly, *Setdb1*^{vav} embryos developed normally with no change in FL cellularity; however, the enhanced lethality at the postnatal stage (3-4 wk) which was accompanied by hypocellularity in the central hematopoietic organs, namely, BM and thymus, pointed to the hematopoietic failure (Figure 3.1). The *Setdb1*^{vav} postnatal phenotype resembled that of adult BM. *Setdb1* ablation in adult HSCs led to expanded apoptosis of these cells, severe BM failure, and mice lethality within 3 weeks after *Setdb1* deletion (Koide et al., 2016). Assessment of hematopoietic compartments in the FL and postnatal (2wk) BM demonstrated a developmental stage-specific phenotype. Expansion of LT-HSCs and MPPs in the FL was followed by the postnatal loss of LT-HSCs (Figure 3.4). Marked decrease of FL LT-HSCs at the G0 phase of cell cycle and lack of apoptosis further supported the fact that FL LT-HSCs devoid of *Setdb1* enhanced cycling capacity while maintaining normal survival (Figure 3.5, Figure 3.6). In contrast, 2wk LT-HSCs exhibited enhanced apoptosis (Figure 3.5). *Setdb1*^{vav} LT-HSC phenotype was indicative of a phenomenon called “stem cell exhaustion,” in which the population of LT-HSC declined progressively after initial expansion (Jacob et al., 2010).

When it came to lineage specification, *Setdb1* ablation resulted in a compromised lymphoid differentiation while at the same enhancing myeloerythroid output. Thymocyte-specific deletion of *Setdb1* induced a partial transition block in the double-positive (DP) to single-positive (SP) cells and subsequent hypocellularity of the thymus (Martin et al., 2015; Takikita et al., 2016). Similarly, *Setdb1* deficiency diminished T cell reservoir in the thymus and spleen, which could be partly attributed to two developmental blocks, first at DN3 to DN4 stage and second at DP to both CD4 and CD8 SP cells (Figure 3.2). Another clue for impaired lymphopoiesis arose from the fact that despite T cell pool shrinkage, surprisingly, the comparable number of CLPs were generated upon *Setdb1* deletion, implying the compromised

homing potential of CLPs to the thymus. Besides, in line with our previous finding (Pasquarella et al., 2016), *Setdb1* was essential for B cell development since no B cell was generated from *Setdb1*^{vav} CLPs. On the other side of the hematopoietic system, myeloerythroid lineage specification enhanced progressively, as demonstrated by the frequency of granulocyte/monocyte cells in *Setdb1*^{vav} FL and 2wk BM. The same held true when we looked at their immediate progenitors, GMPs. In the same way, the early erythroid progenitors continuously expanded in *Setdb1*^{vav} FL and 2wk spleen (Figure 3.3). However, similar to *Setdb1*^{vav} CLPs, the frequency of MEPs remained unaltered in *Setdb1*^{vav} FL. The phenotypic consequences of *Setdb1* deletion during fetal and postnatal hematopoiesis was unique when compared to the previously reported adult hematopoiesis (Koide et al., 2016). Except for adult BM MEPs, which phenocopied the FL counterparts, all the other progenitors severely declined in adult BM upon *Setdb1* loss.

Together, *Setdb1* ablation in the entire hematopoietic system generated a progressive phenotype from fetal to postnatal, as demonstrated by 1) stem cell exhaustion feature of LT-HSCs, 2) myeloerythroid expansion. Importantly, fetal and postnatal hematopoiesis was distinct from that of adult, thereby indicating a developmental stage-specific phenotype (Figure 4.1).

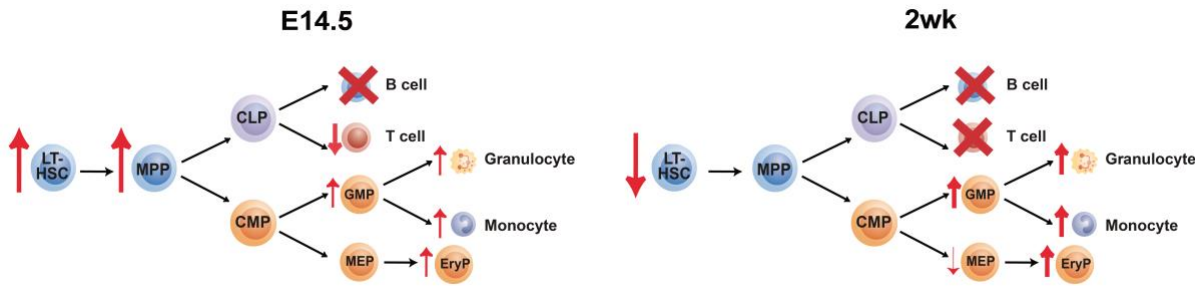

Figure 4.1 | Summary of the progressive *Setdb1*^{vav} phenotype in hematopoietic system

Setdb1 deletion in the fetal liver HSPCs demonstrates a progressive phenotype. Expansion and normal survival of fetal liver LT-HSCs at E14.5 is followed by the apoptosis and depletion of these cells at around two weeks after birth (postnatal). Lymphoid lineage specification is compromised downstream of the CLP population, while at the same time, myeloerythroid expansion becomes more pronounce over time, leading to biased lineage differentiation.

4.2. SETDB1 is central for functional capacity of FL HSPCs

The functional characteristics of HSCs can be assessed by a variety of approaches. In this study, we took advantage of the gold standard transplantation experiment for the assessment of several aspects of HSPCs function. We showed that *Setdb1* presence is vital for the engraftment potential since FL *Setdb1*^{vav} HSPCs were incapable of repopulating the recipient BM in the competitive transplantation setting. Besides, both myeloerythroid and lymphoid colony formation ability of FL *Setdb1*^{vav} hematopoietic progenitors was impaired in *in vitro* culture (Figure 3.7). Reduced number of myeloerythroid colonies, despite the expansion of these cells *in vivo*, hinted to their probable vulnerability to *in vitro* culture. Another fundamental feature of HSCs is the migrating function (Ciriza et al., 2013). Compromised function of FL *Setdb1*^{vav} HSPCs for hematopoietic reconstitution after transplantation raised the question of whether these cells were able to home to the BM niche. Indeed, FL *Setdb1*^{vav} HSPCs endowed with less, but not significant, homing potential (Figure 3.8). However, a significant decrease in the surface expression of homing markers on *Setdb1*^{vav} LSKs substantiated the results of the homing experiment. Coherently, several gene sets, including the ones implicated in cellular communication and homing such as cell adhesion molecules (CAMs) and Cytokine-cytokine receptors, depleted in *Setdb1*^{vav} MPPs (Figure 3.12). Thus, not only the hematopoietic reconstitution was impaired, but it also could be attributed, at least in part, to inefficient homing.

4.3. Transcriptome analysis corroborates the phenotypic and functional features of FL *Setdb1*^{vav} HSPCs

To date, there was no genome-wide transcriptional profiling for *Setdb1*-deleted LT-HSCs and MPPs, let alone the FL stage. Our study provided the first comprehensive transcriptome analysis of these populations to better elucidate their distinct phenotypic and functional properties during FL hematopoiesis, in the absence of *Setdb1*. Previous studies highlighted the importance of *Setdb1* in the repression of tissue-inappropriate genes (Yuan et al., 2009; Karimi et al., 2011; Tan et al., 2012; Koide et al., 2016). Likewise, in FL LT-HSCs and MPPs, *Setdb1* was essential for repressing the non-hematopoietic genes associated with other tissues, including testis, oocyte, germ cell, neuron, and muscle, thereby maintaining the hematopoietic cell identity (Figure 3.9). In the GSEA analysis, enrichment of several pathways related to cell cycle supported the enhanced cycling and subsequent expansion of *Setdb1*^{vav} LT-HSCs and MPPs (Figure 3.10). Enhanced cycling requires higher energy production. In quiescent adult BM HSCs, glycolysis is the main metabolic pathway for energy production (Suda et al., 2011; Klimmeck et al., 2012). Interestingly, cycling FL HSCs are fueled not only

by glycolysis but also additionally by oxidative phosphorylation (OxPhos) (Manesia et al., 2015). In consistence, the OxPhos gene set enriched in *Setdb1*^{vav} LT-HSCs to meet the energy demand of highly proliferating cells as well as in *Setdb1*^{vav} MPPs. The fact that FL *Setdb1*^{vav} LT-HSCs acquired additional energy capacity reasoned their normal survival and proliferation potential despite *Fbp2* upregulation. The muscle gluconeogenic enzyme, *Fbp2*, is normally transcriptionally repressed in other organs, including HSPCs, thereby favoring glycolysis (Ito and Suda, 2014). In *Setdb1*-depleted adult HSPCs, the upregulation of *Fbp2* resulted in ATP depletion and impaired cell repopulation (Koide et al., 2016). Our data supported this notion that FL *Setdb1*^{vav} LT-HSCs could well tolerate the antagonized glycolysis, thanks to having been fueled by OxPhos.

Beyond non-hematopoietic genes, other transcriptional changes occurred. Enhanced proliferation and subsequent abundance of HSPCs seemed contradictory to the impaired function of *Setdb1*^{vav} HSPCs *in vivo*. However, significant downregulation of several stem cell genes, including the FL-specific *Hmga2* gene, all conferring self-renewal advantage, and depletion of the LT-HSC gene signature in *Setdb1*^{vav} LT-HSCs further confirmed the compromised function (Figure 3.11). Our data suggested that the proliferating *Setdb1*^{vav} LT-HSCs lost their cell identity and that the enhanced proliferation could not be attributed to the enhanced self-renewal but rather to other inducing factors, for example, lymphopenia.

In MPPs, lineage segregation is governed by the two master regulators PU.1 and GATA1 (Shivdasani et al., 1997; Laslo et al., 2006). Transcriptome analysis of FL *Setdb1*^{vav} MPPs provided molecular evidence about the tipped lineage priming in these cells (Figure 3.11). Indeed, transcriptional changes of *Setdb1*^{vav} MPPs were similar to that of *PU.1* as well as its target *Mef2c* deletion (Stehling-Sun et al., 2009; Pang et al., 2018). MPPs devoid of *PU.1* demonstrated impaired progression toward LMPPs, resulting in diminished LMPPs and CLPs. Moreover, transcription of several genes that were dependent on *PU.1* decreased, including *Csf1r*, *Flt3*, *Il7r*, and *Mef2c*. Concomitantly, genes involved in myeloid and erythroid differentiation, such as *Cebpe* and *Gfi1*, were upregulated (Pang et al., 2018). Besides, *Mef2c* showed to be involved in transcriptional regulation of lymphoid development and myeloid versus lymphoid cell fate ‘choice’ in MPPs. *Mef2c*-deficient MPPs were incapable of generating CLPs, B cells, T cells, and NK cells, but showed enhanced myeloid output. Transcriptional profiling revealed the downregulation of lymphoid genes such as *Ets1*, *Rag1*, *Flt3*, *Tcf7*, and *Pbx1* and upregulation of myeloid genes, including *Fcgr2b*, *Cebpa,* and *Lyc6c1* (Stehling-Sun et al., 2009). All aforementioned transcriptional events occurred in *Setdb1*^{vav} MPPs, implying the role of PU.1 and its target Mef2c for the biased lineage specification. Of note, despite the shared transcriptional changes, *Setdb1*^{vav} MPPs were potent to generate a comparable number of CLPs to the control. One explanation is that the extent of transcriptional changes in

Setdb1^{vav} MPPs is milder than that of *PU.1* and *Mef2c* complete deletion. Although lymphoid-affiliated genes are significantly downregulated, *Setdb1*^{vav} MPPs are still endowed with the minimal activity of these genes, which allows for lymphoid priming and CLP generation from MPPs. Moreover, the severe developmental block in *Setdb1*^{vav} CLPs toward B and T cell differentiation could account for their accumulation. In line with this, the lymphoid differentiation gene signature was depleted in *Setdb1*^{vav} MPPs (Figure 3.11). Another reason could be the defective homing potential of *Setdb1*^{vav} CLPs to the thymus, leading to their congestion in FL and BM. The chemokine receptors CCR9 and CCR7 are required for migrating and seeding of lymphoid progenitors in the thymus (Ramond et al., 2014). Coherently, the expression of both chemokine receptors markedly decreased (Figure 3.12).

Enhanced myeloerythroid output could be, in part, attributed to the downregulation of lymphoid specific genes, thereby favoring the myeloerythroid lineage specification. For example, genes such as *Cebpe* and *Gfi1* upregulated in *PU.1*-deleted MPPs, and *Fcgr2b* and *Lyc6c1* upregulated in *Mef2c*-deficient MPPs were among the myeloerythroid genes with enhanced expression in *Setdb1*^{vav} MPPs. Another example was the *Pbx1* gene. In CMPs, *Pbx1* gene restrains the expression of GMP specific genes and subsequent myeloid differentiation (Ficara et al., 2013). Assuming that *Pbx1* downregulation endured in *Setdb1*^{vav} CMPs, enhanced GMP commitment and subsequently higher myeloid output could also be attributed to this molecular event. In addition, *Setdb1*^{vav} MPPs demonstrated a striking upregulation of erythroid-affiliated genes, *GATA1* on the top as the master regulator of erythroid lineage priming (Figure. 3.11). Consistently, the gene signature associated with erythropoiesis and heme metabolism positively enriched in *Setdb1*^{vav} MPPs (Figure 3.10, Figure 3.11). Surprisingly, despite the transcriptional activation of erythroid lineage, the number of MEPs in *Setdb1*^{vav} FL remained unchanged compared to control. However, the progressive expansion of erythroid progenitors corroborated the transcriptional changes (Figure 3.3). One explanation could be that the rate of erythroid differentiation exceeded that of MEP commitment from *Setdb1*^{vav} CMPs. This speculation seems plausible if we consider that *Setdb1*^{vav} CMPs are endowed with a premature commitment toward GMPs, as mentioned above, suggesting that the CMPs balanced commitment to their immediate progenitors is tipped.

Previous studies pointed to the fact that *Setdb1* depletion resulted in the expression of distinct classes of retrotransposons in different cell types. Moreover, activation of a given ERV has been attributed to the presence of the cell type-specific transcription factor. For example, in pro-B cell, activation of MLV ERV was linked to the binding of Pax5, the B cell-specific TF (Collins et al., 2015). However, expression of the similar MLV family in *Setdb1*^{vav} LT-HSC and MPPs raised the question of whether binding of the cell-specific TF is sufficient for their expression. In addition, significant but mild expression of non-LTR retrotransposons such as

LINE-L1 and B2 SINE in *Setdb1*^{vav} MPPs has not been reported before in hematopoietic cells. Moreover, expression of MuLV and MMVL30 (class I) ERVs in *Setdb1*^{vav} LT-HSC and MPPs was similar to that of pro-B cells (Figure 3.13).

We previously showed that expression of ERVs and enhanced production of viral proteins, which overwhelmed endoplasmic reticulum (ER), led to the accumulation of misfolded or unfolded proteins and subsequently triggered unfolded protein response (UPR), thereby leading to apoptosis in pro-B cells (Pasquarella et al., 2016). However, despite the enrichment of the UPR gene set in both *Setdb1*^{vav} LT-HSC and MPPs, no apoptosis detected in these cells (Figure 3.5, Figure 3.10). This can be explained by the mechanism which protects the proliferating FL-HSCs during the peak of their expansion (E14.5-E15.5) in FL (Sigurdsson and Miharada, 2018). It was shown that the bile acid pool of either maternal or fetal sources in the FL was the key mechanism to manage ER stress. Consistently, bile acids functioned as chemical chaperons to suppress ER and, consequently, the generation of misfolded or unfolded proteins in the growing FL HSCs (Sigurdsson et al., 2016). Similarly, *Setdb1*^{vav} LT-HSC and MPPs could presumably take advantage of the bile acid pool in the FL and reduce the ER burden by suppressing the excessive production of misfolded or unfolded viral proteins, thereby maintaining their survival.

4.4. SETDB1 directly silences non-hematopoietic genes and retrotransposons in FL LSKs

So far, the direct function of SETDB1 in gene silencing is attributed to the deposition of the H3K9me3 mark on gene promoters, including developmental genes and lineage-specific/non-specific genes (Bilodeau et al., 2009; Yuan et al., 2009; Karimi et al., 2011; Tan et al., 2012; Koide et al., 2016). In fact, in *Setdb1*^{vav} LSKs, genes demonstrating the highest level of expression were those which lost H3K9me3 at their promoters, including *Fbp2*, *Dnah8*, *Gstp2*, and *M1ap*. Of note, none of the promoter-hypomethylated genes were hematopoietic-specific (Figure 3.14). As to retrotransposons, while the majority of derepressed ERVs (MuLV and MMVL30 (class I), RLTR50A, MMERVK10C (class II)) demonstrated hypomethylation, derepression of IAPLTR3 (class II), and MER74C (class III) seemed to be independent of SETDB1 as shown by maintained H3K9me3 level in the absence of *Setdb1* (Figure 3.15). The expression of these ERVs might be due to the other changes in their chromatin environment, like loss of DNA methylation. Moreover, the LINE-L1 element showed mild reduction of the H3K9me3 level, similar to MEF cells (Kato et al., 2018). Generation of chimeric transcripts, which denotes ERV-derived transcripts extending to the nearby genes (aka read-through transcripts), has been reported previously, leading to the upregulation of ERV neighboring

genes (Karimi et al., 2011; Tan et al., 2012; Liu et al., 2014). In *Setdb1*^{vav} MPPs, the orientation of the upregulated genes with respect to the derepressed ERV disputed the possibility of chimeric transcript formation. To this end, no chimeric transcript was detected upon *Setdb1* ablation in other hematopoietic cells (Koide et al., 2016; Pasquarella et al., 2016).

4.5. Chromatin accessibility is modulated by SETDB1-mediated H3K9me3 deposition in FL LSKs

The fact that regulation of hematopoietic genes was not directly regulated by SETDB1 and considering the SETDB1 role in heterochromatinization of the genome, we hypothesized that SETDB1 should control gene expression by modulating chromatin accessibility landscape. Indeed, *Setdb1* loss changed the chromatin state toward a more accessible and less compacted state, as demonstrated by the higher number of ATAC peaks in *Setdb1*^{vav} LSKs (Figure 3.16). More interestingly, the newly emerged ATAC peaks harbored the TF binding sites related to hematopoietic development (PU.1 and other ETS TFs), genome organization, and transcriptional regulator (CTCF). We further showed that the alteration of chromatin accessibility was the direct consequence of H3K9me3 hypomethylation. More specifically, in *Setdb1*^{vav} LSKs, the accessible chromatin regions containing PU.1 and CTCF motifs explicitly lost the H3K9me3 mark, indicating that SETDB1-mediated H3K9me3 deposition was crucial for proper organization of chromatin accessibility (Figure 3.17).

4.6. SETDB1 fine-tunes gene expression by protecting excessive PU.1 and CTCF binding motifs

Expression of PU.1 along with other ETS TFs and CTCF in *Setdb1*^{vav} MPPs further supported this notion that putative binding of the available TFs to newly emerged binding motifs could contribute to gene deregulation (Figure 3.16 F). Indeed, there was an overlap between genes significantly deregulated in *Setdb1*^{vav} MPPs and those within the ± 100 kb window around the PU.1 and CTCF binding motifs in *Setdb1*^{vav}-specific ATAC peaks in LSKs (Figure 3.18 A-D). Surprisingly, significantly downregulated genes neighboring these putative motifs seemed to be more relevant to the hematopoietic phenotype, as demonstrated by the enrichment of the “cytokine-cytokine receptor interaction” pathway in downregulated PU.1 motif-related genes (Figure 3.18 F). Consistently, downregulated CTCF motif-related genes enriched for “antigen processing and presentation” and “immune response” pathways (Figure 3.18 H, J).

Mechanism of action of PU.1 in inducing the expression of its target genes relates to PU.1 concentration and the affinity of binding sites (Pham et al., 2013; Rothenberg et al.,

2019). The excessive PU.1 binding site that emerged upon *Setdb1* loss could shift the genome-wide PU.1 binding, which could also include some of the PU.1 high-affinity motifs. The subsequent shift in the concentration gradient, as well as downregulation of PU.1, could eventually lead to the depletion or low concentration of PU.1 on its actual targets, thereby perturbing the regular PU.1-guided transcriptional events, for example, lymphoid lineage specification in MPPs. Besides, the previous study showed that PU.1 mediated transcriptional repression and activation by redirecting the binding of the co-TFs (Hosokawa et al., 2018). To this end, redistribution of PU.1 binding might lead to aberrant binding of the partner TFs, leading to another layer of gene deregulation. Moreover, PU.1 instructs lineage commitment through its interplay with GATA1 (Burda et al., 2010). It was previously reported that PU.1 repressed GATA1-target genes by binding to GATA1 on DNA, recruiting pRb, Suv39h, and HP1α, depositing of H3K9me, and subsequent formation of the repressive chromatin environment (Stopka et al., 2005). In *Setdb1*^{vav} MPPs, the upregulation of erythroid-specific genes and higher erythroid output might be due to the scarce of PU.1 on GATA1 target genes, leading to disruption of the repressive chromatin complex.

The sequence-specific DNA binding factor CTCF has multifaceted functions. The physical interactions of the genomic regions bound by CTCF with themselves and/or with other regions establish the CTCF as an ‘‘architectural protein’’ (Ong and Corces, 2014). For instance, it can function as a transcriptional insulator, which blocks enhancer-promoter interactions and/or a domain barrier, which protects the active genomic regions from the spread of neighboring repressive epigenetic marks (Bell et al., 1999; Cuddapah et al., 2009). Moreover, CTCF demarcates the boundaries of topologically associating domains (TADs), thereby allowing for the local enhancer-promoter interaction within a defined TAD across which the interactions are restricted (Dixon et al., 2012; Gorkin et al., 2014). In *Setdb1*^{vav} LSKs, enrichment of CTCF motifs in ATAC peaks was suggestive of the implication of CTCF in gene deregulation. As such, potential binding of CTCF to these motifs could lead to 1) downregulation of CTCF-motif neighboring genes due to the insulating function of CTCF, 2) upregulation of CTCF-motif neighboring genes due to the structural collapse or change of domain architecture. The latter was shown in neurons, in which loss of *Setdb1* and excessive CTCF binding shifted the repressive long-range contacts toward facilitative shorter-range promoter-enhancer looping, thereby leading to gene upregulation (Jiang et al., 2017). Other sequence features at TAD boundaries are SINE elements. Moreover, the highest fraction of CTCF binding sites is embedded in SINEs at both TAD and non-TAD boundaries (Kentepozidou et al., 2020). Interestingly, in *Setdb1*^{vav} LSKs, the hypomethylated CTCF motifs in ATAC peaks were embedded in the B3 subfamily of B2 SINEs (Figure 3.18 I, K). This points to the fact that SETDB1-mediated H3K9me3 deposition at SINEs is integral to protect the

genome-wide CTCF binding, thereby suggesting a role for SETDB1 in the maintenance of domain architecture and proper gene expression.

4.7. Conclusion and future directions

In conclusion, our study provided a detailed analysis of *Setdb1* ablation during FL hematopoiesis. We demonstrated that *Setdb1* deletion in FL LT-HSCs and MPPs generated a unique phenotype, which was different from that of adult HSPCs, thereby corroborating the SETDB1 cell type and developmental stage-specific phenotype. To this end, some of the phenotypic features of *Setdb1*-ablated FL HSPCs could be attributed to their developmentally distinct characteristics in comparison to adult HSPCs. This was the first study to show the significance of SETDB1 for the maintenance and function of FL HSPCs. *Setdb1* deletion led to the loss of HSPCs identity and skewed differentiation toward myeloerythroid lineage. We showed that *Setdb1* ablation resulted in both non-hematopoietic and hematopoietic transcriptional events. While SETDB1 governed non-hematopoietic transcriptional changes in adult HSPCs (Koide et al., 2016), our study delineated the first hematopoietic transcriptional events in HSPCs devoid of *Setdb1*. Restriction of SETDB1-silencing function to the promoters of non-hematopoietic genes and retrotransposons, pointed to the existence of an additional mechanism underlying the hematopoietic genes regulation. Indeed, we showed that SETDB1 organized chromatin accessibility through deposition of H3K9me3 at ERVs (class III) and B2 SINEs retrotransposons, which embedded PU.1 and CTCF motifs, respectively. In fact, there was an overlap between deregulated genes, especially the downregulated immune genes, and the PU.1 and CTCF motif-associated genes. Therefore, we postulate that apart from gene promoters and retrotransposons silencing, there is an additional mechanism by which SETDB1 finetunes gene expression that is through protecting inappropriate PU.1 and CTCF binding sites. Putative binding of PU.1 and CTCF to these unprotected and exposed motifs leads to redistribution of TFs, which, for example, in the case of CTCF, results in either enhanced insulation or altered domain architecture, promoter-enhancer interaction, and transcriptional changes (Figure 4.2).

To confirm the proposed model, it would be of high interest to ask whether the binding of PU.1 and CTCF is linked to their biological functions. One option would be to map PU.1 and CTCF in *Setdb1*^{vav} HSPCs to narrow down the analysis on those target genes either bound by these TFs or lost the TF occupancy. In light of advancement in TFs ChIP protocols tailored to low cell numbers, this experiment would be possible in the near future. To complement this experiment, and to gain insight into the target gene activation or repression, the identification of enhancer landscape (H3K4me/H3K27ac) and subsequent integrative analysis using

transcriptome and TF occupancy data are suggested. Given the role of CTCF as architectural protein in TAD formation and redistribution of CTCF binding motifs in the absence of *Setdb1*, analysis of TADs architecture using the Hi-C method will be of particular interest to delineate the transcriptional changes. Collectively, these analyses will shed light on the SETDB1 implication in shaping the chromatin landscape, enhancer-promoter interaction mediated by CTCF, and domain architecture, which can eventually grant or impede access to the transcriptional machinery, thereby fine-tuning the transcriptional changes, fundamental for HSPCs function.

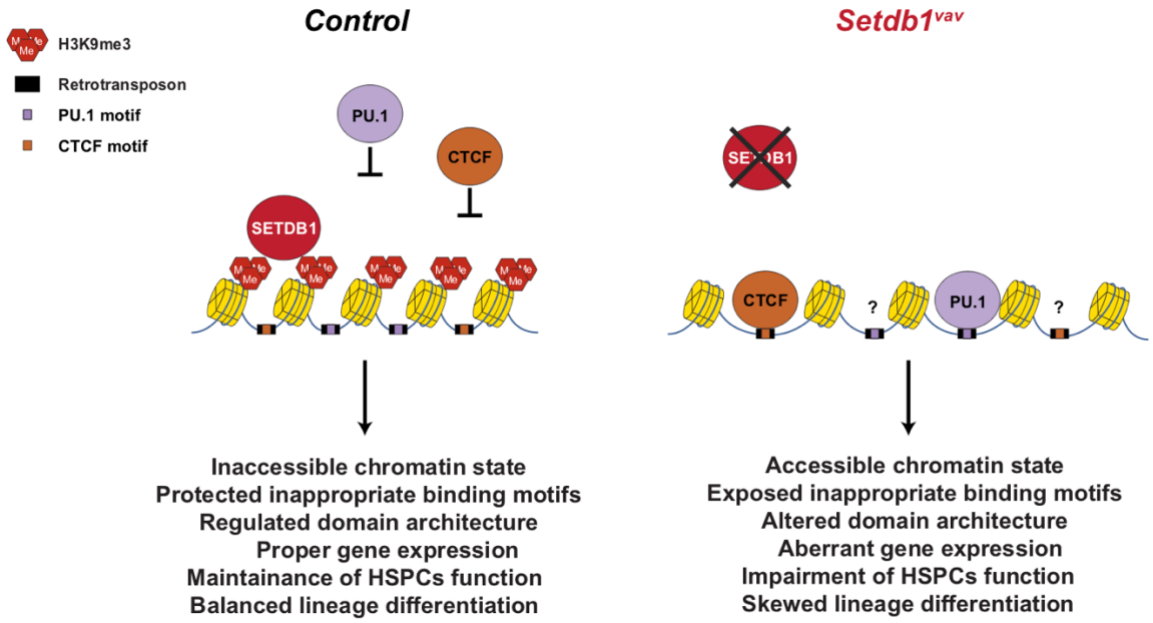

Figure 4.2 | The proposed model of *Setdb1*-mediated gene regulation

SETDB1-mediated H3K9me3 protects the inappropriate, retrotransposon-embedded PU.1 and CTCF binding sites in HSPCs. SETDB1 loss and subsequent hypomethylation shift the chromatin state toward more accessibility on these binding motifs. Putative binding of PU.1 and CTCF to the exposed and unprotected motifs results in the redistribution of transcription factors and subsequent gene deregulation.

5. Materials

5.1. Mice

Transgenic mice	Strain
Setdb1 flox; flox	C57BL/6
Vav-cre	C57BL/6
Wild type (CD45.2)	C57BL/6
Wild type (CD45.1)	B6/SJL
Wild type (CD45.1/2)	B6/SJL

5.2. Antibodies

FACS antibodies

Antibody (anti-mouse)	Clone	Fluorochrome	Provider	Identifier
CD117	2B8	APC-Alexa Fluor 780	Thermo Fischer Scientific	Cat# 47-1171-80
CD127(IL7Rα)	A7R34	PE-Cy5	Thermo Fischer Scientific	Cat# 15-1271-81
CD150	mShad150	APC	Thermo Fischer Scientific	Cat# 17-1502-80
CD150	mShad150	FITC	Thermo Fischer Scientific	Cat# 11-1502-80
CD16/32	93	PE-Cy7	Thermo Fischer Scientific	Cat# 25-0161-81
CD34	RAM34	eFluor 660	Thermo Fischer Scientific	Cat# 50-0341-82
CD3e	145-2C11	APC-eFluor 780	Thermo Fischer Scientific	Cat# 47-0031-80
CD45.1	A20	PE-Cy7	Thermo Fischer Scientific	Cat# 25-0453-81
CD45.2	104	FITC	Thermo Fischer Scientific	Cat# 11-0454-81
CD45R/B220	RA3-SB2	APC-Alexa-Fluor 750	Thermo Fischer Scientific	Cat# 27-0452-82
CD48	HM48-1	PE-Cy7	Thermo Fischer Scientific	Cat# 25-0481-80
CD62L	MEL-14	FITC	Thermo Fischer Scientific	Cat# 11-0621-82
CD71	R17217	PE	Thermo Fischer Scientific	Cat# 12-0711-81
CD8α	53-6.7	PE-Cy7	Thermo Fischer Scientific	Cat# 25-0081-81
Ki67	SolA15	eflour 450	Thermo Fischer Scientific	Cat# 48-5698-80
Ly-6G(Gr-1)	RB6-8C5	PE	Thermo Fischer Scientific	Cat# 12-5931-81
Sca-1	D7	FITC	Thermo Fischer Scientific	Cat# 11-5981-81
Sca-1	D7	PerCP-Cyanine 5.5	Thermo Fischer Scientific	Cat# 45 5981-80
er119	TER119	APC-AlexaFluor 780	Thermo Fischer Scientific	Cat# 47-5921-80
Ter119	TER119	PE	Thermo Fischer Scientific	Cat# 12-5921-81
CD11b/Mac-1	M1/70	PE	BD Bioscience	Cat# 553311
CD11c	HL3	PE	BD Bioscience	Cat# 553802
CD127(IL7Rα)	SB/199	BV421	BD Bioscience	Cat# 566300
CD19	1D3	PE	BD Bioscience	Cat# 553786
CD3e	145-2C11	PE	BD Bioscience	Cat# 553064
CD4	PM4-5	PE	BD Bioscience	Cat# 553049
CD45R/B220	RA3-6B2	PE	BD Bioscience	Cat# 561878
CD49d (VLA-4)	R1-2	BV786	BD Bioscience	Cat# 564397
CD8α	53-6.7	PE	BD Bioscience	Cat# 553033
Mouse BD Fc Block	2.4G2	purified	BD Bioscience	Cat# 553142

ChIP antibody

Target	ID	Weight	Host	Type	Provider	Identifier
H3K9me3	249	17 kDa	rabbit	polyclonal	Active Motif	39161

5.3. Reagents and Commercial assays

Reagent/Commercial assay	Provider	Identifier
Agencourt AMPure XP	Beckman Coulter	Cat# A63882
Agilent High Sensitivity DNA Kit	Agilent	Cat# 5067-4626
Agilent RNA 6000 Pico Kit	Agilent	Cat# 5067-1513
Annexin V Apoptosis Detection Kit FITC	Thermo Fischer Scientific	Cat# 88-8005-72
Anti-PE MicroBeads	Miltenyi	Cat# 130-048-801
Arcturus® PicoPure® RNA Isolation Kit	Thermo Fischer Scientific	Cat# KIT0204
CellTrace CFSE Cell Proliferation Kit	Thermo Fischer Scientific	Cat# C34570
cOmplete, Mini, EDTA-free Protease Inhibitor Cocktail	Roche Diagnostics	Cat# 4693159001
Digitonin	Promega	Cat# G9441
Dynabeads Protein A/Protein G	Thermo Fischer Scientific	Cat# 10015D
Foxp3 / Transcription Factor Staining Buffer Set	Thermo Fischer Scientific	Cat# 00-5523-00
Methocult M3434	STEMCELL Technologies	Cat# 03434
Methocult M3630	STEMCELL Technologies	Cat# 03630
MicroPlex Library Preparation Kit v2	Diagenode	Cat# C05010012
MNase	Biolabs	Cat# M0247S
Nextera DNA Library Preparation Kit	Illumina	Cat# FC-121-1030
Nuclei Isolation Kit: Nuclei EZ Prep	Sigma	Cat# NUC-101
Osteosoft	Merck	Cat# 101728
PCR clean-up MinElute kit	Qiagen	Cat# 28006
Qubit dsDNA HS Assay kit	Thermo Fischer Scientific	Cat# Q33854
red blood cell lysis buffer	BD Bioscience	Cat# 555899
RNase-Free DNase Set	Qiagen	Cat# 79254
SMART-Seq v4 Ultra Low Input RNA Kit	Clontech	Cat# 634888
Zombie Aqua Fixable Viability Dye	BioLegend	Cat# 423101

5.4. High-throughput sequencing libraries

Library Name	ID	Experiment	Sequencing mode	Index
LT-HSC_Cont-2	GS98	RNA-seq	50 bp paired-end	ATCACG
LT-HSC_Cont-3	GS99	RNA-seq	50 bp paired-end	CGATGT
LT-HSC_Cont-4	GS100	RNA-seq	50 bp paired-end	TTAGGC
LT-HSC_Mut-1	GS101	RNA-seq	50 bp paired-end	TGACCA
LT-HSC_Mut-3	GS102	RNA-seq	50 bp paired-end	ACAGTG
LT-HSC_Mut-4	GS103	RNA-seq	50 bp paired-end	GCCAAT
MPP_Cont-1	GS104	RNA-seq	50 bp paired-end	CAGATC
MPP_Cont-2	GS105	RNA-seq	50 bp paired-end	ACTTGA
MPP_Cont-3	GS106	RNA-seq	50 bp paired-end	GATCAG
MPP_Mut-1	GS107	RNA-seq	50 bp paired-end	TAGCTT
MPP_Mut-2	GS108	RNA-seq	50 bp paired-end	GGCTAC
MPP_Mut-4	GS109	RNA-seq	50 bp paired-end	CTTGTA
LSK_Input_con_1	GS353	ULI-NChIP-seq	50 bp single-end	ATCACG
LSK_H3K9me3_con_1	GS344	ULI-NChIP-seq	50 bp single-end	CGATGT
LSK_H3K9me3_con_2	GS229	ULI-NChIP-seq	50 bp single-end	CGATGT
LSK_H3K9me3_con_3	GS346	ULI-NChIP-seq	50 bp single-end	GCCAAT
LSK_H3K9me3_mut_1	GS345	ULI-NChIP-seq	50 bp single-end	TTAGGC
LSK_H3K9me3_mut_2	GS352	ULI-NChIP-seq	50 bp single-end	ACAGTG
LSK_H3K9me3_mut_3	GS347	ULI-NChIP-seq	50 bp single-end	CAGATC
FL_LSK_con1_Omni-ATAC	GS472	Omni-ATAC-seq	50 bp single-end	GCTACGCT
FL_LSK_con2_Omni-ATAC	GS444	Omni-ATAC-seq	50 bp single-end	AGGCAGAA
FL_LSK_mut1_Omni-ATAC	GS473	Omni-ATAC-seq	50 bp single-end	CGAGGCTG
FL_LSK_mut2_Omni-ATAC	GS445	Omni-ATAC-seq	50 bp single-end	CGAGGCTG

6. Methods

6.1. Mice

The *Setdb1* floxed mice were purchased from the EUCOMM project [*Setdb1*$^{tm1a(EUCOMM)Wtsi}$]. *Vav-cre* transgenic mice have been described previously (Ogilvy et al., 1999). All mice colonies were bred and housed in ventilated cages in pathogen-free conditions in the mouse facility at the Adolf Butenandt Institute and Biomedical Center (BMC). All mice experiments were performed in accordance with EU regulations. The 2- to 3-week-old mice and E14.5 embryos were used for experiments.

6.2. Hematoxylin and Eosin (H&E) staining of bone marrow

Sterna collected from 2-week-old control and *Setdb1*^{vav} mice were fixed in 4% formaldehyde, decalcified in Osteosoft (Merck), embedded in paraffin, sectioned, and stained with haematoxylin and eosin following deparaffinization and rehydration.

6.3. Flow cytometry and cell sorting

For FACS analysis, bone marrow cell suspension was prepared by flushing tibiae and femurs and filtered through 70 µm cell strainer. To obtain hematopoietic cells from spleen and thymus, the organs were gently meshed using the thumb rest of a 10 ml plunger on a 70 µm cell strainer. Fetal liver hematopoietic cells were prepared through dissociation of fetal livers using a 1 mL pipette and filtered through 70 µm cell strainer. Single cell suspensions from different organs were incubated with unconjugated CD16/CD32 Fc- blocking antibody (2.4G2) for 20 minutes at 4°C, and then were stained using antibody conjugates listed in section 5.2. Antibodies and dyes for 20 minutes at 4°C. For myeloid progenitor analysis, CD16/CD32 Fc-unblocked sample was subjected for staining. For fetal liver HSPCs analysis, anti-Mac1 (M1/70) was removed from the lineage$^+$ staining antibody cocktail. All antibodies were purchased from BD Bioscience and Thermo Fischer Scientific (listed in section 5.2. Antibodies).

For FACS sorting, fetal liver cells were filtered through a 40 µm filter, pre-treated with red blood cell lysis buffer (BD Bioscience) following the manufacturer's instructions, stained with PE-conjugated antibodies for lineage markers, and then enriched for lineage$^-$ HSPCs using Anti-PE MicroBeads (Miltenyi) through magnetic separation with the QuadroMACS separator. Cells were then labelled with fluorochrome-coupled antibodies specific for LT-HSCs, MPPs, and LSKs (listed in sections 5.2. Antibodies, and 6.4. Definition of hematopoietic cell populations). Based on the purpose of the experiment, the labeled cells were run on BD

FACSCanto or BD LSRFortessa for analysis or on FACSAria III or BD FACSAria Fusion for cell sorting. FACS) data were analyzed with Flowjo software (Tree Star).

6.4. Definition of hematopoietic cell populations

Cell population	Gating strategy
LT-HSC	Living cells, Lin^-, $Sca\text{-}1^+$, $c\text{-}kit^+$, $CD150^+$, $CD48^-$
MPP	Living cells, Lin^-, $Sca\text{-}1^+$, $c\text{-}kit^+$, $CD150^-$, $CD48^+$
LSK	Living cells, Lin^-, $Sca\text{-}1^+$, $c\text{-}kit^+$
CLP	Living cells, Lin^-, $IL7Ra^+$, $Sca\text{-}1^{low}$, $c\text{-}kit^{low}$
CMP	Living cells, Lin^-, $c\text{-}kit^{high}$, $Sca\text{-}1^-$, $CD34^+$,$CD16/32^{-/low}$
MEP	Living cells, Lin^-, $c\text{-}kit^{high}$, $Sca\text{-}1^-$, $CD34^-$, $CD16/32^-$
GMP	Living cells, Lin^-, $c\text{-}kit^{high}$, $Sca\text{-}1^-$, $CD34^+$, $CD16/32^+$
B cell	Living cells, Lymphocyte, $CD19^+$, $B220^+$
DN1	Living cells, $CD44^+$, $CD25^-$
DN2	Living cells, $CD44^+$, $CD25^+$
DN3	Living cells, $CD44^-$, $CD25^+$
DN4	Living cells, $CD44^-$, $CD25^-$
DP	Living cells, $CD3^+$, $CD4^+$, $CD8^+$
SP CD4	Living cells, $CD3^+$, $CD4^+$, $CD8^-$
SP CD8	Living cells, $CD3^+$, $CD4^-$, $CD8^+$
ProE	Living cells, $CD71^+$, $TER119^-$
TER119 erythroblasts	Living cells, $CD71^{+/-}$, $TER119^+$
Granulocyte/Macrophage/Monocyte	Living cells, $Gr\text{-}1^+$, $Mac\text{-}1^+$

6.5. Annexin V staining

One million bone marrow or fetal liver cells first stained for the specific markers to detect LSKs. Labelled cells were washed once with 1mL 1X PBS and then with 1mL 1X Annexin V binding buffer (Thermo Fischer Scientific). 5 µL of fluorochrome-conjugated Annexin V was added to the 100 µL cell suspension in Annexin V binding buffer. Cells were incubated at room temperature for 15 minutes, protected from light. Cell then were washed in 2 mL 1X Annexin V binding buffer and resuspended in 200 µL of 1X Annexin V Binding Buffer. 5 µL of Propidium Iodide Staining Solution added to discriminate the dead cells. Samples were analyzed within 1 hour, while stored at 4°C in the dark.

6.6. Intracellular staining for cell cycle analysis

For intracellular Ki-67 staining, similar to cell preparation for FACS sorting explained above, RBC-lysed fetal liver cells were subjected to MACS cell separation to enrich for $lineage^-$ cells. To eliminate dead cells, 1.5 million cells were first stained with Zombie Aqua Fixable Viability Dye (BioLegend) according to the manufacturer's instructions. After the last wash, cells were labeled for the specific markers to detect LSKs. Fixation and permeabilization were carried out using Foxp3/Transcription Factor Staining Buffer Set (Thermo Fischer Scientific)

following the manufacturer's protocol. After fixation/permeabilization, intracellular staining was performed with Ki-67 (SolA15) antibody. Samples were run on BD LSRFortessa for analysis.

6.7. Transplantation assay

For transplantation, fetal liver cells were collected from CD45.1 wild type (competitor) and CD45.2 *Setdb1*^{vav} or control (donor) E14.5 embryos. One million competitor fetal liver cells were mixed with either *Setdb1*^{vav} (*Setdb1*$^{flox/flox}$*; Vav-cre*) or control (*Setdb1*$^{flox/+}$*; Vav-cre* or *Setdb1*$^{flox/+}$*;* +/+) donor fetal livers cells at the ration of 1:1 and a total of two million cells were transplanted into the lethally irradiated (9.5 Gy) recipient mice (CD45.1/2) by tail vein injection. To analyze donor-derived chimerism, peripheral blood was collected from tail vein of recipients every 2 weeks after transplantation. Percentage of the chimerism in the bone marrow of recipient mice was assessed 8 weeks after transplantation. Additional CD45.1 (A20) and CD45.2 (104) were added to the antibody cocktail to measure the percentage of contribution from each donor.

6.8. Colony forming assay

For methylcellulose assays, 3×10^4 cells were plated in methylcellulose medium supporting myeloerythroid colonies, Methocult M3434 (STEMCELL Technologies), in 60 mm dishes, in duplicate. For pre-B cell colony forming assay, 1×10^5 fetal liver cells, were seeded in Methocult M3630 (STEMCELL Technologies), Plates were incubated at 37°C in 5% CO2 with ≥ 95% humidity. Myeloerythroid and pre-B cell colonies were enumerated on day 10 and day 7 after culture, respectively.

6.9. Homing assay

Fetal liver cells were collected from *Setdb1*^{vav} and control embryos, pre-treated with red blood cell lysis buffer (BD Biosciences), and enriched for lineage$^-$ cells, as described for FACS sorting. Lineage$^-$ cells were labeled with CFSE (Thermo Fischer Scientific) for 10 min at 37°C at the final concentration of 10 μM, and 10 million CFSE-labelled lineage$^-$ cells were injected into the lethally irradiated (9.5 Gy) recipient mice via tail vein. Frequency of CFSE$^+$ cells were analyzed in the bone marrow, 20 hours after injection by flow cytometry.

6.10. RNA-sequencing

To isolate total RNA, E14.5 *Setdb1*^{vav} and control fetal liver LT-HSCs and MPPs were sorted directly into the 100 µl extraction buffer, provided by PicoPure RNA Isolation Kit (Thermo Fischer Scientific). Total RNA isolation was carried out according to the

manufacturer‘s instructions. DNase treatment was performed on column using RNase-Free DNase Set (Qiagen). The RNA quantity and quality were assessed on an Agilent 2100 Bioanalyzer by the Agilent RNA 6000 Pico Kit (Agilent Technologies). High-quality RNA samples with RNA Integrity Number (RIN) > 8 were used for cDNA synthesis with SMART-Seq v4 Ultra Low Input RNA Kit (Clontech) according to the manufacturer’s instruction. Before proceeding to library preparation, cDNA was sheared in a Covaris S220 device (PP 175; DF 10; CB 200; 5 min; 4°C) to the size range of 200–500 bp and were subjected to library preparation with MicroPlex Library Preparation Kit v2 (Diagenode). The quantity of the libraries was assessed in a Qubit 3.0 Fluorometer with Qubit dsDNA HS Assay kit (Thermo Fischer Scientific). Libraries were further qualified by the Agilent High Sensitivity DNA Kit (Agilent Technologies). Libraries were sequenced using Illumina’s HiSeq 1500 sequencer for 50 bp paired end (PE) reads at the Laboratory for Functional Genome Analysis (LAFUGA) within the Gene Center (LMU Munich).

6.11. RNA-seq bioinformatic analysis

Demultiplexing of data was carried out on the Galaxy platform (Afgan et al., 2016). Paired-end reads were mapped to the version mm10 for mouse genome using STAR (Dobin et al., 2013). Normalization of read counts for all genes and differential expression analysis were performed using DESeq2 (Love et al., 2014). Heatmaps were plotted with pheatmap either using rlog-normalized expression values or log-transformed mean TPM (Transcript Per Million) from RSEM-normalized data. plotPCA function of the DESeq2 package was employed for PCA analyses. Gene set enrichment analysis was performed with GSEA software (Subramanian et al., 2005). KEGG pathway and GO analyses on motif-associated genes were carried out using ShinyGO tool (Ge et al., 2020). The expression levels of repeat classes were assessed with Homer using the analyzeRepeats.pl program with “repeats“ function, following loading the repeat definitions from UCSC. Differential expression analysis of repeats was performed using DESeq2.

6.12. ULI-NChIP-sequencing

5000 LSK cells were sorted from E14.5 *Setdb1*^{vav} and control fetal livers in the low binding tubes, centrifuged and cell pellet was resuspended in 20 µL of EZ nuclei isolation lysis buffer (Sigma) containing 0.1% Triton, 0.1% deoxycholate, 1x cOmplete EDTA-free Protease Inhibitor Cocktail (Roche Diagnostics), 1 mM PMSF, flash frozen and kept at -80 °C. Chromatin fragmentation and immunoprecipitation was performed following the ultra-low-input micrococcal nuclease-based native ChIP (ULI-NChIP) protocol with minor modifications (Brind’Amour et al., 2015). Briefly, after thawing cells in nuclei isolation lysis buffer, 10% of the

volume (2 µL) of a 1% Triton/1% deoxycholate solution was added and mixed by pipette up and down 15-20 times while swirling. Chromatin was fragmented using MNase (Biolabs) enzyme at 1.5 U/µL in MNase digestion buffer (1X MNase Reaction Buffer, 100 mM DTT, 50% PEG 6000, and ultrapure H20) for 7.5 minutes at 21°C. Reaction was stopped by adding 10% of the reaction volume of 100 µM EDTA and 1% Triton/1% deoxycholate solution. To 120 µL fragmentated chromatin, 380 µL of complete immunoprecipitation buffer (20 mM Tris-HCl (pH 8.0), 2 mM EDTA, 150 mM NaCl, 0.1% Triton X-100, 1x cOmplete EDTA-free Protease Inhibitor Cocktail, 1 mM PMSF) was added. Chromatin was rotated for 1 hour at 4°C and 13 rpm. For input, 100 µL of sample was taken, 10% volume of 10% SDS (10 µL) was added and mixed together with 90 µL elution buffer (Qiagen). The input sample was kept at 4°C and DNA purification was performed together with IP samples. The remaining 400 µL chromatin was pre-cleared in 2 tubes, each 200 µL together with 5 µL of pre-washed 1:1 protein A:protein G Dynabeads (Thermo Fischer Scientific) and incubated for 3 hours on a rotator at 4°C and 13 rpm. In parallel, per IP tube, 0.25 µg (0.25 µL) of H3K9me3 antibody (Active motif) was incubated with 5 µL of pre-washed 1:1 protein A:protein G Dynabeads (Thermo Fischer Scientific) in 100 µL complete immunoprecipitation buffer for 3 hours on a rotator at 4°C and 13 rpm. After incubation, all tubes were placed on the magnetic rack. The antibody-coated beads were washed 1X with 200 µL complete immunoprecipitation buffer and the pre-cleared chromatin was then added to the antibody-beads complex. The immunoprecipitation was carried out overnight (12 hours) at 4°C whilst rocking at 13rpm. Chromatin-bound beads were first washed 3X, each for 10 min at 4°C and 20 rpm with 500 µL low salt wash buffer (20 mM Tris-HCl (pH 8.0), 2 mM EDTA, 150 mM NaCl, 1% Triton X-100, 0.1% SDS) and then 3X with high salt wash buffer (20 mM Tris-HCl pH 8.0, 2 mM EDTA, 500 mM NaCl, 1% Triton X-100, 0.1% SDS). Per sample, 2 IP tubes were pooled and were eluted in 30 µL freshly prepared ChIP elution buffer (100 mM NaHCO3, 1% SDS) for 1.5 hours at 65°C in a thermo-shaker. To maximize the elution, additional 70 µL freshly prepared ChIP elution buffer was added to the beads. DNA isolation was carried out by Agencourt AMPure XP beads (Beckman Coulter) from input and ChIP samples. Samples were quantified in a Qubit 3.0 Fluorometer with Qubit dsDNA HS Assay kit (Thermo Fischer Scientific). Fragmentation of MNase-treated chromatin was assessed on input sample by the Agilent High Sensitivity DNA Kit (Agilent Technologies). Input and ChIP samples were subjected to library preparation with MicroPlex Library Preparation Kit v2 (Diagenode). The quantity of the libraries was assessed in a Qubit 3.0 Fluorometer with Qubit dsDNA HS Assay kit (Thermo Fischer Scientific). Libraries were further qualified by the Agilent High Sensitivity DNA Kit (Agilent Technologies). Libraries were sequenced using Illumina's HiSeq 1500 sequencer for 50 bp single-end (SE) reads at the Laboratory for Functional Genome Analysis (LAFUGA) within the Gene Center (LMU Munich).

6.13. ULI-NChIP-seq bioinformatic analysis

Data demultiplexing was done on the Galaxy platform. Reads were aligned to the version mm10 for mouse genome using bowtie (Langmead, 2010), excluding multi-mapped reads. Identification of H3K9me3 peaks was carried out by Homer (Heinz et al., 2010). For repeat analysis, multi-mapped reads were included. Enrichment of H3K9me3 on repeats was assessed by Homer using the analyzeRepeats.pl program with “repeats“ function, following loading the repeat definitions from UCSC. Coverage density of H3K9me3 on motifs was assessed with annotatePeaks.pl program from corresponding tag directories, using option “-hist 50 -size 4000”. Plots were generated with ggplot2.

6.13. Omni-ATAC-sequencing

ATAC-seq was performed as previously described (Corces et al., 2017). Briefly, 10,000 LSK cells were sorted from E14.5 *Setdb1*^{vav} and control fetal livers in the low binding tubes. Cells were spun at 500 g for 5 min at 4°C. Cell pellets were resuspended and lysed in cold ATAC Resuspension Buffer (10mM Tris-HCl (pH 7.4), 10 mM NaCl, 3 mM MgCl2) containing 0.1% NP40, 0.1% Tween-20 and 0.01% digitonin. Cell lysis reaction was incubated on ice for 3 min and then 1 ml of ATAC Resuspension Buffer containing only 0.1% Tween-20 was added and centrifuged at 500 g for 5 min at 4°C. Nuclei were then resuspended in 10 µL of Transposition Mix containing 25 µL 2x Tagmentation Buffer (20 mM Tris-HCl (pH 7.6), 10 mM MgCl2, 20% dimethyl Formamide, H2O), 2.5 µL Tn5 Transposase (Illumina), 5.25 µL H2O, 16.5 µL PBS, 0.25 µL of 2% digitonin (Promega) and 0.5 µL of 10% Tween-20. Reactions were proceeded by incubation for 30 min at 37°C in a thermo-shaker at 900 rpm. NA was subsequently purified using PCR clean-up MinElute kit (Qiagen). Transposed DNA was then amplified in 50 µL reactions with custom primers as described previously (Buenrostro et al., 2013). Libraries were amplified for 4 cycles and then were monitored with qPCR in a 15 µL reaction containing the same primers and 5 µL PCR sample. qPCR output was monitored for the ΔRN. The number of additional cycles of the PCR reaction needed for the remaining PCR samples was estimated based on the 0.25 ΔRN cycle number. Amplified libraries were purified with the PCR clean-up MinElute kit (Qiagen) and size selected for fragments less than 600 bp using the Agencourt AMPure XP beads (Beckman Coulter). Libraries were quantified in a Qubit 3.0 Fluorometer with Qubit dsDNA HS Assay kit (Thermo Fischer Scientific). Further qualification of the libraries was by the Agilent High Sensitivity DNA Kit (Agilent Technologies). Libraries were sequenced using Illumina’s HiSeq 1500 sequencer for 50 bp single-end (SE) reads at the Laboratory for Functional Genome Analysis (LAFUGA) within the Gene Center (LMU Munich).

6.14. Omni-ATAC-seq bioinformatic analysis

Data demultiplexing was done on the Galaxy platform. ATAC-seq reads were reads were mapped to the version mm10 for mouse genome using Bowtie. ATAC peaks over Input background were identified with Homer using the findPeaks.pl program with option “-style factor”. Peaks from all samples were merged using mergePeaks. The unified Peak list was filtered for promoter-associated peaks (distance to TSS < 1000bp) with bedtools. ATAC coverage counts were then calculated with Homer using the annotatePeaks.pl from corresponding tag directories. ATAC peaks with log2 fold change > 2 were defined as differentially accessible region. PCA analysis was performed on ATAC peaks coverage data with plotPCA function in R. Transcription factor motif prediction for differential ATAC peak was done with Homer using findMotifsGenome.pl program.

6.15. Data presentation and statistical analyses

Data are presented as mean±SD calculated from “n“ number of independent experiments. Statistical analysis was performed in R.

7. Abbreviations

Ab	antibody(ies)
AGM	aorta-gonad-mesonephros
APC	allophycocyanin
APC-Cy7	allophycocyanin-Cy7 conjugated
ATAC-seq	assay for transposase-accessible chromatin using sequencing
BM	bone marrow
BV	brilliant violet
C/EBPα	CCAAT/enhancer-binding protein alpha
C/EBPε	CCAAT/enhancer-binding protein epsilon
CAM	cell adhesion molecule
CCR7	chemokine (C-C motif) receptor 7
CCR9	chemokine (C-C motif) receptor 9
cDNA	complementary DNA
CFSE	carboxyfluorescein succinimidyl ester
CFU-S	colony forming unit-spleen
CGI	CpG island(s)
ChIP	chromatin immunoprecipitation
CLP	common lymphoid progenitor(s)
CMP	common myeloid progenitor(s)
CpG	cytosine nucleotide followed by a guanine in the 5’ to 3’ direction
CRU	competitive repopulating unit
CTCF	CCCTC-binding factor
CX3CR1	CX3C chemokine receptor 1
CXCL12	chemokine (C-X-C motif) ligand 12
CXCR4	chemokine (C-X-C motif) receptor 4
Def8	defensin 8
dHSC	definitive hematopoietic stem cellv
DN	double negative
DNAme	deoxyribonucleic acid methylation
DNMT	DNA methyltransferase (cytosine-5) 1
DNMT3a	DNA methyltransferase 3A
DNMT3b	DNA methyltransferase 3B
DP	double positive
E	embryonic day
EHT	endothelial-to-hematopoietic transition
Env	envelop protein
EPO	erythropoietin
ERG	ETS-related gene
ERV	endogenous retroviruse(s)
ETS	E-twenty-six
FACS	fluorescence-activated cell sorting
Fbp2	fructose-bisphosphatase 2
FL	fetal liver
Fli-1	friend leukemia integration 1
Flt3	FMS-related tyrosine kinase 3
FOG-1	friend of GATA-1
GATA1	globin transcription factor 1
Gfi1	growth factor independent 1
GM	granulocyte-monocyte
GMP	granulocyte-macrophage progenitor(s)
GO	gene ontology
Gr-1	granulocyte-1
GSEA	gene set enrichment analysis

H3K14ac	histone 3 lysine 14 acetylation
H3K27ac	histone 3 lysine 27 acetylation
H3K27me3	histone 3 lysine 27 trimethylation
H3K36	histone 3 lysine 36
H3K4me3	histone 3 lysine 4 trimethylation
H3K9me/1/2/3	histone 3 lysine 9 mono/ di/ trimethylation
H4K20	histone 4 lysine 20
HDAC4	histone Deacetylase 4
Hmga2	high Mobility Group AT-Hook 2
HoxA10	homeobox A10
HoxA9	homeobox A9
HP1	heterochromatic protein 1
HSC	hematopoietic stem cell(s)
HSPC	hematopoietic stem and progenitor cell(s)
IAP	internal A-type particle
IGF2	insulin-like growth factor 2
IGN	imprinted gene network
IGV	integrated genome browser
IL-3	interleukin 3
IL-6	interleukin 6
IL-7	interleukin 7
IL7Rα	interleukin 7 receptor-α
IP	immunoprecipitation
kb	kilobases
KMT	lysine methyltransferases
KO	knockout
LFA-1	lymphocyte function-associated antigen 1
LINE	long interspersed nuclear element(s)
LMO2	LIM domain only 2
LMPP	lymphoid-primed multipotent progenitor(s)
LPS	lipopolysaccharides
LT-HSC	long-term hematopoietic stem cell(s)
LTR	long terminal repeat
Mac-1	macrophage-1
MACS	magnetic activatd cell sorting
MBD	methyl-CpG binding domain
MEF	mouse embryonic fibroblast(s)
MEP	megakaryocyte-erythroid progenitor(s)
mESC	mouse embryonic stem cell(s)
MkE	megakaryocyte-erythrocyte
MMTV	mouse mammary tumor virus
MPP	multipotent progenitor(s)
mRNA	messenger ribonucleic acid
MSC	mesenchymal stem cell
MuLV (MLV)	murine leukemia viruses
NPC	neural progenitor cells
OxPhos	oxidative phosphorylation
P-Sp	para-aortic splanchnopleura
PBS	phosphate saline buffer
PCA	principal component analysis
PCR	polymerase chain reaction
PE	phycoerythrin
PE-Cy5	phycoerythrin-Cy5 conjugated
PE-Cy7	phycoerythrin-Cy7 conjugated
PGCs	primordial germ cells
Pre-B	precursor B cells

PTM	post-translational modification
rcf	relative centrifugal force
RNA-Seq	RNA high throughput sequencing
RPKM	reads per kilobase of transcript per million mapped reads
rpm	rotations per minute
RT	room temperature
RUNX1	runt-related transcription factor 1
SCF	stem cell factor
SCL/TAL1	stem cell leukemia/T-cell acute lymphoblastic leukemia [T-ALL] 1
SDF1	stromal cell-derived factor 1
SET domain	Su(var)3-9 and 'Enhancer of zeste' protein domain
SETDB1	SET domain bifurcated 1 (also ESET)
Sfpi1 (PU.1)	spleen focus forming virus (SFFV) proviral integration oncogene
SINE	short interspersed nuclear element(s)
SLAM	signaling lymphocyte activation molecule
Sox17	SRY-box transcription factor 17
SP	single positive
ST-HSC	short-term hematopoietic stem cell(s)
SUV39	suppressor of variegation 3-9
TF	transcription factor
Th	T helper
TSS	transcription start site(s)
ULI-NChIP-seq	ultra-low-input native chromatin immunoprecipitation followed by high throughput sequencing
UPR	unfolded protein response
Vav	Vav 1 oncogene
VLA-4	very late antigen-4
wk	week
XEN	extraembryonic endoderm stem cells
ZFP	zinc finger protein

8. Acknowledgments

I would like to express my special and greatest thanks to my PhD supervisor Prof. Dr. Gunnar Schotta, for his guidance and scientific support throughout my PhD life to accomplish this challenging project. His high standard scientific vision has greatly advanced the project and my learning experience as a PhD student.

I would also like to thank Filippo for all his scientific and technical support during my thesis work, and even beyond that as a great lab mate. It was a pleasure to work with him and other former and current lab members, especially Alessandra, Gustavo, Sahra, Rui, Alex, Dennis, Sophia, Helena, Zeyang, Irina, Andrea, and Heike. We shared quite nice moments and made unforgettable memories.

I was also privileged to be a member of the Molecular Biology department and to work with outstanding and friendly colleagues. I want to thank them all for their scientific and fruitful feedback. I would also thank Dr. Elizabeth Schroeder-Reiter, our IRTG program coordinator, for her cordial support during my PhD studies.

My warmest thanks go to my family – Mom and my sister, Minoo – for a lifetime of unconditional love and encouragement. My heartfelt thanks go to my Dad, who I lost during my PhD journey, who always believed in me. I feel his presence every moment in my life.

All my love and sincere thanks to my husband, Mehrdad, who has had faith in me, for having accompanied me with his tremendous support and encouragement. He has been the star in the night sky that showed me the path when I could not see it. I dedicate this work to him.

In the end, I would like to thank myself for my Passion, Perseverance, and Patience. I've never given up and won't! This long journey could have never come to an end without my tireless dedication.

9. Curriculum Vitae

The CV is not accessible in the public version.

10. Appendix

Table 10.1 | List of significantly upregulated genes in *Setdb1^{vav}* LT-HSCs

gene	log2FoldChange	padj	Akap2	0,80739374	6,23E-03
4930550L24Rik	3,91226304	5,81E-43	Zfp709	0,80374616	1,20E-03
Iqcg	3,05452084	5,03E-53	1700001L05Rik	0,80027346	7,34E-03
Stag3	2,96320513	2,11E-86	Pcdhga12	0,7909819	1,10E-02
Dnah8	2,43437381	1,41E-75	Espnl	0,78770911	6,90E-03
Tmem150c	2,3214372	3,94E-10	Hsh2d	0,78424511	8,51E-04
Akap5	2,2954194	1,61E-25	Ly6c1	0,77958271	4,72E-03
M1ap	2,25293503	7,90E-32	Mical2	0,77913449	6,11E-03
1700097N02Rik	2,13473463	9,98E-27	Afap1	0,77826478	1,11E-02
Fcgr2b	2,12454222	1,52E-26	Gpc2	0,77243878	3,73E-04
2810474O19Rik	1,93852159	1,13E-34	Setx	0,77002243	2,98E-05
Gstp2	1,68153886	7,08E-15	1700030C10Rik	0,76140523	1,70E-02
Gm1564	1,65184762	1,40E-11	Skint3	0,75893565	1,51E-02
Car1	1,51888416	3,84E-29	Pla2g5	0,75783223	6,96E-06
Cldn10	1,45283395	1,14E-09	Ahsa2	0,74579887	2,66E-05
Amotl1	1,43147296	1,42E-11	Ttc39b	0,72498535	5,11E-04
Gstp1	1,40856093	2,28E-17	Erdr1	0,72139105	1,93E-02
Entpd3	1,27476849	1,42E-08	Alpl	0,7137502	2,84E-02
Slc1a4	1,23794086	7,45E-08	Gm13154	0,71267247	3,50E-02
Ldoc1l	1,23520375	1,14E-09	Catsperg1	0,70364025	2,26E-02
Def8	1,21784481	4,17E-12	B3gnt7	0,70266079	1,60E-03
Arl14epl	1,14781722	3,85E-08	Vmn2r96	0,69160109	3,53E-06
4930447C04Rik	1,13766289	2,11E-06	Zfp110	0,68804101	2,66E-05
Gapt	1,1132987	1,45E-06	Pcdhgb4	0,68505956	3,80E-02
Klrb1c	1,09468584	1,97E-05	Fbp1	0,6781096	1,89E-02
4930526I15Rik	1,08501191	2,98E-05	Ltbp1	0,6746406	3,17E-02
Ccdc36	1,04715475	6,39E-05	Sdsl	0,67177386	3,84E-02
Alyref2	1,04393917	5,00E-06	Kirrel2	0,6618209	3,06E-05
Ryr2	1,0355964	1,09E-04	Zc3hav1l	0,65717529	1,20E-02
Pkd1l3	1,01737463	1,68E-04	Fam208a	0,65195806	9,95E-03
C1rl	1,01268793	4,88E-07	Mtl5	0,64635484	3,12E-02
Zcwpw1	1,00419496	4,75E-07	Pxt1	0,64588508	4,71E-02
Dmc1	0,98371019	2,45E-04	Ecm1	0,64537822	1,05E-02
Dzip1	0,97594868	3,62E-04	Zfp808	0,64277975	5,86E-03
Slc16a3	0,97411192	3,14E-05	Gdf3	0,64211678	2,04E-02
D330045A20Rik	0,95352279	5,58E-04	Hyou1	0,64155368	7,11E-03
Prr19	0,93537032	1,68E-04	Scml4	0,63985857	4,83E-02
Tex15	0,9319548	1,45E-06	Tdrkh	0,63865777	9,24E-03
Il1rl1	0,92350896	9,24E-04	2610305D13Rik	0,63320556	4,99E-02
Nrg4	0,92274335	8,84E-04	Plcd3	0,63313914	4,02E-02
Ccbl2	0,91384198	3,14E-05	Frmd6	0,63275438	1,51E-02
Tmem132d	0,90442472	6,52E-06	Ept1	0,6299149	7,37E-03
Slc25a31	0,88531814	1,00E-04	Aim2	0,62619114	1,79E-02
4930539E08Rik	0,88075998	1,54E-03	Sema4f	0,62066967	4,94E-02
AI506816	0,87295248	1,14E-03	Fbp2	0,61379998	5,07E-10
Akr1c13	0,8534203	2,01E-05	Gadd45g	0,61311868	3,57E-02
Rnf17	0,84962577	3,62E-03	Cnr2	0,60904949	9,24E-03
Crispld2	0,82653131	1,17E-03	Adad2	0,60027951	1,67E-03
Gal3st3	0,82035737	3,05E-04	Ncf1	0,59481666	4,57E-02

Macrod2	0,58665848	1,10E-02	St6galnac3	0,49404679	2,33E-02
Epha2	0,58236394	1,68E-02	Padi3	0,47657343	1,04E-02
Sh2d5	0,57825578	4,46E-02	Klhl6	0,47395349	1,31E-02
Tex19.1	0,57550772	2,78E-13	Ethe1	0,46944334	1,36E-02
Cep70	0,56873458	4,14E-03	Ppa1	0,45154397	4,83E-02
Morc2a	0,56428549	1,70E-02	Gabrr1	0,43916735	8,51E-04
Smc5	0,54859882	6,56E-05	Ppef1	0,41006352	1,10E-02
Uqcc2	0,5434979	5,09E-03	Ankrd36	0,40929274	3,00E-02
Gm13157	0,54324844	9,07E-03	Cyp2b10	0,39875897	7,42E-04
Tex19.2	0,53885116	3,48E-03	Fmr1nb	0,39526754	1,71E-02
H2-T23	0,53685487	1,77E-02	1700029P11Rik	0,36261379	5,26E-03
Trap1a	0,52944868	4,10E-13	Ntng1	0,34009188	4,46E-02
Ly6k	0,52356629	6,94E-04	Dppa4	0,33673336	4,46E-02
Olfr1372-ps1	0,52195242	4,59E-05	Tuba3a	0,32301932	1,68E-02
Tmem184b	0,51894215	1,40E-02	2310043L19Rik	0,31033314	4,45E-02
Sync	0,51766985	1,60E-02	Ccl12	0,30487065	1,25E-02
Chrnb4	0,51325263	3,07E-02	Fcrlb	0,29110436	1,28E-02
Vill	0,50953625	1,96E-03	Cdsn	0,29059951	1,99E-02
Clstn3	0,5071999	2,74E-02	Capn11	0,2707337	3,02E-02
Arhgap30	0,50497001	2,11E-02	Tcfl5	0,26929407	4,59E-02
Nccrp1	0,50112984	5,86E-03	Ak7	0,26917523	1,52E-03
Pfkp	0,50012056	1,31E-02	Prss42	0,21011662	3,63E-02
Slfn4	0,49968218	1,16E-04	Mmp13	0,03603977	2,47E-05
F11r	0,49427955	4,83E-02			

Table 10.2 | List of significantly downregulated genes in *Setdb1^{vav}* LT-HSCs

gene	log2FoldChange	padj			
Igf1	-1,5556759	4,88E-14	Flt3	-0,9075568	4,75E-07
Muc6	-1,513428	1,73E-10	Epb4.1l3	-0,9038017	7,97E-04
Igf2	-1,4714635	2,42E-11	Fxyd1	-0,8904782	2,16E-03
Ces2b	-1,4415444	1,20E-09	Ctsh	-0,8705468	1,36E-03
Plbd1	-1,3334879	1,01E-08	3632451O06Rik	-0,8443961	3,36E-03
H19	-1,3284269	6,16E-11	Jun	-0,8413209	1,10E-05
Clec1b	-1,3049536	3,46E-08	Fam132a	-0,8324807	1,10E-03
Cd36	-1,3009417	7,63E-08	Efna1	-0,8314191	2,13E-03
Meg3	-1,298693	2,31E-08	Aqp1	-0,8283186	7,07E-04
C6	-1,2898255	3,77E-08	Fpr1	-0,8249161	1,27E-04
Tmem26	-1,2517557	4,49E-07	Lama3	-0,8202546	1,00E-03
Il18bp	-1,2217478	4,90E-07	Nrk	-0,8192814	6,75E-03
Gfra2	-1,2099955	9,34E-07	Mrap	-0,8179833	4,78E-03
Fcgrt	-1,0745087	9,21E-08	Car3	-0,8137523	4,59E-05
Vldlr	-1,0373061	4,27E-05	Epha7	-0,8125505	6,84E-03
Pitx2	-1,014036	1,23E-04	Armcx4	-0,7958166	6,75E-03
Plxna4os1	-1,0111203	1,68E-04	Sqrdl	-0,7957601	9,30E-03
Gimap3	-0,9962522	1,91E-04	Lancl3	-0,7955882	1,05E-02
Cyp4b1	-0,9857281	1,52E-04	Gem	-0,7936787	6,32E-06
Wfdc18	-0,9832358	4,27E-05	Ndnf	-0,7655982	8,76E-03
S100a16	-0,9723587	3,16E-04	Bex2	-0,7482612	1,88E-02
Wfdc17	-0,9707684	3,62E-04	Trf	-0,748031	8,81E-03
Kcna2	-0,9521371	2,19E-06	Serpinf1	-0,7460152	1,33E-03
Syne4	-0,9516352	3,53E-04	Dkk1	-0,7417883	1,10E-02
Tac2	-0,9468217	4,01E-05	Sh2d4a	-0,7403581	2,26E-02
Postn	-0,9452318	3,70E-04	Gpc3	-0,7333674	2,15E-02
Plekhg1	-0,9319419	7,04E-06	Gjb2	-0,7297818	1,35E-05
Dhrs3	-0,9276352	2,45E-04	Scd1	-0,7266717	2,11E-02
			Dlk1	-0,7258604	7,20E-03

Cyp26b1	-0,7250747	1,90E-02	Prodh2	-0,5940125	2,95E-02
S1pr3	-0,7128973	6,00E-04	Cacna2d1	-0,5851662	3,78E-02
Col11a2	-0,712395	6,75E-03	Pparg	-0,584916	3,61E-03
Fxyd7	-0,7084429	3,79E-02	Zfp870	-0,5832662	3,27E-02
Hoxa3	-0,7075926	1,10E-02	Sema6d	-0,5759463	2,94E-02
Ccl6	-0,707321	3,10E-02	Ccr2	-0,5749633	1,42E-03
Hid1	-0,7061947	1,25E-02	Cd82	-0,5728482	9,55E-03
Ecscr	-0,7032363	6,71E-03	Sdc1	-0,5686102	6,75E-03
Angptl3	-0,6909535	5,20E-03	Pld3	-0,568319	1,59E-03
Itih4	-0,6901982	5,90E-04	Itm2a	-0,557254	1,10E-02
Zfp354c	-0,6899704	1,23E-02	Emcn	-0,5399243	4,92E-02
Sepp1	-0,6867481	1,32E-03	Cfi	-0,5364755	2,66E-02
Gsta4	-0,6860896	1,57E-02	Tmem154	-0,5295636	4,04E-02
Pde2a	-0,6777887	1,58E-03	Dsp	-0,5261037	2,95E-02
Sox18	-0,675221	2,04E-02	Serinc5	-0,5241273	1,40E-02
Ikbke	-0,6737371	1,04E-02	Tsc22d1	-0,5239202	4,78E-03
Acox2	-0,6727887	1,76E-02	Paqr9	-0,5238419	4,19E-02
Spon2	-0,6720432	2,44E-03	Cyp2c44	-0,5053779	5,09E-03
Folr2	-0,6699711	5,09E-03	Slc1a2	-0,5002941	9,15E-03
Mafb	-0,6646306	1,49E-02	Otc	-0,4956555	2,66E-02
Hpgd	-0,6636823	4,26E-02	Cnn3	-0,4943356	3,57E-02
Trib2	-0,6589709	3,03E-02	Atg14	-0,4829064	2,40E-02
Tox	-0,6547175	4,83E-02	Chga	-0,4801615	2,86E-02
Enpp2	-0,6539077	1,12E-03	Hoxa9	-0,4741318	3,63E-02
Serpina1c	-0,6534966	2,49E-04	Spp2	-0,4711199	4,32E-02
F2	-0,6519707	1,49E-02	Pcsk5	-0,4652567	3,57E-02
Hmgcs2	-0,6517076	1,10E-02	Ugt2b34	-0,4594334	4,31E-02
Irf6	-0,6478002	2,11E-02	Mat1a	-0,4594317	3,46E-03
Btbd3	-0,6476678	1,43E-02	Serpina1d	-0,45479	4,64E-02
Rdh12	-0,6476189	1,05E-02	F13b	-0,4425091	3,00E-02
Sgsm1	-0,646276	2,94E-02	Hmga2	-0,4272461	2,18E-02
Clec7a	-0,6440714	1,10E-02	Crp	-0,4202027	1,52E-02
Pid1	-0,6414378	1,12E-03	Pipox	-0,4137955	2,24E-02
Snhg11	-0,6402921	9,07E-03	Glul	-0,3975756	4,95E-02
Ccr5	-0,6379448	2,59E-02	Abhd4	-0,3939315	2,66E-02
Cd22	-0,6312287	4,08E-03	Itm2b	-0,3855565	3,23E-02
Vdr	-0,6228348	2,66E-02	Adra2b	-0,3563666	1,25E-02
Serpina1e	-0,6218423	1,58E-03	Vsig4	-0,3463763	8,42E-03
Stab2	-0,6149588	1,23E-02	D10Bwg1379e	-0,3404254	1,05E-02
Prdm5	-0,6025731	2,79E-02	Ugt2b36	-0,2922276	8,99E-03
Itgb5	-0,602156	4,26E-02	BC024386	-0,255519	1,95E-02
Pld2	-0,6013125	4,03E-02	Vcam1	-0,2278482	4,31E-02

Table 10.3 | List of significantly upregulated genes in *Setdb1^{vav}* MPPs

gene	log2FoldChange	padj			
Fbp2	8,2541579	3,44E-91	Vmn2r96	4,4481598	2,00E-13
Tex19.1	8,083226	3,60E-28	Arl14epl	4,2773757	2,08E-11
Tmem150c	7,1041668	4,40E-20	Ryr2	4,1225307	5,12E-42
Car1	6,982836	0,00E+00	Olfr1372-ps1	3,9968248	8,36E-12
Gm1564	5,2794679	1,27E-20	Sec14l4	3,9206038	4,45E-10
Ak7	5,2075651	3,45E-26	Ntng1	3,8200288	9,32E-33
Amotl1	5,1732828	1,78E-31	Tcfl5	3,5923296	1,20E-10
4930550L24Rik	4,8787257	7,91E-54	Akap5	3,4304792	5,76E-74
Gstp2	4,5292684	1,16E-59	Pla2g5	3,3887289	3,32E-08
Fbp1	4,4745765	1,89E-121	Stag3	3,344433	1,74E-123
			Sdsl	3,3285062	3,45E-21

Grhl2	3,2989723	4,27E-08	Gypa	2,2565957	1,10E-32
Iqcg	3,2480146	2,16E-61	Wbp2nl	2,244762	1,16E-06
Aplp1	3,2396361	5,80E-16	Serpinb9g	2,2413306	1,22E-06
M1ap	3,1619179	2,85E-102	Penk	2,2370209	9,01E-08
Cyp2b10	3,1547991	1,35E-09	Popdc2	2,2248377	1,61E-12
Mmp14	3,1159403	4,63E-28	Sgcz	2,1990749	1,60E-06
Slc4a8	3,1105676	2,03E-36	Cbr3	2,1823257	2,10E-07
Ltbp1	3,0817303	4,59E-46	4930433N12Rik	2,1705249	2,71E-05
Homer2	3,0658014	4,47E-17	Tspo2	2,1641035	1,42E-35
Dnah8	3,0363132	9,08E-147	Pcdhga12	2,1629848	1,11E-11
Cdsn	3,0092211	8,83E-09	Ank2	2,1504115	2,09E-09
Ly6k	3,001536	2,35E-11	Gal3st3	2,1444144	9,83E-08
Padi3	2,977548	7,09E-54	Amn	2,1425722	5,55E-06
Kirrel2	2,9753266	2,05E-08	Boll	2,1321832	3,59E-08
Cyp2a12	2,9560387	1,30E-08	Tmod1	2,1304337	3,47E-16
Myrip	2,9076802	2,65E-08	Cbr2	2,1233983	1,38E-06
Ackr1	2,8773135	6,26E-24	Apol8	2,115492	2,97E-11
Gabrr1	2,870101	6,80E-07	Epb4.2	2,1015449	1,98E-36
Vwa5b2	2,8574232	3,31E-14	Grtp1	2,0952139	1,73E-11
Col5a1	2,8514505	6,20E-59	D330045A20Rik	2,0940183	2,19E-17
Lama1	2,8369186	2,66E-08	Sowaha	2,0936704	3,45E-14
Nfatc4	2,8278286	2,76E-08	Hormad2	2,0871257	2,79E-12
Cntn3	2,7769376	2,08E-13	5730507C01Rik	2,072165	1,34E-09
Entpd3	2,7663237	1,96E-10	Cebpe	2,0714911	7,34E-15
Tmem132d	2,7449186	6,42E-10	Dzip1	2,0662841	1,03E-20
Nccrp1	2,743152	2,58E-10	4930447C04Rik	2,063864	4,86E-25
Ly6c1	2,6979353	1,99E-06	Smarca5-ps	2,0600335	1,22E-08
Prr19	2,6942456	3,01E-11	Vangl1	2,0567091	2,03E-28
Dppa4	2,6789908	5,37E-08	Slc7a15	2,0521509	6,50E-05
Ahsa2	2,632368	6,01E-114	Redrum	2,0423822	1,96E-34
Il1rl1	2,6204741	4,03E-31	Snca	2,0400194	1,34E-23
Pcsk9	2,6153912	4,65E-25	Slc30a10	2,0361654	4,85E-23
2410076I21Rik	2,6104434	6,37E-15	D10Bwg1379e	2,0150673	6,88E-08
1700029P11Rik	2,5787021	1,42E-07	Mt1	2,0136056	6,05E-44
Vmn2r24	2,5766322	1,36E-07	Gm10532	2,0102036	8,99E-05
1700097N02Rik	2,5743662	4,85E-13	Plcd3	2,0062575	4,62E-11
Col4a3	2,571029	2,37E-11	1700112E06Rik	1,9883581	3,39E-08
2810474O19Rik	2,5670461	7,96E-135	Stk32b	1,9739019	1,32E-07
Ankrd36	2,5257113	7,14E-08	Optn	1,9674104	9,69E-22
Adad2	2,4764895	1,19E-06	Slc1a4	1,9630441	4,15E-26
Sptb	2,4566872	6,41E-57	Gstp1	1,9605183	1,27E-65
Xlr3a	2,4307363	4,25E-08	Tuba8	1,9585726	8,12E-19
BC051019	2,4271703	1,96E-06	Acacb	1,9553998	1,82E-12
Epcam	2,4271036	1,94E-13	Trap1a	1,9540155	2,32E-17
Ndufa4l2	2,4244287	1,23E-12	Nfxl1	1,9495015	7,94E-41
Ano1	2,4012748	2,23E-12	Klf5	1,9464011	2,19E-12
Tex19.2	2,3893618	9,79E-06	Fech	1,9415137	1,46E-38
Amigo2	2,3524958	1,06E-18	Tdrd9	1,9391623	4,44E-05
Pxt1	2,332726	1,15E-10	Gsdma3	1,9379318	5,30E-06
Gtsf1	2,3087368	4,29E-06	Atp6ap1l	1,9309149	1,15E-04
Upk1b	2,2966229	2,97E-08	Fcgr2b	1,9230629	4,33E-25
Tdrd5	2,2917469	6,90E-08	Acoxl	1,9169993	1,32E-04
Dmc1	2,2666426	1,57E-14	Prss42	1,9152947	3,30E-05
Mt2	2,2587531	2,78E-44	2310043L19Rik	1,9062002	9,84E-06
Podxl	1,9029792	1,41E-30	Pnma5	1,6762174	4,55E-05
Hvcn1	1,8994078	5,73E-17	Gpat2	1,664523	2,09E-05

2210417A02Rik	1,8992132	1,87E-05	Syce1	1,6634882	7,94E-05
Add2	1,899148	1,09E-29	Pklr	1,662053	3,39E-23
Vwce	1,8902033	1,89E-06	Socs2	1,6568173	3,11E-15
Il1bos	1,889921	6,28E-05	Abcb10	1,6509062	2,28E-31
Eif5a2	1,8824409	8,25E-23	Fgl1	1,6505894	3,63E-04
1700030C10Rik	1,8733156	2,59E-10	Fbxl2	1,6486457	6,97E-12
Abcg4	1,8675217	7,23E-25	Ache	1,6460253	5,75E-08
Cpne7	1,8635477	4,05E-07	Fam210b	1,6452739	1,57E-19
Ank1	1,8525289	4,89E-34	LOC100503676	1,6445516	1,34E-04
Rragd	1,8515074	3,07E-05	Gal3st1	1,6435764	8,14E-08
Rnf17	1,8453956	3,41E-06	Lmna	1,642653	1,10E-26
Cnnm1	1,8435696	2,32E-06	Gm364	1,6325516	9,64E-04
Trim10	1,8393796	5,48E-19	Spta1	1,6276725	1,03E-20
Ank3	1,8343701	3,10E-06	Pkhd1l1	1,6273659	2,18E-08
Rgcc	1,8282528	1,96E-30	Icam4	1,6265693	6,75E-20
Itgb2l	1,8263005	3,00E-07	Gm5483	1,6262007	7,28E-10
Clcn2	1,8090039	4,42E-23	Mmp9	1,6246004	2,09E-05
1300017J02Rik	1,8084013	2,29E-13	Gm867	1,6220241	2,16E-04
St6galnac5	1,7994762	7,23E-07	Perp	1,6189502	3,91E-08
Slc6a9	1,7981928	1,51E-18	Reep6	1,6161764	4,95E-18
Rhox5	1,7972429	2,53E-05	Nxpe4	1,6146128	8,18E-18
Prkd1	1,7891198	4,31E-06	Pla2g12a	1,6143016	1,36E-24
Trim24	1,7841554	1,75E-32	Gata1	1,6134772	3,07E-22
Sh3d19	1,780313	7,98E-15	Plxdc1	1,6118327	6,91E-07
Tex15	1,7748523	1,92E-07	Ssx2ip	1,6097941	1,01E-33
Fam83g	1,7733599	2,44E-13	Klf1	1,6071123	4,36E-29
Rhag	1,7696599	1,87E-08	Hecw1	1,6039788	5,99E-04
Irs2	1,7587364	2,28E-16	Epor	1,6016131	3,10E-24
Trem3	1,7576669	2,59E-09	Bicd1	1,6007252	3,90E-13
Adam8	1,7559211	2,07E-14	Dazl	1,6003014	1,68E-04
Arhgef12	1,7542993	2,53E-11	Nrg4	1,592551	8,50E-14
Slc41a3	1,7519053	4,26E-23	Nckap1	1,5916125	2,79E-09
Sdk1	1,7485105	2,10E-05	1700023E05Rik	1,5905708	8,46E-05
Slc16a3	1,7450623	2,38E-30	En2	1,5902971	7,84E-05
Arsg	1,7428601	1,26E-10	Arhgdig	1,5859396	1,44E-09
Bmp7	1,7318167	4,14E-05	Stk31	1,5840745	4,34E-04
Msrb3	1,7301374	1,43E-25	Gmpr	1,5821927	6,01E-32
1700001L05Rik	1,7282591	2,44E-17	Sgms2	1,5808734	1,31E-08
Spats2	1,7270595	1,15E-19	Vnn1	1,5690097	7,40E-05
Ccl2	1,726626	2,04E-06	Kel	1,5547836	9,26E-22
Pak6	1,7219666	1,37E-05	Galnt6	1,5543734	1,47E-15
Tspan33	1,7174177	1,35E-17	Cyp2a5	1,5543306	6,20E-05
Aldh1l2	1,7161724	1,73E-04	P4ha3	1,5510686	5,09E-04
Akap2	1,7146673	1,57E-07	2900041M22Rik	1,5410201	8,77E-05
Hesx1	1,7135531	1,10E-13	Sox6	1,5365372	3,73E-10
Cpox	1,7084151	1,79E-30	Olfml2b	1,5319349	1,30E-04
Ccdc36	1,7040506	1,50E-10	Rfesd	1,5282998	1,74E-24
Asns	1,7006954	3,36E-28	Rims3	1,5249046	5,46E-04
Endod1	1,6951126	4,43E-24	Prokr1	1,5246419	1,68E-07
Topaz1	1,6852439	2,82E-05	Tspan12	1,5241248	6,89E-06
Nipa1	1,6814922	7,72E-11	5730508B09Rik	1,5237157	6,33E-12
Garem	1,6790166	1,87E-20	Slc39a8	1,5192396	3,16E-23
Acmsd	1,5172418	7,78E-07	Slc1a3	1,3948807	5,27E-04
Abca13	1,5155256	1,60E-04	Il1r2	1,3897238	1,91E-10
Dmtn	1,5142034	2,37E-07	Samd14	1,3880603	1,03E-16
Gadd45g	1,5124568	3,82E-13	Ms4a3	1,3857421	1,66E-11

Ell2	1,5102698	2,59E-22	Mrpl52	1,3798184	1,58E-25
Nxt2	1,510148	1,51E-20	2610305D13Rik	1,3791851	3,54E-12
Zar1	1,5095448	1,20E-04	Sycp3	1,3712343	2,51E-03
Hemgn	1,5067942	2,89E-25	Fgd6	1,3700516	5,03E-10
Zfp808	1,5058368	8,46E-18	Gpc1	1,3680986	1,57E-05
Ccbl2	1,5056981	2,77E-40	Cdr2	1,3680124	3,64E-09
Pkd1l3	1,5019453	1,95E-08	2410003L11Rik	1,3639824	1,74E-03
Usp32	1,4948911	6,11E-19	Dpf3	1,3637085	2,43E-04
Tsix	1,4944787	8,50E-04	Dnajc6	1,3621248	2,65E-04
Fam46c	1,4927571	6,52E-10	Slc22a23	1,3602906	1,96E-10
AI506816	1,4925331	3,91E-23	Prnp	1,358702	6,42E-13
Itsn1	1,4906517	5,15E-27	Cyp4b1-ps2	1,355604	4,21E-03
Elane	1,4815307	2,30E-19	Ermap	1,3546804	2,30E-06
Dnajb3	1,4807004	4,24E-06	Alad	1,3520744	2,56E-20
Blvrb	1,4779227	7,87E-27	Cda	1,3420038	2,81E-03
C5ar2	1,46974	4,43E-06	Phyhip	1,3389302	1,79E-04
Gclm	1,4668342	1,15E-16	4930526I15Rik	1,3359027	4,94E-11
Fkbp6	1,4667275	9,11E-04	Tbc1d12	1,3331094	5,65E-05
Plek2	1,4654184	6,16E-07	Ublcp1	1,3310957	1,49E-10
Vps13c	1,4649238	3,62E-16	Syce3	1,3309646	3,42E-04
Ppap2a	1,4640836	9,85E-12	Stfa1	1,3298483	2,03E-04
Fmr1nb	1,4607469	9,79E-04	Abcb4	1,3272718	1,42E-15
Erdr1	1,4580412	1,19E-05	Mylk3	1,3257146	1,58E-04
Usp44	1,457733	2,88E-07	Abhd5	1,3202096	8,59E-14
Rbm44	1,4540022	4,01E-04	6030468B19Rik	1,3180757	4,89E-11
Tmem56	1,4483665	4,74E-15	Lamb3	1,3176752	2,79E-03
Gm14139	1,4474806	1,15E-03	BC100530	1,3150009	5,19E-09
Ces1d	1,4458937	1,16E-03	Pcnxl2	1,3129104	4,29E-03
Mfhas1	1,438352	3,27E-09	Ston2	1,3127169	2,25E-07
Fcnb	1,436572	2,52E-10	Smim1	1,3126779	7,26E-17
Rnf128	1,4345709	1,35E-08	Bcl2l15	1,3109579	2,13E-03
Reps2	1,433266	5,26E-07	Mtl5	1,3101552	9,46E-05
Osgepl1	1,4312724	7,79E-18	Mst1	1,3056858	1,01E-03
Cited4	1,4286447	7,51E-19	Myh7b	1,305101	5,39E-05
Rhd	1,4282228	1,12E-19	Pdia2	1,3048265	1,35E-11
Ppp1r36	1,4278205	1,64E-03	2310039L15Rik	1,301563	4,58E-04
Nap1l3	1,4240382	2,90E-06	Igsf3	1,3006249	1,49E-09
Pcdhgb8	1,4194969	1,93E-03	Rab11fip4os1	1,2994452	5,13E-04
Emc9	1,4194416	1,22E-11	Pglyrp1	1,2969445	2,22E-11
Hsd17b6	1,4144886	2,30E-04	Ccl7	1,2946305	3,34E-03
Frmpd1	1,4125338	2,09E-04	Clpx	1,2885359	4,04E-25
Erbb3	1,4123573	6,98E-07	Alas2	1,2854249	8,40E-07
Cachd1	1,4113574	9,87E-06	Farp2	1,2845056	2,78E-03
Mfsd2b	1,4095582	8,99E-17	Map3k6	1,2821448	3,96E-11
Zfp575	1,4088379	2,43E-04	Cftr	1,2811985	5,68E-04
6720489N17Rik	1,4037807	6,56E-15	Epn2	1,2746952	7,39E-04
Rec8	1,4036048	5,01E-07	Uros	1,2745687	4,94E-19
Hspa1a	1,3985543	1,88E-03	Wnk4	1,2743006	4,67E-08
Myo5b	1,3979162	4,74E-04	Enpp3	1,2694104	4,30E-03
Hmbs	1,395101	4,43E-24	Ripply3	1,2663648	3,64E-03
Wipi1	1,2648356	5,55E-09	Lyve1	1,1910053	4,22E-04
Slc22a4	1,2630646	7,29E-09	Prelid2	1,1897801	4,17E-11
G530011O06Rik	1,2597319	3,38E-03	Clca1	1,1895123	9,58E-03
Slc25a31	1,2594419	8,98E-06	Cldn10	1,1882766	8,65E-03
Lama4	1,2580391	2,14E-03	Setx	1,1881732	1,36E-25
1810055G02Rik	1,2573239	3,49E-11	Nxf7	1,1863227	9,75E-03

Pramef12	1,2546984	5,82E-03	3300005D01Rik	1,1857306	1,82E-04
Camsap2	1,2545461	5,20E-13	Spire2	1,1853021	1,91E-03
Hspbap1	1,254303	3,99E-11	Gab2	1,1828941	7,62E-13
Tom1l1	1,254079	2,29E-12	Dnah7a	1,1814929	1,04E-02
Hbq1b	1,2521642	4,26E-03	Xk	1,1809902	8,32E-16
Serpinb8	1,251895	2,32E-03	Smc5	1,180768	3,41E-36
Mgarp	1,251894	4,63E-03	Slc25a38	1,1770311	5,34E-17
Daam1	1,2505969	1,88E-09	1100001G20Rik	1,1709256	4,74E-03
S100a8	1,2498969	3,78E-04	Bex4	1,1707571	7,85E-12
Izumo1	1,249097	4,61E-03	Hormad1	1,1691531	8,78E-04
Slc38a4	1,2472511	1,65E-04	St3gal2	1,1683048	1,79E-16
Mar8	1,2453252	7,49E-17	Ampd3	1,1600172	1,49E-12
Ryk	1,2452368	8,28E-08	Hsd11b1	1,1581237	5,99E-05
Cttn	1,240266	6,19E-21	Rb1	1,1555064	2,59E-10
Tjp1	1,2396396	1,92E-07	C4b	1,1554892	1,21E-02
Slc25a21	1,2396214	5,55E-09	Atp7b	1,1548394	4,63E-11
Fhdc1	1,2370709	8,76E-07	Abcb6	1,1470478	1,76E-16
Cacna1h	1,2362695	7,37E-03	Gm13152	1,1400409	7,84E-05
4933431E20Rik	1,2353712	2,91E-06	Pcdhgb4	1,1383426	6,91E-04
Glrx5	1,2351277	3,47E-14	Lefty1	1,1365613	1,39E-03
Cldn13	1,2338363	3,10E-12	Lrig1	1,1362258	2,36E-03
Sema4f	1,233763	1,95E-03	Dusp27	1,1354405	4,22E-03
Arhgef25	1,2321451	1,13E-08	Zadh2	1,132897	2,33E-13
5730460C07Rik	1,2304122	3,82E-03	Tfrc	1,1312059	5,34E-15
Tnfrsf23	1,2289339	8,47E-04	Nqo1	1,1299371	2,34E-05
Pkd1l2	1,226263	2,77E-03	Trib3	1,128866	2,51E-03
Myo1d	1,2250176	4,65E-08	Pmm1	1,1285747	6,84E-11
Zcwpw1	1,2232959	3,06E-14	Adamtsl5	1,1274244	2,69E-03
Wdr65	1,2232584	2,37E-04	Slc9b1	1,1271927	1,45E-02
Ero1l	1,2219676	2,36E-20	Rfx2	1,1269467	6,19E-08
6820408C15Rik	1,2182958	6,82E-03	Mael	1,1264387	9,85E-04
Tmem40	1,2160405	1,84E-15	C330013F16Rik	1,1252908	7,36E-03
Gm4841	1,215788	4,46E-03	Pcdhgb2	1,1218606	1,54E-02
Ccnb3	1,2133227	3,52E-03	Syt5	1,1214958	1,28E-02
Meiob	1,2130682	6,97E-03	Hsd17b14	1,1210328	9,30E-04
Asb17	1,2118463	2,06E-03	Cldn15	1,1202908	5,78E-04
Gstm5	1,2110594	4,45E-12	D730045A05Rik	1,1202768	1,46E-03
Ttc39b	1,209798	2,28E-12	Pcyt1b	1,1193293	1,33E-07
Sgpp1	1,2086942	2,31E-12	Igsf21	1,1188752	1,44E-03
Zdhhc14	1,2056865	1,33E-06	Serpinb9c	1,1180001	1,45E-03
Tbc1d24	1,2023516	9,51E-17	Bag3	1,1138171	5,75E-06
Cables1	1,2004873	8,27E-07	Prom1	1,1127976	1,23E-03
C5ar1	1,1990816	3,02E-05	Tnfaip2	1,1106008	1,25E-13
Kcnj5	1,1975686	4,58E-03	Aqp3	1,1092911	2,73E-08
Epdr1	1,1971631	6,84E-12	Alpl	1,1091924	1,75E-03
Zfpm1	1,1964252	3,49E-04	Atg2b	1,1059037	4,07E-21
Gml	1,1937558	8,01E-03	Asb17os	1,1016322	8,51E-03
Lrig3	1,192448	3,63E-03	St6galnac3	1,1014295	1,35E-15
Itch	1,1012271	4,50E-24	Ifnlr1	1,0451652	2,06E-02
Hspa1b	1,1004319	1,56E-02	Stx11	1,0399989	2,41E-04
I730030J21Rik	1,0980987	2,29E-03	Iqcd	1,039749	5,97E-03
Rcvrn	1,0962681	8,19E-03	Oaf	1,0375675	9,31E-06
Samd11	1,0942726	9,52E-03	Prdx3	1,0359271	1,58E-13
Hemt1	1,0931393	1,80E-02	Chrnb4	1,0319736	2,54E-02
Alox5	1,092578	4,84E-05	Lcn2	1,0309829	2,27E-02
Prkar2b	1,0877592	4,69E-14	C1galt1	1,0303033	4,76E-05

Agrn	1,0876958	3,98E-08	C330024C12Rik	1,0279956	2,77E-02
Cpd	1,0864386	3,71E-14	Nxpe2	1,0268056	5,40E-09
Tmem150cos	1,0822279	2,11E-03	Mgst3	1,026474	1,03E-11
Xlr4a	1,0819899	2,73E-04	Casp4	1,0251107	1,99E-05
Ctcflos	1,0796263	1,53E-02	Tarsl2	1,0231074	1,54E-09
Slc6a13	1,0782761	4,45E-09	Osbpl3	1,0215155	9,54E-10
Gpr150	1,0774187	5,69E-03	Steap3	1,0190118	2,55E-12
4921525O09Rik	1,0769818	1,92E-02	Ubac1	1,0189399	1,55E-13
Gm13154	1,0769119	2,91E-03	Fam124a	1,0185269	2,34E-02
Cnnm2	1,0750862	1,83E-07	Larp1b	1,0169644	7,89E-04
Pard3	1,0750438	1,99E-02	Car2	1,015679	8,60E-17
Chac2	1,0726741	6,07E-08	Clec2i	1,0147633	3,49E-04
Fam208a	1,0698819	2,87E-17	Cyth3	1,0144599	2,50E-08
Gpsm2	1,0687973	1,12E-12	Atp8b5	1,0128026	2,95E-02
Mob1b	1,0685954	1,15E-06	Baz1a	1,0127915	3,14E-12
Zbtbd6	1,0676747	9,98E-05	Tmem14c	1,010262	1,81E-15
Mgll	1,0675934	1,25E-05	Papola	1,0075784	9,10E-20
Chchd10	1,0650286	1,03E-08	Tango2	1,0031604	5,72E-12
Map10	1,0642454	4,45E-05	Tada2b	1,0005125	1,83E-03
Cep76	1,0634093	3,27E-12	Stfa2l1	0,9994915	2,72E-02
Dcbld2	1,063319	1,84E-03	Mar3	0,997418	4,45E-05
Fndc5	1,0627381	2,03E-02	Asb1	0,9956015	7,46E-08
Nt5c3	1,0627334	1,10E-14	Hipk2	0,9941047	1,21E-09
BC021767	1,0622386	1,99E-02	2210016F16Rik	0,9926616	4,43E-08
Fry	1,0604794	1,93E-11	Cd55	0,9909568	4,80E-07
Asnsd1	1,0598504	2,40E-15	Ccdc150	0,9908859	1,87E-02
Scube2	1,0597103	1,02E-02	Hebp1	0,9901782	4,57E-08
Ttbk2	1,0583909	3,70E-07	Rnf43	0,9889909	4,37E-03
Arrb1	1,0568952	9,51E-17	Smoc1	0,9870762	3,31E-05
Sh3tc2	1,0545377	1,10E-02	Foxh1	0,9863471	1,12E-02
Wdr63	1,0540753	2,20E-03	Gas6	0,9855312	1,32E-02
Ldoc1l	1,0537434	1,87E-09	Nadk2	0,9837194	2,72E-10
BC049635	1,0535643	2,31E-02	1110008P14Rik	0,983182	4,36E-06
Fam20a	1,0535276	1,02E-02	B3gnt7	0,9824974	1,65E-13
Prkab1	1,0527458	1,81E-16	Akr1c13	0,9777232	7,50E-11
Gca	1,0516229	1,20E-04	Stx2	0,9766895	6,34E-12
Cetn4	1,0506594	1,22E-02	Ehd3	0,9758416	1,54E-04
Etv4	1,050582	1,70E-02	Dennd4a	0,9753763	4,86E-16
Fam188a	1,0497368	5,88E-17	Syne1	0,9750336	2,92E-10
Abcb9	1,0492254	2,69E-07	Gpr64	0,97461	3,83E-02
0610010F05Rik	1,0489886	1,25E-16	Gm19589	0,9703624	2,70E-02
2410088K16Rik	1,0489763	2,66E-03	Ntn4	0,967827	1,80E-02
Lactb2	1,0481825	1,48E-09	Plekhg4	0,9651027	3,50E-02
Caprin2	1,0474423	9,85E-12	Galnt2	0,9635011	1,27E-12
Abcg2	1,0470941	1,45E-12	Mpp2	0,9633888	2,87E-05
Dnaja4	1,0464699	8,94E-05	9830132P13Rik	0,9626518	3,57E-02
Atp1b1	0,9625034	1,47E-06	Crip2	0,892633	4,88E-06
Qpct	0,9593827	3,46E-02	Pacs1	0,8923571	4,93E-12
Hk1	0,9590892	7,79E-20	Mtus2	0,8922704	2,60E-02
Slc14a1	0,9574914	4,36E-08	Usp45	0,8919834	3,88E-08
Lrrc20	0,955788	1,19E-07	Lyar	0,8908595	4,69E-14
Aplp2	0,9554736	1,18E-11	Zfp709	0,8880914	1,13E-06
Mical2	0,9552635	2,00E-06	Mylk	0,8870875	1,22E-03
Spo11	0,9551951	1,53E-02	Tmem9b	0,8826568	5,91E-07
Pvt1	0,9533239	1,30E-04	Rexo2	0,8815325	1,52E-10
Ccrn4l	0,952622	2,93E-07	4930459C07Rik	0,8811962	7,56E-03

3110043O21Rik	0,9504952	5,32E-06	Tnfrsf14	0,8808207	4,21E-04
Txnrd2	0,9503811	7,57E-13	Clec4b2	0,8800382	3,93E-02
Tnk2	0,9493799	1,58E-05	Zdhhc25	0,8791541	7,77E-03
Soga1	0,9477204	5,71E-11	Nars2	0,8760206	6,21E-11
Tmem64	0,9476011	4,98E-08	Cdc73	0,8744485	8,11E-07
Clstn3	0,9475192	9,21E-14	Tdrkh	0,8739256	4,65E-10
Bdh1	0,9458047	1,07E-10	Ank	0,8738972	5,42E-05
Slc4a1	0,9449419	3,55E-02	Stab1	0,8733585	3,47E-02
Sep8	0,9446096	3,78E-12	Orc5	0,8733242	1,61E-07
Zfp882	0,9410827	5,11E-06	Mcts2	0,871966	2,52E-04
Spock2	0,9382296	4,40E-02	Dopey2	0,8713884	1,97E-08
Rtn4r	0,9378714	3,96E-02	Atp6v0a1	0,8702985	1,02E-07
Myh10	0,9375839	8,81E-09	Slc35g1	0,8699333	7,85E-06
Pip5k1b	0,9363386	8,38E-04	Olr1	0,8694383	1,11E-02
Atp1b2	0,9346824	1,12E-11	9430020K01Rik	0,8692793	3,74E-06
S100a9	0,9345382	1,80E-02	Klhl12	0,8687579	2,53E-10
Fitm1	0,9338341	4,71E-02	Unc5cl	0,8679008	1,06E-02
A630007B06Rik	0,9312392	6,20E-07	E2f4	0,8667167	9,85E-12
Bai2	0,9265123	1,79E-02	4930430F08Rik	0,8658788	2,39E-05
Cela1	0,9262024	1,18E-05	Tmem120b	0,865233	1,31E-04
Gm10825	0,9227843	5,06E-03	Prss57	0,8635195	1,04E-05
Clcn3	0,9185335	6,31E-12	Dclre1a	0,8612354	7,12E-08
1700012B07Rik	0,9178158	5,35E-03	Mtfr1	0,8596182	8,55E-11
Gatsl3	0,9167123	2,57E-02	Bola3	0,8587923	1,24E-06
Glo1	0,9164363	2,75E-13	2610524H06Rik	0,8578213	2,05E-11
Adcy6	0,9108907	3,94E-06	Tex21	0,8567956	4,59E-02
Ankrd9	0,9101948	3,95E-04	Cpt1c	0,8553236	4,36E-02
Bambi	0,9100579	7,13E-05	Klhl23	0,8544994	2,34E-07
Plxna2	0,9094029	4,57E-04	Ufsp1	0,8543189	2,37E-02
Rmdn3	0,9075287	1,65E-10	Pnpo	0,8540311	4,30E-10
Zfp951	0,9064102	1,53E-04	Ntn3	0,8524026	2,32E-02
Phf10	0,9055038	6,55E-09	Otub2	0,8516456	2,39E-05
Def8	0,9049531	1,30E-10	Rnf125	0,8487836	2,39E-04
Tspan8	0,9039813	1,66E-05	Sycn	0,8474739	9,78E-03
Gpr155	0,9011906	4,65E-04	Ppp1r15a	0,8467743	3,53E-07
Ept1	0,8996499	2,27E-08	Gsr	0,8438917	6,21E-08
1300002E11Rik	0,8963692	1,10E-07	Pdk1	0,8407762	2,36E-13
Clint1	0,8963311	1,29E-12	Hcfc2	0,8403569	1,85E-07
Trim58	0,8959682	1,82E-04	Xlr4b	0,8402054	1,67E-02
St3gal6	0,895684	8,98E-07	Cox17	0,8389155	1,03E-10
Slc11a2	0,8949372	2,62E-08	Dhx40	0,8374628	1,93E-06
Chil1	0,8947832	3,37E-02	Chst11	0,8371221	2,24E-04
Acsl1	0,8941551	3,62E-09	Man1a	0,8358205	1,05E-13
Ctsg	0,8936148	1,73E-06	Bcas2	0,8357261	7,60E-13
Mical3	0,8354692	2,53E-05	Galnt10	0,7742541	5,89E-07
Svip	0,8353705	8,58E-07	Desi2	0,7738541	4,36E-09
Fhod3	0,8341317	4,37E-02	Tfr2	0,7728281	8,21E-10
5730420D15Rik	0,8334663	3,06E-02	Nt5dc2	0,7725827	9,25E-07
Pbx3	0,8305708	1,47E-03	Grina	0,7705256	2,43E-06
Pi4k2b	0,8247634	4,15E-08	Asap1	0,7702292	2,45E-08
Tnnt1	0,8220667	1,24E-03	Odc1	0,7683192	4,91E-07
Tuba3a	0,82043	4,71E-02	Lpcat1	0,7677041	4,20E-08
0610040J01Rik	0,8200192	8,92E-04	Mospd3	0,767452	3,15E-09
Cpeb4	0,8200172	1,13E-05	Tsnax	0,7665593	5,89E-11
1810006J02Rik	0,8185635	4,03E-02	Dusp4	0,7663975	3,58E-02
Pip4k2c	0,8182758	4,33E-10	Usp7	0,7645412	7,87E-09

Epha8	0,8178547	3,29E-02	Cd59a	0,7638595	3,50E-04
Gtf2h1	0,8168741	1,67E-10	Slc38a5	0,7625067	1,22E-04
Crnde	0,8149574	3,04E-03	Homer1	0,761705	2,94E-04
Glcci1	0,8142211	5,55E-03	Lgals1	0,7598754	7,28E-11
Cd24a	0,8127435	2,65E-10	Guk1	0,759131	2,32E-08
Agfg1	0,8117973	2,12E-06	Usp46	0,7587114	7,75E-09
Gm13251	0,8107755	3,70E-02	Ift140	0,7580814	2,35E-09
BC021614	0,8103604	1,69E-02	Rnf19a	0,756649	4,33E-08
Klf9	0,808723	4,17E-02	Ddah1	0,7566064	4,29E-02
Ttll12	0,8078066	8,51E-12	Gm16793	0,7549367	1,73E-02
Hace1	0,8050122	2,30E-05	Lgr4	0,7545065	3,49E-02
Bahd1	0,8044307	5,42E-05	Ankrd6	0,754494	5,75E-06
Mgl2	0,8025303	3,27E-02	Tm7sf3	0,7540679	6,54E-07
Btaf1	0,8013901	2,22E-11	Morc2a	0,7531969	2,76E-11
Zfp110	0,8009823	4,45E-10	Adamts3	0,7523382	8,08E-04
Frmd4a	0,7989081	1,59E-09	Ttll4	0,7521936	3,04E-11
Lnp	0,7982031	2,96E-06	Zfp78	0,7511897	2,66E-02
Lpin1	0,7976243	1,23E-07	Idh3a	0,749251	5,72E-10
Slc25a33	0,7973638	4,51E-03	Ehbp1	0,7479924	1,39E-03
Acaa2	0,7966919	6,35E-10	Olfml1	0,7476354	4,68E-02
Tgm2	0,7962094	5,82E-08	Bcl2l11	0,7459766	3,71E-06
Pgp	0,7960079	1,91E-07	Htatip2	0,7455717	4,83E-07
Zfp69	0,7934059	4,00E-04	Zc3hav1l	0,7451702	4,18E-06
Ermp1	0,7884162	2,72E-10	Mar2	0,744695	1,55E-06
4732471J01Rik	0,787227	1,49E-02	8430419L09Rik	0,7442279	1,54E-07
Yod1	0,7867483	1,44E-05	Ankrd13c	0,7439803	1,39E-04
Hif3a	0,7866956	4,35E-11	Zfp800	0,7439242	1,57E-06
Tab3	0,7848308	3,86E-06	Klf11	0,7435058	1,65E-03
Slc16a1	0,7844482	6,61E-12	Ago2	0,741156	1,08E-08
Spire1	0,7840142	1,31E-06	Eps15	0,740532	1,07E-08
Mbd2	0,7839611	2,00E-04	Mns1	0,740437	3,94E-06
Pik3cb	0,7832014	3,29E-05	Ehd1	0,7386676	5,65E-07
Ethe1	0,7827175	8,12E-09	Pycr2	0,7369781	8,52E-09
Folr1	0,7806482	3,99E-02	Zfp934	0,7361178	3,01E-04
Smap1	0,7777494	1,10E-03	Scml4	0,7350946	1,19E-03
Slc12a4	0,7771733	1,18E-05	Ash2l	0,7349267	2,84E-08
Hmgb3	0,7758455	1,29E-11	Prss50	0,7345276	9,53E-04
Sssca1	0,7757501	1,66E-09	Eml5	0,7344801	4,84E-03
Clec10a	0,7755102	4,61E-02	Narf	0,7337628	3,43E-07
Dnajc19	0,7750467	4,57E-08	Wsb2	0,7336889	3,00E-04
Ppp2r3a	0,7743764	2,26E-05	Tlk1	0,7334515	2,73E-09
Pithd1	0,7743377	9,17E-06	Uap1	0,7333008	2,32E-07
Ubxn2a	0,7327981	1,93E-06	Xpo4	0,6921726	1,26E-06
Gas2l1	0,7324854	6,68E-03	Per2	0,6910965	2,21E-05
Dram1	0,7320583	3,12E-02	Slc16a6	0,6909977	5,85E-05
Tmem69	0,7320553	1,15E-05	Fth1	0,6899175	7,31E-08
Orc2	0,7313007	2,05E-10	Uimc1	0,688576	6,90E-09
Ptpdc1	0,7311657	3,60E-02	Gm3604	0,6878223	2,61E-03
4930452B06Rik	0,7311215	1,61E-02	Tal1	0,6877877	2,01E-05
Pcyt1a	0,7301649	2,10E-07	Hic2	0,6876636	7,46E-05
Mthfd2	0,7299765	6,61E-08	Hdac11	0,6862127	3,71E-02
Esyt2	0,7298282	5,61E-07	Higd1a	0,6859963	1,39E-07
Fndc3b	0,7295063	7,05E-04	Fam195a	0,6859003	5,36E-05
Gm13283	0,7275837	1,96E-02	Donson	0,6858579	6,19E-04
Polm	0,7263392	3,68E-02	Arl5a	0,6851914	2,03E-06
Pnp2	0,7254367	2,96E-03	Fam126a	0,6851381	8,07E-08

Golph3	0,7241041	2,81E-08	Hiatl1	0,6838614	5,85E-08
Atp8a1	0,7239534	4,84E-08	Nudt4	0,6836934	1,20E-05
4921513I03Rik	0,72357	1,81E-02	Ptpn12	0,6836712	2,82E-06
Napepld	0,7235289	5,75E-03	Parm1	0,6833196	3,80E-02
Hp	0,7222128	2,98E-04	Sord	0,6812483	5,87E-07
Isca1	0,7221847	3,19E-08	Ydjc	0,6790798	1,84E-04
Cdk14	0,7214768	2,32E-03	Gid8	0,6786611	3,36E-07
Acss1	0,7204761	2,95E-06	8030462N17Rik	0,6784936	1,70E-02
Csgalnact1	0,7203869	3,03E-04	Acer2	0,678286	5,10E-03
Ciart	0,7193812	4,23E-02	Acp5	0,6773214	2,60E-06
Clybl	0,7192084	2,71E-06	Hspa4l	0,6761067	2,68E-06
Mapk13	0,7189865	1,08E-02	Sfxn1	0,6743105	1,62E-09
Ythdc2	0,7181701	3,70E-05	Tmc1	0,6729012	2,98E-02
Nudt9	0,7179982	4,11E-08	Bag2	0,6716375	4,11E-07
Map4k5	0,7171224	2,58E-04	Exoc5	0,6712813	7,49E-08
Snhg3	0,7156589	8,59E-05	Atp13a3	0,6709501	4,63E-07
Ap3s1	0,7144224	7,88E-05	Zfp511	0,6708682	7,91E-05
Tmem185b	0,7139619	4,46E-07	Asf1a	0,6686796	7,02E-06
Klhdc2	0,7122124	6,14E-06	Gfm1	0,6684343	1,77E-07
Slc7a7	0,7120652	6,57E-03	Ppa1	0,6677958	9,73E-09
Ankrd27	0,711391	1,18E-09	Wapal	0,6669064	2,00E-07
Sphk1	0,7112978	5,35E-04	Slc30a1	0,6653256	3,15E-02
Zc3h6	0,7109434	4,47E-03	Sorbs1	0,664583	8,26E-04
Afap1	0,709759	8,41E-03	Ddx39	0,6645788	9,57E-09
Slc26a1	0,7087572	1,11E-03	Xpnpep1	0,6640636	3,70E-08
Dhrs11	0,7087264	2,41E-06	Eif2b3	0,6629546	5,97E-06
Pno1	0,7085771	2,02E-08	Piezo1	0,6619721	1,74E-05
Mcu	0,7082665	5,92E-04	Rom1	0,661665	4,83E-02
Wrn	0,7071422	9,82E-06	Lysmd3	0,6616073	5,05E-05
Rnf123	0,7055923	5,22E-09	Aqp9	0,6613916	4,96E-07
Msh2	0,7029918	8,34E-11	Mff	0,6612152	9,10E-07
Cox11	0,7024608	5,75E-05	Gcsh	0,6597228	1,55E-07
Ninl	0,6986568	1,14E-04	Hspe1	0,6593156	1,87E-08
Hyou1	0,6983821	6,88E-10	Rnf139	0,65896	3,79E-05
Bnip3	0,6969537	2,80E-06	C1qbp	0,6587693	1,53E-06
Casc4	0,6963895	2,09E-04	Gss	0,6580912	7,59E-06
Sec24a	0,6963008	9,55E-05	Slc2a8	0,6569316	6,54E-04
Ammecr1	0,6962557	2,89E-04	Tprgl	0,6559553	1,97E-04
Mettl20	0,6949764	3,99E-05	Hs6st1	0,6555012	4,23E-04
Golm1	0,6947288	4,40E-06	Gm13212	0,6551413	1,86E-02
Ppox	0,6548845	3,74E-06	Slc25a16	0,6308011	5,85E-04
Plaa	0,6548733	1,22E-08	Ly6c2	0,6302022	2,69E-02
Uqcc2	0,6546951	1,20E-09	Ifrd2	0,6289086	1,43E-06
Atf4	0,6545735	2,17E-07	Kctd7	0,6284464	1,13E-03
Ap2a1	0,6539915	7,42E-08	Psme3	0,6281503	7,19E-08
Prkaa1	0,6530668	2,25E-05	Scd1	0,6280168	5,73E-03
Taf10	0,652192	1,41E-03	Psmg2	0,6275666	6,40E-07
Rpia	0,6521529	1,39E-02	Casp3	0,6272755	1,13E-05
Spryd7	0,6509974	5,60E-04	Tcam1	0,6268134	1,01E-02
Iba57	0,6506159	2,48E-04	Hras	0,6266456	7,31E-03
Ubxn2b	0,6504017	2,34E-05	Timm23	0,6265248	8,20E-07
Rab10os	0,650098	4,64E-05	Srm	0,6258352	7,32E-07
Rabgef1	0,6487272	5,67E-06	Tmem131	0,6255609	2,75E-06
Nudt19	0,6485445	1,58E-06	Gars	0,6252969	1,88E-07
Grb10	0,6485291	6,99E-10	Prkag1	0,6248185	1,52E-06
Clic4	0,6481199	1,24E-08	Pus7	0,6232391	1,60E-07

Fbxo10	0,6478837	1,53E-03	Metap2	0,6227054	1,08E-07
Slc19a2	0,6477122	2,26E-03	Slc25a37	0,6226508	2,51E-05
Cnr2	0,6474856	3,18E-06	Ube2j1	0,6220545	8,64E-06
Ppa2	0,6473058	1,93E-06	2410127L17Rik	0,6214658	9,21E-03
St3gal5	0,6469284	2,28E-05	Fabp5	0,6214432	2,17E-05
Anxa9	0,6469159	1,39E-02	Gfpt1	0,6212071	2,59E-05
Tshz1	0,6467994	2,87E-04	Tmtc3	0,6209384	1,48E-04
Pir	0,6467547	4,58E-02	Eps8	0,6206337	6,77E-04
Egln3	0,6467367	1,61E-05	Orc1	0,620102	1,98E-04
Slc35a3	0,6467304	1,06E-04	Gpc2	0,6195882	7,21E-04
Bysl	0,6448274	8,58E-07	Mthfd1	0,6194103	6,23E-08
Stom	0,6446454	1,23E-04	Ube2c	0,6191685	3,65E-09
Ube3c	0,644592	1,39E-06	Hsph1	0,6188204	1,16E-07
Abcc4	0,6436441	3,43E-05	Lsr	0,6187547	6,80E-03
Ccdc71l	0,6436222	8,75E-03	Stk38l	0,617531	2,32E-03
Tceal8	0,6435865	5,85E-05	Sun1	0,6174729	1,10E-06
Vkorc1l1	0,641859	3,44E-05	Pabpc4	0,6174712	2,28E-05
Scrn3	0,6410343	2,04E-04	3110002H16Rik	0,617327	5,20E-06
Mllt3	0,6406979	1,57E-04	Stt3b	0,6165417	1,99E-08
Zbtb46	0,6405201	3,47E-02	Hdgf	0,6165356	3,59E-02
Mrs2	0,6394935	5,59E-03	Gcnt1	0,6162731	2,44E-05
Gm13157	0,6391396	3,45E-05	Kti12	0,6147202	1,13E-06
Ccrl2	0,6390424	1,20E-02	Etf1	0,6137101	3,62E-08
Psmd5	0,6388889	1,89E-06	C1rl	0,6133274	9,00E-03
Mylpf	0,6388189	6,68E-03	Wdsub1	0,6118009	1,17E-04
Ranbp17	0,6374578	6,19E-03	Olfr417	0,6115816	4,27E-02
B3galnt2	0,6373383	3,49E-07	Pitrm1	0,6115753	5,10E-07
AI662270	0,6357565	1,26E-07	Cry2	0,6113988	1,18E-04
Gclc	0,6356941	1,71E-04	Faf1	0,6111681	7,34E-04
Tprkb	0,6336265	4,53E-04	Sod2	0,6108655	1,42E-06
A430005L14Rik	0,6333942	8,42E-06	Nhp2	0,6099265	3,40E-08
Rab44	0,6331293	3,05E-04	Gfi1b	0,6090423	2,09E-04
Clptm1l	0,6331176	1,10E-04	1700037H04Rik	0,6088818	4,70E-06
Ush1c	0,6328381	3,63E-02	Lonrf1	0,6079326	4,06E-02
Crat	0,63206	2,72E-05	Mtfp1	0,6076385	1,33E-04
Mtf1	0,6316884	3,79E-05	Dld	0,6073976	1,64E-05
Nek1	0,6313988	6,81E-06	Ahctf1	0,6066918	9,11E-09
Smim5	0,6311694	3,43E-05	Dmkn	0,6065729	4,43E-02
Cdc20	0,6065583	1,12E-05	Ankrd22	0,5773667	4,14E-02
Atxn1	0,6051999	4,48E-03	Gab1	0,577093	4,81E-04
Pon2	0,6044485	2,54E-06	Uqcrq	0,5761557	5,23E-07
Tomm40	0,6040646	3,93E-06	Gm608	0,5759607	1,02E-03
Dnajc12	0,6037823	8,78E-03	Idi1	0,5759576	1,42E-02
Eef1e1	0,6031091	3,08E-05	Pfkp	0,5758569	4,91E-05
Ccdc23	0,60216	2,91E-05	2700097O09Rik	0,5726082	1,64E-03
Fnip2	0,6021377	1,60E-03	Wdr55	0,5726059	2,91E-05
Dpy19l1	0,6008246	2,39E-04	Ring1	0,5719358	2,60E-03
Acss2	0,6000951	2,61E-03	Mrto4	0,5712006	1,17E-06
Lrrc8b	0,5989471	3,27E-03	Usp33	0,5708612	1,39E-05
Utp18	0,5988192	6,49E-06	Fbxo30	0,5706454	2,02E-04
Eaf1	0,5980557	1,09E-07	Gga2	0,5699683	2,34E-05
Mrpl20	0,5971043	3,52E-06	Rae1	0,5696157	7,48E-07
Ska1	0,5966339	2,53E-05	Rn45s	0,5695793	2,71E-06
Eri2	0,5965838	6,87E-05	Mpv17l2	0,5690084	1,37E-03
Fbxo9	0,5957671	4,53E-05	Usp14	0,5689006	1,76E-06
Urod	0,595732	4,12E-05	Mbd1	0,568882	5,45E-08

Trappc10	0,5954488	3,43E-04	Ppm1l	0,5686889	2,25E-03
Scamp1	0,5949974	1,80E-05	Helq	0,5665441	6,15E-04
Hnrnpll	0,5938576	1,92E-05	Pigg	0,5655552	1,66E-03
Fam98a	0,5935472	8,63E-06	Cars	0,5651461	1,60E-05
Htra2	0,5931226	7,14E-07	Alg3	0,5649196	4,70E-06
Sccpdh	0,5926563	3,58E-04	Uqcrfs1	0,5636912	8,16E-05
Epb4.1	0,5922842	2,57E-08	Psmd7	0,5636049	1,06E-07
Slc7a5	0,591367	3,77E-06	Sav1	0,563494	1,50E-02
Erc1	0,5905507	1,36E-03	Bmp2k	0,5623472	8,37E-03
Heatr3	0,5904979	4,57E-08	Atp1b3	0,5612319	1,44E-05
Minpp1	0,5902235	5,47E-06	Mars	0,5610752	4,87E-08
Txnl1	0,5901191	6,31E-07	Srp19	0,5607797	2,17E-06
Bcl2l13	0,5897559	6,82E-07	D10Wsu102e	0,5604552	2,06E-06
4930523C07Rik	0,5897002	1,31E-03	Atp2a2	0,5603772	1,88E-05
Ppp2r1b	0,5891303	2,12E-06	Plk1	0,5600315	9,49E-08
6030458C11Rik	0,5886115	1,52E-06	Nsun2	0,5599403	3,22E-06
Ranbp2	0,5882885	1,30E-06	Dr1	0,5598202	8,42E-07
F2r	0,5869993	1,50E-05	Lmtk2	0,5569446	7,21E-04
Degs1	0,5864157	4,54E-06	Parp16	0,5545051	4,24E-03
Cdyl	0,5864121	5,24E-03	C230052I12Rik	0,5540036	2,92E-04
Serpinb9e	0,5854068	4,81E-02	2410004N09Rik	0,5537946	1,58E-02
Gnai3	0,5852112	8,73E-08	Pqlc1	0,5531674	1,36E-05
Kif5b	0,5845918	4,45E-09	Msh6	0,5529643	3,77E-06
Afg3l2	0,5836475	1,96E-05	Dhx29	0,5517945	1,76E-05
Cish	0,5832678	1,30E-02	Cat	0,5508204	2,47E-05
Nol10	0,5831733	4,93E-05	Psmg4	0,5507113	3,86E-04
Dph3	0,5829716	8,47E-06	Gpr146	0,5505052	8,99E-03
Tram1	0,5825256	1,67E-07	Timm17a	0,5502314	1,61E-05
Flt3l	0,5822472	6,41E-03	Comt	0,5492316	1,52E-06
Brpf3	0,5815607	1,35E-03	Ampd2	0,5488647	4,67E-08
Adk	0,5798451	1,57E-05	Akap1	0,5486392	5,88E-05
Xpot	0,5794386	1,07E-08	Get4	0,5484935	1,93E-03
Ehhadh	0,5793959	1,36E-02	Ccna2	0,5481532	8,30E-05
Rabggtb	0,5787522	5,16E-04	Iars2	0,5478725	7,02E-06
Lrrc8c	0,5782896	7,44E-05	Eif2ak1	0,5476023	5,72E-05
Tnfrsf26	0,5773675	5,80E-03	Psma8	0,547562	2,50E-02
Cdc25b	0,5465676	2,57E-05	Mrpl12	0,5214136	2,15E-05
Slc7a1	0,5464856	1,70E-06	Sdf2l1	0,5211818	4,15E-04
Ubp1	0,5460983	5,26E-05	Rcor1	0,5208767	2,37E-03
Slc48a1	0,5448063	5,42E-05	Atpif1	0,5207759	1,88E-06
Jmy	0,5445135	7,70E-03	Arfgef2	0,5207437	9,69E-05
Mettl16	0,5444307	3,17E-05	Slc25a44	0,520564	2,59E-03
Cenpw	0,5444254	3,99E-05	Dctn6	0,519989	6,30E-05
Surf2	0,5438119	2,69E-04	Pigq	0,5196697	3,71E-05
Nupl2	0,5435059	1,12E-03	Bsg	0,5195	1,07E-04
Mbp	0,5432329	5,22E-06	Ppm1g	0,5192672	1,59E-05
Tbrg4	0,5430038	2,27E-05	Ormdl3	0,5179825	4,26E-05
Pgm1	0,542636	9,13E-06	Nsun5	0,5177999	2,46E-05
Mtx2	0,5423633	3,15E-04	Cep70	0,5173382	9,26E-04
Deptor	0,5422021	1,79E-03	Hmmr	0,5163015	3,35E-04
Hectd1	0,5419766	1,17E-06	Manf	0,5162834	5,85E-05
Cltc	0,5405592	1,04E-05	Fam136a	0,5161691	4,86E-06
Tstd3	0,5404537	1,25E-02	Prrc1	0,516154	2,56E-05
Ube2q2	0,5404142	4,68E-04	Tomm70a	0,5160315	6,73E-06
Myo19	0,5393532	5,87E-03	Cdk8	0,5159343	2,14E-03
Rhoq	0,5387401	1,19E-02	Slc25a32	0,5157853	1,51E-03

Ecsit	0,5382975	1,96E-04	Larp1	0,5137087	2,67E-05
Phykpl	0,5380695	1,57E-03	Tmed7	0,5135818	5,10E-03
Prdx2	0,5379231	1,21E-05	C030006K11Rik	0,513375	9,70E-03
Tmem184c	0,5362207	2,23E-03	Pkn2	0,5132744	1,43E-04
Bcat2	0,5360382	1,52E-05	Ddx21	0,513243	1,27E-04
Whamm	0,5353676	4,94E-02	Cdkn3	0,511882	2,99E-03
Atl2	0,5353609	1,38E-04	Psmd3	0,5116396	2,72E-05
Tuba1c	0,535008	1,04E-05	Micu2	0,5113027	8,61E-04
Ppid	0,5347937	3,52E-06	Memo1	0,5112038	2,97E-04
Slmo2	0,5347516	5,68E-06	Kpna2	0,5105942	4,41E-05
Chd7	0,5347318	3,29E-03	Akap7	0,5101998	3,36E-02
Arhgap28	0,5339273	5,32E-03	Ankrd54	0,5095454	4,22E-03
Acp1	0,5337045	1,20E-04	Uso1	0,5084325	8,47E-06
Kpna1	0,5317489	3,89E-06	Strap	0,5083744	2,41E-05
Caap1	0,5314196	1,89E-02	Uck2	0,5071547	1,99E-04
Phb2	0,5311154	2,48E-05	Ccnb1	0,5062627	1,40E-04
Ap4e1	0,529691	7,21E-04	Hprt	0,5062015	1,80E-05
Ptdss2	0,5295754	1,18E-04	Mettl8	0,5058326	5,00E-03
Scoc	0,5286552	2,06E-03	Slc35b1	0,505724	7,86E-05
Nploc4	0,5283704	7,77E-05	Ltb	0,5053209	1,22E-02
D630045J12Rik	0,5270822	3,36E-02	L2hgdh	0,5053105	2,45E-04
Pik3r2	0,5268815	3,36E-04	Naa50	0,5049237	8,47E-06
Ppp2r4	0,5262515	2,34E-05	Ttc7b	0,5044168	4,58E-02
Eif2b5	0,5261087	6,33E-05	Gucd1	0,5042563	6,07E-04
Mcph1	0,5259838	6,85E-06	Aars	0,5038992	5,04E-06
Amfr	0,5255639	5,27E-04	Bckdhb	0,5033792	6,16E-03
Rasa2	0,5255451	8,03E-04	Comtd1	0,5028444	1,01E-03
Rab6a	0,5249846	4,65E-04	Tomm5	0,5026668	2,73E-05
Fancd2	0,5242548	2,30E-04	Lrpprc	0,5018591	1,84E-05
C330018D20Rik	0,5240794	7,95E-03	Nup210	0,5017762	1,77E-05
Pacsin2	0,5234241	1,57E-06	Atmin	0,5012198	1,97E-03
Necap2	0,5230182	2,00E-05	Fam109b	0,5009905	1,46E-04
Tmc8	0,5217169	7,38E-04	Setd6	0,5009746	1,87E-02
Piga	0,5215545	1,43E-03	Herc4	0,5008448	1,21E-05
Cdc34	0,5006156	3,27E-03	Rmnd5b	0,5001513	4,01E-05
Hbs1l	0,500534	2,58E-04	Sqle	0,5000749	3,19E-05

Table 10.4 | List of significantly downregulated genes in *Setdb1*^{vav} MPPs

gene	log2FoldChange	padj			
Vcam1	-5,4074127	2,37E-80	Pltp	-3,2992584	6,14E-16
Clec7a	-5,4058569	2,99E-61	Prss34	-3,2488261	1,06E-09
Ccr2	-4,8967092	2,02E-133	Sdpr	-3,1150944	1,07E-11
Ccr9	-4,5525165	1,44E-103	Clec4a3	-3,1031785	2,30E-33
Rnd3	-4,4248291	2,55E-35	Pid1	-3,0992277	1,59E-22
Hpgd	-4,3093908	6,78E-71	Gjb2	-3,0859113	4,95E-09
Postn	-4,093155	1,12E-51	Lpar1	-3,073066	2,38E-30
Sema3d	-3,5585212	3,63E-30	Cd209a	-3,0425222	1,02E-08
Ly86	-3,542128	2,94E-74	Tmem26	-3,0296908	8,42E-12
Ms4a4c	-3,5253334	1,55E-19	Mafb	-3,0245151	4,77E-18
Ccr5	-3,5034223	1,54E-29	Wfdc17	-2,9862564	4,28E-38
Siglech	-3,3643387	3,43E-08	Il13ra1	-2,9714949	5,66E-32
Emr4	-3,3610712	1,41E-32	Lilra6	-2,9674334	2,17E-12
Plbd1	-3,3578508	3,74E-36	H2-Aa	-2,9599805	6,02E-14
Ifi204	-3,3529713	3,20E-34	Thbs1	-2,9365948	2,66E-30
Ctsh	-3,3387773	1,26E-75	Mpeg1	-2,8640384	9,38E-29
			Rag1	-2,8637889	1,10E-19

Mar1	-2,8413055	2,89E-14	Csf1r	-2,2286088	8,15E-17
Stc1	-2,833702	1,20E-33	Fn1	-2,2215622	1,27E-28
Pou2af1	-2,8124613	1,25E-06	Kcng1	-2,2173779	2,16E-10
Tcf7	-2,7717945	6,11E-13	Cfh	-2,2164097	2,07E-20
Stab2	-2,7650413	7,41E-17	H19	-2,2137373	2,59E-17
Ifi205	-2,758035	1,70E-06	Mycl	-2,2028114	2,70E-09
Klrk1	-2,7500934	5,66E-08	Mertk	-2,190118	5,51E-13
Sema6d	-2,7317772	1,97E-13	Batf3	-2,1823704	6,83E-07
Dlk1	-2,7182217	1,03E-16	Cmah	-2,1705985	1,77E-15
Vldlr	-2,6788624	5,60E-12	AI607873	-2,1542661	5,35E-17
Mnda	-2,6707619	7,56E-10	Ebf1	-2,1494537	1,26E-11
Cx3cr1	-2,6588658	1,09E-32	Tifab	-2,1482091	1,00E-42
Gpr35	-2,6579691	1,44E-19	Ahnak	-2,1467883	5,15E-27
Gfra2	-2,6474696	1,89E-13	Gbp4	-2,1387747	1,35E-09
Fpr1	-2,6308953	6,91E-10	Cd5l	-2,1281076	2,97E-08
Klra2	-2,6201419	3,89E-09	Icos	-2,1144106	2,83E-14
Slfn2	-2,610413	2,87E-47	Gm5086	-2,1086339	4,01E-06
Clec4n	-2,5932684	1,86E-26	Plxnb2	-2,1045352	1,73E-24
Cd74	-2,5932501	1,65E-35	Rassf4	-2,100909	4,62E-50
Ctss	-2,590086	6,47E-76	Pla2g7	-2,0961615	7,41E-12
Cd36	-2,5853029	1,26E-11	Nrp1	-2,0917921	4,05E-16
Igf1	-2,5847121	3,34E-22	Fcgr1	-2,0889853	5,25E-20
Abca9	-2,5720594	2,32E-14	Pld4	-2,0882868	1,12E-72
Aif1	-2,5691085	3,47E-24	Ddit4l	-2,0863323	4,32E-07
Ms4a6c	-2,5448136	3,47E-14	Il2rb	-2,0664099	6,09E-06
Spic	-2,5262097	1,20E-15	Cttnbp2nl	-2,0654302	2,49E-08
Prss2	-2,5200202	2,56E-07	Kcna2	-2,0611454	4,08E-06
Kmo	-2,5182755	2,07E-24	Lifr	-2,0610041	9,57E-09
Tlr8	-2,5116811	4,30E-10	Ppfia4	-2,0444201	3,47E-27
Mcpt8	-2,5090508	1,92E-09	Arl5c	-2,0411605	7,44E-09
Lgals3	-2,5031593	1,93E-55	Cdh5	-2,0381145	1,62E-08
Pyhin1	-2,4976351	2,67E-22	Ifit3	-2,0213025	3,40E-10
Il7r	-2,417381	1,40E-10	Pygm	-2,0091391	2,94E-20
C6	-2,4169116	3,60E-07	Pirb	-2,0079476	1,19E-31
Cd7	-2,4138772	2,73E-09	Cd22	-2,004892	1,17E-09
Ifitm6	-2,4018993	3,48E-17	A630033H20Rik	-1,9990304	2,79E-09
Hes1	-2,4005381	3,28E-07	Meg3	-1,9921457	4,69E-07
Cybb	-2,398386	5,12E-45	Ms4a4b	-1,9916285	2,99E-06
Nr1h3	-2,3921167	4,43E-18	Ephb6	-1,9851969	1,90E-17
Kynu	-2,3906499	1,30E-10	Tns4	-1,9830353	1,04E-05
Slfn1	-2,3877714	2,06E-10	Slfn5	-1,9745198	1,86E-11
Klf4	-2,3833561	2,39E-10	Klrd1	-1,9705501	1,65E-07
Cysltr1	-2,3772425	1,37E-20	Nes	-1,9582329	3,19E-15
Emr1	-2,3584438	1,20E-33	Ly6d	-1,9581221	9,82E-06
Id2	-2,3482178	2,02E-74	Il18bp	-1,946556	6,00E-07
Asb2	-2,3286787	7,43E-11	AI839979	-1,9443522	3,12E-09
Fcgrt	-2,321982	2,31E-23	Fcgr4	-1,9398975	5,16E-08
P2ry12	-2,3132761	6,13E-15	Hck	-1,9388011	4,65E-25
Scel	-2,3110194	2,51E-05	Cd79a	-1,9282907	4,67E-08
Ptpro	-2,3063502	9,20E-18	Atf3	-1,9239394	1,42E-06
Ccl3	-2,2932413	5,60E-11	Glis3	-1,9155224	3,66E-06
Abcc3	-2,2818739	1,42E-22	Gm5431	-1,9132182	2,18E-06
Zbp1	-2,280832	1,71E-14	Itgax	-1,8982539	1,83E-08
Blnk	-2,2612918	4,33E-07	Cd28	-1,8931908	3,32E-08
Olfm1	-2,2552868	9,89E-10	Slc11a1	-1,8826082	6,14E-18
Gbp8	-2,239311	3,58E-11	Dse	-1,882562	1,72E-19
Apoc1	-1,8812602	3,33E-14	C2	-1,665694	2,62E-05
Irf4	-1,8807927	1,04E-08	Tlr7	-1,6627748	1,75E-13

Ecscr	-1,8785281	7,72E-20	Timd4	-1,6625381	2,21E-05
Gria3	-1,8762189	1,23E-17	Rorc	-1,6617329	1,83E-04
Serpinf1	-1,8715602	6,59E-23	Gpr183	-1,6546554	4,28E-11
Sdc4	-1,8694957	4,96E-11	Clec4a1	-1,6503457	6,59E-05
Nlrp3	-1,8629391	4,51E-07	Anpep	-1,6421843	1,10E-07
Ccl4	-1,8508087	1,21E-16	Btla	-1,6420338	8,93E-09
Axl	-1,8500573	1,07E-18	Plxna4os1	-1,6404161	7,42E-06
Selp	-1,8499318	2,69E-08	Ctsc	-1,6294221	8,07E-48
Mx1	-1,8497908	1,32E-08	Ccl24	-1,6234155	9,62E-08
Cadm1	-1,8481502	3,10E-11	Fos	-1,6219334	6,66E-09
Lyz2	-1,8461667	3,14E-35	Scimp	-1,61913	7,40E-05
Zfp366	-1,8316268	3,92E-05	Pydc3	-1,6189354	2,08E-06
Wfdc18	-1,8312903	1,13E-04	Lgmn	-1,6145778	2,43E-21
Ccl9	-1,8152705	2,30E-08	Kif26a	-1,6142458	7,22E-04
Thbd	-1,8103834	6,51E-18	Pnck	-1,6067702	4,26E-10
Spib	-1,8083394	7,55E-05	Vpreb3	-1,6049473	4,28E-04
Mrc2	-1,7973253	4,99E-04	I830012O16Rik	-1,6044924	2,57E-04
Cd86	-1,7938354	6,84E-22	Arhgef37	-1,6010229	2,39E-04
Acvrl1	-1,7928862	1,86E-07	H2-Eb1	-1,6002486	1,81E-04
P2ry13	-1,7850357	8,87E-15	Trim30a	-1,5994976	3,54E-19
Nrk	-1,782986	9,42E-07	Colq	-1,5970673	3,68E-05
Gbp9	-1,7818278	5,50E-11	Tpm2	-1,5967537	3,43E-15
Irf5	-1,7812948	1,90E-37	Ptprk	-1,5947029	1,26E-08
Rtn1	-1,7801928	9,35E-08	Pmaip1	-1,5926463	7,99E-12
Gimap3	-1,7785429	6,13E-08	Adora3	-1,5849687	7,99E-05
Il10ra	-1,7680568	1,17E-21	Dysf	-1,5836788	2,80E-04
Treml4	-1,7656782	2,54E-08	Mycbpap	-1,5827049	1,98E-04
Dhrs3	-1,7600241	1,37E-18	Il18	-1,5811421	1,02E-09
Gpr141	-1,7555441	3,01E-11	Rasgrp1	-1,5795187	1,28E-04
Fam129a	-1,754933	2,04E-21	Gpr18	-1,5745299	5,78E-05
Bcl6	-1,7505235	6,98E-07	Trps1	-1,5716731	1,84E-16
Auts2	-1,7468042	4,11E-06	Lpxn	-1,5715808	4,52E-11
Slc15a3	-1,7460864	6,53E-07	Sema4c	-1,5714217	1,03E-11
Trf	-1,7402186	2,99E-35	Ms4a6b	-1,5669264	5,14E-13
Ifi27l2a	-1,7379938	1,85E-05	Fgl2	-1,5575199	9,86E-17
Phf11b	-1,7287378	2,19E-08	Filip1l	-1,5575101	2,21E-14
Klhl30	-1,7236675	3,55E-04	Mx2	-1,5523418	3,27E-05
Ctnnd2	-1,7211756	8,74E-11	Hmga2	-1,5453016	4,36E-38
Apoe	-1,7088749	1,04E-24	H2-DMb2	-1,5431627	3,41E-06
Slc7a2	-1,7058127	2,41E-05	Tmem37	-1,5418866	9,98E-08
Ccr1	-1,7057971	1,62E-11	Slc37a2	-1,5340094	7,21E-09
Igfbp5	-1,7044485	3,75E-04	Irf7	-1,5305285	6,89E-06
Atp1a3	-1,7033662	1,90E-15	Trim12a	-1,5276771	3,08E-10
Naaa	-1,7032304	8,29E-08	Camkv	-1,5158424	3,37E-07
Lilra5	-1,7013531	4,12E-04	Rin2	-1,5130748	6,09E-10
AF251705	-1,6987586	1,65E-10	Hfe	-1,5129377	2,06E-11
Plxnb3	-1,6922161	6,32E-05	Zc3h12d	-1,5089608	6,58E-05
Itgb5	-1,6900285	1,09E-07	Blk	-1,5088925	1,03E-03
Ckb	-1,6900103	4,33E-21	Slc1a2	-1,502363	1,26E-03
Hlx	-1,6823443	3,72E-11	Acad12	-1,4965664	4,76E-05
Spon2	-1,6814634	2,62E-04	Pydc4	-1,4962093	4,83E-04
P2ry6	-1,678071	5,81E-09	Nfil3	-1,4945068	1,98E-14
Pparg	-1,6712556	6,82E-05	Gpr34	-1,4855137	6,54E-04
Cfb	-1,6711213	1,37E-12	Tmem51	-1,4812699	2,82E-08
Cd302	-1,4774174	6,88E-10	Pgap1	-1,3545791	2,29E-04
Irf8	-1,4724332	4,71E-24	Igf2	-1,3513571	1,68E-03
Gm14446	-1,4717703	2,56E-04	Nefh	-1,3506228	3,87E-11
Sdc3	-1,4690987	2,20E-04	Abca1	-1,3489794	2,68E-14

5430435G22Rik	-1,4679953	4,13E-06	Il1a	-1,3480882	2,27E-03
Adap2	-1,4612555	8,97E-05	Dkk1	-1,3460885	3,16E-03
Sox18	-1,4576578	1,57E-07	Fgf13	-1,345646	8,49E-04
Cd14	-1,4544787	1,69E-04	Paqr5	-1,335888	9,86E-10
9930111J21Rik1	-1,4540719	7,09E-08	Klhl13	-1,335337	1,26E-03
Dmpk	-1,4533935	5,62E-04	Ciita	-1,3334408	3,88E-03
Igsf10	-1,4506238	1,41E-07	Tyrobp	-1,3323784	1,89E-23
Gbp2	-1,4493342	7,72E-09	Coro2a	-1,3311413	5,00E-28
Socs3	-1,4412545	2,48E-04	Tmem229b	-1,3287737	1,01E-15
Gm12250	-1,4404174	2,94E-07	Dhx58	-1,3283027	1,59E-09
Cxx1c	-1,4393111	9,61E-05	Itih3	-1,3273286	2,79E-03
Cd300ld	-1,4382541	6,74E-06	Trim34a	-1,3269491	9,21E-13
Lancl3	-1,4376658	5,46E-04	Cd300a	-1,326873	1,39E-14
Rag2	-1,4300147	1,66E-11	Cox6a2	-1,3263286	4,88E-06
Tnip3	-1,4299933	4,77E-09	Slamf8	-1,3242757	4,61E-04
Cmbl	-1,4276517	1,01E-03	Grifin	-1,3230616	2,43E-03
Ms4a6d	-1,4254737	6,28E-08	Trim30d	-1,3229386	9,39E-06
Sdc1	-1,424995	2,42E-15	Serpina1b	-1,3218024	2,77E-03
Ctsf	-1,4210583	1,52E-07	Mcoln3	-1,3216679	4,26E-04
H2-DMa	-1,4205207	9,20E-18	Cyp11a1	-1,319631	4,24E-03
Nlrp1a	-1,4194446	7,23E-16	Cd300lg	-1,3194569	1,25E-03
C1qb	-1,4184018	1,13E-04	Adam11	-1,3155774	5,12E-08
Clic5	-1,4137276	1,34E-03	Hspg2	-1,3152964	1,66E-03
Olfr433	-1,4134381	1,58E-03	C1qa	-1,3127395	6,43E-04
Treml1	-1,4107544	4,80E-04	Clu	-1,3103869	2,09E-03
Jph1	-1,4105675	2,99E-04	Rmst	-1,3093747	4,53E-03
Sall2	-1,409046	5,43E-07	Lilrb4	-1,3057967	3,32E-08
Sowahc	-1,4055449	3,70E-04	Havcr2	-1,3026679	3,45E-04
Padi2	-1,4039684	1,18E-15	Lacc1	-1,3006018	1,83E-07
Gpc3	-1,4033329	3,89E-09	Lpar6	-1,2999057	9,71E-15
Pld1	-1,4011345	3,69E-06	Aldob	-1,2988427	3,43E-03
Gpnmb	-1,4008442	6,71E-05	Phactr1	-1,2981037	4,50E-03
Ifit1	-1,4006418	5,29E-06	Tmem86a	-1,2980674	1,84E-08
I830077J02Rik	-1,396705	1,36E-08	Col17a1	-1,2978453	3,76E-03
Evi2a	-1,3925984	7,70E-12	Ffar2	-1,2931086	6,79E-05
1600010M07Rik	-1,3908728	9,19E-04	Gm7694	-1,2868877	6,49E-06
Mc5r	-1,3892887	4,18E-10	Evl	-1,2853572	1,61E-19
Tbc1d9	-1,3878677	1,40E-04	Cd38	-1,2830324	1,70E-05
Trim12c	-1,3870262	1,02E-08	Sell	-1,2818703	6,21E-11
Ptms	-1,3851261	3,74E-06	Zbtb4	-1,2810861	9,51E-06
Ets1	-1,3803185	9,59E-15	Tmem229a	-1,2777212	6,29E-04
Cd4	-1,3786204	8,49E-10	Nkd1	-1,2765098	1,38E-03
Enpp2	-1,3752699	3,44E-03	Tnfrsf25	-1,2757653	1,39E-04
Hid1	-1,3729278	9,82E-06	Prr33	-1,2755006	3,10E-04
Kctd12b	-1,3727054	1,42E-05	BC064078	-1,2739594	1,55E-05
Sat1	-1,3720014	7,67E-26	Ptprf	-1,273826	3,55E-04
Nlrp1b	-1,3700947	1,65E-04	8430408G22Rik	-1,2735829	2,71E-06
Jun	-1,3686154	4,62E-14	Cpxm1	-1,2715937	4,88E-06
Gpx3	-1,3677761	8,55E-14	Adamtsl2	-1,2677314	6,22E-03
Rtp4	-1,3653578	2,58E-04	Slfn8	-1,2675032	1,37E-09
Themis2	-1,3644602	7,21E-16	Lsp1	-1,2661507	9,08E-30
Tlr3	-1,3600285	2,02E-03	Prdm1	-1,2648871	2,47E-03
Cd200r3	-1,2632802	4,15E-03	2210010C04Rik	-1,1748291	1,13E-02
Lrrc34	-1,2627582	4,21E-03	Ifitm3	-1,1738809	1,97E-16
Ddx60	-1,2604433	3,18E-05	Mfsd7a	-1,1675323	1,08E-02
Clcf1	-1,257868	4,59E-04	Trim36	-1,1665149	1,20E-03
Aim1	-1,2576876	2,86E-06	Pcgf2	-1,1663533	4,63E-03
Adgb	-1,2569654	1,45E-03	Fgd2	-1,1655627	2,06E-16

Trib2	-1,2539573	1,68E-03	Kcnk13	-1,1630489	1,09E-02
Sirpa	-1,2529949	3,16E-22	Zfp462	-1,1612246	1,08E-02
Rgs2	-1,2516032	5,40E-24	Fcer1g	-1,1609871	1,56E-15
Dock4	-1,2506704	5,63E-04	Vtn	-1,160787	9,39E-03
Evpl	-1,2488727	1,12E-03	Amica1	-1,1605983	9,35E-03
Apobec1	-1,2483816	1,26E-11	Sema4a	-1,1604497	3,16E-06
B3gnt8	-1,2467274	1,67E-06	Lpl	-1,1604464	7,28E-09
Ddit4	-1,2462708	5,48E-08	Ak8	-1,1599853	5,98E-03
Ccdc148	-1,244628	4,43E-03	Tlr1	-1,159059	4,45E-04
Oas2	-1,2435596	8,02E-04	Clec4f	-1,1547087	1,97E-03
Apob	-1,2425465	4,85E-03	Ptprm	-1,1530287	1,36E-03
Gpr97	-1,2381719	4,08E-15	Siglec1	-1,1512296	9,21E-03
Slc18a1	-1,237026	2,87E-17	Gngt2	-1,1506787	1,09E-05
Neat1	-1,2354191	7,89E-10	Ccr7	-1,1499429	2,57E-08
Sqrdl	-1,2308901	2,78E-04	Unc93b1	-1,1488443	9,31E-22
Cd200r4	-1,2241209	6,03E-03	Chrnb1	-1,1476848	6,72E-05
BC147527	-1,2237041	5,69E-08	C1qc	-1,1473213	8,82E-03
Pdlim4	-1,2229679	3,36E-03	Zik1	-1,1466373	8,74E-09
Zfp703	-1,2229566	1,48E-05	Fgg	-1,1457102	1,09E-02
Nos1ap	-1,2209646	1,48E-04	Agpat9	-1,1455402	6,10E-03
Isg15	-1,218903	5,29E-06	Tle2	-1,1452057	4,98E-05
Cdh1	-1,2171892	9,54E-03	Ccnjl	-1,1446486	2,76E-04
Hmox1	-1,2142054	9,12E-05	Rasgrp3	-1,1441024	2,58E-08
Grn	-1,2135307	2,98E-19	Clec4a2	-1,1438496	3,82E-05
Amz1	-1,2121429	4,86E-06	Lrrc25	-1,1421929	4,51E-06
Zeb2os	-1,2120774	3,61E-03	Myo1b	-1,1412251	3,94E-04
Xaf1	-1,2103731	3,76E-07	Igll1	-1,1396407	1,31E-02
Marco	-1,210284	1,92E-03	Krt80	-1,1391598	4,36E-05
Nupr1	-1,2097512	1,87E-04	Myadml2	-1,1374121	9,91E-03
Rarg	-1,209413	1,53E-06	Nr4a1	-1,13695	3,96E-04
Ephx1	-1,2085894	2,77E-03	Rasal1	-1,136841	1,13E-03
Tox	-1,2071676	5,55E-08	Gsap	-1,1325548	1,01E-06
Cxcl16	-1,2007985	9,46E-03	Psap	-1,1323748	1,18E-23
Trim21	-1,1986431	4,54E-13	AI854703	-1,1299054	1,41E-04
Mndal	-1,197516	2,88E-17	Arhgef9	-1,1277112	4,08E-03
Aldh1l1	-1,1975109	3,15E-05	Gria2	-1,1276122	1,11E-03
Fpr2	-1,196264	8,98E-03	Csf2rb2	-1,1267904	1,53E-09
Lrp1	-1,1930273	2,64E-19	Cd207	-1,1265193	1,46E-03
Btbd11	-1,1904848	2,15E-04	Entpd1	-1,1262696	3,24E-10
Cd68	-1,1891699	1,50E-12	Apoc2	-1,1259481	9,17E-03
Angptl2	-1,1879684	1,24E-05	1700026L06Rik	-1,1256945	1,71E-03
Sparc	-1,1832012	9,63E-03	Pdcd1	-1,1254029	1,43E-02
Gm4951	-1,1814744	1,02E-02	Cd52	-1,1252093	1,12E-19
Fam184b	-1,1806353	9,64E-03	Nlrp1c-ps	-1,1246021	7,61E-03
Raph1	-1,1795257	9,55E-06	Ednrb	-1,1239923	1,54E-03
Itih2	-1,17841	8,30E-03	Pdzd4	-1,1236366	1,10E-02
Armcx4	-1,1772066	3,49E-07	Acsl6	-1,1224955	5,25E-03
Zfyve9	-1,1760734	1,09E-02	Calm4	-1,1213186	1,50E-02
Dpp4	-1,1757686	7,41E-12	4632428N05Rik	-1,1212519	3,53E-15
Grm6	-1,1755671	1,04E-02	Gm15987	-1,1205938	1,80E-03
F630111L10Rik	-1,1188439	1,06E-02	Gng11	-1,0666742	3,82E-05
Slc9a7	-1,117124	5,13E-04	H2-Q10	-1,0617956	1,78E-02
Vpreb2	-1,11654	1,49E-02	Slc13a3	-1,061385	2,10E-02
Ms4a7	-1,1164926	1,57E-02	Tnni2	-1,0607343	6,57E-08
4930506M07Rik	-1,1150188	1,20E-02	Marcks	-1,0593661	2,78E-10
Ndnf	-1,1146826	1,59E-02	Ptplad2	-1,0591684	9,45E-12
Rtkn	-1,1143595	6,48E-10	Ifitm1	-1,0573565	4,78E-12
Rasgef1b	-1,1119777	1,16E-07	Col18a1	-1,057245	1,03E-09

Camk1d	-1,1104852	7,39E-15	Ltbp3	-1,0560595	2,20E-02
Notch1	-1,1084809	5,35E-15	E230029C05Rik	-1,055442	2,24E-02
Rnase6	-1,1082972	8,00E-12	Mef2b	-1,0552395	1,95E-02
Pcdhga6	-1,1056685	9,01E-03	3632451O06Rik	-1,0540825	2,34E-02
Plekhg1	-1,1036259	1,46E-03	Dusp22	-1,0535406	9,91E-08
Kifc3	-1,1034848	6,68E-03	Gm11545	-1,0530387	2,15E-02
Phf11d	-1,1034015	1,28E-02	5031439G07Rik	-1,0525405	5,70E-07
Prdm5	-1,1027645	9,81E-07	Ccdc135	-1,0519363	2,66E-04
Pilrb1	-1,1026155	3,84E-03	St8sia1	-1,0519151	2,43E-07
Paqr9	-1,102305	1,68E-02	Plod1	-1,0476118	2,65E-09
Ptafr	-1,1022654	3,78E-06	Ap3m2	-1,0475222	4,47E-05
Igf2bp1	-1,1017636	1,30E-16	Abtb2	-1,0475078	1,94E-04
Depdc7	-1,1013965	6,62E-03	Cyp2j6	-1,047214	9,45E-04
Maf	-1,0999559	3,87E-04	Bst1	-1,0452297	2,34E-02
Mmp17	-1,0990699	2,70E-03	Gbp3	-1,0441069	6,06E-07
Il6ra	-1,0989623	2,07E-09	Mpped2	-1,0437413	6,01E-04
Gprc5c	-1,0977616	1,57E-02	Tmem44	-1,0435367	1,08E-03
Zfp711	-1,097241	3,91E-05	Htra3	-1,0433409	2,27E-02
Prkag3	-1,0946195	1,83E-02	Gatm	-1,0430599	5,36E-11
Epha7	-1,0936625	9,10E-05	Klf12	-1,0422944	3,49E-03
Plg	-1,0920086	1,61E-02	Cd101	-1,0413144	2,52E-02
Atp4a	-1,0919988	1,90E-03	E330013P04Rik	-1,0411517	2,01E-02
Gm10584	-1,0912309	1,86E-02	Obsl1	-1,0410637	1,13E-05
Rbfox2	-1,0900673	1,39E-04	Alpk3	-1,0410575	3,47E-06
AB124611	-1,086543	1,20E-04	Fam174a	-1,0399944	1,08E-07
1700040L02Rik	-1,0858941	1,16E-04	Myl4	-1,0396071	2,42E-03
Pyroxd2	-1,082638	5,02E-03	Plxna3	-1,0395451	1,45E-07
Aadac	-1,0806172	1,55E-02	Pxdn	-1,0391095	2,60E-02
Smad7	-1,0804016	1,02E-04	Prkcdbp	-1,0390554	1,60E-02
Zcchc18	-1,0795523	1,37E-03	Folr2	-1,03882	7,31E-03
Il1rn	-1,0792563	1,79E-02	Id3	-1,0382857	1,57E-10
Sepp1	-1,0779541	3,57E-19	Dlc1	-1,0374737	1,27E-02
Mmp11	-1,0778794	6,82E-03	Cyp2j9	-1,035438	2,94E-04
Sardh	-1,0764838	2,03E-02	Trim14	-1,0340141	4,32E-07
Slc35d3	-1,0760163	1,89E-10	L1cam	-1,033874	2,53E-02
6030408B16Rik	-1,075866	2,15E-02	Arrdc3	-1,0338421	1,37E-10
Tmem71	-1,0756204	1,58E-05	Rtn4rl1	-1,0318274	2,73E-02
Cyp4b1	-1,0751959	1,87E-02	Trem2	-1,031188	8,66E-04
Cd96	-1,0740698	9,82E-04	Pik3r5	-1,0310771	3,95E-08
Trex1	-1,0740397	1,24E-12	AW112010	-1,0304931	5,71E-03
Lair1	-1,0721864	3,17E-04	Stard13	-1,0298426	9,52E-03
Ifi203	-1,0716611	5,35E-17	Pros1	-1,0292274	1,44E-05
Aph1c	-1,0712111	1,22E-04	Tmem106a	-1,0287108	1,85E-05
Dcbld1	-1,0702131	1,51E-03	Magee2	-1,0286442	1,79E-02
2010300C02Rik	-1,0684195	2,09E-02	2810410L24Rik	-1,0284433	2,90E-05
Peg12	-1,0683187	1,27E-03	Ctsw	-1,0274437	7,73E-05
Acot1	-1,0679588	5,39E-04	Apof	-1,0269373	8,82E-03
Rab20	-1,0667144	1,98E-02	Fmo1	-1,0260376	1,23E-02
Fam26f	-1,0251919	2,92E-04	Cd248	-0,9779708	3,81E-02
Pkdcc	-1,0246336	2,57E-02	C130050O18Rik	-0,9777631	3,28E-05
Irgm2	-1,0237103	5,63E-07	Arhgap22	-0,9762929	3,86E-02
Sp140	-1,0219332	1,06E-09	Nsg2	-0,975039	1,30E-03
Gm1966	-1,0196387	8,49E-12	Serpinc1	-0,974412	3,19E-02
Sytl4	-1,0187353	6,05E-05	Ceacam1	-0,9733202	9,92E-05
Tmem98	-1,0181465	1,25E-12	Gfra1	-0,9705211	2,08E-05
Fkbp9	-1,0179503	1,21E-05	Gm10640	-0,9703344	3,99E-02
Tead3	-1,017795	2,89E-02	Tagap	-0,9702614	2,26E-06
Gm13710	-1,0173846	2,87E-02	Bmp1	-0,9698164	8,89E-04

Bin1	-1,0157069	1,05E-10	Rgs8	-0,9691661	2,74E-02
Sema4g	-1,0155822	3,05E-02	Myof	-0,9691396	9,92E-03
Sp100	-1,0147197	1,87E-07	Rasa4	-0,9691132	5,31E-06
Nfam1	-1,013422	6,97E-17	Abhd4	-0,96838	4,48E-11
Cyp4f18	-1,0131357	1,13E-04	Il12a	-0,9679845	1,79E-09
3830408C21Rik	-1,0122468	2,27E-02	Spef2	-0,9679839	1,99E-02
S100a10	-1,0105199	6,07E-15	Rgs3	-0,9665307	2,54E-04
Spp1	-1,0084715	2,35E-02	2900026A02Rik	-0,9662791	4,17E-08
Il1b	-1,0061654	2,65E-02	Itfg3	-0,9645941	7,68E-09
Rbpms2	-1,0050167	3,15E-02	Mmp8	-0,96339	6,06E-03
Vcan	-1,0050033	3,04E-02	C3ar1	-0,9633022	1,15E-03
Fkbp1b	-1,0048643	1,19E-02	Pilra	-0,9628296	7,49E-03
Bend6	-1,0029569	2,67E-02	Slc9a9	-0,9608417	5,94E-11
Pacsin1	-1,0028389	4,08E-03	Kctd12	-0,9599193	2,24E-08
Sh3pxd2a	-1,0024268	3,43E-03	Ly6a	-0,9593243	1,19E-07
Lgals3bp	-1,0001917	2,07E-08	Rab39	-0,9590954	3,84E-03
Tlr13	-1,0001305	7,52E-04	Slc27a1	-0,9574998	1,25E-05
Tiam2	-0,9999396	3,12E-04	Mzb1	-0,9565917	3,22E-06
Rnf150	-0,9995618	1,56E-03	Trp53inp1	-0,9555302	3,10E-06
Fcna	-0,9992397	2,77E-02	S100a11	-0,9549942	8,20E-16
Slc12a9	-0,9978716	4,66E-10	Hivep2	-0,9535841	2,76E-03
Tfeb	-0,9974269	1,15E-04	Fam155a	-0,9535014	3,86E-02
Mpl	-0,997047	7,49E-17	Rgl1	-0,9531637	2,18E-08
Iqsec2	-0,9964331	1,04E-03	Zfp658	-0,9531418	1,94E-04
Degs2	-0,9961554	3,15E-03	Hmga2-ps1	-0,9527233	4,88E-03
A530088E08Rik	-0,9952747	1,82E-03	Rpgrip1	-0,952609	1,26E-04
Rhbdf1	-0,9944581	3,38E-02	Cx3cl1	-0,9524701	3,36E-02
Mira	-0,993422	6,04E-05	Ssh3	-0,9507561	7,39E-03
Slc43a2	-0,9922683	3,06E-13	Itpripl2	-0,9506481	6,72E-04
Cd93	-0,9905786	9,01E-13	Neo1	-0,950623	4,24E-02
Fzd6	-0,9898476	1,79E-04	Rasd1	-0,9504065	2,72E-04
Pde2a	-0,9895166	4,51E-03	Fam46a	-0,95001	1,81E-04
Phf11a	-0,9889286	2,60E-02	1700015E13Rik	-0,9498365	4,45E-02
Tmem38a	-0,9889157	1,50E-04	Oas1a	-0,9492059	4,11E-05
Snx29	-0,9886851	6,68E-07	Gpr133	-0,9487769	4,00E-02
Chad	-0,9863154	1,87E-02	Parp14	-0,9476997	2,10E-08
Fxyd7	-0,9853029	1,53E-02	Sgsm1	-0,947195	1,33E-05
Alcam	-0,9845637	1,83E-02	BC035044	-0,9465398	1,72E-11
Cc2d2a	-0,9838697	4,18E-03	Rsad2	-0,9460003	3,61E-04
Dtx4	-0,9838591	3,48E-06	Plekhh1	-0,945793	3,70E-02
Sulf2	-0,9836109	1,97E-02	Gpm6b	-0,9452185	1,84E-02
Egr1	-0,983365	7,32E-03	Stat1	-0,9441332	1,31E-08
Prrt2	-0,9830077	6,93E-03	Eepd1	-0,9439541	9,45E-04
Ldhd	-0,9823896	2,87E-02	Abcd2	-0,9433716	1,39E-04
H1f0	-0,982284	4,34E-14	Gpr137b	-0,9431737	2,20E-02
Serpind1	-0,9783575	3,58E-02	Cyth4	-0,9429623	1,26E-12
Cd300e	-0,9413985	4,36E-02	AI429214	-0,9003355	1,99E-02
Aldh5a1	-0,9413316	3,64E-02	Clec9a	-0,9001132	7,09E-03
Pde5a	-0,9407561	1,15E-02	She	-0,89987	2,58E-02
Spsb1	-0,9398832	5,92E-03	Irf1	-0,8997555	1,21E-11
Syne4	-0,939395	2,44E-02	Adamts6	-0,8995998	7,48E-03
Samd9l	-0,9387165	7,14E-07	Epha2	-0,8980226	2,74E-02
Tnni1	-0,9385977	1,18E-02	Hmcn1	-0,8976248	2,27E-02
Slc4a4	-0,9382311	4,20E-02	Jup	-0,8973942	1,99E-05
Capsl	-0,9382259	1,83E-02	Flt3	-0,8970808	3,09E-13
Plekho1	-0,9382057	3,03E-06	B3gnt5	-0,8963016	3,32E-03
Ticam2	-0,938122	2,01E-09	Gm4759	-0,8960163	1,39E-06
Rgag4	-0,9377818	2,54E-03	Snx7	-0,8956427	5,24E-03

Bex2	-0,9376283	1,95E-02	Zfp36	-0,8949202	3,71E-11
Dsel	-0,9362896	7,27E-03	Itpr1	-0,894806	9,52E-10
Proc	-0,9347875	3,37E-02	Slfn10-ps	-0,894268	4,71E-05
Aph1b	-0,9340798	1,32E-02	Sh2d4a	-0,8941862	1,35E-04
Tgtp1	-0,9288956	3,72E-02	Tlr4	-0,894161	1,76E-05
Fscn1	-0,9280656	7,30E-08	Ctsl	-0,8932862	1,09E-08
Acsbg1	-0,9280022	4,60E-02	Accs	-0,8927601	4,67E-06
Zfp579	-0,9263151	2,23E-04	2310040G24Rik	-0,8925915	9,34E-03
Oasl2	-0,9263035	8,56E-03	Oplah	-0,8898287	4,41E-02
Bend5	-0,926261	2,34E-04	Sh2d1b1	-0,8867068	4,71E-02
Hoxa7	-0,9256458	4,95E-06	Itgb7	-0,8862298	3,09E-07
Zbtb16	-0,9248318	5,63E-03	Maged2	-0,8856443	7,23E-10
Gja1	-0,9238585	5,36E-08	Slc40a1	-0,8855074	8,59E-10
Dusp18	-0,9220748	5,38E-03	Cldn1	-0,8853761	3,78E-02
H2-K2	-0,9219558	1,45E-02	Csf3r	-0,8838813	1,67E-16
Plekha1	-0,9205892	1,65E-07	Tlr9	-0,8838352	4,67E-02
Tsc22d1	-0,9179893	1,75E-17	Scn3a	-0,8822717	4,91E-02
Gabre	-0,9164902	4,49E-02	Rogdi	-0,8812855	2,01E-10
Tcp11l2	-0,9160603	2,29E-07	Trafd1	-0,8811857	7,38E-09
Rab32	-0,9159217	7,99E-12	Csf2rb	-0,8811603	8,69E-11
Irgm1	-0,9157148	1,84E-07	Cd1d2	-0,8797387	1,79E-02
Pcbd1	-0,9155501	1,46E-03	Tead2	-0,8795012	1,02E-02
Gm15708	-0,9142678	5,00E-02	Hoxa9	-0,8794351	1,51E-09
St8sia4	-0,914202	1,59E-12	Aif1l	-0,8791667	2,35E-02
Zfp551	-0,9132235	2,48E-03	Emcn	-0,8773391	1,01E-05
Tmem91	-0,9130705	3,03E-05	Chp2	-0,8773214	4,90E-02
Zbtb7b	-0,9124491	1,95E-04	Vash2	-0,8772787	1,68E-02
Fndc4	-0,9100902	1,49E-02	Cnn2	-0,8766449	4,38E-15
Mdk	-0,9092867	4,15E-02	Trim47	-0,8764887	2,40E-03
Mrvi1	-0,9091093	2,78E-05	Cd276	-0,8759988	3,36E-03
Ctxn1	-0,9084336	9,13E-05	Acot3	-0,8742207	1,44E-02
Myo15	-0,908062	3,36E-02	Icam1	-0,8737206	3,50E-09
Art1	-0,9075891	4,45E-02	Tlr2	-0,8733425	3,09E-07
Abcg3	-0,9068382	3,25E-08	Fbxo32	-0,8720067	1,88E-04
Sp110	-0,9055007	5,28E-10	Large	-0,871378	2,32E-02
Ccdc60	-0,9044048	5,08E-03	Smtnl2	-0,8711465	4,93E-02
Tyro3	-0,9041937	4,40E-02	Ypel3	-0,870864	2,04E-07
Tnfsf10	-0,9037896	2,40E-04	Tmsb4x	-0,8707721	2,77E-19
Tmem132a	-0,9014447	1,42E-03	Cd97	-0,8703379	2,07E-10
Pou2f2	-0,9012835	8,11E-10	Rab11fip4	-0,8701038	2,88E-02
Clec1b	-0,9012734	1,07E-02	Parp8	-0,8700008	4,06E-10
Cpq	-0,9011249	7,76E-11	Lrrc32	-0,8695568	1,09E-02
6330416G13Rik	-0,9011163	2,24E-10	Med12l	-0,8694606	1,23E-03
Fam43a	-0,90077	4,87E-07	Lbh	-0,8683833	1,17E-06
Gyltl1b	-0,8671267	2,91E-02	9130008F23Rik	-0,8337109	3,76E-02
Pisd-ps2	-0,8671031	2,96E-05	Acox3	-0,8329871	2,22E-06
Rgs1	-0,8669807	5,23E-03	Tnfaip8l2	-0,8325833	8,33E-10
Gm12216	-0,8662931	1,66E-02	Serping1	-0,8323225	9,33E-03
Slamf7	-0,865089	4,92E-02	Fam98c	-0,8320966	1,20E-04
Fgr	-0,8648744	2,22E-03	6430548M08Rik	-0,831689	6,52E-03
Zfp773	-0,8647816	4,75E-04	Robo4	-0,8314394	1,20E-05
Phactr2	-0,8636041	8,99E-09	Nynrin	-0,8310923	1,92E-06
Pcdhgb6	-0,8619454	2,48E-02	Neurl2	-0,8310532	1,33E-02
Hoxa3	-0,8616576	4,18E-03	Emp1	-0,8300187	1,11E-03
Gab3	-0,8614689	2,54E-02	Sv2a	-0,8296573	5,04E-03
Mxd4	-0,8614494	6,48E-03	Zbtb10	-0,8276952	5,23E-03
Jam3	-0,8605052	1,75E-05	Vwa5a	-0,8276409	1,06E-08
Zfp831	-0,860317	2,99E-06	Selplg	-0,827442	3,14E-12

Dyrk1b	-0,8596131	1,51E-03	Slc8a1	-0,8274268	2,37E-03
Ggt5	-0,8590853	5,95E-03	Efna4	-0,8269128	1,11E-02
Evc	-0,8585716	4,91E-02	Ophn1	-0,826362	2,83E-02
Klf7	-0,8582828	9,02E-03	Ptgr1	-0,8242998	9,23E-07
Myadm	-0,8573839	1,30E-12	Slc29a3	-0,8241945	4,28E-10
Bok	-0,8572717	1,03E-03	Slc22a18	-0,8240924	1,32E-02
H2-Ob	-0,8569886	5,90E-06	Cd180	-0,822442	5,13E-04
Cd1d1	-0,8562222	2,57E-07	Mpdz	-0,8222983	5,73E-03
Fosl2	-0,8559102	3,87E-04	Pard3b	-0,8221206	5,73E-04
Unc5a	-0,8552826	2,34E-02	Litaf	-0,8218776	2,07E-10
Slc25a45	-0,8547673	2,96E-11	Tgif1	-0,8215556	1,79E-09
Tor3a	-0,8544601	1,86E-08	Cyp4v3	-0,8206987	1,74E-04
Cyp27a1	-0,8542764	3,24E-05	Igf2bp2	-0,8206705	9,64E-09
Sep4	-0,8541475	5,38E-03	Tgtp2	-0,8200192	3,22E-03
Slc25a23	-0,8530446	2,58E-07	4930451G09Rik	-0,8199919	4,28E-02
Tshz3	-0,8519453	2,27E-02	Traf5	-0,8198342	6,65E-04
Dlg2	-0,8507446	4,58E-02	Tle3	-0,8197839	2,80E-09
Mtss1l	-0,8491252	4,25E-02	Rph3al	-0,8197054	2,70E-02
P2ry2	-0,8483258	1,39E-04	Zfp799	-0,8193395	4,45E-05
Vdr	-0,8482227	5,88E-03	Slit2	-0,8183111	4,20E-02
Celsr2	-0,8472957	1,34E-02	2610307P16Rik	-0,8178251	7,52E-05
Vamp1	-0,8472664	2,39E-08	Gbp5	-0,8178099	1,51E-03
Celsr1	-0,8466869	1,01E-02	Lat2	-0,8167706	1,28E-05
Fkbp7	-0,8466218	8,13E-03	Boc	-0,816637	3,59E-02
Aldh1b1	-0,8454444	1,75E-05	Sash1	-0,8159274	2,92E-02
Cyb561a3	-0,8454257	1,06E-15	Pald1	-0,8155813	3,90E-03
Serpina1e	-0,844437	4,33E-02	Ift122	-0,8148899	5,77E-06
Tcn2	-0,8443602	3,75E-07	Lpp	-0,8146222	2,04E-07
Sytl1	-0,8443424	3,00E-06	Hc	-0,8145886	2,92E-02
Calhm2	-0,8443128	2,27E-05	Stau2	-0,8126577	3,82E-03
Bex1	-0,8443122	1,81E-04	Slc9b2	-0,8105115	4,59E-02
Cd79b	-0,8430856	2,74E-09	Myo1f	-0,8094981	7,63E-16
Fam167a	-0,8405883	2,48E-02	Tmem119	-0,8094597	1,63E-03
Nat8l	-0,8400105	1,15E-02	Loxl3	-0,8090634	3,61E-02
Cep112	-0,8394444	4,39E-02	Bcl3	-0,8088879	8,74E-03
Irf9	-0,8387748	2,97E-08	Uaca	-0,8069487	7,93E-06
Ctsa	-0,8381789	2,49E-12	Mdfi	-0,8050811	3,86E-02
Arl4c	-0,8368909	5,10E-03	Cds1	-0,80501	2,05E-02
Dbn1	-0,8366196	2,26E-03	Ccdc8	-0,8049792	1,49E-08
Usp18	-0,8360337	4,95E-02	Bach2	-0,8048002	5,30E-03
Fam196b	-0,8359238	1,11E-02	Epsti1	-0,8043426	2,20E-08
Oas3	-0,8342452	5,89E-04	Fads3	-0,8033755	2,35E-05
Snn	-0,8026721	1,18E-04	Acy3	-0,7640569	1,06E-04
Ap1s2	-0,8026594	6,40E-05	Acsf2	-0,7638691	5,09E-05
Pi16	-0,8025026	7,21E-03	Hoxa5	-0,7635971	1,47E-02
Cd27	-0,8024981	3,15E-08	Mtus1	-0,762586	3,06E-04
Msantd3	-0,8023645	3,56E-02	Rassf5	-0,762445	2,15E-10
Ikbke	-0,8022793	1,51E-06	Gstm7	-0,7616639	1,29E-02
Slc7a8	-0,802272	8,19E-04	Fhl2	-0,7616386	4,58E-02
P2rx1	-0,8013547	3,16E-05	Adck3	-0,7615315	2,69E-06
Dnmt3a	-0,8009986	1,32E-10	Bckdha	-0,7614154	5,13E-09
Tctn3	-0,8009872	1,31E-05	Arid5b	-0,760917	2,79E-04
Dcaf12l1	-0,8006651	2,71E-02	Tubb6	-0,7607224	4,07E-04
Asah1	-0,7998325	1,59E-12	Map3k8	-0,7578198	2,47E-03
Tbc1d16	-0,7982887	4,98E-05	Arpp21	-0,7574363	6,70E-03
A630001G21Rik	-0,7979153	8,09E-06	Baiap2	-0,7559006	5,08E-05
Gbp7	-0,7971046	2,93E-08	Cnn3	-0,7550549	4,18E-10
Cacna2d4	-0,7954594	2,67E-02	Fgd4	-0,7543585	2,34E-04

Isoc2b	-0,7942477	8,30E-03	AI504432	-0,7542712	1,38E-02
Firre	-0,7900964	1,13E-07	Arhgap26	-0,7538338	1,52E-04
Muc6	-0,7895735	1,81E-02	Fam214a	-0,7530558	3,50E-04
Hddc3	-0,7882808	5,83E-03	Gm16897	-0,7525301	6,85E-03
Chn2	-0,7875968	5,50E-04	Cxcr4	-0,7523913	6,81E-06
Lyplal1	-0,7871481	1,99E-03	Pdk2	-0,7521171	2,05E-04
Ppm1h	-0,7862192	1,03E-05	H2-M3	-0,7517905	1,90E-03
Hsd3b7	-0,7853418	1,06E-07	Btbd3	-0,751781	1,45E-06
Sirpb1b	-0,7824101	4,39E-02	Satb1	-0,7513264	3,65E-06
Plek	-0,7820226	5,59E-06	Sfxn4	-0,7510349	1,06E-02
Gcsam	-0,7820201	1,42E-03	Basp1	-0,7505878	8,81E-03
Btg1	-0,7812744	5,30E-05	Tlr11	-0,7504217	1,81E-02
Irf6	-0,7805568	1,36E-02	Gimap8	-0,7499566	1,58E-07
Gpr174	-0,779559	4,60E-03	Marveld1	-0,7499348	1,97E-02
Dusp10	-0,7787984	1,98E-02	Gpr160	-0,7488062	7,39E-04
Speg	-0,7784761	4,65E-02	2500004C02Rik	-0,7462511	1,97E-03
Plac8	-0,7781022	3,45E-07	Pea15a	-0,7460543	3,85E-04
Fut7	-0,7777192	2,05E-05	Calcoco1	-0,7455786	1,19E-07
6330403K07Rik	-0,7775558	3,74E-02	Ccdc102a	-0,7446969	9,03E-03
C030034L19Rik	-0,7772152	1,19E-07	D930048N14Rik	-0,7446155	2,10E-02
Ppt2	-0,7766933	1,98E-06	Fam181b	-0,7443336	3,21E-02
Mn1	-0,7765929	6,73E-06	Gpr171	-0,7441212	1,33E-08
Marveld2	-0,7764218	1,76E-02	Zbtb18	-0,7433715	1,01E-04
Rilpl1	-0,7762638	1,59E-02	Laptm5	-0,742114	4,38E-12
Tmem108	-0,7748947	5,34E-03	Lst1	-0,7413761	1,46E-07
Arhgef5	-0,7747322	4,04E-05	Ldlrad4	-0,7404752	1,04E-02
Grrp1	-0,7733894	8,80E-03	Ppm1k	-0,7404404	1,30E-03
Phldb1	-0,772076	1,82E-02	Pak1	-0,7387605	1,22E-11
Peg13	-0,7719362	9,64E-09	Acot4	-0,738575	4,82E-02
Arid5a	-0,7710534	3,48E-06	Epb4.1l3	-0,7373635	2,70E-04
Fggy	-0,7707816	3,63E-04	Abhd14b	-0,7362995	3,51E-04
Cst3	-0,7706927	2,28E-12	Rcbtb2	-0,7361458	3,79E-09
Itm2a	-0,7697209	1,09E-08	Plekhg5	-0,735206	1,68E-04
Fam64a	-0,7695565	4,05E-11	Sgce	-0,7347701	9,09E-04
Lyn	-0,7694504	3,01E-11	Fmnl2	-0,7347425	8,30E-03
Scpep1	-0,7694407	6,43E-07	Tnfrsf1b	-0,7332508	9,42E-09
Rnase4	-0,7681882	3,82E-04	Vasn	-0,7328462	4,20E-02
E030024N20Rik	-0,765275	8,49E-03	Myom1	-0,7320167	4,95E-02
B430306N03Rik	-0,7647257	3,91E-03	Kcnh2	-0,7309331	1,65E-03
Ikzf2	-0,7642567	7,39E-07	Ptger2	-0,730056	1,96E-04
Vangl2	-0,7289031	2,23E-03	Efnb1	-0,6949475	2,34E-02
Gpr132	-0,728325	5,75E-05	Tmco4	-0,6949165	4,72E-05
Hnf4a	-0,7276453	8,75E-05	Frmd4b	-0,6945781	2,60E-05
Slc22a17	-0,7275467	6,04E-03	Cd53	-0,693884	5,46E-07
Ppapdc3	-0,7265127	1,06E-02	Nlrc5	-0,6931022	4,59E-02
Tcf4	-0,7254929	2,09E-09	Arhgap4	-0,6922778	1,85E-06
2810408A11Rik	-0,7252551	1,46E-03	Tmem198b	-0,6922674	6,91E-03
Cfp	-0,7236559	4,73E-06	Rad9b	-0,6905625	4,68E-02
Slc26a11	-0,7216522	3,56E-03	Clk1	-0,6903021	3,98E-08
Cers6	-0,7215776	2,61E-03	Atp6v1g2	-0,6894039	3,76E-02
4930486L24Rik	-0,7214662	4,85E-02	Zfp90	-0,6891671	3,17E-04
Slc5a11	-0,721	3,56E-02	Carns1	-0,6875667	2,54E-03
Hsd17b11	-0,7206281	3,22E-03	Pbx1	-0,6868547	1,11E-03
Magee1	-0,7203204	1,60E-02	Herc6	-0,6866836	1,73E-04
Tha1	-0,7203051	1,53E-02	Lax1	-0,6859249	3,60E-05
Tapbpl	-0,7201377	4,30E-06	Fnbp1l	-0,6857331	1,00E-02
Cotl1	-0,7195176	2,25E-07	Abhd15	-0,6855954	9,11E-04
Pik3ap1	-0,7185339	1,54E-07	Zfp521	-0,6855948	1,44E-04

Tgfbr2	-0,7184545	9,34E-06	E130317F20Rik	-0,6854156	4,72E-02
Traf3ip3	-0,7179701	1,78E-09	Lekr1	-0,6838519	2,19E-02
Cd200r1	-0,7171529	1,00E-03	Zfp184	-0,6830481	8,00E-04
Slc25a53	-0,7154362	6,12E-03	Slc50a1	-0,6829447	4,26E-08
Rcor2	-0,7145147	1,08E-02	Osbpl5	-0,6827531	3,12E-02
Prr5l	-0,7137652	1,89E-02	BC037704	-0,6823641	4,91E-02
Capg	-0,7125763	1,21E-10	Esam	-0,6815206	1,26E-04
Hes6	-0,7117092	1,01E-05	Ly96	-0,681469	1,57E-02
Nrros	-0,7092843	1,02E-09	Zyx	-0,680856	4,71E-07
Cnksr3	-0,7091858	2,10E-04	Efcc1	-0,6808511	1,85E-03
2900005J15Rik	-0,7091697	3,09E-02	Arl10	-0,6800501	1,28E-02
Slc38a6	-0,7082104	4,50E-02	Arhgap25	-0,6800349	1,04E-06
Arsa	-0,7081612	3,57E-05	Hcls1	-0,6797088	1,61E-09
Prkca	-0,7060685	8,44E-04	Tspan6	-0,6796496	5,35E-07
Mb21d1	-0,7058145	4,53E-05	Tie1	-0,6795492	1,68E-04
Srgap3	-0,7048504	1,49E-02	Fes	-0,6792422	9,90E-06
Kcnd1	-0,7040779	3,64E-02	Ddx58	-0,6792247	3,37E-04
Yes1	-0,7033257	1,14E-02	Dock10	-0,6782504	3,24E-07
Zdhhc15	-0,7024677	1,84E-04	Ids	-0,677712	2,00E-03
H2-DMb1	-0,7019128	1,20E-02	Abcd1	-0,6774104	3,07E-08
Cmtm8	-0,701709	1,33E-02	4933412E12Rik	-0,6773771	2,54E-03
Ctso	-0,7011216	1,69E-05	Fam129c	-0,6771024	4,63E-02
Syk	-0,6999864	5,69E-09	Phpt1	-0,6770095	7,79E-08
Gimap4	-0,6996507	1,35E-03	Fam188b	-0,6767457	1,67E-02
Vsig4	-0,6995829	2,68E-02	Emb	-0,6763947	8,16E-09
Nradd	-0,6995443	4,91E-02	Amot	-0,6760246	2,27E-02
Msl3l2	-0,6994979	1,59E-02	Sla	-0,6759274	3,32E-07
Map3k14	-0,6992842	2,30E-04	Il15ra	-0,6747452	1,56E-02
2810442I21Rik	-0,6990017	7,33E-03	Igtp	-0,6744844	5,88E-04
Slc30a4	-0,6988529	2,50E-02	Nuak2	-0,6742043	1,32E-02
Tmem173	-0,698655	1,75E-07	Inf2	-0,6738545	6,23E-03
2610035D17Rik	-0,6983933	2,03E-04	Tacc2	-0,6719117	1,20E-03
Helz2	-0,6977275	6,59E-05	Rora	-0,6716863	5,00E-02
Guca1a	-0,6974922	4,07E-02	Nudt16	-0,6712865	4,09E-03
Car12	-0,6966997	3,23E-02	Fabp7	-0,6709716	3,25E-02
Armcx6	-0,6965476	2,28E-03	Zc2hc1a	-0,6698084	2,33E-03
Tbc1d10c	-0,695286	4,50E-07	5830416P10Rik	-0,6697148	2,30E-02
Ppfibp2	-0,6952215	3,36E-03	Fam105a	-0,6689656	8,83E-06
H2-Oa	-0,6684265	1,82E-02	Rcbtb1	-0,6341702	1,07E-04
Nhsl1	-0,6680974	4,32E-02	Il21r	-0,6341167	8,57E-06
Rnls	-0,6680052	1,88E-02	Sox13	-0,6335615	3,50E-03
Aoah	-0,6676113	1,13E-02	Mylip	-0,6326814	9,26E-04
Map4k2	-0,6671604	6,16E-07	Slc35f5	-0,6326214	3,11E-03
Rnf180	-0,6667821	3,61E-02	Lysmd2	-0,6325804	4,76E-02
Slc38a7	-0,6664608	5,47E-04	Wls	-0,6317891	3,39E-06
Btg2	-0,6661118	6,45E-06	Vipr2	-0,631766	1,64E-03
Pik3r6	-0,6653957	1,21E-04	Gjb3	-0,631273	2,58E-02
Inadl	-0,6649329	6,34E-03	Cytip	-0,6293549	1,50E-05
Cmtm3	-0,6646822	1,64E-05	Gsdmd	-0,6288017	7,32E-06
Rhob	-0,6641785	4,64E-03	Ncf4	-0,6285508	1,04E-06
Tbxas1	-0,6631616	9,82E-04	Tmem154	-0,6283112	6,64E-05
Stambpl1	-0,6617327	3,68E-03	Smpd2	-0,6278466	3,45E-04
Hexa	-0,6614873	8,54E-06	Igsf6	-0,6276919	1,04E-03
Ly6e	-0,6609655	2,33E-09	Slc35f2	-0,6272732	1,21E-02
Map3k5	-0,6608633	1,22E-03	Cd69	-0,6269648	3,26E-03
Trip6	-0,6606105	1,04E-04	Ifit2	-0,6268494	1,35E-03
Hgf	-0,6584083	4,48E-03	Tmem159	-0,6262934	1,13E-02
Nr2f6	-0,6583218	2,82E-02	Wdpcp	-0,6261695	5,07E-03

Npc2	-0,6579718	5,37E-09	Ypel1	-0,6242923	1,35E-02
Sh3bp2	-0,657775	2,09E-06	Gm6548	-0,6234431	2,73E-02
Emilin2	-0,6564991	1,00E-03	Muc13	-0,623302	1,72E-02
Ifitm2	-0,6548325	1,25E-07	Dtx3l	-0,6231803	1,16E-04
Nrep	-0,6546046	4,40E-02	Atp10a	-0,6226984	7,24E-04
Nfkbiz	-0,6533524	6,37E-03	Man2b1	-0,622657	8,25E-09
Ifnar1	-0,6526707	4,12E-08	Renbp	-0,6225067	4,38E-04
Nedd9	-0,6522847	9,49E-05	Nabp1	-0,6220399	4,44E-05
Arid3a	-0,650588	1,23E-06	Zfp422	-0,6218838	4,73E-08
Smad6	-0,6501647	2,27E-02	Tpmt	-0,6218501	3,91E-02
Ssfa2	-0,649068	1,96E-04	Myo6	-0,6199751	5,00E-02
Ivd	-0,6483729	4,82E-07	Bmyc	-0,6195077	4,04E-04
Ankrd44	-0,6479016	6,13E-06	Lipa	-0,6181935	3,40E-05
Gcat	-0,6473492	6,02E-05	Trim32	-0,6179628	1,10E-05
Parp9	-0,6472405	7,44E-05	Hexb	-0,6169284	5,12E-04
Napsa	-0,6466571	3,95E-08	Ctnnbip1	-0,6165494	2,02E-02
Ttpa	-0,6461052	2,10E-04	Lck	-0,6154691	3,68E-04
Smim24	-0,6450718	8,51E-03	Rnf215	-0,6153413	1,62E-02
Ncoa3	-0,644847	1,13E-06	Cyba	-0,6152677	6,89E-10
Sh2d3c	-0,6439379	1,01E-06	Madd	-0,6152421	3,38E-06
Tmem191c	-0,6424152	7,91E-03	Timd2	-0,6150367	4,10E-02
Prx	-0,6422575	2,44E-02	Fyb	-0,6142808	5,65E-07
Fam49a	-0,6414478	4,03E-05	Cxcr3	-0,6142277	1,76E-03
Cnp	-0,6411462	1,39E-07	Pld3	-0,6130147	3,19E-05
Pold4	-0,6400069	4,89E-05	Gprasp2	-0,6124776	1,04E-02
Vstm4	-0,6397968	4,00E-02	Adamts10	-0,6114384	5,80E-05
Txndc16	-0,6387483	5,91E-05	Csad	-0,6111347	1,73E-03
Zeb2	-0,6381877	8,84E-06	Rin3	-0,6107904	2,96E-06
2010111I01Rik	-0,6371571	3,05E-05	Itga6	-0,6104725	1,21E-04
Trim26	-0,6371374	3,93E-05	Dleu2	-0,6103344	2,42E-02
Stk10	-0,6365795	9,88E-07	Cand2	-0,6100726	2,13E-04
Kank2	-0,6351947	2,60E-02	Lrrk1	-0,6097779	5,41E-05
Adar	-0,635099	1,18E-05	Mov10	-0,6087146	5,55E-06
Tns3	-0,6348054	4,69E-04	Tmem176a	-0,6086142	4,58E-05
Dhdh	-0,6344815	2,87E-02	Cd33	-0,6080022	2,18E-04
Tnks1bp1	-0,6342086	4,47E-02	Abr	-0,6070489	9,82E-06
Itgam	-0,6069979	1,23E-05	Galm	-0,5747014	2,57E-02
N4bp3	-0,6065067	3,56E-03	Pde4b	-0,5746402	2,25E-05
Foxp1	-0,6059293	8,80E-09	Ppp1r9a	-0,574593	3,56E-03
Oas1b	-0,6055963	4,35E-02	Eogt	-0,5742426	2,89E-02
Lztfl1	-0,6055177	8,06E-05	Rhoh	-0,5729018	3,94E-05
Rab27a	-0,6053649	1,69E-07	Crem	-0,5726792	1,79E-02
Ankrd13d	-0,6047178	5,63E-03	Igflr1	-0,5725823	2,44E-03
Ing4	-0,6043961	2,32E-08	Slc12a6	-0,5725687	1,21E-05
Tcf7l2	-0,6043079	7,46E-06	Tpcn2	-0,5721549	9,78E-03
Glis2	-0,6040528	1,53E-02	Ppic	-0,5719087	4,12E-04
Stat2	-0,6040136	1,53E-05	Hdac9	-0,5708198	6,81E-03
Nrgn	-0,6037895	4,38E-04	Siae	-0,56965	1,29E-03
Il12rb2	-0,6032127	9,56E-04	Mctp2	-0,5685589	4,24E-03
Cdyl2	-0,6028362	1,09E-03	Sorbs3	-0,5684326	1,85E-03
Klc4	-0,6015285	1,27E-03	Akna	-0,5681342	6,30E-05
Suox	-0,6011089	3,64E-02	Ctps2	-0,5679717	6,16E-06
Gpr137b-ps	-0,6004376	2,02E-02	Idh1	-0,567858	2,56E-05
Siglece	-0,6000926	1,02E-02	Hpgds	-0,5676912	1,62E-02
Zfp53	-0,5996444	2,42E-03	Tnfrsf13c	-0,5675557	4,60E-03
Runx2	-0,5984529	2,94E-05	Galns	-0,5675484	4,84E-04
Zfhx3	-0,5976528	4,60E-04	Map2k6	-0,5673904	3,26E-03
Rltpr	-0,5973918	3,15E-03	Rara	-0,5668572	1,15E-03

Cep19	-0,597288	3,63E-04	Ptpn22	-0,5667558	2,71E-04
Gnaq	-0,5965837	8,32E-05	Mef2c	-0,5666158	7,39E-06
Kank3	-0,5961072	2,65E-02	Slc5a3	-0,5662945	2,67E-03
1600014C10Rik	-0,5956184	9,52E-06	Limk1	-0,5662721	1,05E-03
Morn4	-0,5954413	1,33E-02	Zfp608	-0,5661899	2,10E-05
Zfp286	-0,5950214	2,25E-02	Ralgps1	-0,5647717	4,56E-03
Nagk	-0,5947217	1,25E-03	Prkra	-0,5645088	1,39E-03
Mctp1	-0,592577	7,46E-05	Cnnm4	-0,5642653	1,21E-03
Psmb8	-0,5923751	7,92E-05	Mex3a	-0,5641558	2,18E-03
Slc44a2	-0,5922586	2,34E-06	Wdr45	-0,5634529	5,88E-05
Acp2	-0,5910674	1,10E-03	Smo	-0,5625014	1,63E-03
Plxnd1	-0,5910476	3,30E-04	S100a16	-0,5622752	4,86E-02
Ypel5	-0,5906195	3,79E-05	Tmem176b	-0,5615493	3,53E-05
Nmi	-0,5904739	2,80E-04	Gstk1	-0,5614858	3,18E-02
Ndst1	-0,5903853	3,01E-04	Prkab2	-0,5611174	3,56E-02
Gm2a	-0,590246	4,09E-06	Nudt14	-0,5610711	2,40E-04
Car11	-0,5902266	4,95E-02	Egfl7	-0,559395	3,53E-07
Ppm1m	-0,5896045	1,93E-03	9030617O03Rik	-0,559348	8,57E-04
5430427O19Rik	-0,5891622	1,74E-03	Stard5	-0,5592477	1,55E-03
Il16	-0,588847	4,04E-06	Abi3	-0,5586098	2,51E-04
Actn1	-0,588796	1,36E-02	Pycard	-0,5583594	1,20E-06
Ptgs1	-0,5879326	1,75E-07	Zfp783	-0,5580006	7,57E-04
Samhd1	-0,5864098	5,47E-06	D5Ertd605e	-0,5577858	2,65E-02
Ttc38	-0,5843988	6,01E-03	Tspyl4	-0,5565277	2,87E-02
Il3ra	-0,5820283	2,82E-02	Ltbr	-0,555804	2,02E-03
Tmcc2	-0,5816193	4,85E-03	Plekhm3	-0,5556024	1,27E-03
Il11ra1	-0,5813092	1,74E-03	Cnrip1	-0,5552749	1,03E-03
BC005764	-0,5810297	7,60E-05	Tapbp	-0,5542351	2,05E-06
Arrdc1	-0,5800613	2,52E-07	Slc36a1	-0,5530747	4,88E-02
Prkce	-0,5779632	2,91E-02	Sertad3	-0,5529195	2,24E-03
Dgkg	-0,5763908	2,47E-03	Dhrs1	-0,5527328	9,48E-05
Cxcr2	-0,5756822	4,40E-02	Sigirr	-0,5527209	2,88E-05
Parp12	-0,5751817	2,58E-02	Ift22	-0,5519075	8,78E-04
Athl1	-0,5747417	4,59E-04	Prr5	-0,551493	1,91E-03
Fam21	-0,5512699	3,31E-05	Sh3kbp1	-0,5299598	8,40E-05
Haao	-0,5510735	5,30E-04	Itgal	-0,5289109	1,54E-04
Pcdh7	-0,5474294	5,33E-03	Osgin1	-0,5284532	2,19E-02
Emid1	-0,5469261	6,78E-03	Arhgap6	-0,5278686	2,37E-03
Ehd4	-0,5468142	2,35E-04	Tmtc4	-0,5277502	1,66E-02
Nrxn1	-0,5467882	2,89E-02	1700025G04Rik	-0,527638	5,98E-03
Gimap6	-0,5466042	3,98E-06	Mxd3	-0,5273198	4,65E-02
Tgfbi	-0,5465559	4,35E-04	Zmym3	-0,5272046	1,14E-04
Ptprc	-0,5464297	4,38E-05	Glb1l	-0,5256631	1,33E-02
Psmb9	-0,5461697	4,45E-04	Igfbp4	-0,5246845	9,61E-05
Agtrap	-0,5453801	4,04E-04	Klk8	-0,5234794	4,34E-04
Cdh17	-0,5452301	3,85E-02	Fam101b	-0,5227723	7,13E-03
Luzp1	-0,5451904	1,37E-03	Tbc1d13	-0,5223989	1,66E-02
Ccdc28a	-0,5449366	1,39E-02	Sfxn3	-0,5221425	2,83E-04
Ociad2	-0,5446894	3,11E-02	Zbtb20	-0,5219777	2,74E-02
Il1rap	-0,5445608	1,36E-02	Prkar2a	-0,5219531	1,54E-02
Tbc1d5	-0,5442739	6,67E-06	Arhgap18	-0,521925	2,72E-04
Cdip1	-0,544182	2,51E-04	Bloc1s1	-0,5218327	1,18E-04
Gpatch11	-0,54305	1,04E-03	Serf1	-0,5207708	8,17E-03
Hdac8	-0,5429439	1,41E-03	Pot1b	-0,5205806	1,74E-02
Peak1	-0,5428748	5,45E-04	Bcl2	-0,5202049	4,06E-03
Sfmbt2	-0,542416	4,31E-02	Ctns	-0,5199397	8,51E-03
Lzts2	-0,542135	1,16E-02	Zfp629	-0,5196193	8,61E-04
Stard10	-0,5419589	5,33E-03	Camkk1	-0,5191244	4,25E-03

Epb4.1l2	-0,5414762	9,81E-05	Spice1	-0,5187062	1,29E-03
Fmo5	-0,5413034	3,60E-02	Nckap1l	-0,5185927	5,80E-05
Cbx8	-0,5411201	8,41E-03	Fut10	-0,5165683	1,38E-02
Eif4e3	-0,5405992	1,63E-02	Birc3	-0,516298	5,60E-04
Itm2c	-0,5405304	2,21E-04	Apobr	-0,5161388	3,30E-03
Cox4i2	-0,5403324	4,30E-02	Inpp4a	-0,5159228	1,68E-02
Nfat5	-0,5401072	1,40E-03	Treml2	-0,5157747	2,15E-05
Casp6	-0,5395538	2,67E-04	Stx16	-0,5146943	2,20E-04
Sik1	-0,5390982	3,92E-03	Prkcd	-0,513545	5,78E-05
Shisa5	-0,538847	1,81E-06	Ppm1f	-0,5127768	4,24E-04
Elk3	-0,5383877	7,43E-06	Ip6k2	-0,5126136	4,80E-02
Chst15	-0,5378296	1,41E-03	Ldhb	-0,5124742	4,60E-04
Usf1	-0,5358572	7,31E-05	Spns3	-0,5119172	1,57E-02
Zcchc24	-0,5356841	4,48E-02	Rasa3	-0,5119109	3,47E-04
Fcgr3	-0,5344401	2,94E-03	Mapk3	-0,5117559	2,92E-04
Iqcb1	-0,5344323	1,55E-03	Slc31a2	-0,5116122	1,06E-02
Gpr56	-0,5342464	5,90E-06	3110056K07Rik	-0,511472	3,84E-02
Cnpy3	-0,5338293	1,06E-05	Tsc22d3	-0,5107125	3,71E-05
Cbx7	-0,5338025	2,03E-02	Sestd1	-0,5101197	2,54E-02
Bahcc1	-0,5335525	1,76E-03	Sh3pxd2b	-0,5100521	2,77E-02
Tex264	-0,5333889	4,23E-03	Dgka	-0,509812	3,69E-02
Gdap10	-0,5331691	4,40E-02	Ncf2	-0,5079398	6,65E-05
Gdi1	-0,5331532	5,55E-08	6330419J24Rik	-0,5074271	4,48E-02
Sirt3	-0,5329569	2,35E-05	Nicn1	-0,5071723	4,37E-02
Pitpnm1	-0,5323364	1,21E-02	Maml3	-0,506724	2,70E-03
Akr1b10	-0,5321715	2,16E-03	Acot11	-0,5060973	6,06E-03
Cdk19	-0,53179	5,59E-06	Pkn3	-0,5059785	2,28E-02
Rel	-0,5307849	2,97E-02	Tmsb10	-0,5059723	3,84E-06
Appl2	-0,530723	1,09E-03	Pla2g15	-0,505713	9,63E-04
4931406C07Rik	-0,5303378	2,45E-03	Tcirg1	-0,5057083	9,10E-05
A230050P20Rik	-0,5303269	1,16E-02	Khnyn	-0,5055369	3,15E-04
Enkd1	-0,5300604	1,95E-03	Ifnar2	-0,5050715	8,19E-04
Parp10	-0,5048953	6,07E-03	Cyth1	-0,5017325	1,41E-02
Ift74	-0,5048308	9,21E-03	Idua	-0,5016355	9,45E-04
Pdlim7	-0,5047423	8,72E-04	Ptpn6	-0,5015001	9,80E-06
Zfp667	-0,5046161	3,72E-02	Mob3c	-0,5013894	4,89E-03
Clec12a	-0,5037711	1,46E-02	Cers4	-0,5013071	7,33E-03
F630028O10Rik	-0,5033071	3,02E-02	Map3k12	-0,5009038	4,89E-02
Gpr65	-0,5025576	1,40E-03	9030619P08Rik	-0,5006843	2,76E-02
Kctd14	-0,5024867	1,02E-02	Itpk1	-0,5001285	1,24E-03
Tor4a	-0,5021209	6,04E-05			

Table 10.5 | List of significantly upregulated ERVs in *Setdb1*^{vav} LT-HSCs

ERVs	log2FoldChange	padj
RLTR50A|LTR|ERVK	4,533159221	1,76E-19
MER74C|LTR|ERVL	3,872425015	5,42E-14
IAPLTR3-int|LTR|ERVK	3,533401388	2,39E-24
ERVB4_1-I_MM-int|LTR|ERVK	3,4898036	1,81E-19
MuLV-int|LTR|ERV1	3,039734155	4,17E-36
ERVB4_2-I_MM-int|LTR|ERVK	2,968110392	2,30E-09
RLTR6C_Mm|LTR|ERV1	2,69618733	2,19E-15
RLTR45|LTR|ERVK	2,493699688	4,20E-14
IAPLTR4|LTR|ERVK	2,422171983	5,39E-11
MMERVK10C-int|LTR|ERVK	2,330897416	9,05E-13
RLTR10C|LTR|ERVK	2,300374391	3,31E-06

MMVL30-int|LTR|ERV1	2,271243474	1,38E-17
MMTV-int|LTR|ERVK	2,177523161	0,000404423
RLTR3_Mm|LTR|ERVK	2,009509415	5,06E-06
MMERVK9C_I-int|LTR|ERVK	1,813424411	0,000643022
RLTR45-int|LTR|ERVK	1,537845251	1,82E-21
RLTR4_Mm|LTR|ERV1	1,431960201	6,96E-16
RMER17A-int|LTR|ERVK	1,378754235	0,000287049
IAP1-MM_LTR|LTR|ERVK	1,344447962	5,94E-05
IAP-d-int|LTR|ERVK	1,171041168	0,000484206
RLTR27|LTR|ERVK	1,014595359	0,000404423

Table 10.6 | List of significantly upregulated ERVs in *Setdb1*^{vav} MPPs

	log2FoldChange	padj
RLTR50A|LTR|ERVK	6,929567457	1,48E-22
IAPLTR3-int|LTR|ERVK	5,957725342	0
ERVB4_2-I_MM-int|LTR|ERVK	5,910899848	3,26E-136
MER74C|LTR|ERVL	5,554551083	1,07E-30
ERVB4_2-LTR_MM|LTR|ERVK	5,082019253	3,78E-06
MURVY-int|LTR|ERV1	4,575814994	3,65E-31
ERVB4_1-I_MM-int|LTR|ERVK	4,463654539	4,11E-78
RLTR6C_Mm|LTR|ERV1	4,36015532	1,00E-50
IAPLTR4|LTR|ERVK	4,255906444	1,34E-82
RLTR10C|LTR|ERVK	4,104850424	1,86E-105
MMERVK10C-int|LTR|ERVK	4,072903087	2,17E-125
RLTR45|LTR|ERVK	4,04025705	6,08E-92
MuLV-int|LTR|ERV1	3,952581031	0
RLTR45-int|LTR|ERVK	3,505584294	5,48E-121
RMER17A-int|LTR|ERVK	3,468191276	2,87E-65
MMERVK9C_I-int|LTR|ERVK	3,4538709	1,86E-74
MMVL30-int|LTR|ERV1	3,225050534	8,08E-69
RLTR44E|LTR|ERVK	3,184298209	2,42E-10
MMTV-int|LTR|ERVK	3,045928684	2,52E-46
ERVB3_1-I_MM-int|LTR|ERVK	2,745359668	5,70E-25
RLTR10B2|LTR|ERVK	2,543976306	6,97E-21
IAP-d-int|LTR|ERVK	2,4991614	3,65E-28
ERVB7_3-LTR_MM|LTR|ERVK	2,105487905	3,56E-11
RLTR4_Mm|LTR|ERV1	2,078628927	2,49E-115
MMERVK10D3_I-int|LTR|ERVK	2,007497073	6,23E-28
RLTR44D|LTR|ERVK	1,792437478	0,001084028
RLTR1B-int|LTR|ERV1	1,740523579	6,08E-36
RLTR44B|LTR|ERVK	1,720522959	0,001791936
IAPLTR1a_Mm|LTR|ERVK	1,690250188	2,09E-32
RLTR13D6|LTR|ERVK	1,66631935	1,47E-18
RLTR3_Mm|LTR|ERVK	1,647747567	1,42E-10
MMERGLN-int|LTR|ERV1	1,605707858	7,99E-13
RLTR1B|LTR|ERV1	1,546579957	2,78E-25
RLTR10B|LTR|ERVK	1,434639777	5,29E-06
IAPEY4_I-int|LTR|ERVK	1,375984536	2,73E-49
RLTR10D2|LTR|ERVK	1,351069369	0,004535435
RLTR6-int|LTR|ERV1	1,342205529	2,05E-12
ERVB7_2-LTR_MM|LTR|ERVK	1,320835098	2,21E-11
ETnERV3-int|LTR|ERVK	1,22415767	3,57E-10
IAP1-MM_LTR|LTR|ERVK	1,171322935	0,00136433
RLTR6_Mm|LTR|ERV1	1,137927028	1,17E-08
IAPEz-int|LTR|ERVK	1,127922157	1,89E-11

ETnERV-int|LTR|ERVK	1,06976194	4,27E-10
RLTR10F|LTR|ERVK	1,053555807	5,02E-06
ERVB4_1B-I_MM-int|LTR|ERVK	1,03679133	1,36E-07
RMER16A3|LTR|ERVK	1,026735636	0,003301675

Table 10.7 | List of significantly upregulated LINEs in *Setdb1^{vav}* MPPs

	log2FoldChange	padj
L1_Mm|LINE|L1	0,627558688	4,23E-12
L1M2b|LINE|L1	0,4546018	9,72E-06
X9_LINE|LINE|L1?	0,363004007	0,005456843
L1Md_T|LINE|L1	0,307181867	2,57E-07
L1_Mus2|LINE|L1	0,262388523	1,01E-07
L1_Mus3|LINE|L1	0,2379632	5,36E-08
L1MB2|LINE|L1	0,216896528	0,004045762

Table 10.8 | List of significantly upregulated SINEs in *Setdb1^{vav}* MPPs

	log2FoldChange	padj
B2_Mm1a|SINE|B2	0,477513027	3,19E-52
B2_Mm1t|SINE|B2	0,319605564	1,43E-27

Table 10.9 | List of top 20 enriched motifs in *Setdb1^{vav}*-specific ATAC peaks

Motif Name	Consensus	P-value	Log P-value	# of Target Sequences with Motif(of 708)	% of Target Sequences with Motif
Fli1(ETS)/CD8-FLI-ChIP-Seq(GSE20898)/Homer	NRYTTCCGGH	1,00E-115	-2,66E+02	324	45,76%
CTCF(Zf)/CD4+-CTCF-ChIP-Seq(Barski_et_al.)/Homer	AYAGTGCCMYCTRGTGGCCA	1,00E-113	-2,61E+02	145	20,48%
PU.1(ETS)/ThioMac-PU.1-ChIP-Seq(GSE21512)/Homer	AGAGGAAGTG	1,00E-108	-2,49E+02	237	33,47%
BORIS(Zf)/K562-CTCFL-ChIP-Seq(GSE32465)/Homer	CNNBRGCGCCCCCTGSTGGC	1,00E-100	-2,33E+02	147	20,76%
ETS1(ETS)/Jurkat-ETS1-ChIP-Seq(GSE17954)/Homer	ACAGGAAGTG	1,00E-99	-2,30E+02	306	43,22%
ELF3(ETS)/PDAC-ELF3-ChIP-Seq(GSE64557)/Homer	ANCAGGAAGT	1,00E-98	-2,26E+02	251	35,45%
ELF5(ETS)/T47D-ELF5-ChIP-Seq(GSE30407)/Homer	ACVAGGAAGT	1,00E-94	-2,17E+02	245	34,60%
EHF(ETS)/LoVo-EHF-ChIP-Seq(GSE49402)/Homer	AVCAGGAAGT	1,00E-83	-1,93E+02	310	43,79%
ERG(ETS)/VCaP-ERG-ChIP-Seq(GSE14097)/Homer	ACAGGAAGTG	1,00E-79	-1,83E+02	349	49,29%
ETV1(ETS)/GIST48-ETV1-ChIP-Seq(GSE22441)/Homer	AACCGGAAGT	1,00E-79	-1,82E+02	320	45,20%
GABPA(ETS)/Jurkat-GABPa-ChIP-Seq(GSE17954)/Homer	RACCGGAAGT	1,00E-73	-1,68E+02	246	34,75%
Etv2(ETS)/ES-ER71-ChIP-Seq(GSE59402)/Homer(0.967)	NNAYTTCCTGHN	1,00E-70	-1,61E+02	247	34,89%
Klf9(Zf)/GBM-Klf9-ChIP-Seq(GSE62211)/Homer	GCCACRCCCACY	1,00E-62	-1,43E+02	172	24,29%
Ets1-distal(ETS)/CD4+-PolII-ChIP-Seq(Barski_et_al.)/Homer	MACAGGAAGT	1,00E-57	-1,33E+02	132	18,64%
EWS:FLI1-fusion(ETS)/SK_N_MC-EWS:FLI1-ChIP-Seq(SRA014231)/Homer	VACAGGAAAT	1,00E-49	-1,15E+02	163	23,02%

Sp5(Zf)/mES-Sp5.Flag-ChIP-Seq(GSE72989)/Homer	RGKGGGCGGAGC	1,00E-49	-1,13E+02	238	33,62%
ELF1(ETS)/Jurkat-ELF1-ChIP-Seq(SRA014231)/Homer	AVCCGGAAGT	1,00E-46	-1,06E+02	141	19,92%
RUNX1(Runt)/Jurkat-RUNX1-ChIP-Seq(GSE29180)/Homer	AAACCACARM	1,00E-43	-1,01E+02	219	30,93%
EWS:ERG-fusion(ETS)/CADO_ES1-EWS:ERG-ChIP-Seq(SRA014231)/Homer	ATTTCCTGTN	1,00E-43	-1,01E+02	165	23,31%
ETS(ETS)/Promoter/Homer	AACCGGAAGT	1,00E-43	-1,00E+02	109	15,40%

11. References

Adolfsson, J., Månsson, R., Buza-Vidas, N., Hultquist, A., Liuba, K., Jensen, C.T., Bryder, D., Yang, L., Borge, O.-J., Thoren, L.A.M., et al. (2005). Identification of Flt3+ Lympho-Myeloid Stem Cells Lacking Erythro-Megakaryocytic Potential. Cell *121*, 295–306.

Adoue, V., Binet, B., Malbec, A., Fourquet, J., Romagnoli, P., van Meerwijk, J.P.M., Amigorena, S., and Joffre, O.P. (2019). The Histone Methyltransferase SETDB1 Controls T Helper Cell Lineage Integrity by Repressing Endogenous Retroviruses. Immunity *50*, 629-644.e8.

Afgan, E., Baker, D., van den Beek, M., Blankenberg, D., Bouvier, D., Čech, M., Chilton, J., Clements, D., Coraor, N., Eberhard, C., et al. (2016). The Galaxy platform for accessible, reproducible and collaborative biomedical analyses: 2016 update. Nucleic Acids Res. *44*, W3–W10.

Akashi, K., Traver, D., Miyamoto, T., and Weissman, I.L. (2000). A clonogenic common myeloid progenitor that gives rise to all myeloid lineages. Nature *404*, 193–197.

An, J., Zhang, X., Qin, J., Wan, Y., Hu, Y., Liu, T., Li, J., Dong, W., Du, E., Pan, C., et al. (2014). The histone methyltransferase ESET is required for the survival of spermatogonial stem/progenitor cells in mice. Cell Death Dis. *5*, e1196–e1196.

Ariki, R., Morikawa, S., Mabuchi, Y., Suzuki, S., Nakatake, M., Yoshioka, K., Hidano, S., Nakauchi, H., Matsuzaki, Y., Nakamura, T., et al. (2014). Homeodomain Transcription Factor Meis1 Is a Critical Regulator of Adult Bone Marrow Hematopoiesis. PLoS One *9*, e87646.

Arinobu, Y., Mizuno, S. ichi, Chong, Y., Shigematsu, H., Iino, T., Iwasaki, H., Graf, T., Mayfield, R., Chan, S., Kastner, P., et al. (2007). Reciprocal Activation of GATA-1 and PU.1 Marks Initial Specification of Hematopoietic Stem Cells into Myeloerythroid and Myelolymphoid Lineages. Cell Stem Cell *1*, 416–427.

Barker, J.E. (1968). Development of the mouse hematopoietic system. Dev. Biol. *18*, 14–29.

Becker, A., McCulloch, E., Siminovitch, L., and Till, J. (1965). The effect of differing demands for blood cell production on DNA synthesis by hemopoietic colony-forming cells of mice. Blood *26*, 296–308.

Bell, A.C., West, A.G., and Felsenfeld, G. (1999). The protein CTCF is required for the enhancer blocking activity of vertebrate insulators. Cell *98*, 387–396.

Berger, S.L. (2007). The complex language of chromatin regulation during transcription. Nature *447*, 407–412.

Bertrand, J.Y., Desanti, G.E., Lo-Man, R., Leclerc, C., Cumano, A., and Golub, R. (2006). Fetal spleen stroma drives macrophage commitment. Development *133*, 3619–3628.

Beyer, S., Pontis, J., Schirwis, E., Battisti, V., Rudolf, A., Le Grand, F., and Ait-Si-Ali, S. (2016). Canonical Wnt signalling regulates nuclear export of Setdb1 during skeletal muscle terminal differentiation. Cell Discov. *2*, 16037.

Bilodeau, S., Kagey, M.H., Frampton, G.M., Rahl, P.B., and Young, R.A. (2009). SetDB1 contributes to repression of genes encoding developmental regulators and maintenance of ES cell state. Genes Dev. *23*, 2484–2489.

Bird, A. (2002). DNA methylation patterns and epigenetic memory. Genes Dev. *16*, 6–21.

Bowie, M.B., McKnight, K.D., Kent, D.G., McCaffrey, L., Hoodless, P.A., and Eaves, C.J. (2006). Hematopoietic stem cells proliferate until after birth and show a reversible phase-specific engraftment defect. J. Clin. Invest. *116*, 2808–2816.

Bowie, M.B., Kent, D.G., Dykstra, B., McKnight, K.D., McCaffrey, L., Hoodless, P.A., and Eaves, C.J. (2007). Identification of a new intrinsically timed developmental checkpoint that reprograms key hematopoietic stem cell properties. Proc. Natl. Acad. Sci. *104*, 5878–5882.

Brind'Amour, J., Liu, S., Hudson, M., Chen, C., Karimi, M.M., and Lorincz, M.C. (2015). An ultra-low-input native ChIP-seq protocol for genome-wide profiling of rare cell populations. Nat. Commun. *6*, 6033.

Broxmeyer, H.E., Maze, R., Miyazawa, K., Carow, C., Hendrie, P.C., Cooper, S., Hangoc, G., Vadhan-Raj, S., and Lu, L. (1991). The kit receptor and its ligand, steel factor, as regulators of hemopoiesis. Cancer Cells *3*, 480–487.

Buenrostro, J.D., Giresi, P.G., Zaba, L.C., Chang, H.Y., and Greenleaf, W.J. (2013). Transposition of native chromatin for fast and sensitive epigenomic profiling of open chromatin, DNA-binding proteins and nucleosome position. Nat. Methods *10*, 1213–1218.

Burda, P., Laslo, P., and Stopka, T. (2010). The role of PU.1 and GATA-1 transcription factors during normal and leukemogenic hematopoiesis. Leukemia *24*, 1249–1257.

Cao, H., Cao, B., Heazlewood, C.K., Domingues, M., Sun, X., Debele, E., McGregor, N.E., Sims, N.A., Heazlewood, S.Y., and Nilsson, S.K. (2019). Osteopontin is An Important Regulative Component of the Fetal Bone Marrow Hematopoietic Stem Cell Niche. Cells *8*, 985.

Capel, B., Hawley, R., Covarrubias, L., Hawley, T., and Mintz, B. (1989). Clonal contributions of small numbers of retrovirally marked hematopoietic stem cells engrafted in unirradiated neonatal W/Wv mice. Proc. Natl. Acad. Sci. *86*, 4564–4568.

Capel, B., Hawley, R.G., and Mintz, B. (1990). Long- and short-lived murine hematopoietic stem cell clones individually identified with retroviral integration markers. Blood *75*, 2267–2270.

Carotta, S., Dakic, A., D'Amico, A., Pang, S.H.M., Greig, K.T., Nutt, S.L., and Wu, L. (2010). The transcription factor PU.1 controls dendritic cell development and Flt3 cytokine receptor expression in a dose-dependent manner. Immunity *32*, 628–641.

Chambers, S.M., Boles, N.C., Lin, K.Y.K., Tierney, M.P., Bowman, T. V., Bradfute, S.B., Chen, A.J., Merchant, A.A., Sirin, O., Weksberg, D.C., et al. (2007). Hematopoietic Fingerprints: An Expression Database of Stem Cells and Their Progeny. Cell Stem Cell *1*, 578–591.

Chen, M.J., Yokomizo, T., Zeigler, B.M., Dzierzak, E., and Speck, N.A. (2009). Runx1 is required for the endothelial to haematopoietic cell transition but not thereafter. Nature *457*, 887–891.

Christensen, J.L., Wright, D.E., Wagers, A.J., and Weissman, I.L. (2004). Circulation and Chemotaxis of Fetal Hematopoietic Stem Cells. PLoS Biol. *2*, e75.

Ciriza, J., Thompson, H., Petrosian, R., Manilay, J.O., and García-Ojeda, M.E. (2013). The migration of hematopoietic progenitors from the fetal liver to the fetal bone marrow: Lessons learned and possible clinical applications. Exp. Hematol. *41*, 411–423.

Clark, E.R. (1909). Observations on living growing lymphatics in the tail of the frog larva. Anat. Rec. *3*, 183–198.

Cobb, M. (2017). 60 years ago, Francis Crick changed the logic of biology. PLOS Biol. *15*, e2003243.

Collins, P.L., Kyle, K.E., Egawa, T., Shinkai, Y., and Oltz, E.M. (2015). The histone methyltransferase SETDB1 represses endogenous and exogenous retroviruses in B lymphocytes. Proc. Natl. Acad. Sci. *112*, 8367–8372.

Copley, M.R., Babovic, S., Benz, C., Knapp, D.J.H.F., Beer, P.A., Kent, D.G., Wohrer, S., Treloar, D.Q., Day, C., Rowe, K., et al. (2013). The Lin28b–let-7–Hmga2 axis determines the higher self-renewal potential of fetal haematopoietic stem cells. Nat. Cell Biol. *15*, 916–925.

Corces, M.R., Trevino, A.E., Hamilton, E.G., Greenside, P.G., Sinnott-Armstrong, N.A., Vesuna, S., Satpathy, A.T., Rubin, A.J., Montine, K.S., Wu, B., et al. (2017). An improved ATAC-seq protocol reduces background and enables interrogation of frozen tissues. Nat. Methods *14*, 959–962.

Cuddapah, S., Jothi, R., Schones, D.E., Roh, T.Y., Cui, K., and Zhao, K. (2009). Global analysis of the insulator binding protein CTCF in chromatin barrier regions reveals demarcation of active and repressive domains. Genome Res. *19*, 24–32.

Cumano, A., Dieterlen-Lievre, F., and Godin, I. (1996). Lymphoid Potential, Probed before Circulation in Mouse, Is Restricted to Caudal Intraembryonic Splanchnopleura. Cell *86*, 907–916.

Dambacher, S., Hahn, M., and Schotta, G. (2010). Epigenetic regulation of development by histone lysine methylation. Heredity (Edinb). *105*, 24–37.

DeKoter, R.P., Lee, H.-J., and Singh, H. (2002). PU.1 Regulates Expression of the Interleukin-7 Receptor in Lymphoid Progenitors. Immunity *16*, 297–309.

Dias, S., Månsson, R., Gurbuxani, S., Sigvardsson, M., and Kee, B.L. (2008). E2A Proteins Promote Development of Lymphoid-Primed Multipotent Progenitors. Immunity *29*, 217–227.

Dixon, J.R., Selvaraj, S., Yue, F., Kim, A., Li, Y., Shen, Y., Hu, M., Liu, J.S., and Ren, B. (2012). Topological domains in mammalian genomes identified by analysis of chromatin interactions. Nature *485*, 376–380.

Djaldetti, M., Bessler, H., and Fishman, P. (1975). Hematopoiesis in the embryonic mouse spleen. II. Alterations after phenylhydrazine administration to the mothers. Anat. Rec. *182*, 123–136.

Dobin, A., Davis, C.A., Schlesinger, F., Drenkow, J., Zaleski, C., Jha, S., Batut, P., Chaisson, M., and Gingeras, T.R. (2013). STAR: Ultrafast universal RNA-seq aligner. Bioinformatics *29*, 15–21.

Dodge, J.E., Kang, Y., Beppu, H., and Lei, H. (2004). Histone H3-K9 Methyltransferase ESET Is Essential for Early Development Histone H3-K9 Methyltransferase ESET Is Essential for Early Development. Mol. Cell. Biol. *24*, 2478–2486.

Douagi, I., Vieira, P., and Cumano, A. (2002). Lymphocyte commitment during embryonic development, in the mouse. Semin. Immunol. *14*, 361–369.

Drissen, R., Buza-Vidas, N., Woll, P., Thongjuea, S., Gambardella, A., Giustacchini, A., Mancini, E., Zriwil, A., Lutteropp, M., Grover, A., et al. (2016). Distinct myeloid progenitor-differentiation pathways identified through single-cell RNA sequencing. Nat. Immunol. *17*, 666–676.

Eissenberg, J.C., and Shilatifard, A. (2010). Histone H3 lysine 4 (H3K4) methylation in development and differentiation. Dev. Biol. *339*, 240–249.

Ema, H., and Nakauchi, H. (2000). Expansion of hematopoietic stem cells in the developing liver of a mouse embryo. Blood *95*, 2284–2288.

Falandry, C., Fourel, G., Galy, V., Ristriani, T., Horard, B., Bensimon, E., Salles, G., Gilson, E., and Magdinier, F. (2010). CLLD8/KMT1F Is a Lysine Methyltransferase That Is Important for Chromosome Segregation. J. Biol. Chem. *285*, 20234–20241.

Ferreira, R., Ohneda, K., Yamamoto, M., and Philipsen, S. (2005). GATA1 function, a paradigm for transcription factors in hematopoiesis. Mol. Cell. Biol. *25*, 1215–1227.

Ficara, F., Crisafulli, L., Lin, C., Iwasaki, M., Smith, K.S., Zammataro, L., and Cleary, M.L. (2013). Pbx1 restrains myeloid maturation while preserving lymphoid potential in hematopoietic progenitors. J. Cell Sci. *126*, 3181–3191.

Fleming, W., Alpern, E., Uchida, N., Ikuta, K., Spangrude, G., and Weissman, I. (1993). Functional heterogeneity is associated with the cell cycle status of murine hematopoietic stem cells. J. Cell Biol. *122*, 897–902.

Frenette (2008). Hematopoietic stem cell trafficking. StemBook.

Ge, S.X., Jung, D., and Yao, R. (2020). ShinyGO: a graphical gene-set enrichment tool for animals and plants. Bioinformatics *36*, 2628–2629.

Gekas, C., Dieterlen-Lièvre, F., Orkin, S.H., and Mikkola, H.K.A. (2005). The Placenta Is a Niche for Hematopoietic Stem Cells. Dev. Cell *8*, 365–375.

Godin, I., and Cumano, A. (2002). The hare and the tortoise: an embryonic haematopoietic race. Nat. Rev. Immunol. *2*, 593–604.

Goldberg, A.D., Allis, C.D., and Bernstein, E. (2007). Epigenetics: A Landscape Takes Shape. Cell *128*, 635–638.

Goll, M.G., and Bestor, T.H. (2005). Eukaryotic cytosine methyltransferases. Annu. Rev. Biochem. *74*, 481–514.

Gorkin, D.U., Leung, D., and Ren, B. (2014). The 3D Genome in Transcriptional Regulation and Pluripotency. Cell Stem Cell *14*, 762–775.

Göttgens, B., Nastos, A., Kinston, S., Piltz, S., Delabesse, E.C.M., Stanley, M., Sanchez, M.J., Ciau-Uitz, A., Patient, R., and Green, A.R. (2002). Establishing the transcriptional programme for blood: The SCL stem cell enhancer is regulated by a multiprotein complex containing Ets and GATA factors. EMBO J. *21*, 3039–3050.

Greenberg, M.V.C., and Bourc'his, D. (2019). The diverse roles of DNA methylation in mammalian development and disease. Nat. Rev. Mol. Cell Biol. *20*, 590–607.

Greer, E.L., and Shi, Y. (2012). Histone methylation: A dynamic mark in health, disease and inheritance. Nat. Rev. Genet. *13*, 343–357.

Hachiya, R., Shiihashi, T., Shirakawa, I., Iwasaki, Y., Matsumura, Y., Oishi, Y., Nakayama, Y., Miyamoto, Y., Manabe, I., Ochi, K., et al. (2016). The H3K9 methyltransferase Setdb1 regulates TLR4-mediated inflammatory responses in macrophages. Sci. Rep. *6*, 28845.

Hall, M.A., Curtis, D.J., Metcalf, D., Elefanty, A.G., Sourris, K., Robb, L., Gothert, J.R., Jane, S.M., and Begley, C.G. (2003). The critical regulator of embryonic hematopoiesis, SCL, is vital in the adult for megakaryopoiesis, erythropoiesis, and lineage choice in CFU-S12. Proc. Natl. Acad. Sci. *100*, 992–997.

Hart, A., Melet, F., Grossfeld, P., Chien, K., Jones, C., Tunnacliffe, A., Favier, R., and Bernstein, A. (2000). Fli-1 Is Required for Murine Vascular and Megakaryocytic Development and Is Hemizygously Deleted in Patients with Thrombocytopenia. Immunity *13*, 167–177.

He, S., Kim, I., Lim, M.S., and Morrison, S.J. (2011). Sox17 expression confers self-renewal potential and fetal stem cell characteristics upon adult hematopoietic progenitors. Genes Dev. *25*, 1613–1627.

Heinz, S., Benner, C., Spann, N., Bertolino, E., Lin, Y.C., Laslo, P., Cheng, J.X., Murre, C., Singh, H., and Glass, C.K. (2010). Simple Combinations of Lineage-Determining Transcription Factors Prime cis-Regulatory Elements Required for Macrophage and B Cell Identities. Mol. Cell *38*, 576–589.

Hock, H., Hamblen, M.J., Rooke, H.M., Schindler, J.W., Saleque, S., Fujiwara, Y., and Orkin, S.H. (2004a). Gfi-1 restricts proliferation and preserves functional integrity of haematopoietic stem cells. Nature *431*, 1002–1007.

Hock, H., Meade, E., Medeiros, S., Schindler, J.W., Valk, P.J.M., Fujiwara, Y., and Orkin, S.H. (2004b). Tel/Etv6 is an essential and selective regulator of adult hematopoietic stem cell survival. Genes Dev. *18*, 2336–2341.

Hosokawa, H., Ungerbäck, J., Wang, X., Matsumoto, M., Nakayama, K.I., Cohen, S.M., Tanaka, T., and Rothenberg, E. V. (2018). Transcription Factor PU.1 Represses and Activates Gene Expression in Early T Cells by Redirecting Partner Transcription Factor Binding. Immunity *48*, 1119-1134.e7.

Houssaint, E. (1981). Differentiation of the mouse hepatic primordium. II. Extrinsic origin of the haemopoietic cell line. Cell Differ. *10*, 243–252.

Huisinga, K.L., Brower-Toland, B., and Elgin, S.C.R. (2006). The contradictory definitions of heterochromatin: transcription and silencing. Chromosoma *115*, 110–122.

Ikuta, K., and Weissman, I.L. (1992). Evidence that hematopoietic stem cells express mouse c-kit but do not depend on steel factor for their generation. Proc. Natl. Acad. Sci. *89*, 1502–1506.

Ito, K., and Suda, T. (2014). Metabolic requirements for the maintenance of self-renewing stem cells. Nat. Rev. Mol. Cell Biol. *15*, 243–256.

Ivanova, N.B., Dimos, J.T., Schaniel, C., Hackney, J.A., Moore, K.A., and Lemischka, I.R. (2002). A stem cell molecular signature Supporting Online Material. Science (80-.). *298*, 1–45.

Jacob, B., Osato, M., Yamashita, N., Wang, C.Q., Taniuchi, I., Littman, D.R., Asou, N., and Ito, Y. (2010). Stem cell exhaustion due to Runx1 deficiency is prevented by Evi5 activation in leukemogenesis. Blood *115*, 1610–1620.

Jaenisch, R., and Bird, A. (2003). Epigenetic regulation of gene expression: How the genome integrates intrinsic and environmental signals. Nat. Genet. *33*, 245–254.

Jenuwein, T., and Allis, C.D. (2001). Translating the histone code. Science (80-.). *293*, 1074–1080.

Jiang, Y., Loh, Y.-H.E., Rajarajan, P., Hirayama, T., Liao, W., Kassim, B.S., Javidfar, B., Hartley, B.J., Kleofas, L., Park, R.B., et al. (2017). The methyltransferase SETDB1 regulates a large neuron-specific topological chromatin domain. Nat. Genet. *49*, 1239–1250.

Jordan, C.T., McKearn, J.P., and Lemischka, I.R. (1990). Cellular and developmental properties of fetal hematopoietic stem cells. Cell *61*, 953–963.

Kang, Y.-K. (2015). SETDB1 in Early Embryos and Embryonic Stem Cells. Curr. Issues Mol. Biol. *17*, 1–10.

Karamitros, D., Stoilova, B., Aboukhalil, Z., Hamey, F., Reinisch, A., Samitsch, M., Quek, L., Otto, G., Repapi, E., Doondeea, J., et al. (2018). Single-cell analysis reveals the continuum of human lympho-myeloid progenitor cells. Nat. Immunol. *19*, 85–97.

Karimi, M.M., Goyal, P., Maksakova, I.A., Bilenky, M., Leung, D., Tang, J.X., Shinkai, Y., Mager, D.L., Jones, S., Hirst, M., et al. (2011). DNA methylation and SETDB1/H3K9me3 regulate predominantly distinct sets of genes, retroelements, and chimeric transcripts in mescs. Cell Stem Cell *8*, 676–687.

Kato, M., Takemoto, K., and Shinkai, Y. (2018). A somatic role for the histone methyltransferase Setdb1 in endogenous retrovirus silencing. Nat. Commun. *9*, 1–13.

Kawamoto, H. (1997). Direct evidence for the commitment of hematopoietic stem cells to T, B and myeloid lineages in murine fetal liver. Int. Immunol. *9*, 1011–1019.

Kawamoto, H., Ohmura, K., and Katsura, Y. (1998). Presence of Progenitors Restricted to T, B, or Myeloid Lineage, but Absence of Multipotent Stem Cells, in the Murine Fetal Thymus. J. Immunol. *161*, 3799 LP – 3802.

Kawamoto, H., Ohmura, K., Fujimoto, S., and Katsura, Y. (1999). Emergence of T Cell Progenitors Without B Cell or Myeloid Differentiation Potential at the Earliest Stage of Hematopoiesis in the Murine Fetal Liver. J. Immunol. *162*, 2725 LP – 2731.

Keniry, A., Gearing, L.J., Jansz, N., Liu, J., Holik, A.Z., Hickey, P.F., Kinkel, S.A., Moore, D.L., Breslin, K., Chen, K., et al. (2016). Setdb1-mediated H3K9 methylation is enriched on the inactive X and plays a role in its epigenetic silencing. Epigenetics Chromatin *9*, 16.

Kentepozidou, E., Aitken, S.J., Feig, C., Stefflova, K., Ibarra-Soria, X., Odom, D.T., Roller, M., and Flicek, P. (2020). Clustered CTCF binding is an evolutionary mechanism to maintain topologically associating domains. Genome Biol. *21*, 5.

Kiel, M.J., Yilmaz, Ö.H., Iwashita, T., Yilmaz, O.H., Terhorst, C., and Morrison, S.J. (2005). SLAM Family Receptors Distinguish Hematopoietic Stem and Progenitor Cells and Reveal Endothelial Niches for Stem Cells. Cell *121*, 1109–1121.

Kieusseian, A., de la Grange, P.B., Burlen-Defranoux, O., Godin, I., and Cumano, A. (2012). Immature hematopoietic stem cells undergo maturation in the fetal liver. Development *139*, 3521–3530.

Kim, I., Yilmaz, O.H., and Morrison, S.J. (2005). CD144 (VE-cadherin) is transiently expressed by fetal liver hematopoietic stem cells. Blood *106*, 903–905.

Kim, I., He, S., Yilmaz, O.H., Kiel, M.J., and Morrison, S.J. (2006). Enhanced purification of fetal liver hematopoietic stem cells using SLAM family receptors. Blood *108*, 737–744.

Kim, I., Saunders, T.L., and Morrison, S.J. (2007). Sox17 Dependence Distinguishes the Transcriptional Regulation of Fetal from Adult Hematopoietic Stem Cells. Cell *130*, 470–483.

Klimmeck, D., Hansson, J., Raffel, S., Vakhrushev, S.Y., Trumpp, A., and Krijgsveld, J. (2012). Proteomic Cornerstones of Hematopoietic Stem Cell Differentiation: Distinct Signatures of Multipotent Progenitors and Myeloid Committed Cells. Mol. Cell. Proteomics *11*, 286–302.

Knudsen, K.J., Rehn, M., Hasemann, M.S., Rapin, N., Bagger, F.O., Ohlsson, E., Willer, A., Frank, A.K., Søndergaard, E., Jendholm, J., et al. (2015). ERG promotes the maintenance of hematopoietic stem cells by restricting their differentiation. Genes Dev. *29*, 1915–1929.

Koide, S., Oshima, M., Takubo, K., Yamazaki, S., Nitta, E., Saraya, A., Aoyama, K., Kato, Y., Miyagi, S., Nakajima-Takagi, Y., et al. (2016). Setdb1 maintains hematopoietic stem and progenitor cells by restricting the ectopic activation of nonhematopoietic genes. Blood *128*, 638–649.

Kondo, M., Weissman, I.L., and Akashi, K. (1997). Identification of Clonogenic Common Lymphoid Progenitors in Mouse Bone Marrow. Cell *91*, 661–672.

Kornberg, R.D., and Lorch, Y. (1999). Twenty-Five Years of the Nucleosome, Fundamental Particle of the Eukaryote Chromosome. Cell *98*, 285–294.

Kouzarides, T. (2007). Chromatin Modifications and Their Function. Cell *128*, 693–705.

Langmead, B. (2010). Aligning Short Sequencing Reads with Bowtie. Curr. Protoc. Bioinforma. *32*.

Laslo, P., Spooner, C.J., Warmflash, A., Lancki, D.W., Lee, H.-J., Sciammas, R., Gantner, B.N., Dinner, A.R., and Singh, H. (2006). Multilineage Transcriptional Priming and Determination of Alternate Hematopoietic Cell Fates. Cell *126*, 755–766.

Laslo, P., Pongubala, J.M.R., Lancki, D.W., and Singh, H. (2008). Gene regulatory networks directing myeloid and lymphoid cell fates within the immune system. Semin. Immunol. *20*, 228–235.

Lawrence, H.J., Christensen, J., Fong, S., Hu, Y.-L., Weissman, I., Sauvageau, G., Humphries, R.K., and Largman, C. (2005). Loss of expression of the Hoxa-9 homeobox gene impairs the proliferation and repopulating ability of hematopoietic stem cells. Blood *106*, 3988–3994.

Lawson, K.A., Teteak, C.J., Gao, J., Li, N., Hacquebord, J., Ghatan, A., Zielinska-Kwiatkowska, A., Song, G., Chansky, H.A., and Yang, L. (2013a). ESET histone methyltransferase regulates osteoblastic differentiation of mesenchymal stem cells during postnatal bone development. FEBS Lett. *587*, 3961–3967.

Lawson, K.A., Teteak, C.J., Zou, J., Hacquebord, J., Ghatan, A., Zielinska-Kwiatkowska, A., Fernandes, R.J., Chansky, H.A., and Yang, L. (2013b). Mesenchyme-specific knockout of ESET histone methyltransferase causes ectopic hypertrophy and terminal differentiation of articular chondrocytes. J. Biol. Chem. *288*, 32119–32125.

Lekstrom-Himes, J.A. (2001). The Role of C/EBPε in the Terminal Stages of Granulocyte Differentiation. Stem Cells *19*, 125–133.

Liu, S., Brind???Amour, J., Karimi, M.M., Shirane, K., Bogutz, A., Lefebvre, L., Sasaki, H., Shinkai, Y., and Lorincz, M.C. (2014). Setdb1 is required for germline development and silencing of H3K9me3-marked endogenous retroviruses in primordial germ cells. Genes Dev. *28*, 2041–2055.

Lohmann, F., Loureiro, J., Su, H., Fang, Q., Lei, H., Lewis, T., Yang, Y., Labow, M., Li, E., Chen, T., et al. (2010). KMT1E mediated H3K9 methylation is required for the maintenance of embryonic stem cells by repressing trophectoderm differentiation. Stem Cells *28*, 201–212.

Loughran, S.J., Kruse, E.A., Hacking, D.F., de Graaf, C.A., Hyland, C.D., Willson, T.A., Henley, K.J., Ellis, S., Voss, A.K., Metcalf, D., et al. (2008). The transcription factor Erg is essential for definitive hematopoiesis and the function of adult hematopoietic stem cells. Nat. Immunol. *9*, 810–819.

Love, M.I., Huber, W., and Anders, S. (2014). Moderated estimation of fold change and dispersion for RNA-seq data with DESeq2. Genome Biol. *15*, 550.

Luger, K., and Richmond, T.J. (1998). The histone tails of the nucleosome. Curr. Opin. Genet. Dev. *8*, 140–146.

Lux, C.T., Yoshimoto, M., McGrath, K., Conway, S.J., Palis, J., and Yoder, M.C. (2008). All primitive and definitive hematopoietic progenitor cells emerging before E10 in the mouse embryo are products of the yolk sac. Blood *111*, 3435–3438.

Ma, Q., Jones, D., Borghesani, P.R., Segal, R.A., Nagasawa, T., Kishimoto, T., Bronson, R.T., and Springer, T.A. (1998). Impaired B-lymphopoiesis, myelopoiesis, and derailed cerebellar neuron migration in CXCR4- and SDF-1-deficient mice. Proc. Natl. Acad. Sci. *95*, 9448–9453.

Magnusson, M., Brun, A.C.M., Miyake, N., Larsson, J., Ehinger, M., Bjornsson, J.M., Wutz, A., Sigvardsson, M., and Karlsson, S. (2007). HOXA10 is a critical regulator for hematopoietic stem cells and erythroid/megakaryocyte development. Blood *109*, 3687–3696.

Majumder, P., and Boss, J.M. (2010). CTCF Controls Expression and Chromatin Architecture of the Human Major Histocompatibility Complex Class II Locus. Mol. Cell. Biol. *30*, 4211–4223.

Maksakova, I.A., Goyal, P., Bullwinkel, J., Brown, J.P., Bilenky, M., Mager, D.L., Singh, P.B., and Lorincz, M.C. (2011). H3K9me3-binding proteins are dispensable for SETDB1/H3K9me3-dependent retroviral silencing. Epigenetics and Chromatin *4*, 12.

Maksakova, I.A., Thompson, P.J., Goyal, P., Jones, S.J., Singh, P.B., Karimi, M.M., and Lorincz, M.C. (2013). Distinct roles of KAP1, HP1 and G9a/GLP in silencing of the two-cell-specific retrotransposon MERVL in mouse ES cells. Epigenetics and Chromatin *6*, 15.

Manaia, A., Lemarchandel, V., Klaine, M., Max-Audit, I., Romeo, P., Dieterlen-Lièvre, F., and Godin, I. (2000). Lmo2 and GATA-3 associated expression in intraembryonic hemogenic sites. Development *127*, 643–653.

Manesia, J.K., Xu, Z., Broekaert, D., Boon, R., van Vliet, A., Eelen, G., Vanwelden, T., Stegen, S., Van Gastel, N., Pascual-Montano, A., et al. (2015). Highly proliferative primitive fetal liver hematopoietic stem cells are fueled by oxidative metabolic pathways. Stem Cell Res. *15*, 715–721.

Månsson, R., Hultquist, A., Luc, S., Yang, L., Anderson, K., Kharazi, S., Al-Hashmi, S., Liuba, K., Thorén, L., Adolfsson, J., et al. (2007). Molecular Evidence for Hierarchical Transcriptional Lineage Priming in Fetal and Adult Stem Cells and Multipotent Progenitors. Immunity *26*, 407–419.

Manz, M.G., and Boettcher, S. (2014). Emergency granulopoiesis. Nat Rev Immunol *14*, 302–314.

Manz, M.G., Miyamoto, T., Akashi, K., and Weissman, I.L. (2002). Prospective isolation of human clonogenic common myeloid progenitors. Proc. Natl. Acad. Sci. *99*, 11872–11877.

Martin, D.I.K., Zon, L.I., Mutter, G., and Orkin, S.H. (1990). Expression of an erythroid transcription factor in megakaryocytic and mast cell lineages. Nature *344*, 444–447.

Martin, F.J., Xu, Y., Lohmann, F., Ciccone, D.N., Nicholson, T.B., Loureiro, J.J., Chen, T., and Huang, Q. (2015). KMT1E-mediated chromatin modifications at the FcγRIIb promoter regulate thymocyte development. Genes Immun. *16*, 162–169.

Matsui, T., Leung, D., Miyashita, H., Maksakova, I. a, Miyachi, H., Kimura, H., Tachibana, M., Lorincz, M.C., and Shinkai, Y. (2010). Proviral silencing in embryonic stem cells requires the histone methyltransferase ESET. Nature *464*, 927–931.

McCulloch, E., Siminovitch, L., Till, J., Russell, E., and Bernstein, S. (1965). The cellular basis of the genetically determined hemopoietic defect in anemic mice of genotype Sl/Sld. Blood *26*, 399–410.

McGrath, K.E., Koniski, A.D., Maltby, K.M., McGann, J.K., and Palis, J. (1999). Embryonic Expression and Function of the Chemokine SDF-1 and Its Receptor, CXCR4. Dev. Biol. *213*, 442–456.

Mebius, R.E., Miyamoto, T., Christensen, J., Domen, J., Cupedo, T., Weissman, I.L., and Akashi, K. (2001). The Fetal Liver Counterpart of Adult Common Lymphoid Progenitors Gives Rise to All Lymphoid Lineages, CD45 + CD4 + CD3 − Cells, As Well As Macrophages. J. Immunol. *166*, 6593–6601.

Medvinsky, A., and Dzierzak, E. (1996). Definitive Hematopoiesis Is Autonomously Initiated by the AGM Region. Cell *86*, 897–906.

Mercier, F.E., and Scadden, D.T. (2015). Not All Created Equal: Lineage Hard-Wiring in the Production of Blood. Cell *163*, 1568–1570.

Moore, M.A.S., and Metcalf, D. (1970). Ontogeny of the Haemopoietic System: Yolk Sac Origin of In Vivo and In Vitro Colony Forming Cells in the Developing Mouse Embryo. Br. J. Haematol. *18*, 279–296.

Morrison, S.J., and Weissman, I.L. (1994). The long-term repopulating subset of hematopoietic stem cells is deterministic and isolatable by phenotype. Immunity *1*, 661–673.

Morrison, S.J., Hemmati, H.D., Wandycz, A.M., and Weissman, I.L. (1995). The purification and characterization of fetal liver hematopoietic stem cells. Proc. Natl. Acad. Sci. *92*, 10302–10306.

Morrison, S.J., Wandycz, A.M., Hemmati, H.D., Wright, D.E., and Weissman, I.L. (1997). Identification of a lineage of multipotent hematopoietic progenitors. Development *124*, 1929–1939.

Mozzetta, C., Boyarchuk, E., Pontis, J., and Ait-Si-Ali, S. (2015). Sound of silence: The properties and functions of repressive Lys methyltransferases. Nat. Rev. Mol. Cell Biol. *16*, 499–513.

Muller-Sieburg, C.E., Whitlock, C.A., and Weissman, I.L. (1986). Isolation of two early B lymphocyte progenitors from mouse marrow: A committed Pre-Pre-B cell and a clonogenic Thy-1lo hematopoietic stem cell. Cell *44*, 653–662.

Müller, A.M., Medvinsky, A., Strouboulis, J., Grosveld, F., and Dzierzakt, E. (1994). Development of hematopoietic stem cell activity in the mouse embryo. Immunity *1*, 291–301.

Nagasawa, T., Hirota, S., Tachibana, K., Takakura, N., Nishikawa, S., Kitamura, Y., Yoshida, N., Kikutani, H., and Kishimoto, T. (1996). Defects of B-cell lymphopoiesis and bone-marrow myelopoiesis in mice lacking the CXC chemokine PBSF/SDF-1. Nature *382*, 635–638.

Ng, A.P., Loughran, S.J., Metcalf, D., Hyland, C.D., de Graaf, C.A., Hu, Y., Smyth, G.K., Hilton, D.J., Kile, B.T., and Alexander, W.S. (2011). Erg is required for self-renewal of hematopoietic stem cells during stress hematopoiesis in mice. Blood *118*, 2454–2461.

Ng, S.Y.-M., Yoshida, T., Zhang, J., and Georgopoulos, K. (2009). Genome-wide Lineage-Specific Transcriptional Networks Underscore Ikaros-Dependent Lymphoid Priming in Hematopoietic Stem Cells. Immunity *30*, 493–507.

Notta, F., Zandi, S., Takayama, N., Dobson, S., Gan, O.I., Wilson, G., Kaufmann, K.B., McLeod, J., Laurenti, E., Dunant, C.F., et al. (2016). Distinct routes of lineage development reshape the human blood hierarchy across ontogeny. Science (80-.). *351*, aab2116.

Ogilvy, S., Metcalf, D., Gibson, L., Bath, M.L., Harris, A.W., and Adams, J.M. (1999). Promoter elements of vav drive transgene expression in vivo throughout the hematopoietic compartment. Blood *94*, 1855–1863.

Oguro, H., Ding, L., and Morrison, S.J. (2013). SLAM Family Markers Resolve Functionally Distinct Subpopulations of Hematopoietic Stem Cells and Multipotent Progenitors. Cell Stem Cell *13*, 102–116.

Okada, S., Nakauchi, H., Nagayoshi, K., Nishikawa, S., Miura, Y., and Suda, T. (1992). In vivo and in vitro stem cell function of c-kit- and Sca-1-positive murine hematopoietic cells. Blood *80*, 3044–3050.

Ong, C.T., and Corces, V.G. (2014). CTCF: An architectural protein bridging genome topology and function. Nat. Rev. Genet. *15*, 234–246.

Orkin, S.H. (2000). Diversification of haematopoietic stem cells to specific lineages. Nat. Rev. Genet. *1*, 57–64.

Osawa, M., Hanada, K. -i., Hamada, H., and Nakauchi, H. (1996). Long-Term Lymphohematopoietic Reconstitution by a Single CD34-Low/Negative Hematopoietic Stem Cell. Science (80-.). *273*, 242–245.

Ottersbach, K., and Dzierzak, E. (2005). The Murine Placenta Contains Hematopoietic Stem Cells within the Vascular Labyrinth Region. Dev. Cell *8*, 377–387.

Palis, J., Robertson, S., Kennedy, M., Wall, C., and Keller, G. (1999). Development of erythroid and myeloid progenitors in the yolk sac and embryo proper of the mouse. Development *126*, 5073 LP – 5084.

Pang, S.H.M., de Graaf, C.A., Hilton, D.J., Huntington, N.D., Carotta, S., Wu, L., and Nutt, S.L. (2018). PU.1 Is Required for the Developmental Progression of Multipotent Progenitors to Common Lymphoid Progenitors. Front. Immunol. *9*, 1264.

Park, I., Qian, D., Kiel, M., Becker, M.W., Pihalja, M., Weissman, I.L., Morrison, S.J., and Clarke, M.F. (2003). Bmi-1 is required for maintenance of adult self-renewing haematopoietic stem cells. Nature *423*, 302–305.

Pasquarella, A., Ebert, A., Pereira de Almeida, G., Hinterberger, M., Kazerani, M., Nuber, A., Ellwart, J., Klein, L., Busslinger, M., and Schotta, G. (2016). Retrotransposon derepression leads to activation of the unfolded protein response and apoptosis in pro-B cells. Development *143*, 1788–1799.

de Pater, E., Kaimakis, P., Vink, C.S., Yokomizo, T., Yamada-Inagawa, T., van der Linden, R., Kartalaei, P.S., Camper, S.A., Speck, N., and Dzierzak, E. (2013). Gata2 is required for HSC generation and survival. J. Exp. Med. *210*, 2843–2850.

Paul, F., Arkin, Y., Giladi, A., Jaitin, D.A., Kenigsberg, E., Keren-Shaul, H., Winter, D., Lara-Astiaso, D., Gury, M., Weiner, A., et al. (2015). Transcriptional Heterogeneity and Lineage Commitment in Myeloid Progenitors. Cell *163*, 1663–1677.

Pawliuk, R., Eaves, C., and Humphries, R.K. (1996). Evidence of both ontogeny and transplant dose-regulated expansion of hematopoietic stem cells in vivo. Blood *88*, 2852–2858.

Perié, L., Duffy, K.R., Kok, L., de Boer, R.J., and Schumacher, T.N. (2015). The Branching Point in Erythro-Myeloid Differentiation. Cell *163*, 1655–1662.

Pham, T.H., Minderjahn, J., Schmidl, C., Hoffmeister, H., Schmidhofer, S., Chen, W., Längst, G., Benner, C., and Rehli, M. (2013). Mechanisms of in vivo binding site selection of the hematopoietic master transcription factor PU.1. Nucleic Acids Res. *41*, 6391–6402.

Pietras, E.M., Reynaud, D., Kang, Y.-A., Carlin, D., Calero-Nieto, F.J., Leavitt, A.D., Stuart, J.M., Göttgens, B., and Passegué, E. (2015). Functionally Distinct Subsets of Lineage-Biased Multipotent Progenitors Control Blood Production in Normal and Regenerative Conditions. Cell Stem Cell *17*, 35–46.

Ponting, C.P. (1997). Tudor domains in proteins that interact with RNA. Trends Biochem. Sci. *22*, 51–52.

Qian, H., Georges-Labouesse, E., Nyström, A., Domogatskaya, A., Tryggvason, K., Jacobsen, S.E.W., and Ekblom, M. (2007). Distinct roles of integrins α6 and α4 in homing of fetal liver hematopoietic stem and progenitor cells. Blood *110*, 2399–2407.

Ramond, C., Berthault, C., Burlen-Defranoux, O., De Sousa, A.P., Guy-Grand, D., Vieira, P., Pereira, P., and Cumano, A. (2014). Two waves of distinct hematopoietic progenitor cells colonize the fetal thymus. Nat. Immunol. *15*, 27–35.

Rea, S., Eisenhaber, F., O'Carroll, D., Strahl, B.D., Sun, Z.-W., Schmid, M., Opravil, S., Mechtler, K., Ponting, C.P., Allis, C.D., et al. (2000). Regulation of chromatin structure by site-specific histone H3 methyltransferases. Nature *406*, 593–599.

Rebel, V.I., Miller, C.L., Eaves, C.J., and Lansdorp, P.M. (1996a). The repopulation potential of fetal liver hematopoietic stem cells in mice exceeds that of their liver adult bone marrow counterparts. Blood *87*, 3500–3507.

Rebel, V.I., Miller, C.L., Thornbury, G.R., Dragowska, W.H., Eaves, C.J., and Lansdorp, P.M. (1996b). A comparison of long-term repopulating hematopoietic stem cells in fetal liver and adult bone marrow from the mouse. Exp. Hematol. *24*, 638–648.

Robb, L., and Begley, C.G. (1997). The SCL/TAL1 gene: Roles in normal and malignant haematopoiesis. BioEssays *19*, 607–613.

Robb, L., Lyons, I., Li, R., Hartley, L., Kontgen, F., Harvey, R.P., Metcalf, D., and Begley, C.G. (1995). Absence of yolk sac hematopoiesis from mice with a targeted disruption of the scl gene. Proc. Natl. Acad. Sci. *92*, 7075–7079.

Robertson, S.M., Kennedy, M., Shannon, J.M., and Keller, G. (2000). A transitional stage in the commitment of mesoderm to hematopoiesis requiring the transcription factor SCL/tal-1. Development *127*, 2447 LP – 2459.

Rossi, L., Lin, K.K., Boles, N.C., Yang, L., King, K.Y., Jeong, M., Mayle, A., and Goodell, M.A. (2012). Less is more: Unveiling the functional core of hematopoietic stem cells through knockout mice. Cell Stem Cell *11*, 302–317.

Rothenberg, E. V, Hosokawa, H., and Ungerbäck, J. (2019). Mechanisms of Action of Hematopoietic Transcription Factor PU.1 in Initiation of T-Cell Development. Front. Immunol. *10*, 228.

Sabin, F.R. (1920). Studies on the origin of blood-vessels and of red blood-corpuscles as seen in the living blastoderm of chicks during the second day of incubation: contributions to embryology. Contrib Embryol *9*, 213–262.

Saha, A., Wittmeyer, J., and Cairns, B.R. (2006). Chromatin remodelling: The industrial revolution of DNA around histones. Nat. Rev. Mol. Cell Biol. *7*, 437–447.

Sánchez, M.-J., Holmes, A., Miles, C., and Dzierzak, E. (1996). Characterization of the First Definitive Hematopoietic Stem Cells in the AGM and Liver of the Mouse Embryo. Immunity *5*, 513–525.

Sasaki, K., and Matsumura, G. (1988). Spleen lymphocytes and haemopoiesis in the mouse embryo. J. Anat. *160*, 27–37.

Sasaki, K., and Sonoda, Y. (2000). Histometrical and Three-Dimensional Analyses of Liver Hematopoiesis in the Mouse Embryo. Arch. Histol. Cytol. *63*, 137–146.

Scelfo, and Fachinetti (2019). Keeping the Centromere under Control: A Promising Role for DNA Methylation. Cells *8*, 912.

Schofield, R. (1970). Comparative study of repopulating potential of grafts from various haemopoietic sources: CFU repopulation. Cell Prolif. *3*, 119–130.

Schofield, R. (1978). The relationship between the spleen colony-forming cell and the haemopoietic stem cell. Blood Cells *4*, 7–25.

Schultz, D.C., Ayyanathan, K., Negorev, D., Maul, G.G., and Rauscher, F.J. (2002). SETDB1: A novel KAP-1-associated histone H3, lysine 9-specific methyltransferase that contributes to HP1-mediated silencing of euchromatic genes by KRAB zinc-finger proteins. Genes Dev. *16*, 919–932.

Scott, E., Simon, M., Anastasi, J., and Singh, H. (1994). Requirement of transcription factor PU.1 in the development of multiple hematopoietic lineages. Science (80-.). *265*, 1573–1577.

Semerad, C.L., Mercer, E.M., Inlay, M.A., Weissman, I.L., and Murre, C. (2009). E2A proteins maintain the hematopoietic stem cell pool and promote the maturation of myelolymphoid and myeloerythroid progenitors. Proc. Natl. Acad. Sci. *106*, 1930–1935.

Shivdasani, R.A., Mayer, E.L., and Orkin, S.H. (1995). Absence of blood formation in mice lacking the T-cell leukaemia oncoprotein tal-1/SCL. Nature *373*, 432–434.

Shivdasani, R.A., Fujiwara, Y., McDevitt, M.A., and Orkin, S.H. (1997). A lineage-selective knockout establishes the critical role of transcription factor GATA-1 in megakaryocyte growth and platelet development. EMBO J. *16*, 3965–3973.

Sigurdsson, V., and Miharada, K. (2018). Regulation of unfolded protein response in hematopoietic stem cells. Int. J. Hematol. *107*, 627–633.

Sigurdsson, V., Takei, H., Soboleva, S., Radulovic, V., Galeev, R., Siva, K., Leeb-Lundberg, L.M.F., Iida, T., Nittono, H., and Miharada, K. (2016). Bile Acids Protect Expanding Hematopoietic Stem Cells from Unfolded Protein Stress in Fetal Liver. Cell Stem Cell *18*, 522–532.

Song, Y.J., Choi, J.H., and Lee, H. (2015). Setdb1 is required for myogenic differentiation of C2C12 myoblast cells via maintenance of MyoD expression. Mol. Cells *38*, 362–372.

Spangrude, G., Heimfeld, S., and Weissman, I. (1988). Purification and characterization of mouse hematopoietic stem cells. Science (80-.). *241*, 58–62.

Sparmann, A., and Van Lohuizen, M. (2006). Polycomb silencers control cell fate, development and cancer. Nat. Rev. Cancer *6*, 846–856.

Spyropoulos, D.D., Pharr, P.N., Lavenburg, K.R., Jackers, P., Papas, T.S., Ogawa, M., and Watson, D.K. (2000). Hemorrhage, Impaired Hematopoiesis, and Lethality in Mouse Embryos Carrying a Targeted Disruption of the Fli1 Transcription Factor. Mol. Cell. Biol. *20*, 5643–5652.

Stehling-Sun, S., Dade, J., Nutt, S.L., DeKoter, R.P., and Camargo, F.D. (2009). Regulation of lymphoid versus myeloid fate “choice” by the transcription factor Mef2c. Nat. Immunol. *10*, 289–296.

Steiner, R., and Vogel, H. (1973). On the kinetics of erythroid cell differentiation in fetal mice. I. Microspectrophotometric determination of the hemoglobin content in erythroid cells during gestation. J. Cell. Physiol. *81*, 323–337.

Stockard, C.R. (1915). An Experimental Analysis of the Origin and Relationship of Blood Corpuscles and the Lining Cells of Vessels. Proc. Natl. Acad. Sci. *1*, 556–562.

Stocking, C., and Kozak, C.A. (2008). Endogenous retroviruses: Murine endogenous retroviruses. Cell. Mol. Life Sci. *65*, 3383–3398.

Stopka, T., Amanatullah, D.F., Papetti, M., and Skoultchi, A.I. (2005). PU.1 inhibits the erythroid program by binding to GATA-1 on DNA and creating a repressive chromatin structure. EMBO J. *24*, 3712–3723.

Subramanian, A., Tamayo, P., Mootha, V.K., Mukherjee, S., Ebert, B.L., Gillette, M.A., Paulovich, A., Pomeroy, S.L., Golub, T.R., Lander, E.S., et al. (2005). Gene set enrichment analysis: A knowledge-based approach for interpreting genome-wide expression profiles. Proc. Natl. Acad. Sci. *102*, 15545–15550.

Suda, T., Takubo, K., and Semenza, G.L. (2011). Metabolic Regulation of Hematopoietic Stem Cells in the Hypoxic Niche. Cell Stem Cell *9*, 298–310.

Takano, H., Ema, H., Sudo, K., and Nakauchi, H. (2004). Asymmetric Division and Lineage Commitment at the Level of Hematopoietic Stem Cells. J. Exp. Med. *199*, 295–302.

Takikita, S., Muro, R., Takai, T., Otsubo, T., Kawamura, Y.I., Dohi, T., Oda, H., Kitajima, M., Oshima, K., Hattori, M., et al. (2016). A Histone Methyltransferase ESET Is Critical for T Cell Development. J. Immunol. *197*, 2269–2279.

Tan, S.-L., Nishi, M., Ohtsuka, T., Matsui, T., Takemoto, K., Kamio-Miura, A., Aburatani, H., Shinkai, Y., and Kageyama, R. (2012). Essential roles of the histone methyltransferase ESET in the epigenetic control of neural progenitor cells during development. Development *139*, 3806–3816.

Till, J.E., and McCulloch, E.A. (1961). A direct measurement of the radiation sensitivity of normal mouse bone marrow cells. Radiat. Res. *14*, 213–222.

Tober, J., Yzaguirre, A.D., Piwarzyk, E., and Speck, N.A. (2013). Distinct temporal requirements for Runx1 in hematopoietic progenitors and stem cells. Development *140*, 3765–3776.

Toyama, H., Hosokawa, K., Ikushima, Y.M., Suda, T., and Arai, F. (2012). Role of N-Cadherin in the Regulation of Hematopoietic Stem Cells in the Fetal Liver and Bone Marrow. Blood *120*, 1205–1205.

Traver, D., Miyamoto, T., Christensen, J., Iwasaki-Arai, J., Akashi, K., and Weissman, I.L. (2001). Fetal liver myelopoiesis occurs through distinct, prospectively isolatable progenitor subsets. Blood *98*, 627–635.

Truong, A.H., and Ben-David, Y. (2000). The role of Fli-1 in normal cell function and malignant transformation. Oncogene *19*, 6482–6489.

Tsai, F.Y., and Orkin, S.H. (1997). Transcription factor GATA-2 is required for proliferation/survival of early hematopoietic cells and mast cell formation, but not for erythroid and myeloid terminal differentiation. Blood *89*, 3636–3643.

Tsai, F.-Y., Keller, G., Kuo, F.C., Weiss, M., Chen, J., Rosenblatt, M., Alt, F.W., and Orkin, S.H. (1994). An early haematopoietic defect in mice lacking the transcription factor GATA-2. Nature *371*, 221–226.

Vlaeminck-Guillem, V., Carrere, S., Dewitte, F., Stehelin, D., Desbiens, X., and Duterque-Coquillaud, M. (2000). The Ets family member Erg gene is expressed in mesodermal tissues and neural crests at fundamental steps during mouse embryogenesis. Mech. Dev. *91*, 331–335.

Waddington, C. (1942). The Epigenotpye. Endeavour 18–20.

Waddington, C. (1957). The strategy of the genes. A discussion of some aspects of theoretical biology (London: George Allen & Unwin, Ltd.).

Wagner, E.J., and Carpenter, P.B. (2012). Understanding the language of Lys36 methylation at histone H3. Nat. Rev. Mol. Cell Biol. *13*, 115–126.

Wang, L.D., and Wagers, A.J. (2011). Dynamic niches in the origination and differentiation of haematopoietic stem cells. Nat. Rev. Mol. Cell Biol. *12*, 643–655.

Wang, Q., Stacy, T., Binder, M., Marin-Padilla, M., Sharpe, A.H., and Speck, N.A. (1996). Disruption of the Cbfa2 gene causes necrosis and hemorrhaging in the central nervous system and blocks definitive hematopoiesis. Proc. Natl. Acad. Sci. *93*, 3444–3449.

Wilson, A., Laurenti, E., Oser, G., van der Wath, R.C., Blanco-Bose, W., Jaworski, M., Offner, S., Dunant, C.F., Eshkind, L., Bockamp, E., et al. (2008). Hematopoietic Stem Cells Reversibly Switch from Dormancy to Self-Renewal during Homeostasis and Repair. Cell *135*, 1118–1129.

Wolber, F.M., Leonard, E., Michael, S., Orschell-Traycoff, C.M., Yoder, M.C., and Srour, E.F. (2002). Roles of spleen and liver in development of the murine hematopoietic system. Exp. Hematol. *30*, 1010–1019.

Wu, A.M., Till, J.E., Siminovitch, L., and McCulloch, E.A. (1967). A cytological study of the capacity for differentiation of normal hemopoietic colony-forming cells. J. Cell. Physiol. *69*, 177–184.

Wu, A.M., Till, J.E., Siminovitch, L., and McCulloch, E.A. (1968). Cytological evidence for a relationship between normal hemotopoietic colony-forming cells and cells of the lymphoid system. J. Exp. Med. *127*, 455–464.

Yamada, Y., Warren, A.J., Dobson, C., Forster, A., Pannell, R., and Rabbitts, T.H. (1998). The T cell leukemia LIM protein Lmo2 is necessary for adult mouse hematopoiesis. Proc. Natl. Acad. Sci. *95*, 3890–3895.

Yang, L., Xia, L., Wu, D.Y., Wang, H., Chansky, H. a, Schubach, W.H., Hickstein, D.D., and Zhang, Y. (2002). Molecular cloning of ESET, a novel histone H3-specific methyltransferase that interacts with ERG transcription factor. Oncogene *21*, 148–152.

Yang, L., Lawson, K.A., Teteak, C.J., Zou, J., Hacquebord, J., Patterson, D., Ghatan, A.C., Mei, Q., Zielinska-Kwiatkowska, A., Bain, S.D., et al. (2013). ESET histone methyltransferase is essential to hypertrophic differentiation of growth plate chondrocytes and formation of epiphyseal plates. Dev. Biol. *380*, 99–110.

Yang, Q., Kardava, L., St. Leger, A., Martincic, K., Varnum-Finney, B., Bernstein, I.D., Milcarek, C., and Borghesi, L. (2008). E47 Controls the Developmental Integrity and Cell Cycle Quiescence of Multipotential Hematopoietic Progenitors. J. Immunol. *181*, 5885–5894.

Ye, M., Zhang, H., Amabile, G., Yang, H., Staber, P.B., Zhang, P., Levantini, E., Alberich-Jordà, M., Zhang, J., Kawasaki, A., et al. (2013). C/EBP controls acquisition and maintenance of adult haematopoietic stem cell quiescence. Nat. Cell Biol. *15*, 385–394.

Yuan, P., Han, J., Guo, J., Orlov, Y.L., Huss, M., Loh, Y.H., Yaw, L.P., Robson, P., Lim, B., and Ng, H.H. (2009). Eset partners with Oct4 to restrict extraembryonic trophoblast lineage potential in embryonic stem cells. Genes Dev. *23*, 2507–2520.

Zhang, C.C., and Lodish, H.F. (2004). Insulin-like growth factor 2 expressed in a novel fetal liver cell population is a growth factor for hematopoietic stem cells. Blood *103*, 2513–2521.

Zhang, C.C., Kaba, M., Ge, G., Xie, K., Tong, W., Hug, C., and Lodish, H.F. (2006). Angiopoietin-like proteins stimulate ex vivo expansion of hematopoietic stem cells. Nat. Med. *12*, 240–245.

Zon, L.I., Yamaguchi, Y., Yee, K., Albee, E.A., Kimura, A., Bennett, J.C., Orkin, S.H., and Ackerman, S.J. (1993). Expression of mRNA for the GATA-binding proteins in human eosinophils and basophils: potential role in gene transcription. Blood *81*, 3234–3241.